University of Southampton

Palaeoceanography and Sedimentology of the Gulf of Cadiz (0 – 30ka, BP)

by

Michael Rogerson

Doctor of Philosophy

(September 2003)

Faculty of Science

School of Ocean and Earth Science

This thesis was submitted in partial fulfilment of the requirements for the degree of Doctor of Philosophy and is the result of research carried out whilst in registered candidature at the University of Southampton.

University of Southampton

Abstract

Faculty of Science

Geology

Doctor of Philosophy

PALAEOCEANOGRAPHY AND SEDIMENTOLOGY OF THE GULF OF CADIZ

(0 – 30ka BP)

by Michael Rogerson

Evidence is presented for the presence of the Azores Front in the northern Gulf of Cadiz prior to 16ka BP, and its subsequent withdrawal during the last deglaciation. It is concluded that the North Atlantic warm water sphere was comparable in extent to today during the latter parts of the last glaciation.

It is also proposed that the Mediterranean Outflow plume settled to greater depths during the last glaciation, on the basis that evidence for its presence is found on the Gil Eanes Drift (the lowermost part of the Gulf of Cadiz contourite) but is not found in the modern flow path of the plume. This observation is consistent with predictions made from the physical constraints on the current system, and will have significant and potentially wide-ranging impact for the circulation of the Atlantic at all depths. In addition to its direct influence, the relatively shallow settling depth of the modern Mediterranean Outflow plume may promote the formation of North Atlantic Deep Water and thus enhance the meridional overturning.

Sea-level / climatic variation are proposed as the cause of contourite cycles on both large and small scales. The implications of observed anti-phasing of depositional cycles on the Gil Eanes Drift and the rest of the Gulf of Cadiz drift are discussed. Sediment deposited on the Gil Eanes Drift is found to be ultimately sourced from southwestern Iberia, initially deposited on the continental shelf and then reworked onto the slope where it is energetically sorted by the waning Mediterranean Outflow Plume and deposited on the sediment drift.

High-resolution colour data scanning is investigated as a tool for palaeoceanography, both as a correlation tool and for delineation of sedimentary flux to a location. Supply of terrigenous material to the western Gulf of Cadiz is found to be significantly enhanced during glacial times.

Contents

Illustrations

Tables

Accompanying Material

1 CD-ROM containing raw data collected during this study.

Acknowledgements

A large number of people have contributed to the work presented in this thesis. Only a few can be named here, and I express my gratitude to those that have been missed off. I would like to thank my supervisors, Phil Weaver and John Murray, whose support has been invaluable and particularly to Phil whose steadfast financial backing has made all the difference. An important role was also played by Eelco Rohling, without whose guidance this manuscript would have been very different. I thank James Casford, Mark Siddall and particularly Andy Hogg for thier help in coming to terms with new subject areas, Michal Kucera, Babette Hoogakker and Michael Winkelhofer for their interest and encouragement and John Thomson for not letting me get away with *anything*. Neville Barker and Simon Dean are also thanked for their help with knotty computing problems. The committee, chairman and staff of the NERC-RCL are thanked for providing the ^{14}C dates used in this work and for their support and encouragement.

I thank the members of the SOC cricket club for keeping my sprits up, particularly the Andies (Roberts and Bullock) whose enthusiasm has been invigorating, and the members of the Jet-Set Outdoor Club for keeping me sane when no end was in sight. Most of all I would like to thank my wife, Caroline, who married me in the first year of this work and presented me with our first child, Joseph Morton, in its final weeks. I cannot imagine how I could have got through it without you any more than I can imagine the future in your absence.

1 Rationale

The presence of the Mediterranean Outflow current on the northern GoC margin has lead to the deposition of a thick contourite deposit. Bottom-current derived deposits in the sediment record hold a distinctive signature of past bottom circulation, and are therefore of great potential use for constraining models of past ocean circulation and climate (Robinson and McCave, 1994). In addition, it is contended that sands deposited by bottom currents may act as hydrocarbon reservoirs (Shanmugam et al., 1993). It is therefore becoming important to gain what understanding we can about the history, origin and sedimentary architecture of these systems.

The North Atlantic Ocean and the Mediterranean Sea are the most intensively studied regions in the world in terms of their palaeoceanography. The response of these basins to cyclic climate change ("Milankovitch" and "Dansgaard-Oeschger" cyclicity), and transient climatic and environmental effects (e.g. Heinrich Events) are beginning to be understood. Atmospheric teleconnection between these regions has also been shown to exist (Allen et al., 1999; Allen and Huntley, 1996; Bar-Matthews et al., 1999; Cacho et al., 1999; Moreno et al., 2002; Rohling et al., 1998b; Roucoux et al., 2001; Sanchez-Goni et al., 2002; Sanchez-Goni et al., 2000), and marine and terrestrial records of environmental variability in the Mediterranean can now be correlated to, and put in the wider context of, the climatic variability seen in the northern high latitudes.

The Gulf of Cadiz (GoC) is located at the connection between the Atlantic Ocean and the Mediterranean Sea. The history of water mass exchange between the Atlantic and Mediterranean will be recorded in the sediment deposited in the GoC, making this a location at which further constraint can be placed upon the past budgets of the Mediterranean Sea. In addition, it is a location at which the influence of saline waters derived from the Mediterranean on the circulation of the Atlantic can be assessed.

1.2 Thesis Aims

This thesis has two main aims:-

1) To use planktonic foraminiferal assemblage and stable isotopic ($\delta^{13}C$, $\delta^{18}O$) data to describe the behaviour of palaeoceanographic features that have been present in the Gulf of Cadiz over the last 30,000 years. Specifically, the Azores Front is investigated, the history of which will be used to give insight into past surface circulation in the North Atlantic. In addition, micropalaeontological and sedimentological data are combined to give insight into the history of the Mediterranean Outflow current, which dominates the eastern Atlantic at intermediate depths and influences the meridional overturning of the Atlantic.

2) To describe the transportation pathway of sediment supplied to the Gil Eanes Drift, and its sedimentary behaviour over the last 30,000 years. Petrological, geochemical and micropalaeontological methods are used to indicate a dominantly western Iberian, rather than Mediterranean, origin for the sand found on the lowermost part of the Gulf of Cadiz contourite drift.

3) To investigate the history of the Gil Eanes Drift, and the implications for the sedimentology of the wider Gulf of Cadiz contourite and other contourite deposits in the sediment record.

4) To assess the validity and implications of the use of sediment colour for the development of astronomically tuned chronostratigraphic frameworks for sediment cores recovered from the Atlantic Ocean. To combine colour, geochemical and micropalaeontological methods to investigate the history of sedimentation in the western Gulf of Cadiz during the past 16,000 years.

5) To make an initial assessment of the benthic foraminiferal assemblages on the Gil Eanes Drift.

2 Introduction

2.1 Regional Geography and Geomorphology

The Gulf of Cadiz (GoC) is a large embayment located at the connection between the Atlantic Ocean and the Mediterranean Sea (Fig. 1). To the north and east lie Portugal and Spain respectively, Morocco lies to the south and the GoC is open to the Atlantic in the west. At the eastward extremity is the shallow and narrow Strait of Gibraltar, which is the only connection between the Mediterranean Sea and the open ocean. The Strait of Gibraltar forms a channel between the Betic and Atlas mountain chains, which lie to the north (in Spain) and south (in Morocco and Algeria) respectively (see fig 1), and are both part of the Alpine orogen (Jimenez-Munt et al., 2001). Both these mountain belts fall away rapidly along the margins of the GoC (northwest and southwest respectively), which are both relatively low-lying, with only Algarve (southern Portugal) having land above 500m close to the coast. The highlands of Gibraltar and the spur of the Rif mountains, which form an arc northwest of the High Atlas, thus form a narrow topographic barrier between the Atlantic and Mediterranean which is broken only at the Strait of Gibraltar.

Southwest Iberia is highly arid region, and is designated a semi-desert (Nicolau et al., 1996), experiencing ~350mm rain $year^{-1}$ (INM (Instituto Nacional de Meteororogia; www.inm.es) record for Granada, 1971-2000). The surrounding regions of southern Iberia and Morocco are generally areas with high aridity, high relief (see Fig. 1) and thus often poor cover by vegetation, and are rich sources of aeolian sediment (Grousset et al., 1998). The dust plume derived from the Sahara transports mineral grains from North Africa at least as far as northwest Europe (Ryall et al., 2002). However, the dry, dusty south of Iberia stands in contrast to northwest Iberia which is characterised by high precipitation (1000mm $year^{-1}$ (INM record for La Corunna 1971-2000)) derived from westerly winds supplying moisture from the Atlantic. Precipitation increases in central Spain during the autumn and winter when the Azores High pressure belt weakens enough for these damp westerlies to penetrate further south (www.inm.es) resulting in significant, though seasonally limited, rainfall in this region. Five major river systems are present within Iberia, two of which (the Guadiana and Guadalquivir) flow though the most arid parts of Iberia to drain into the

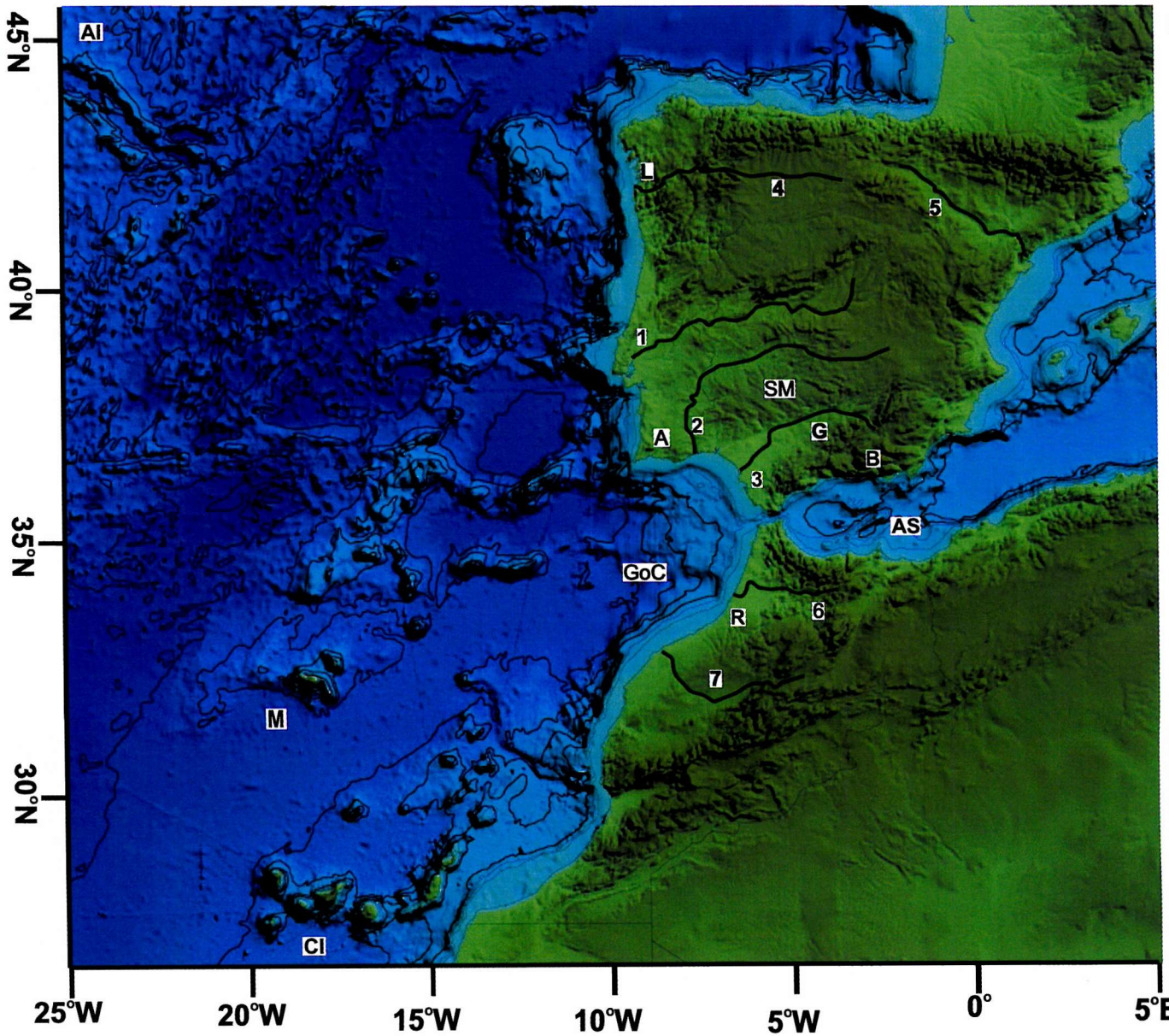

Figure 1.

Figure 1. Geography of the regionsurrounding the Gulf of Cadiz.

1 - Rio Tejo
2 - Rio Guadiana
3 - Rio Guadalquivir
4 - Rio Duero
5 - Rio Ebro
6 - Oued Sebou
7 - Oued Oum Er-Rbia
A - Algarve
AI - Azores Islands
AS - Alboran Sea
B - Betics
CI - Canary Islands
G - Granada
GoC - Gulf of Cadiz
L - La Corunna
M - Madeira
R - Rabat
S - Spain
SM - Sierra Morena

GoC. Deltas have formed at the debouchments of both of these rivers, and in addition the lowest reaches of the Guadalquivir are the Doñana wetlands, an extended area of low lying marsh where a large proportion of the sediment load of the Guadalquivir is deported today (Lopez-Galindo et al., 1999). It is believed that this wetland has been absent in the past, allowing increased sediment supply to the shelf of the GoC (Morales, 1997; Borrego et al., 1999; Lobo et al., 2001).

The Guadalquivir Basin marks the northern boundary of the Betic chain in Iberia (Fig. 1). South of the Guadalquivir, polycyclic Tertiary sedimentary rocks outcrop (Sierro et al., 1996), though the Betics have a core of older meta-sediments (Azanon et al., 1996). To the north and northwest of the basin lie the rich mining areas of the Iberian Pyrite Belt and the Sierra Morena (vanGeen et al., 1997), which are dominated by hydrothermally altered metamorphic rocks. In the east and northeast, the outcrops of Tertiary sediments, mixed with Mesozoic sediments, continue round in an arc north of the Sierra Morena and extend west along the valleys of the Guadiana and Tejo (Geological Map of the World (1994)).

Northern Morocco is essentially a mirror-image of southwest Iberia, and is divided from it by the Africa – Iberia plate boundary that lies within the channel of the Strait of Gibraltar (Jimenez-Munt et al., 2001). There are no major rivers draining into the GoC on its southern margin, the largest being the Oued Sabou which debouches close to Rabat (Fig. 1). The outcrops are of similar Tertiary and Mesozoic sediments as those found in Iberia, and in the drainage basin of the Sebou (i.e. west of the Rif mountains) there is negligible outcrop of either metamorphic or igneous material (Geological Map of the World (1994)).

Relative to most of the Iberian margin, the GoC continental shelf (Fig. 2) is quite wide (10 to 82km) and the continental slope is gentle (~13m km^{-1}). It is in an area believed to be tectonically active, and the Africa – Iberia plate boundary continues west from Gibraltar roughly bisecting the embayment (Calvert et al., 2000). The eastern and northern continental slopes of the GoC have high topography (~500m) related to a series of normal faults, which form asymmetric ridges, and evaporite diapirs, which in turn form symmetric ridges (Nelson et al., 1999). Both sets of ridges

Figure 2.

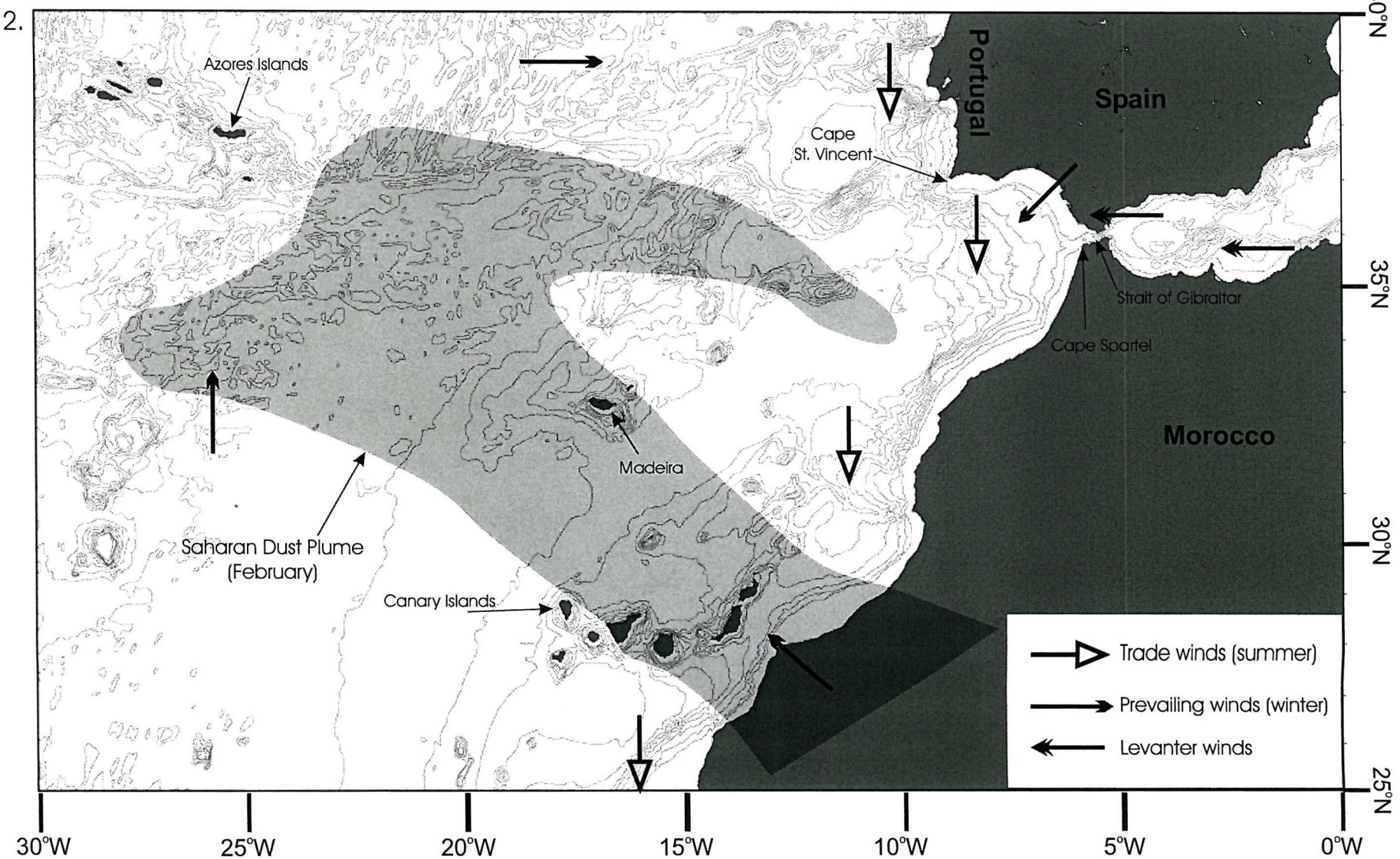

Figure 2. Prevailing winds in the Gulf of Cadiz Region and the rough position of the Saharan Dust Plume.

are oriented northeast to southwest, and are thus perpendicular to the strike of the slope (Nelson et al., 1999).

2.2 General Oceanographic and Climatic Setting

The Mediterranean basin has a high net evaporation, (0.5 – 0.8m yr^{-1}) which results in a net export of atmospheric water out of the basin (Bethoux, 1979; Garrett et al., 1990; Bryden and Kinder, 1991). As the surface water in the Mediterranean passes eastwards, it therefore becomes progressively enriched in salt and loses its buoyancy. Eventually the increasingly dense surface layer reaches the far eastern limit of the basin, where it is further concentrated and cooled during the dry winters of the Levantine basin and sinks to form a high density water mass that turns back on itself and returns westward at intermediate depth (Bryden and Stommel, 1984).

With the water level constantly being depressed by evaporation, to maintain sea level water must be constantly supplied to the Mediterranean, and this is achieved at Gibraltar (Bryden and Stommel, 1984). Atlantic water is drawn eastwards at the surface forming a plume of relatively fresh and buoyant water in the western Mediterranean basin. The excess salt in the Mediterranean is lost as a deep outflowing current that passes westwards through the Strait of Gibraltar and forms a plume of Mediterranean derived water at intermediate depth in the Atlantic (Ambar and Howe, 1979; Reid, 1979; Price et al., 1993; O'Neill-Baringer and Price, 1997, 1999). This transfer of water into and out of the Mediterranean at the Strait of Gibraltar is known as the Gibraltar Exchange.

The Alboran Sea is adjacent to the GoC, lying at the eastern end of the Strait of Gibraltar and its hydrographic structure impacts on the GoC. The water column in this basin is strongly stratified and is derived from three sources:- the eastern Mediterranean, the western Mediterranean (esp. the Gulf of Lions) and the Atlantic (Kinder and Parilla, 1987). The West Mediterranean Deep Water (WMDW) forms in the Gulf of Lions as a result of cooling and evaporation when the Mistral winds blow off southern Europe (Stommel, 1972; Rohling and Bryden, 1994) and accumulates in the deep basins of the western Mediterranean (Kinder and Parilla, 1987). Overlying this is the Levantine Intermediate Water (LIW), which forms in the Eastern Mediterranean and flows westwards through the Strait of Sicily. In the Alboran Sea it

occurs only in the northern two thirds of the basin, and occupies a depth band between 200 and 600m. The surface layer is modified Atlantic water, derived from the Atlantic Inflow Water (AIW) and generally flowing east (Kinder and Parilla, 1987).

The 12.9°C isotherm, defined as being coincident with the top of the WMDW, is several hundred metres below sill depth in the Alboran Sea (Stommel et al., 1973; Pettigrew, 1989). However, the westward transport of the overlying LIW causes a net transport of WMDW towards the Strait by the Bernoulli effect, as proposed by Stommel et al. (1973). At the entrance of the Strait the isotherm is less than 100m below sill depth (Bryden and Stommel, 1982), and water cooler than 12.9°C has been found to be passing over the deepest part of the sill nearly two thirds of the time (Pettigrew, 1989). This aspiration of deep water probably contributes less than 10% of the total flux (Bryden, 1993), but estimates from measurements have been as high as 0.2Sv (10^6 m^3 s^{-1}) (Pettigrew, 1989).

Viewed simply, the GoC is an extension of the Mediterranean anti-estuarine circulation west of Gibraltar and into the Atlantic. Close to Gibraltar, water is lost at the surface as it flows into the Mediterranean, and this must be resupplied to the eastern GoC by constant eastward flow at the surface (Bryden et al., 1988; Bryden et al., 1994). Strong flow of the dense plume of Mediterranean water at depth causes a general westward flow below the surface throughout the GoC, which is in contact with the bottom in the east but lifts off the sea floor roughly half way across the GoC to become an intermediate water mass before it is exported into the open Atlantic (O'Neill-Baringer and Price, 1997, 1999). Both the inflowing and outflowing currents are mainly confined to discrete flow paths in the northern half of the GoC (O'Neill-Baringer and Price, 1997, 1999). The northern and eastern margins of the GoC are therefore swept by strong currents throughout the water column, whereas the southern margin is relatively quiet (Ambar and Howe, 1979).

The surface current in the GoC is termed the Atlantic Inflow Current (AI), and flows northwest to southeast along the northern continental shelf of the GoC. It increases in strength as it nears Gibraltar and it is this water that passes though the Strait of Gibraltar to form the plume of Atlantic water in the western Mediterranean (Ambar and Howe, 1979). This flow probably extends westwards into the Atlantic as it is

genetically linked to the flow found south of the Azores Islands termed the Azores Current (Johnson et al., 2002). The mechanism of mass transformation by which the Azores Current is formed, which is also linked to the behaviour of the MO on the GoC slope, will be described in chapter 4. The impact of the AI on the sedimentology of the continental shelf will be described in more detail in chapters 6 and 7. The deep current in the GoC is termed the Mediterranean Outflow (MO), and flows southeast to northwest impinging on the northern continental slope from Cape Spartel to Cape St. Vincent (Kenyon and Belderson, 1973) (Fig. 1). The behaviour of the plume of the Mediterranean Outflow on the slope of the GoC is rather complex, and will be described in chapter 5.

Throughout much of the year the Azores high pressure system extends as far east as the Strait of Gibraltar (Dorman et al., 1995). In the winter, the mean wind is north-easterly with low pressure dominating over Italy (Dorman et al., 1995), and Sea Surface Temperatures (SSTs) in the Gulf of Cadiz are ~16°C (Antonov et al., 1998). The northerly Portuguese Trades are persistent on the Portuguese coast in the summer, blowing >50% of the time (Fiuza et al., 1982). In the Strait of Gibraltar, the mean summer wind is gentle and north-westerly, but is punctuated by stronger easterly "levanter" winds (Dorman et al., 1995). These form as a result of eastward migrating Atlantic pressure troughs which temporarily collapse the Azores High when they reach the east Atlantic margin, reversing the pressure gradient in the western Mediterranean (Dorman et al., 1995). The levanter winds are particularly strong at Gibraltar as a result of topographic channelling of the wind into the narrows of the Strait (Dorman et al., 1995). At Cadiz, north westerly and levanter winds both occur in the summer (Dorman et al., 1995), but the northerly trade is dominant (Fiuza et al., 1982). Summer Sea Surface Temperatures in the Gulf of Cadiz are in the range 20-22°C (Antonov et al., 1998).

The sub-tropical eastern margin of the north Atlantic is the site of significant upwelling, due to the presence of strong and persistent northerly trade winds causing separation of surface water from the coast (Fiuza et al., 1982). The Gulf of Cadiz lies in the northern part of the sub-topical belt and would therefore be expected to be the site of summer upwelling, particularly as the northerly trade winds are common and strong. However, few summer SST anomalies have been recorded within the Gulf of

Cadiz itself (Fiuza, 1981; Fiuza et al., 1982). Upwelling is strong and consistent throughout the summer at Cape St. Vincent, and to some extent is extended along the 200m isobath into the Gulf of Cadiz. However, it does not seem to extend further east than the mouth of the Guadiana river (Fiuza, 1981) (Fig. 1). This may be due to the coast being oriented northeast to southwest on the eastern margin of the GoC, which does not favour upwelling under northerly winds (Fiuza et al., 1982).

2.3 The Gibraltar Exchange

The fluxes of the Atlantic and Mediterranean water transported through the Strait of Gibraltar are controlled by the hydraulics of the sill and narrow configuration in the Strait itself, which acts like a bottle-neck between the Atlantic and Mediterranean water masses. The analytical treatment of this hydraulic control is described in more detail in chapter 5. A general overview of the configuration of the Strait is given here and the importance of the observation that the Gibraltar Exchange is maximal (i.e. that jet-like flow exists within the Strait section) is discussed. Estimates of the fluxes of the out- and inflow are given, and finally the significance of annual to sub-annual flux variability is discussed.

The Strait of Gibraltar (Fig. 3) is a narrow sea passage, 60km long and about 15km wide, narrowing to 12km at the Tarifa Narrows. At the western end of the Strait is the Camarinal sill, which has a maximum depth of 284m and extends from Point Paloma (Spain) to Point Altares (Morocco) (Candela et al., 1989). To the west of the Camarinal sill lies the relatively deep Tangier Basin (depth 450m), which is separated from the Atlantic by a second sill (the Spartel sill), with a depth of 350m (Armi and Farmer, 1988; Farmer and Armi, 1988). Though it has little effect on flow through the Straits, the Spartel sill has a profound effect on the variability of the flux of the outflow as it enters the Atlantic (Thorpe, 1976).

The effect of the bottle-neck of the Strait is to cause the flow to be jet-like, and therefore "hydraulic jumps" form at either end of the Strait (Kinder et al., 1988). The energetic state of the flow is determined by the Froude number, a dimensionless number that indicates whether a flow is sub- or super-critical (i.e. whether the flow is flat or jet-like). The maximum exchange possible occurs when the flow is a jet and the two layer Froude number (G^2) exceeds 1, i.e.:

Figure 3.

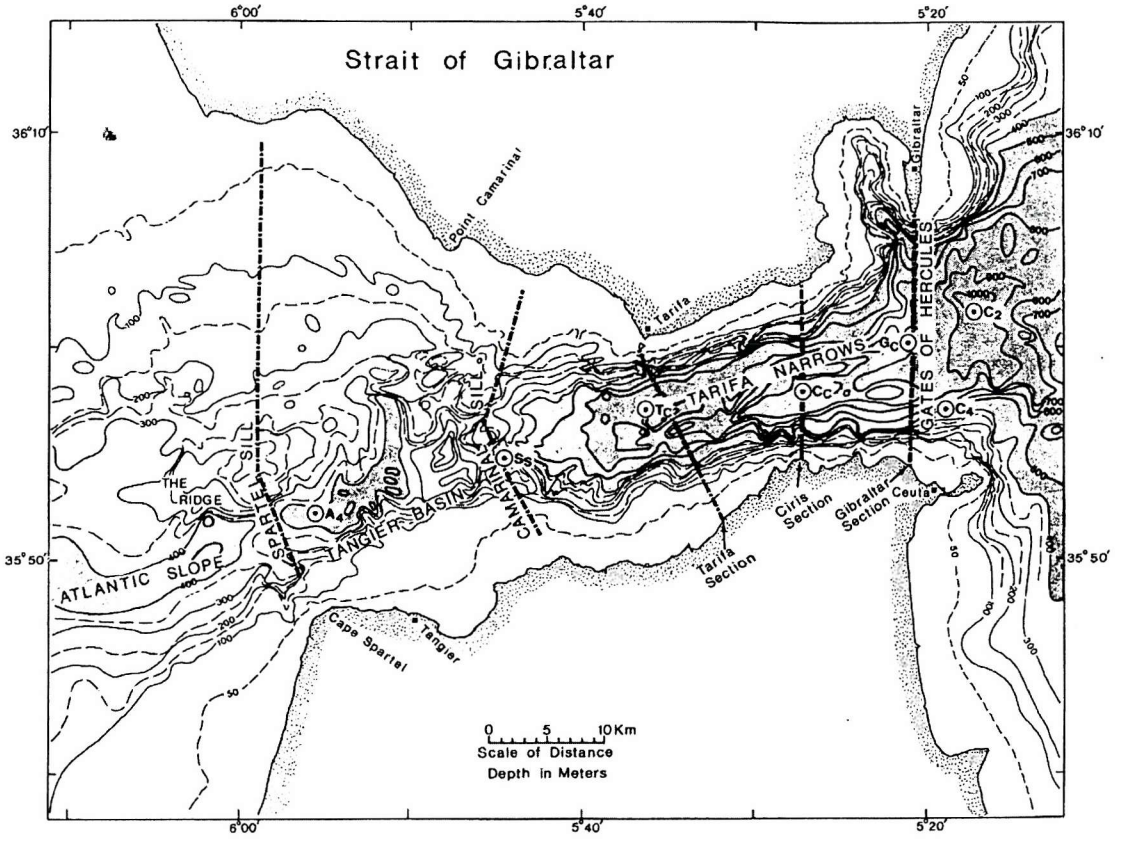

Figure 3. The Strait of Gibraltar (Lacombe and Richez 1978).

$$G^2 = (u_{AI}^2 / g' H_{AI}) + (u_{MO}^2 / g' H_{MO}) \geq 1$$

Where u_{AI} and u_{MO} are the velocities of the upper and lower layer respectively, H_{AI} and H_{MO} are the thicknesses of the upper and lower layers respectively and $g' = g\beta(S_{MO} - S_{AI})$ where β is determined from the equation of state for seawater (g is the acceleration due to gravity) and S_{AI} and S_{MO} are the salinities of the upper and lower layers respectively. Under these conditions, the flow is termed *critical*, and the exchange is termed *maximal* (Armi and Farmer, 1986; Farmer and Armi, 1986; Armi and Farmer, 1988; Farmer and Armi, 1988).

The hydraulic jumps at both ends of the Strait of Gibraltar are analogous to the flow of water over a weir, and prevent signals from being propagated through the Strait section (i.e. the velocity of the flow is greater than the internal velocity of waves within it) (Bryden and Kinder, 1991). The Mediterranean Sea is thus isolated from the Atlantic and each basin can be practically treated as being separate from the other, a fact that has been exploited during efforts to develop models of the Mediterranean (e.g. (Bethoux, 1979; Bigg, 1994; Rohling and Bryden, 1994; Bigg, 1995; Myers et al., 1998; Myers, 2002; Rohling et al., 2003b)). The presence of critical flow may also be exploited when considering the history of the Gibraltar Exchange. Though without critical flow the fluxes of the in- and outflows can be predicted by the statements of mass and salt conservation, with the presence of critical flow these statements can be combined with the equations describing the hydraulics of the sill to predict not only the fluxes but also the properties of the Mediterranean water exported west (Armi and Farmer, 1988; Farmer and Armi, 1988). In addition, with a maximal exchange the out- and inflow currents must be active permanently, with relatively little variability compared to the sub-critical scenario (Armi and Farmer, 1988; Farmer and Armi, 1988).

Modern estimates of the exchanged fluxes are based on measurements taken during the Gibraltar Experiment of the 1980's, and suggest an outflow value of 0.79×10^6 m^3 s^{-1}, with a corresponding estimate of inflow flux of 0.95×10^6 m^3 s^{-1} (Bryden and Kinder, 1991). Though this is lower than traditional estimates (eg. (Lacombe and

Richez, 1982)), it is consistent with estimates derived from a steady-state hydraulic model (Bryden and Kinder, 1991).

Though the exchange is usually viewed as a steady-state, within the Strait of Gibraltar section it shows significant cyclicity on annual, sub-annual and diurnal timescales. Approximately half of the total flux is effected by tidal fluctuations alone (Bryden et al., 1994), with bores of Atlantic and Mediterranean water passing through the Strait with the rising and falling tides respectively. Due to the large tidal effect on the exchange, the transport over the Camarinal sill to the Tangier Basin is highly variable on diurnal timescales (Bryden et al., 1994). The height of the reservoir in the Tangier Basin is therefore also variable, but despite this, throughout the tidal cycle the flow out of the Tangier Basin over the Spartel sill is almost constant (Bryden et al., 1988). As it is this sill that partitions the Tangier Basin from the Atlantic, this means that the outflow can be viewed as having little significant short term variability (Thorpe, 1976; Armi and Farmer, 1988; Farmer and Armi, 1988), making steady–state treatment of the outflow valid on short timescales.

Annual cyclicity in the exchange is primarily caused by variation in the rate of formation of deep and intermediate water in the Mediterranean (Garrett et al., 1990). The sea level difference between the Atlantic and Mediterranean at Gibraltar also varies annually, and this may also have an effect (Bormans et al., 1986). The outflow flux varies by 0.03Sv, and reaches its maximum in January – February, when the Mediterranean deep reservoir is being refilled. The inflow flux varies by 0.12Sv annually, reaching a maximum in September, when the newly formed deep water has drained over the sill (Bryden et al., 1994). Atmospheric pressure fluctuations over the Mediterranean also have an effect, with low pressures leading to enhanced inflow, and high pressures leading to increased outflow (Candela et al., 1989). As the annual variability in the outflow may be as much as 15% of the total flux, steady-state models of the exchange are not valid on ~1 year timescales. However, these effects will tend to negate through an annual cycle and so a steady-state model of the mean fluxes on timescales greater than 1 year, as is used in Chapter 5, is likely to be a reasonable approximation.

2.4 The Oceanography of the Wider North Atlantic

Between 10° and 50° latitude, the surface circulation of the North Atlantic is dominated by the sub-tropical gyre (Fig. 4). This is a wind-driven circulation, that is not quite closed in its northeastern extremity allowing the Gulf Stream Extension to flow directly into the Nordic seas (Riverdin et al., 2003). An effective eastern boundary current only exists south of the GoC where it is termed the Canary Current (Knoll et al., 2002), though the weak Portuguese Current is active on the western margin of Iberia which extends the eastern boundary current to the north (Fiuza, 1981; Martins et al., 2002). The western boundary current is the Gulf Stream, and this transports significant water and heat out of the Gulf of Mexico and along the eastern coast of North America (Sturges and Hong, 2001). Estimates of water export from the Gulf of Mexico are in the range of 30-32 Sv (Schmitz and McCartney, 1993), and have been shown in time-series to exhibit <5% variability from a mean of 31Sv (Larsen, 1992). The wind driven component of this export, which is passed into the North Atlantic Gyre and eventually recirculated to the Caribbean Sea via the eastern and southern boundary currents, is believed to be in the range of 17Sv (Schmitz and McCartney, 1993). Roughly 13Sv of water lost from the Arctic Seas during deep and intermediate water production are also replaced by this flow, which accounts for the remaining portion of the Gulf Stream transport (Schmitz and McCartney, 1993).

At the Newfoundland Grand Banks, the Gulf Stream separates from the coast to flow generally northwestwards across the North Atlantic, eventually passing to the north of Britain and into the Nordic seas (Riverdin et al., 2003). The transport of the Gulf Stream Extension north of Britain is much reduced compared to that on the east coast of North America (~18.5Sv (Sturges and Hong, 2001)). This reflects the deterioration of the structure of the Gulf Stream as it crosses the North Atlantic and the meridional and gyre components separate (Fratantoni, 2001). A major part of this deterioration occurs at the Newfoundland Grand Banks, where part of the Gulf Stream is recirculated into the North Atlantic to flow directly eastwards at a latitude of ~40°N as the Azores Current / Azores Front (Gould, 1985). This is recirculation is estimated to represent >10Sv of transport (Schmitz and McCartney, 1993; Alves and DeVerdière, 1999) and links with the Canary Current close to Madeira, thus forming a closed "sub-gyre" within which water sourced from the Sargasso Sea is contained (Schiebel

Figure 4.

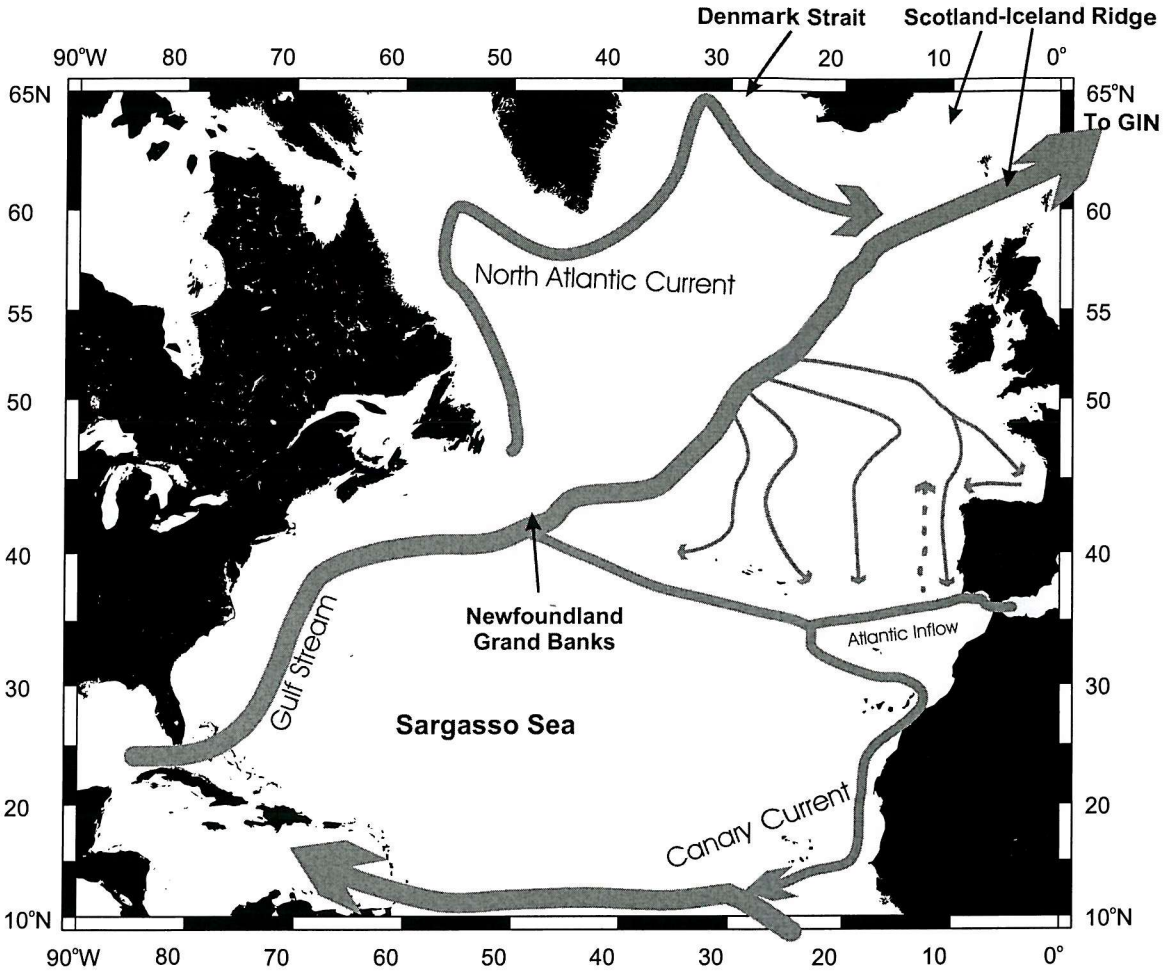

Figure 4. General surface circulation in the North Atlantic today. The Portuguese Counter Current is shown as a broken line, and is active only during winter.

et al., 2002). The Azores Front therefore defines the northern limit of the warm water sphere in the Atlantic (Gould, 1985). Further recirculation of the Gulf Stream to small, unstable and generally southward transporting currents occurs east of the grand Banks as far as the Irish Slope, where a more stable current flows south causing some clockwise circulation in the Bay of Biscay (Paillet and Mercier, 1997). It is also this recirculating water that causes the development of the Portuguese Current (Paillet and Mercier, 1997).

The northern boundary of the gyre is formed by the Gulf Stream and the North Atlantic Current, which lies further north than the Gulf Stream close to the southern tip of Greenland (Riverdin et al., 2003). The wind-driven North Atlantic Current originates on the continental Newfoundland Shelf (Sheng and Thompson, 1996) and flows northwards along the east coast of northern North America before turning west at the mouth of the Labrador Sea (Riverdin et al., 2003). From here it generally flows westwards, south of Greenland where it forms the subpolar front which devides the sub-tropical and sub-polar gyres (Dutkiewicz et al., 2001). This picture is complicated by a complex series of loops, topographically forced standing meanders and recirculations that are too small to be resolvable on Figure 4 (McCartney and Mauritzen, 2001). In addition, these structures are only quasi-stable and so substantial cross-frontal exchange occurs in this region (Dutkiewicz et al., 2001). As they near Iceland, the North Atlantic and Gulf Stream Extension currents join and are caught in a complex configuration of flow into the Nordic Seas, recirculation into the sub-polar and sub-tropical gyres and downwelling which are controlled jointly by the dynamics of the basin-strait exchanges between Greenland and Scotland and the wind regime (McCartney and Mauritzen, 2001; Orvik and Skagseth, 2003).

The subtropical gyre extends to less than 2000m, below which wind-driven circulation is negligible (Pickard and Emery, 1990). In the eastern North Atlantic between 500 and 1500m lies the plume of Mediterranean water sourced from the GoC (Reid, 1979; O'Neill-Baringer and Price, 1999). This plume flows west and north and causes elevated salinities as far west as the Bahama Banks (Armi and Bray, 1982). It is possible that salt derived from the plume also penetrates into the Nordic seas (Greenland-Iceland-Norwegian seas, or GIN) where it decreases the buoyancy of the surface water and promotes sinking (Reid, 1979). Though this assertion is still

debated (McCartney and Mauritzen, 2001), general circulation modelling of the Atlantic meridional overturning has shown sensitivity to the properties of the water exported from the Mediterranean (Rahmstorf, 1998).

Cold and arid conditions in the GIN, particularly in winter, cause surface water supplied mainly by the Gulf Stream and North Atlantic Current to become dense and sink (Girton et al., 2001). The GIN is connected to the Atlantic at the Denmark Strait (between Greenland and Iceland) and between Iceland and Scotland (the Iceland-Faroe ridge and the Faroe-Scotland ridge, termed herein the Scotland-Iceland Ridge) (McCartney and Mauritzen, 2001). The dense water formed in the GIN spills through these straits, analogously to the way Mediterranean water passes through the Strait of Gibraltar (Price and O'neill-Baringer, 1994). With the addition of dense waters formed in a similar way in the non-enclosed Labrador Sea, it is this water that forms the North Atlantic Deep Water (NADW) that can be observed in all the deep ocean basins worldwide (Pickard and Emery, 1990). It is thought that it is the formation of NADW that drives the great Ocean Conveyor (Broecker, 1991), and thus the worldwide thermohaline circulation.

In addition to Mediterranean Outflow water, three other intermediate waters are found in the eastern North Atlantic, characterised by thermal and salinity minima which reflect the high input of fresh water to their source areas (vanAken, 2000). The upper part of the water exported as a deep flow from the Labrador Sea forms one of these intermediate waters and acts as a deep western boundary current that spreads north-eastwards into the Irminger Sea, and then southwards under the North-Atlantic Current towards the eastern Atlantic basins (Talley and McCartney, 1982). Labrador Sea Water is identified by a salinity minimum at intermediate depths in the Porcupine Sea Bight (vanAken, 2000), and south into the Bay of Biscay (Talley and McCartney, 1982). A frontal zone extends southwest from the Bay of Biscay marking the southeastern extent of the Labrador Sea water (Talley and McCartney, 1982). Southeast of this zone, modified Mediterranean water occupies the water column at intermediate depth (Talley and McCartney, 1982; vanAken, 2000).

Winter downwelling between the North Atlantic Current and the coasts of Iceland and Greenland cause the formation of an additional dense water, part of which is

circulated in the sub-polar gyre and part of which subducts below the sub-polar front to be exported into the Atlantic as the North Atlantic Intermediate Water (Arhan, 1990). This is generally found above the Labrador Sea Water at high latitudes, and has been recognised as an intermediate salinity minimum at ~600m water depth at least as far south as 33°N (Tsuchiya et al., 1992).

Antarctic Intermediate Water is found on the northwest African margin (Tsuchiya et al., 1992), and has been shown to extend at least as far north as 32° (Roemmich and Wunsch, 1985). This northward flowing intermediate water is denser than North Atlantic Intermediate Water, and is recognised as a salinity minimum at ~900m (vanAken, 2000).

The southward flowing NADW is present at depth (1km to bottom (Pickard and Emery, 1990)) off Portugal and North Africa, though it is believed that Antarctic Bottom Water has some influence (Shackleton et al., 2000) and is known to penetrate at least as far as 40°N (Roemmich and Wunsch, 1985). The GoC and Iberian margin lie between the sub-polar and Azores Fronts and above the NADW in this region lie the southward flowing North Atlantic Intermediate water (Gould, 1985; Schiebel et al., 2002) (see Fig. 5), and potentially the northward flowing Antarctic Intermediate Water (Roemmich and Wunsch, 1985). However, at intermediate depths the hydrography and properties of the water are dominated by the Mediterranean Outflow (Iorga and Lozier, 1999). South of the Azores Front lies the 18°C Mode Water, which originates in the Sargasso Sea (Pickard and Emery, 1990; Schiebel et al., 2002) and is warm, salty and poor in nutrients relative to the water north of the Front (Fasham et al., 1985; Fernandez and Pingree, 1996; Doval et al., 2001; Schiebel et al., 2002).

2.5 Bottom Currents and the Deposition of Deep-Sea Sand

Geostrophic bottom currents that are derived from the oceans' thermohaline circulation often impinge on the sea floor, reworking the sediment and causing the formation of sediment drifts (Stow and Lovell, 1979). These are generally termed contourites due to the tendency of these geostrophic currents to follow bathymetric contours. This is a problematic definition, as not all bottom currents follow bathymetric contours and very few follow contours throughout their length (Shanmugam, 2000). The type area for many models of contourite deposition is the

Figure 5.

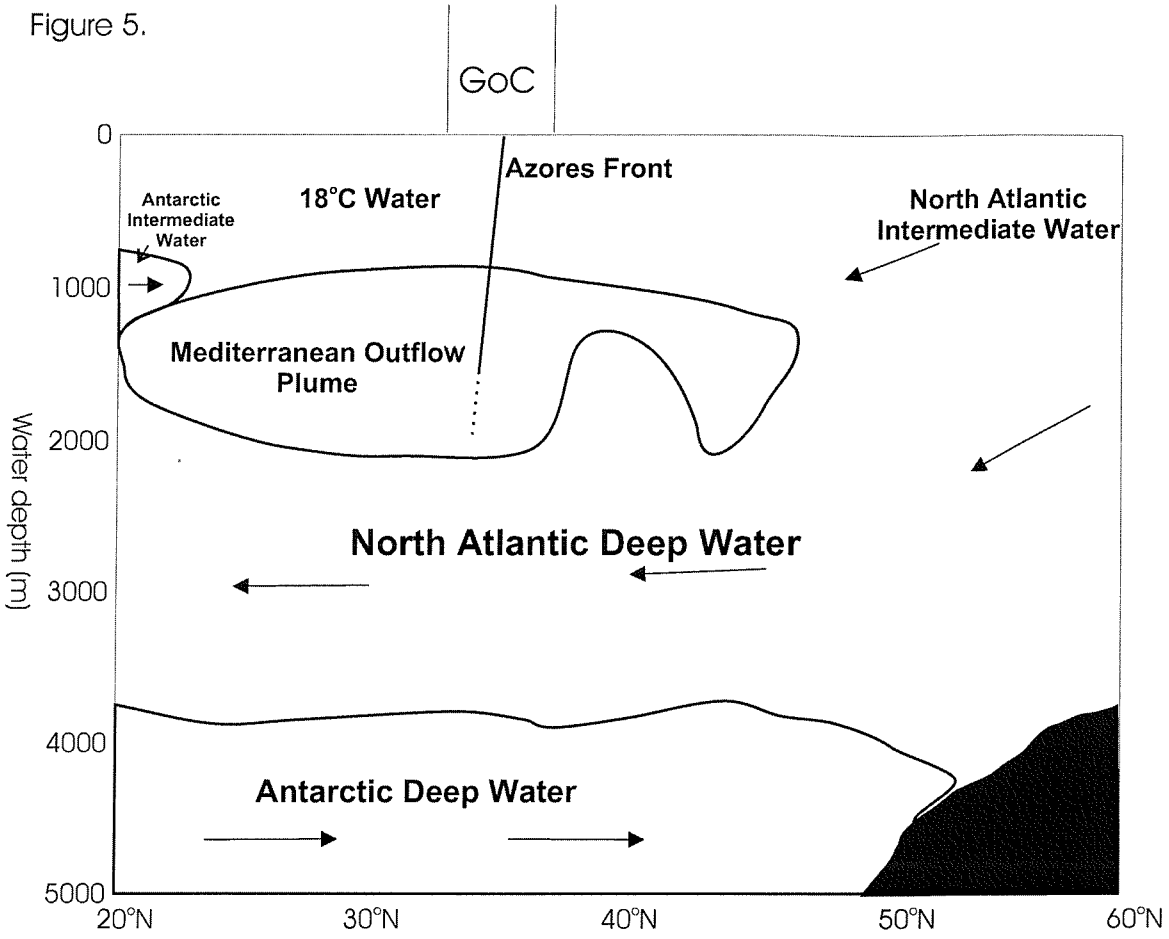

Figure 5. Vertical water column structure in eastern north Atlantic (Pickard and Emery 1990).

GoC (e.g. (Stow and Lovell, 1979; Stow et al., 1986; Stow et al., 1998)), and the GoC sediment drift highlights the problem of non-contouring bottom current flow, as throughout the GoC the current that is causing the drift to form, the MO, is slowly descending the slope and is therefore not parallel to contours (Ambar and Howe, 1979; O'Neill-Baringer and Price, 1999). "Contourite" channels on the GoC slope are often locally oriented downslope as a result of interaction with the high topography of the continental slope (Hernandez-Molina et al., 2003). Some are oriented down slope along their entire length without any apparent topographic steering (the "free-standing" channels of Habgood *et al.*, 2003). To avoid problems of terminology, in this report, sedimentary deposits lain down under a ocean-bottom currents are therefore described in preference as "sediment drifts", and "contourite" when used should be viewed as synonymous with this definition.

The characteristics by which bottom-current derived sediment drifts can be recognised are still a hotly debated issue, particularly for fossil contourites (Stow et al., 1998; Shanmugam, 2000). To definitively show that a particular deposit has been lain down by, or experienced reworking from, a bottom current without substantial contextual information is often impossible (Stow et al., 1998). The sedimentary characteristics of bottom-current derived sediment drifts may all be potentially mimicked by turbidite/mass flow sequences (Shanmugam, 2000). Even those characteristics of bottom-current derived drifts that can be universally agreed upon, such as inverse grading of laminae and beds, lenticular bedding and starved ripples can be produced by gravity flow processes in some contexts (Stow et al., 1998; Shanmugam, 2000; Mulder et al., 2001). Consequently, it is in the modern oceans where context can be readily established that these important sedimentary environments must be investigated further (Stow et al., 1998).

Contourites and sediment drifts in the modern ocean are generally classified as being Muddy or Sandy (Stow and Lovell, 1979), with Sandy contourites often occurring within sequences of Muddy contourite (Stow et al., 1998). This is traditionally thought to represent a full cycle of waxing and waning of the strength of the bottom current though time, and is expressed as the classic "contourite cycle" of Stow (1986) (See figure 6). Both Muddy and Sandy contourites are bioturbated throughout, and often mottled in appearance (Stow and Lovell, 1979).

The ideal, or complete, sequence was first identified on the Faro Drift in the northeastern GoC (Faugères et al., 1984; Gonthier et al., 1984; Stow et al., 1986; Faugères and Stow, 1993). This shows overall negative grading from muddy through silty to sandy sediment, then positive grading back through silt to mud. Lenses, lags and small layers of coarser sediment within the generally massive and bioturbated material are found throughout. Contacts between layers may be graded, sharp or erosional. Just as the Bouma turbidite sequence is rarely found in its entirety, it is often the case that only part of the cycle is preserved. In these cases, a graded or inversely graded bed is deposited, often with one gradational and one sharp contact (Shanmugam, 2000).

Inversely graded beds are the feature most commonly viewed as diagnostic of a bottom-current origin of a sediment in recent reviews of the subject (Stow et al., 1998; Shanmugam, 2000; Stow and Mayall, 2000). Other characteristics of deep-sea sediment drifts, as reported by Shanmugam (2000), are shown below. This is included here as a list of common features of deposits of this origin rather than as a diagnostic criteria, as none of these characteristics is unique to sediment drifts or contourite deposits (Stow et al., 1998).

- Predominantly fine-grained sand and silt composition.
- Thin-bedded to laminated sand (usually less than 5cm) in deep-water mud.
- Rhythmic occurrence of sand and mud layers.
- Numerous sand layers (50 or more per 1 metre of core).
- Sharp (non-erosional) upper contacts and sharp to gradational bottom contacts in layers with inverse grading.
- Internal erosion surfaces.
- Well-sorted sand and low depositional matrix (clean sand).
- Horizontal lamination and low-angle cross lamination.
- Cross bedding.
- Lenticular bedding/starved ripples at the core scale.
- Current ripples with preserved crest or eroded crest.
- Flaser bedding.

Figure. 6

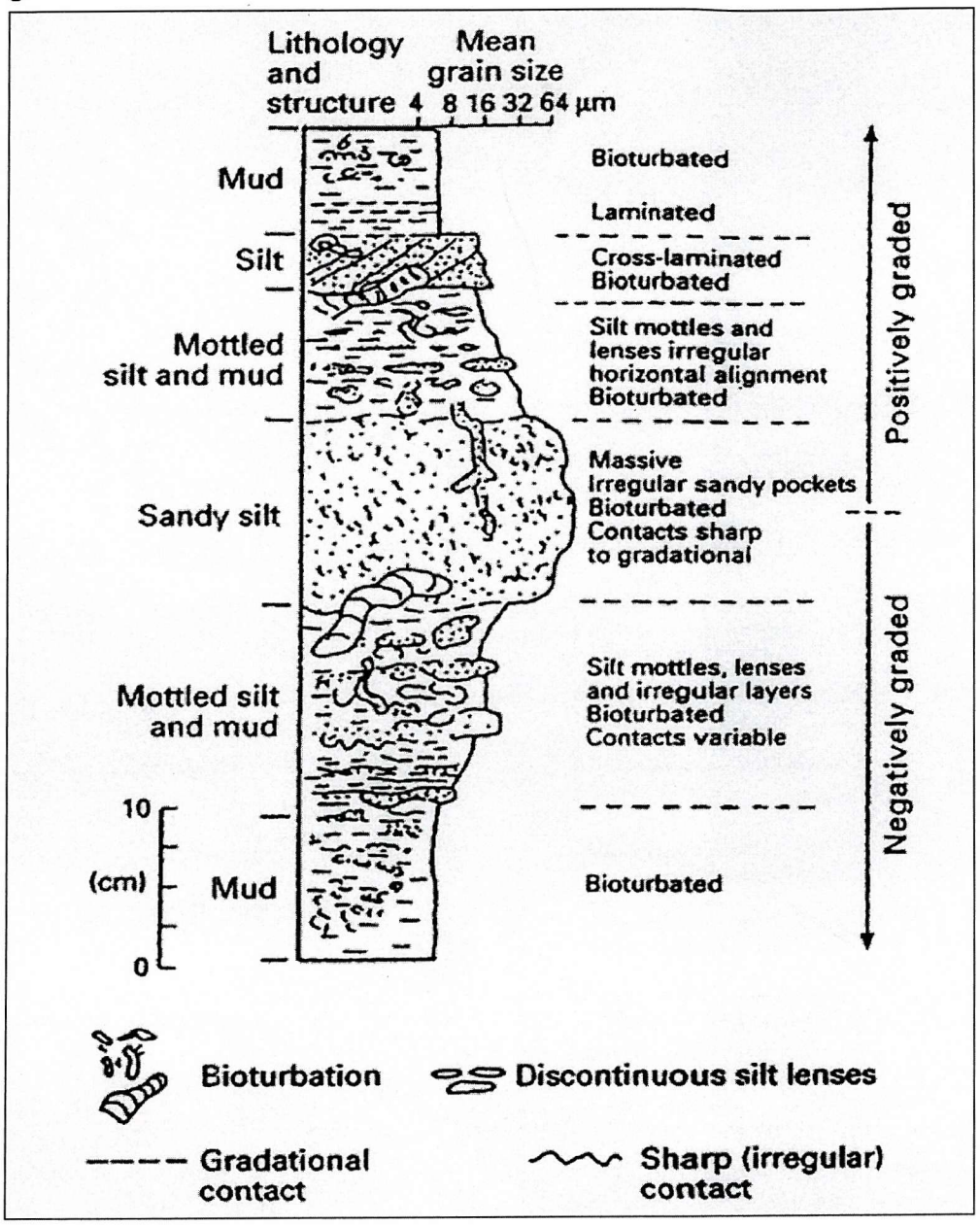

Figure 6. Composite contourite facies showing grain-size variation through a mud-silt-sand contourite sequence (Stow et al., 1998).

- Occurence of layers with traction structures in discrete units, but not as part of a vertical sequence of structures.

The Gulf of Cadiz contourite has formed a sediment wedge up to 300m thick on the continental slope between 1500m and 500m and has been forming since the opening of the Strait of Gibraltar at the end of the Messinian (Nelson et al., 1999; Rodero et al., 1999). The drift is complex on all scales, a result of the complexity of the flow path of the Mediterranean Outflow as it passes over the high topography of the upper slope (Hernandez-Molina et al., 2003). Substantial effort has been exerted into understanding the controls on sedimentation occurring in this area on a variety of timescales (e.g. (Faugères et al., 1986; Nelson et al., 1993; Lopez-Galindo et al., 1999; Nelson et al., 1999; Rodero et al., 1999; Lobo et al., 2001; Habgood et al., 2003; Hernandez-Molina et al., 2003), and the salient parts of this work will be summarised in chapter 5.

It has been proposed that deep-sea sediment drifts record the history of the thermohaline circulation (Robinson and McCave, 1994). In the North Atlantic, these deep-water currents are ultimately derived from high-density water that is generally formed at the surface of a marginal sea and passed into the deep ocean as a flow over a sill (e.g. the NADW in the GIN and the MO in the Mediterranean Sea) (Price and O'neill-Baringer, 1994). The properties of these flows will be determined by the amount of buoyancy loss they experience before sinking (promoted by low temperatures and high aridities) and sea level, which regulates the water-depth at the sill and thus the level of hydraulic limitation it exerts over the flow (Price and O'neill-Baringer, 1994). Temperature, aridity and sea level have all varied cyclically throughout the Quaternary, and it is therefore anticipated that this cyclicity will be represented in deep-sea sediment drifts (Robinson and McCave, 1994).

2.6 Climatic oscillations:- their origin and character .

The history of the Holocene and Quaternary is characterised by a sequence of climatic stages related to the advance and retreat of the polar ice caps. The climatic variation found in the Quaternary is cyclic, and is preconditioned by variations in the Earth's orbit and rotation, which are termed the "Milankovitch Cyclicities" (Emiliani, 1955; Shackleton and Opdyke, 1973). Major advances and retreats of high latitude ice occur

on timescales of 100,000 years, and this dominant variability is superimposed on a 400,000 year cycle (Berger, 1978, 1979). Unlike the 400,000 year cyclicity however, the 100,000 year cycle only dominates the record subsequent to the middle Pleistocene (Park and Maasch, 1993). These cyclicities are controlled by the eccentricity of the orbit of the Earth around the sun, i.e. the ratio of the long and short axes of the ellipse that defines the Earths orbit (the ecliptic) (Berger, 1978, 1979). Interglacial (relatively ice-free) periods occur when eccentricity is low, the orbit of the Earth round the sun is near circular and the supply of heat to the Earth (insolation) is high (Berger, 1978, 1979).

Superimposed upon the 100,000-year climate cyclicity are two further orbitally driven cyclicities with wavelengths clustering at 40,000 and at 19,000 and 21,000 years, which are termed the Obliquity and the Precession cycles respectively (Berger, 1978, 1979). These are related to the variability of the angle between the geographic north pole (the pole of rotation) and the Earths celestial pole (the extended diameter of the Earth that is normal to the plane of the ecliptic) and the "wobble" in the Earths rotation caused by the gravitational action of the Sun and Moon respectively (Berger, 1978, 1979). Though Obliquity and Precession do not effect the total insolation, they do affect the distribution of insolated heat, with high angles between the rotational and celestial poles leading to relatively warm high latitudes and relatively cool low latitudes. Low high latitude insolation promotes the deposition of snow in winter, and reduces the amount of snow melt during the summer, thus promoting the growth of continental ice sheets (Berger, 1978, 1979).

Mean insolation at 65°N has varied between ~390 and ~490 w/m^2 over the last 1.5 million years (Berger and Loutre, 1988). Obliquity related variability is in the order of 6w/m^2 and the 23 and 19kyr precessional cyclicities contribute variabilities of 15 and 21 w/m^2 respectively, with eccentricity (the 400ka wavelength dominating) accounting for the majority of the residual when these are extracted (Short et al., 1989). The small magnitude of this forcing does not account for the large scale of past climatic changes, and the smooth variability exhibited in orbital reconstructions does not compare well with the rapid jumps between extreme climatic states the Earth has experienced in the past, implicating non-linear mechanisms and strong feedbacks within the climate system (Broecker, 2000). Though air, sea surface and deep-ocean

temperatures and global ice volume over the last million years correlate well to the 100ka eccentricity cycle, ice volume lags insolation (and air and oceanic temperature) by ~14ka (Shackleton, 2000), indicating further complexity in the response of the climate system to orbital forcing.

There is a lack of consensus in the literature regarding exactly which mechanisms are important in governing the response of the climate system to orbital forcing, and indeed as to the importance of astronomical forcing relative to other factors such as the internal dynamics of ice sheets (Imbrie et al., 1993; Sarnthein et al., 1999; Shackleton, 2000; Mix et al., 2001). However, the observation that the concentration of atmospheric CO_2; 1, correlates very well with orbital forcing in ice core records (Anklin et al., 1997) and; 2, is in phase with the 100,000 year cyclicity, air temperature and deep-ocean temperature over the last glacial cycle and thus leads ice volume (Shackleton, 2000) implicate this, and the atmospheric concentration of other strong "greenhouse gasses" such as methane, as being an important factor in transmitting and magnifying orbital forcing to the Earths climate system. A considerable impact of albedo (the reflectiveness of the Earths surface) resulting from both variable snow and ice cover and changing vegetation has been found in numerical simulations of the climate system (Berger et al., 1990; Weaver et al., 1998; Bintanja et al., 2002; Brovkin, 2002). This provides a particularly strong feedback for ice volume development, as the very high albedo of snow cover provides significant additional cooling at high latitudes during ice-sheet advance (Bintanja et al., 2002).

Non-linearity in the climate system may in part also represent the behaviour of the continental ice sheets (Imbrie and Imbrie, 1980). The characteristic "saw-tooth" pattern of the Pleistocene glaciations, with slow descent into glacial periods and rapid recovery during deglaciations, has been successfully simulated by models of continental ice sheet development, especially when the slow response of the lithosphere to ice-loading is taken into account (Weaver et al., 1998). Changes in the fresh water budget in the regions of deep-water production at high latitudes and migration of the deep-water production regions as a result, of this and of sea-ice cover, also provides a feedback in the climate system (Broecker et al., 1985; Broecker, 2000). Reduced or more southward NADW production would be anticipated to cause reduced "heat piracy" in the North Atlantic, and therefore

stimulate further cooling (Broecker et al., 1985). The climatic and oceanographic systems are thus linked, with increased cooling causing altered thermohaline circulation as a result of increased high latitude ice volume, which in turn allows increased high latitude cooling and stimulates further ice growth. (Alley, 1998). Virtually all General Circulation Models developed for analysis of the last glacial cycle show a hysteresis behaviour during glacial transitions, which implies that the ocean plays a significant role in "holding" the climate in its glacial or interglacial state (Broecker, 2000).

Atmospheric temperature (Dansgaard et al., 1993; Grimm et al., 1993; GRIP_Members, 1993; Jouzel et al., 1997; Allen et al., 1999) and sea surface temperature (Shackleton and Opdyke, 1973; Zahn and Mix, 1991; Imbrie et al., 1992; Cacho et al., 1999; Weaver et al., 1999; Chapman et al., 2000; Shackleton, 2000; Shackleton, 2001), continental aridity (An et al., 1991; Grimm et al., 1993; Balsam et al., 1995; Bigg, 1995; Allen and Huntley, 1996; Grousset et al., 1998; Bar-Matthews et al., 1999; Lowe et al., 1999; Sanchez-Goni et al., 2000; Bateman and Diez-Herrero, 2001; Roucoux et al., 2001; Moreno et al., 2002), the strength of the windfield (Mayewski et al., 1994a; Hughen et al., 1996) and the turbulence of the atmosphere (Mayewski et al., 1994a; Grousset et al., 1998; Rohling et al., 2003a) have all be recorded as varying at the Milankovitch orbital wavelengths. In addition to the state of the climate, the dominant factor governing the eustatic sea level is the size of the continental ice sheets and sea level is thus also believed to have varied on these timescales (Shackleton, 1987). Orbitally driven climate variability is well represented in the region surrounding the GoC, though few records have been presented from within it. On the Portuguese margin, mean sea surface temperature is believed to have been reduced by ~10°C (from SIMMAX (Lebreiro et al., 1997)) during the last glaciation and in the Alboran Sea by ~7°C (from alkenones (Cacho et al., 1999)); both regions show Milankovitch periodicities in SST (Lebreiro et al., 1997; Cacho et al., 1999; Shackleton et al., 2000). The transport of aeolian dust by the Saharan dust plume has been shown to have been greater by at least a factor of four during the last glacial maximum (Grousset et al., 1998). The thermohaline circulation of the ocean is also thought to have been altered, and more sluggish at this time (Duplessy et al., 1988; Zahn and Mix, 1991; Sarnthein et al., 1999; Seidov and Maslin, 1999), and so the oceanography of the GoC would also be anticipated to be altered.

The palaeoceanographic record of the last glacial cycle (0 to 80 kyr b.p. (see fig. 7) has been particularly well studied, due to the abundance of good deep sea, lake and ice core records. This cycle was punctuated by a series of warm-cold oscillations, termed Dansgaard-Oeschger cycles, each of ~1.5kyr in length (see Fig. 7) (Bond et al., 1993; Dansgaard et al., 1993; Grootes et al., 1993; Cacho et al., 1999). These seem "grouped" within larger cooling cycles lasting 10 to 15 kyr (Bond cycles), which culminate in the vast discharge of icebergs from the Laurentide and European ice sheets, which are termed the Heinrich events (Bond et al., 1993). There are six Heinrich events (Heinrich, 1988), numbered with increasing age. The Dansgaard-Oeschger cycles are not strongly developed in the record of the last 30,000 years (Grootes et al., 1993), the time period this thesis is concerned with, and so their climatic impact will not be described in detail here. Heinrich Events do occur however, and their general characteristics and origin are described below.

The effects of the Heinrich events (Heinrich, 1988; Bond et al., 1993; vanKreveld et al., 1996; Grousset et al., 2000; Grousset et al., 2001) and their atmospheric equivalents (Grimm et al., 1993; Mayewski et al., 1994a; Hostetler et al., 1999; Vidal et al., 1999; Roucoux et al., 2001) are complex. In the deep sea, Heinrich events are synonymous with periods of input of ice rafted debris (IRD) from Europe and more importantly the Laurentide ice sheet of North America (Bond et al., 1993). IRD was mainly depsosited in the northern North Atlantic (between 40 and 55° latitude (Grousset et al., 2001)) and has been found as far south as the Portuguese margin (Thomson et al., 1995; Lebreiro et al., 1997; Thouveny et al., 2000), and has been reported from the GoC (Kudrass, 1973; Heilemann, 2000; Cacho et al., 2001; Mulder et al., 2002) though it is often found to be absent (Duprat, 1983; Sierro et al., 1999). This may reflect the strong surface circulation within the GoC itself. Some IRD has also been reported from the Moroccan margin, which may repflect bypass of the dominantly west-east flowing GoC surface system (Kudrass, 1973). Heinrich Event periods are also characterised by very cold sea surface temperatures (<10°C) in the North Atlantic that last for roughly 1,000 years (Bond et al., 1993; McManus et al., 1994), with planktonic foraminiferal assemblages dominated by the sinistral form of *Neogloboquadrina pachyderma* (Grousset et al., 2001), and low salinity surface waters due to the large input of meltwater derived from the icebergs themselves

Figure 7.

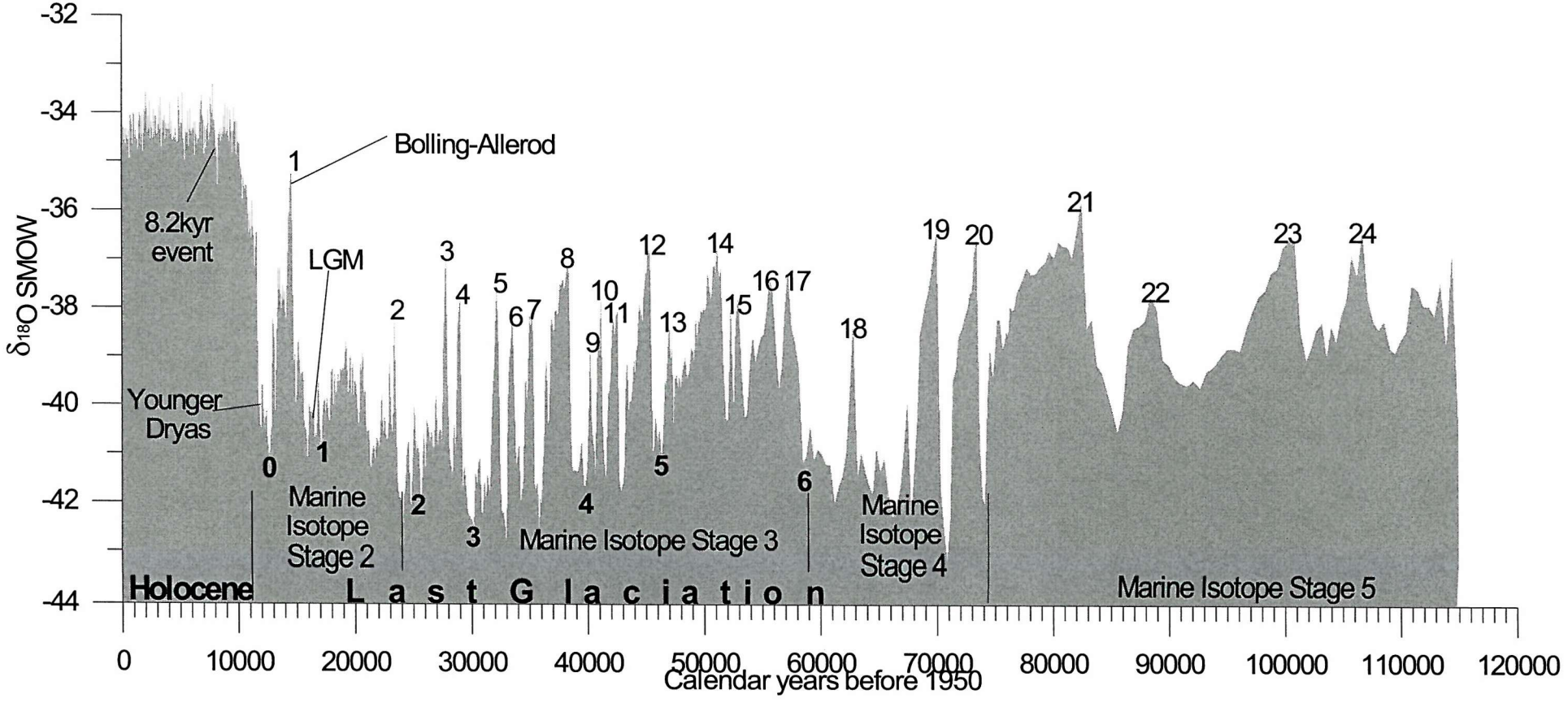

Figure 7. GISP2 oxygen istope series. Non-bold numbers represent Dansgaard-Oeschger interstadials (Dansgaard, 1993). Bold numbers represent Heinrich Events (Rohling et al., 2003).

(Chapman et al., 2000). The Heinrich Events have been shown to coincide with the most extreme "glacial" conditions recorded, and are thus also maxima in aridity and windfield strength (Rohling et al., 2003a). Changes in regions remote from the northern North Atlantic were also altered, particularly in terms of temperature and aridity, during the Heinrich Events which indicates a common forcing or atmospheric transmission of the signal derived from the northern high latitudes or both (Hostetler et al., 1999).

There is evidence that some of the Heinrich events caused a collapse in deep water formation throughout the North Atlantic, as a result of the vast quantity of fresh water debouched into the northern North Atlantic as icebergs (Seidov and Maslin, 1999; Vidal et al., 1999). This prevented the development of negative buoyancy in the nascent NADW resulting in a collapse of the thermohaline circulation (Alley, 1998), thus making conditions favourable for the development of land ice in Europe and North America (Vidal et al., 1999). The very cold sea surface temperatures that were present over much of the North Atlantic allowed southward penetration of the polar air masses (Sanchez-Goni et al., 2000), causing strong cooling and enhanced aridity as far south as the northern Mediterranean (Rohling et al., 1998b; Bar-Matthews et al., 1999; Cacho et al., 1999). In the Gulf of Lions the Heinrich Events are characterised by increases in the abundance of the very low SST planktonic foraminifer *N. pachyderma* sinistral, as is found in the northern North Altantic (Rohling et al., 1998b) and oxygen isotopes from a speleothem in Soreq cave in Israel also show cold periods coincident with HE1, HE2 and HE5 (Bar-Matthews et al., 1999). Enhanced aridity consistent with the southward expansion of the polar air masses is indicated by decreased abundance of the temperate arboreal pollen of the *Juniperus* (juniper), *Betula* (beech) and *Quercus* (oak) taxa in Iberia and Italy found in Heinrich event age layers of marine and lacustrine cores (Allen et al., 1999; Roucoux et al., 2001), and enhanced buoyancy loss in surface waters of the Gulf of Lions (Rohling et al., 1998b). The compression of the meridional thermal gradient by the southward penetration of polar air caused a significant enhancement in the wind field that increased dust transport from Asia to Greenland (Mayewski et al., 1994a; Mayewski et al., 1994b; Rohling et al., 2003a) and enhanced the supply of aeolian dust to the Atlantic and Mediterranean (Grousset et al., 1998; Allen et al., 1999; Sanchez-Goni et al., 2000).

The origin of Heinrich Events is not fully understood. The "canonical" Heinrich Event (Hostetler et al., 1999) begins with precursor cooling in the North Atlantic region with a concurrent increase in the size of the Laurentide ice sheet which then becomes unstable and collapses (MacAyeal, 1993). Candidates for the cause of the initial cooling are changes in atmospheric circulation (Broecker, 1994; Clark and Bartlein, 1995; Porter and An, 1995; Mikolajewicz et al., 1997), changes in atmospheric composition (including water vapour) (Broecker, 1994, 1997) and changes in ocean thermohaline circulation (Broecker, 1994; Behl and Kennett, 1996; Lund and Mix, 1998; Alley and Clark, 1999). Variability on "Heinrich-like" timescales has been found in marine records that pre-date the formation of the northern Hemisphere ice sheets (Ortiz et al., 1999), which disputes the suggestion that all of the non-orbital variability is related to processes internal to the Earth's climatic system under glacial conditions (MacAyeal, 1993). Dansgaard-Oeschger stadials appear to be similar to Heinrich events, though of smaller magnitude, and it has also been proposed that these two features of the climate record are linked with Heinrich Events being extreme Dansgaard-Oeschger stadials (Bond et al., 1993; Cacho et al., 1999). Though of small amplitude, solar forcing could potentially drive significant variability through mediating processes such as stochastic resonance (Renssen et al., 2000; Alley et al., 2001). A solar origin of some climatic variability is supported by records of the Maunder Minimum, which indicates a period of cool conditions in Europe that coincide with reduced sun-spot activity (Renssen et al., 2000). It has also been proposed that the Dangaard-Oeschger cyclicity could be a harmonic of the precessional cycle (Berger and Loutre, 1988).

2.7 Climate and sea level over the last 30,000 years

The last 30,000 years brackets both extremes of the Earth's climate, from the Last Glacial Maximum (LGM; 18-17kyr BP (Chapman et al., 2000)), through the last deglaciation (Termination1) and into the Holocene interglacial, which is a period of relative climatic stability and the warmest temperatures recorded in the last 100,000 years (See fig 7). The last two Heinrich Events also occur within this period (H1 at 17ka BP; H2 at 24ka BP (Rohling et al., 2003a)).

Figure 8.

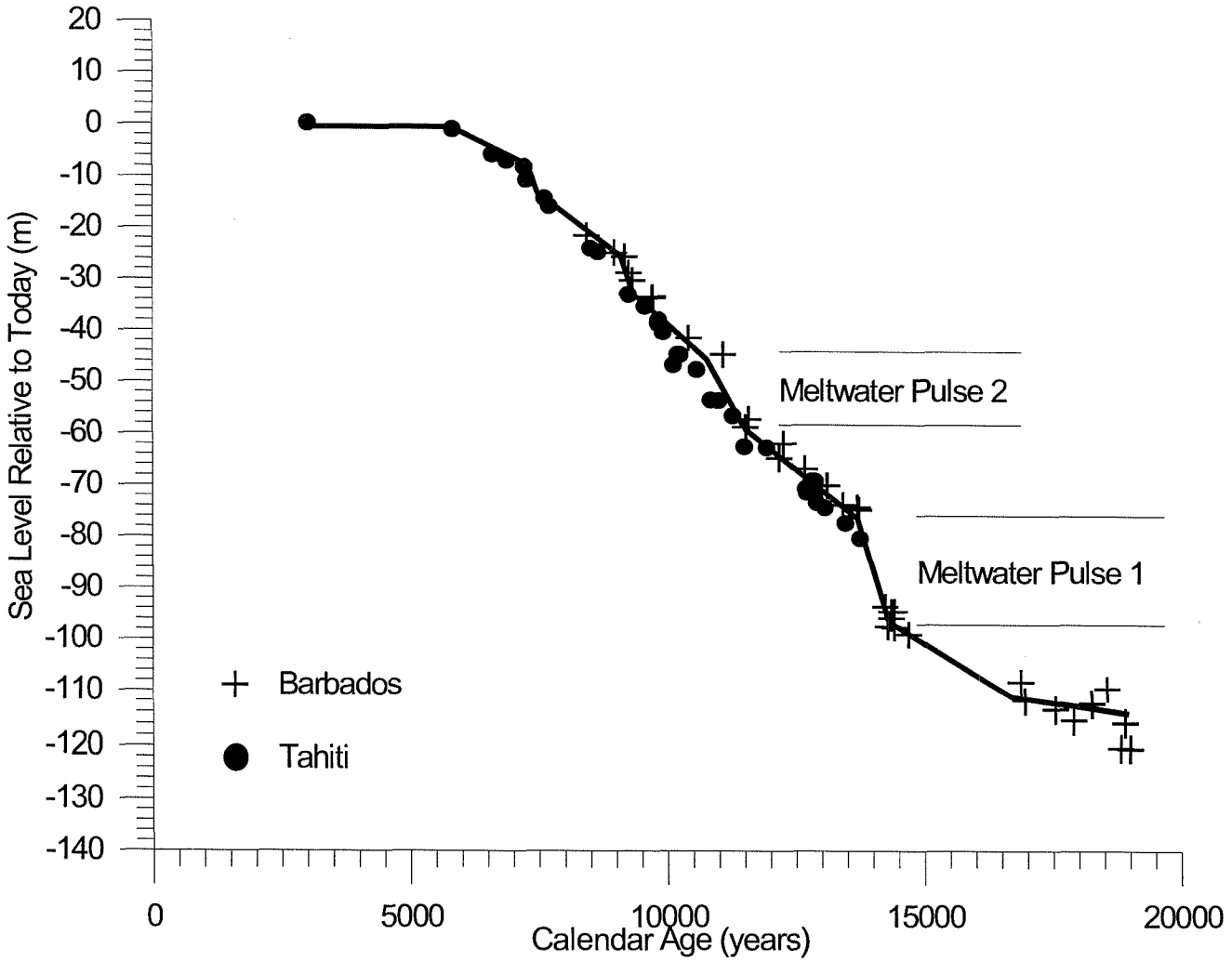

Figure 8. Relative sea level recorded in corals from Tahiti and Barbados. (Fairbanks, 1989, Bard et al., 1990, Bard et al., 1990, Fairbanks, 1990, Bard et al., 1993, Bard et al., 1998, Bard et al., 1996, Montaggioni et al., 1997, Montaggioni & Bard, 1998, Bard et al., 1998.)

During the LGM the northern hemisphere glaciation reached its maximum extent (Clague and James, 2002) and as a result, sea level reached its lowest point during the last glacial cycle (~-120m relative to today (Rohling et al., 1998a)). The LGM is also characterised by extremely "glacial" (i.e. cold, arid, windy, etc.) conditions (CLIMAP, 1976; GRIP_Members, 1993; Grootes et al., 1993; Chapman et al., 2000).

The last deglaciation is a time of generally rising sea level that commenced roughly 16ka BP (Bard et al., 1996). Sea level rose fairly constantly from the onset of the deglaciation until the early Holocene, though it is punctuated by a series of meltwater pulses related to the retreat of the continental ice sheets (MWPs see fig. 8) (Bard et al., 1996). The largest of these are termed MWP1 (13.8ka BP), and MWP2 (~11ka BP). The deglaciation is also a period of climatic improvement (Alley and Clark, 1999), though the latter occurred mainly in two phases. Termination 1a (~14.7kyrs BP (Grootes et al., 1993)) marks the end of the last glaciation and the beginning of the Bølling-Alleröd warm period (~14.7 – ~13kyrs BP (Grootes et al., 1993)), during which time essentially interglacial conditions prevailed e.g. (Watts et al., 1996). A return to glacial conditions (~13 – ~11.7kyrs BP (Grootes et al., 1993)) occurred at the end of the Bølling-Alleröd and is termed the Younger Dryas. The second major climatic improvement is termed Termination 1b, occurred at the end of the Younger Dryas and marks the beginning of the Holocene. The Bølling-Alleröd / Younger Dryas pair is particularly strongly displayed by the Greenland ice cores (GISP2 and GRIP (Grootes et al., 1993) see Fig. 7), which indicate that the climate went from an essentially glacial state to an essentially interglacial state in a matter of decades during each termination.

The Younger Dryas is dynamically similar to the Heinrich Events, had a similar impact on the climate, lasted for a similar duration (~1,000 years) and is thus often termed H0 (Veiga-Pires and Hillaire-Marcel, 1999). It is widely believed to be the large input of freshwater during melting of the ice sheets which triggered the return to glacial conditions (Fairbanks, 1990). In this scenario, the melt water pulse freshened the northern North Atlantic causing the thermohaline circulation to collapse, as in the Heinrich Events (Broecker et al., 1985). However, as in the case of the Heinrich Events precursor coolings have been found within climatic records (Renssen et al., 2000), and MWP1 occurred 1,000 years too early to be the source of fresh water

(Bard et al., 1996). It is therefore also argued that the trigger was an external forcing, such as solar activity. The Younger Dryas coincides with maxima in the cosmogenic isotopes ^{14}C and ^{10}B and it is argued that this is evidence for a minimum in irradiance (Renssen et al., 2000). Supporting evidence comes from the ~2.5 kyr quasi-cycle in the ^{14}C record the maxima of which coincide with coolings during the last glaciation and Holocene (e.g. the Younger Dryas) and which is believed to be of solar origin and the registration of the Younger Dryas in low latitude records, which would not be influenced by a purely oceanic event as proposed above (Renssen et al., 2000).

A further cooling event of smaller magnitude occurred as a result of the emptying of lake Agassiz in North America at 8.2 ka BP (Barber et al., 1999) and is thus termed the 8.2kyr event. This caused a transient cooling that did not collapse the thermohaline circulation but that is noted in records far remote from its source (eg. (Alley et al., 1997; vonGrafenstein et al., 1998). This event lasted for <1,000 years and marks the final retreat of the northern hemisphere glaciers to roughly their modern position, the end of rising sea levels and a slight climatic improvement (Bard et al., 1996; Alley et al., 1997; Barber et al., 1999).

True Holocene conditions began subsequent to the 8.2kyr event, and the atmospheric and oceanic systems achieved their modern configuration. However, though the Holocene has been generally very climatically stable it was punctuated by small amplitude oscillations on roughly a 1.5kyr wavelength such as is observed during the Little Ice Age / Medieval Warm Period (Lamb, 1966) and other oscillations with even lower amplitudes and higher frequencies such as the El Niño Southern Oscillation (Rasmusson, 1985) and the North Atlantic Oscillation (Uppenbrink, 1999). In addition, between 9 and 6kyrs BP a period termed the Holocene Climatic Optimum, which is believed to coincide with a maximum in insolation, occurred (Rossignol-Strick, 1999; Kalis et al., 2003). At this time, global climate was slightly warmer than it is today (+2°C, up to + 4°C (Kalis et al., 2003)) and North Africa and the Mediterranean region experienced significantly increased precipitation (Rossignol-Strick, 1999). This may have been significant enough to reduce or temporarily halt the anti-estuarine circulation of the Mediterranean (Myers et al., 1998), and allowed the stagnation of the deep Mediterranean which preconditioned the basin for the formation of saporopel S1 (Casford et al., 2002).

2.8 Assessment of past climate in sediment core records by stable isotope and planktonic foraminiferal assemblage methods.

This project aims to produce sediment core chronostratigraphies based on radiometric (^{14}C) dating and supported by the identification of the events described in section 2.6 and 2.7 in the micropalaeontological record. Planktonic foraminifera are the most widely used microfossil for this purpose, and both the total planktonic assemblage and the chemical composition of their shells are used. The concentrations of a variety of elements relative to calcium and the balance of the stable isotopes of elements within the $CaCO_3$ of foraminiferal tests are controlled by environmental conditions, primarily temperature (eg. Mg/Ca (Hastings et al., 1998); $\delta^{18}O$ (Shackleton and Opdyke, 1973; Rohling and Cooke, 1999); $^{44}Ca/^{40}Ca$ (Heuser, 2002)). This knowledge can be exploited in two ways; firstly it can be used to define the temperature at which a test was secreted at some time in the recent or distant past. Secondly, where the history of a location can largely be predicted from another local proxy record (e.g. (Shackleton et al., 2000) or a global climate record (e.g. (Grootes et al., 1993), a proxy record can be used as a tool to develop an age model for the record by correlation (Martinson et al., 1987). The most widely used proxy for the latter is the ratio of the stable isotopes of oxygen ($\delta^{18}O$).

Light isotopes of oxygen are incorporated into calcite preferentially at high temperatures by equilibrium fractionation according to the equation:-

$$\alpha_{c\text{-}w} = \exp\{(2.78T^{-2}) \times 10^3 - 3.39 \times 10^{-3}$$

where $\alpha_{c\text{-}w}$ is the fractionation factor between calcite and water and T is the temperature in Kelvin (O'Neil et al., 1969). $\delta^{18}O$ in planktonic foraminifera is therefore commonly used as an indicator of SST. Though oxygen isotopes incorporated into carbonate undergo temperature moderated equilibrium fractionation, this will be dominated by the ratio of the isotopes present in the environment in which the carbonate formed (Rohling and Cooke, 1999). In the case of foraminifera, the environment of formation is the sea water in which the organism is living, and is determined primarily by the global ice volume (Shackleton and Opdyke, 1973) and secondarily by variations in the water cycle (Rohling, 1999).

Water evaporated to form atmospheric moisture is enriched in the light isotopes of oxygen and hydrogen relative to the water mass it is sourced from. The most commonly used equation to describe the fractionation factor is:-

$$\alpha_{l\text{-}v} = \exp\{(1.137T^{2}) \times 10^{3} - (0.1456T^{-1}) - 2.0667 \times 10^{-3}\}$$

where $\alpha_{l\text{-}v}$ is the fractionation factor between the liquid and the vapour (Majoube, 1971). In addition, molecules incorporating heavy isotopes will be preferentially lost during precipitation, causing a gradual enrichment in ^{18}O of the remaining water vapour (termed Rayleigh distillation). Continental ice sheets are built up by precipitation at high latitudes and low temperatures, and thus lie at the far end of the Rayleigh distillation (Rohling and Cooke, 1999). Light oxygen is therefore preferentially sequestered into ice sheets, and when the global ice volume is high the ocean is enriched in ^{18}O (Shackleton, 1987). A similar loss of ^{16}O would be associated with a large storage of fresh water in lakes or groundwater, but this is not of significant magnitude (Rohling and Cooke, 1999).

Practically in terms of $\delta^{18}O$ in foraminiferal tests, times of high ice volume will usually coincide with times of low temperature (glaciations), and the enrichment in $\delta^{18}O$ caused by ice volume will be enhanced by the equilibrium fractionation which will also cause an enrichment in $\delta^{18}O$. Though this is a major problem for quantitative environmental reconstructions from oxygen isotope records, it is advantageous when developing chronostratigraphic correlations as it causes events such as glacial terminations to be of very large magnitude.

Additional complexity in $\delta^{18}O$ is caused by the local conditions in the water cycle and by processes that cause the $\delta^{18}O$ in foraminiferal calcite to be in disequilibrium with the environment (Rohling and Cooke, 1999). The high enrichment of ^{16}O in atmospheric vapour will mean that where a water mass experiences net evaporation it will become enriched in ^{18}O, and conversely where it receives net fresh water by precipitation or runoff it will become enriched in ^{16}O (Rohling and Cooke, 1999). In locations such as the Mediterranean, Baltic, Black and Red Seas these effects can be

important (e.g. (Aksu et al., 1995; Hemleben et al., 1996). However, in open ocean settings they are unlikely to cause more than a transient effect such as is found in the northern North Atlantic during the Heinrich Events (Chapman et al., 2000).

Abiotic disequilibria that cause foraminiferal $\delta^{18}O$ to be out of equilibrium by a constant, independent of biological factors are caused by pH and the concentration of carbonate ions (Spero et al., 1997). These are of low magnitude compared to biological disequilibria and are not anticipated to vary significantly. They therefore have not been investigated in such detail, though it has been shown that $\delta^{18}O$ decreases with increasing carbonate ion concentration. Biological disequilibria are caused by symbiont photosynthesis, respiration, gametogenesis and the ontogenic effect. Juvenile tests of *G. bulloides* have been found to be strongly depleted in $\delta^{18}O$ relative to equilibrium (1.15‰), and this depletion has been shown to decline with shell growth (final chamber depleted by 0.3‰) with constant temperature and $\delta^{18}O_{water}$ (Spero and Lea, 1996). In addition, several species of planktonic foraminifera deposit a veneer of calcite on the surface of their tests at the end of their life-cycles (Duplessy et al., 1981; Deuser, 1987; Spero and Lea, 1993; Bemis et al., 1998). In the case of *Globigerinoides sacculifer* this may contribute 18 – 28% of the total carbonate mass (Duplessy et al., 1981). Due to these effects, it is common practice throughout a study to analyse only tests within a defined and narrow size range.

Respiration and symbiont photosynthesis (termed the "vital effects") cause substantial disequilibria that are more difficult to compensate for. Laboratory assessment has shown that the offset of $\delta^{18}O_{test}$ to $\delta^{18}O_{equilibrium}$ ($\Delta\delta^{18}O$) varies near-linearly with temperature and displays a similar gradient for all species (Bemis et al., 1998; Bemis et al., 2000). However, the vital effects remain a substantial hurdle to be crossed when comparing $\delta^{18}O_{test}$ records between species where individual $\Delta\delta^{18}O$ is not known (Bemis et al., 2002). Substantial effort has therefore been exerted into methods to derive $\delta^{18}O_{equilibrium}$ from a range of species specific $\delta^{18}O_{test}$ measurements (Spero et al., 2003). These require local calibration, independent and accurate insight into the local thermal history and even when these conditions are satisfied can be complicated by the presence of cryptic populations within a species (Williams et al., 1988; Healy-

Williams, 1992; Spero et al., 2003). In addition, where a species carries photosynthetic symbionts, both the gradient and intercept of $\Delta\delta^{18}O$ with temperature may be altered by the light level (Bemis et al., 1998).

It has been shown that in the case of *Orbulina universa,* the isotopic composition of tests secreted by individuals in high light, and low light conditions are so different that these populations should be considered as separate for the purposes of $\Delta\delta^{18}O$ assessment (Bemis et al., 1998). A similar effect is noted in *G. sacculifer* and would be anticipated in other species with symbionts (Spero et al., 2003).

Though it is not primarily controlled by temperature, the ratio of the stable isotopes of carbon ($\delta^{13}C$) in the tests of planktonic foraminifera can also be instructive about the state of the environment (Berger, 1981). The environmental $\delta^{13}C$ (i.e. $\delta^{13}C_{equilibrium}$) is the primary determinant of $\delta^{13}C_{test}$. ^{12}C is preferentially incorporated into organic matter and is exported from surface water in the ocean by productivity, leaving the surface enriched and the deep oceans depleted in $\delta^{13}C$ respectively (Rohling and Cooke, 1999). The $\delta^{13}C$ enrichment between the thermocline and the surface is steep, and the relative dwelling depth of species can, in principal, be reconstructed from their relative $\delta^{13}C_{test}$. $\delta^{13}C_{equilibrium}$ will vary on long (10^8kyr) timescales as a result of burial of organic matter in sediment and burial of carbonate (both of which will enrich environmental $\delta^{13}C$) and changes in the location of deep-water formation and thermohaline turnover, which control the magnitude of the $\delta^{13}C$ enrichment in the deep sea and the rate of resupply of ^{12}C to the atmosphere (Rohling and Cooke, 1999). This is not expected to be important for the purposes of this report.

$\delta^{13}C$ has much of the same complexity as $\delta^{18}O$, resulting from the behaviour of the organism secreting the test, the presence of symbionts and the carbonate ion concentration in the seawater. As in $\delta^{18}O$, foraminiferal $\delta^{13}C$ decreases with increasing carbonate ion concentration, independent of the other factors (Spero et al., 1997). In addition to the relatively small control on $\delta^{13}C_{carbonate}$ by temperature ($\varepsilon_{b\text{-}c} = 10.51 - 2980T^{-1}$ (Grossman, 1984) where $\varepsilon_{b\text{-}c}$ is the isotopic enrichment of the calcite relative to the bicarbonate in seawater), it is also depleted as the respiration rate of the

organism increases. This is the result of the incorporation of respired CO_2 into the test calcite (Rohling and Cooke, 1999). This depletion follows the equation:-

$$\delta^{13}C_b = \delta^{13}C_{test} + \Delta\delta^{13}C_0 Q_{10}^{(T - To)/10} - 1$$

Where T_0 and $\Delta\delta^{13}C_0$ are the temperature and disequilibrium offset of $\delta^{13}C_{test}$ at $time_0$ respectively and Q_{10} is the change in metabolic rate over a change of 10°C (not constant over broad temperature ranges (Ortiz et al., 1996)). Physiological changes in the organism as it grows causes indirect additional deviation from $\delta^{13}C_{equilibrium}$ particularly when the organism is symbiotic, as larger cells have higher symbiont densities (Spero and Parker, 1985). Small cells will have relatively high metabolic rate, and few symbionts (if present) resulting in heavily depleted $\delta^{13}C$ (Bouvier-Soumagnac and Duplessy, 1985; Ravelo and Fairbanks, 1995), and this depletion will decline towards equilibrium with increasing test size (Berger, 1978; Wefer and Berger, 1991). As with $\delta^{18}O$, light intensity will also affect $\Delta\delta^{13}C$ in species with symbionts, with increasing enrichment associated with increasing light intensity (McConnaughey, 1989; Spero and Lea, 1993).

Sea surface temperature (SST) can be estimated from the planktonic foraminiferal assemblage assuming that 1, temperature is the dominant control on species distributions and 2, that species occupied similar ecological niches in the past as they do today. A number of estimation methods have been used, ranging from the ratio of left- and right coiling *Neogloboquadrina pachyderma* (e.g. (Martinez, 1994) to the application of specifically trained artificial neural networks (Malmgren et al., 2000). The most commonly used methods and their acronyms are summarised in Table 1. In a statistical assessment of the error of prediction of each method on a set of core top assemblages with known climatic origin and fossil assemblages with independently defined SSTs (Malmgren et al., 2000), the IKTF method was shown to be inaccurate relative to the other methods. SIMMAX was shown to be the most accurate within the Holocene, though the ANN achieved similar accuracy when geographic information was incorporated as is done in SIMMAX (termed ANND). For the last glaciation, the ANN method was shown to be at least as accurate as MAT and RAM which both outperformed SIMMAX.

Table 2.8.1 Methods for predicting SST of fossil planktonic foraminifera assemblages.

Method	Description
IKTF	Imbrie-Kipp Transfer Functions (Imbrie and Kipp, 1971). A linear equation is empirically derived from a set of artificial end-member assemblages defined by principal component analysis of linked core-top and climatic data. The mean or seasonal SST for a sample assemblage is defined by solution of the equation.
MAT	Modern Analogue Technique (Hutson, 1980). The closest modern assemblage (with known SST) is found in a regional database for each sample assemblage by finding the minimum dissimilarity coefficient. The climatic conditions in which the sample assemblage lived are defined by analogy, or by placing the sample assemblage at a point on a linear interpolation between the 2 or more (often 10) closest analogue assemblages.
SIMMAX	Similar to the MAT (Pflaumann et al., 1996), however incorporates a weighting towards those analogue assemblages geographically closest to the sample assemblage. Climatic conditions are defined as in MAT.
RAM	Revised Analogue Technique (Waelbroeck et al., 1998). Similar to the MAT, but statistically interpolates unevenly spaced sample points into a grid of uniform mesh size. Climatic conditions are defined as in MAT, but additionally searches for "jumps" in the dissimilarity coefficient, which are used to reduce the number of closest analogues used.
ANN	Artificial Neural Network (Malmgren et al., 2000). In principle similar to MAT, but rather than linear statistics a neurogenetic algorithm that automatically searches for the configuration that gives the lowest error of prediction is used. The ANN thus "learns" how to predict the climatic conditions for a sample assemblage from a regional database of analogue assemblages.

2.9 Modern Planktonic Foraminifera Assemblage and Ecology in the GoC

The ecology and habitat (seasonal and depth) of species studied are important for the assemblage-based SST methods outlined above, and are vital when considering chemical proxy data. A brief review of the ecology of those planktonic foraminifera species present in the GoC today is therefore given below. Additional relevant detail is given in chapter 4.

Plankton tows in the Gulf of Cadiz indicate that the dominant foraminiferal species is *Globigerina bulloides*, which makes up between 30 and 54% of the individuals in the study area. *Globigerinoides ruber, Globorotalia inflata*, *Globigerinella aequilateralis* and *Globigerinoides sacculifer* are also common, each contributing 5-15% of the living fauna (Cifelli, 1974). Core top records indicate a similar dominance of *G. bulloides*. *Gs. ruber* and *Gs. sacculifer* together make up ~23% of dead fauna (Sierro et al., 1999).

The abundance of *G. bulloides* decreases rapidly out into the open Atlantic west of Gibraltar. It is the most important species in the Strait of Gibraltar and the western Alboran Sea, but reduces to less than 10% of the living assemblage in the eastern Alboran Sea (Cifelli, 1974). *G. bulloides* is usually associated with upwelling zones or with the polar and transitional water masses (Hemleben et al., 1989), but none of these associations gives an adequate explanation for the high abundance of *G. bulloides* on either side of the Strait of Gibraltar. It is possible that positions in mixed surface waters close to strait exchanges may suit *G. bulloides,* though this concept requires further examination.

In the western Alboran Sea *G. bulloides* has been found to gain maximum abundances in the spring, during the time of restratification of the water column in the western Mediterranean (Vergnaud-Grazzini, 1974; Pujol and Vergnaud-Grazzini, 1989). At this time a strong pycnocline develops, above which nutrients accumulate to form a nutricline upon which *G. bulloides* may graze (Hemleben and Spindler, 1983; Pujol and Vergnaud-Grazzini, 1989). Similar behaviour has been noted in the eastern North Atlantic (Schiebel et al., 2001). Vertical mixing associated with the currents active in

both the GoC (Atlantic Inflow current) and western Alboran Sea (Atlantic Inflow plume) will actively resupply surface waters with nutrients that would otherwise be exported to depth. It is likely that the high abundances of *G. bulloides* in these locations reflect eutrophic conditions stimulated by this resupply of nutrients. Significantly, the most abundant dinoflagellate cyst found in the GoC today is *Lingulodinium machaerophorum*, a species that is associated with eutrophic conditions but not with upwelling (Harland, 1983). In the modern eastern North Atlantic, maximum abundance of living *G. bulloides* is found above 60m in Spring (Schiebel et al., 2001). Later in the year, peak abundance of *G. bulloides* descends to below 20m, becomes broader and more weakly defined and extends as deep as 100m by October (Schiebel et al., 2001).

Gr. inflata is particularly associated with the transitional water mass (Hemleben et al., 1989), and has been linked to environments where winter cooling leads to increased vertical mixing (Pujol and Vergnaud-Grazzini, 1989). In the upwelling zone off North Africa, *Gr. inflata* is a winter species (Ganssen and Sarnthein, 1983).

Gs. ruber and Gs. sacculifer are tropical / sub-tropical species that are shallow dwelling and carry dinoflagellate symbionts (Hemleben et al., 1989). The Gulf of Cadiz lies towards the northern end of their range (Hemleben et al., 1989; Arnold and Parker, 1999), and so these species would be expected to react strongly to SST variation. In the Mediterranean these species have been identified as being summer fauna (Vergnaud-Grazzini, 1974). Off North Africa temperature estimates derived from $\delta^{18}O$ of living *Gs. ruber* specimens correlated well with SST in the late summer (Ganssen and Sarnthein, 1983).

Neogloboquadrina pachyderma (d) is not found in abundance in the GoC today, but is the dominant species during the LGM (Sierro et al., 1999). *N. pachyderma* is a deep dwelling planktonic species that grazes on highly abundant cryptoplankton and diatoms at the deep chlorophyll maximum (Pujol and Vergnaud-Grazzini, 1989; Rohling et al., 1993; Rohling et al., 2003b; Spero et al., 2003). The ecological behaviour of *N. pachyderma* (d) is thus well defined in terms of its preferred dwelling depth. The properties of the water mass (temperature, salinity etc.) at the Deep Chlorophyll maximum (pycnocline) are "set" in the winter, and thus geochemical

measurements made on the tests of *N. pachyderma* (d) will be representative of winter conditions (Pujol and Vergnaud-Grazzini, 1989; Rohling et al., 1993; Rohling et al., 1995). Proxy measurements on *N. pachyderma* (d) are therefore at an advantage to those made on other species, as downcore variability is unlikely to be related to a change in the organisms dwelling depth or season of maximum test production.

Also present in low abundances in plankton tows and core tops are *Turborotalita quinqueloba*, *Globigerinita glutinata*, *Globigerinita humilis*, *Globigerinoides tenellus*, *Globorotalia hirsuta*, *Globorotalia scitula*, *Globorotalia truncatulinoides*, *Neogloboquadrina pachyderma* dextral and *Orbulina universa* (Cifelli, 1974; Lebreiro et al., 1997; Cayre et al., 1999; Sierro et al., 1999). *Hasterina pelagica* has been reported in plankton tows but not in core tops. *Neogloboquadrina pachyderma* sinistral is not known to be living in the GoC today (Cifelli, 1974), and indeed is rarely found in abundance south of Cape St, Vincent even during the Heinrich Events (Duprat, 1983), though peaks in this species have been reported during the Heinrich Events in the northern GoC (Reguera, 2001).

2.10 General Introduction to Subsequent Chapters

Chapter 3 will describe the material available for this study and the methods used during this work. This chapter aims to give the important details on how sample preparation and analysis were carried out, and how the data are presented in forthcoming chapters.

Stable isotope and planktonic foraminiferal abundance data from core D13898 are presented in Chapter 4. This record is compared to a published record from the Portuguese margin to give insight into the local hydrographic conditions. It is proposed that the Azores Front was present in the northern Gulf of Cadiz prior to 16ka bp and during the Younger Dryas.

Physical constraints on the history of the Mediterranean Outflow are discussed in Chapter 5, and grainsize records for a suite of cores from the Gil Eanes Drift are presented. Implications for the behaviour of the Mediterranean Outflow and its impact on the North Atlantic as a response to climatic/sea level variability are discussed.

The palaeoceanographic significance of colour, and the potential use of high-resolution colour logging for the development of chronostratigraphic frameworks for sediment cores is discussed in Chapter 6. Colour, oxygen isotope, ANN-SST and geochemical records for core D13892 are presented. Conclusions are made regarding the origin of colour variability in this core and the source of the terrigenous detritus deposited at this location.

Evidence of reworking of sediment from the Gulf of Cadiz continental shelf and its subsequent sorting and deposition on the continental slope is presented in Chapter 7.

This work is summarised in Chapter 8 and potential further developments of this study are described in Chapter 9.

3 Methods

3.1 Coring

Three types of corer were used (Weaver, 2000), the SOC giant piston corer (GPC) of the Calypso type (Skinner and McCave, 2003), a conventional diameter piston corer, of the "Kullenberg" type (Swedish Deep-Sea Expedition Reports, 1947-1948) and a "Kasten" corer (Zangger and McCave, 1990). The cores collected have diameters of 100mm or 65mm respectively for the piston corers, and are sub-sections of variable dimensions of a 3m long 15cm x 15cm box in the case of the Kasten corer. Giant piston coring is known to cause distortion in the upper part of the collected sediment (Thomson et al., 1999; Thouveny et al., 2000), which is termed "stretching". Cores taken with giant piston corers therefore often falsely display increasing accumulation rates up-core. The stretching is thought to be non-linear and "patchy", with undisturbed layers over- and under-lain by severely stretched material (Skinner and McCave, 2003). This process is thought to be dependant on the length of cable the corer is suspended on during deployment, and so the position of these coring locations in relatively shallow water (1200 – 1000m) may prevent this from being as severe as in some other cases (Skinner and McCave, 2003). Kasten coring causes some slight compression of the sediment, as in this case the barrel is forced into the sea-floor under gravity with no piston mechanism to create negative pressure as it does so. The compression is not thought to be so complex as the stretching, though the lower parts of the core would be expected to be more compressed than the upper (Weaver and Schultheiss, 1982).

Table 3.1.1 Cores used during this study

Core Number	Corer	Cruise	Latitude	Longitude	Bottom Environment
D13680	Piston	244	35°52	7°13	Axis of Gil Eanes Channel
D13682	Piston	244	35°52	7°10.5	Sandy lobe below sediment drift
D13686	Piston	244	35°46.5	7°37	Southern Levee of Gil Eanes Channel
D13892	Kasten	249	35°47.01	7°43.02	Hemipelagic slope below sediment drift
D13896	GPC	249	36°02.60	7°18.00	Sandy-mud drift
D13897#2	GPC	249	35°58.04	7°18.05	Muddy drift
D13898#3	GPC	249	35°54.00	7°24.58	Muddy drift
D13899	GPC	249	35°50.57	7°29.00	Muddy drift
D13900	GPC	249	35°48.57	7°31.01	Termination of Gil Eanes Channel

3.2 Core logging

Cores were logged for p-wave travel time, Gamma-ray attenuation (wet bulk density) and magnetic susceptibility using the British Ocean Sediment COre Repository (BOSCOR) Geotek Multi-sensor core logger at SOC. Measurements were made at 2cm intervals and corrected for variations in temperature and core diameter. A split core section is passed through the analyser array, and irradiated with a 2.5 or 5mm diameter gamma-ray stream determined by the diameter of the collimator used. The intensity of the attenuated stream is measured by a scintillometer positioned below the section using 3 x 5 second counting cycles. The bulk density of the core is derived by comparison of this measured intensity compared to measured intensities after transmission though an empty liner and a series of aluminium blocks of varying thickness. P-Wave velocity is analysed by measuring the travel-time of a compressional wave applied to the surface of the core by a transducer to a receiver placed in contact with the liner below the section. The calipers by which thickness is

measured are attached to the transducer and receiver. Measured gamma-wave intensities were converted to wet bulk density using the equation:-

$$\ln I = A(\rho H)^2 + B\rho H + C$$

Where I is the measured gamma-ray intensity, ρ is the bulk density of the material, H is the measured thickness of the section and A, B and C are constants derived from a polynomial fit to calibration measurements made on aluminium blocks of variable thickness. Measured P-wave travel times were converted to P-wave velocity using the equation:-

$$V = \frac{(H \times 10^4) \times V_{water}}{T_{total} - T_{offset}}$$

Where V is the P-wave velocity (ms^{-1}), H is the measured thickness of the section (in cm), V_{water} is a correction for temperature (derived from the ratio of the velocity of water *in situ* to that of water under controlled conditions), T_{total} is the measured travel time and T_{offset} is a constant offset caused by the transducer, receiver and liner.

3.3 Colour logging

The colour of a sediment is considered to be diagnostic of its composition, particularly with reference to its carbonate and organic carbon content and the redox state of the iron held as minerals or as iron bound within clay lattices (Balsam and Deaton, 1996; Giosan et al., 2002; Grutzner et al., 2002; Mix et al., 1995; Mix et al., 1992; Nagao and Nakashima, 1992; Ortiz et al., 1999). Though it may be altered or obscured by diagenetic processes, much of this variation is likely to be stratigraphic and represent sedimentary or environmental variation through time.

The surfaces of core sections to be imaged are first prepared by osmotic knife or with a glass slide to produce a surface that clearly shows core structure and has minimum unevenness. The camera is calibrated to a white tile and refocused for each section. This maximises reproducibility while ensuring that variable core diameter (resulting from uneven splitting) does not result in measurement artefacts derived from the surface moving in and out of focus. In addition, the "brightness window" allowed by

the aperture is narrow, and it is occasionally necessary to change the aperture diameter between sections. This can potentially cause discrepancies between sections, and so was only done when absolutely necessary.

The colour curves used in this project are derived from line scans taken by the GEOSCAN colour line scan camera at BOSCOR. The GEOSCAN camera is a 3 CCD (Charge-Coupled Device) tool using 3 x 1024 pixel CCD arrays that measure absolute red-green-blue (RGB) colour intensities to produce a finely pixelated image of the sediment surface. Data are produced as continuous curves both down and across core, which are then averaged for each pixel area ($14\mu m^2$) to produce RGB values. These pixels are then combined into a series of bitmap files for each core, into which section number and section depth are encrypted to allow the Geotek MSCL software to accurately combine the bitmap file array into a continuous image.

A panel of this image covering a whole core, core section or part of a section may be selected visually for conversion into downcore RGB curves. Downcore resolution can be set at any level up to a maximum of 100μm, though in the case of D13892, a 1mm resolution curve is sufficient to capture the systematic variation. Averaging pixel values down and across each depth interval then produces the final RGB curves, which show the average red, green and blue colour intensity across the width of the selected panel for each depth interval. The results can be expressed as absolute intensity or relative intensity.

Data for D13892 have been produced at 1mm intervals. The data points therefore represent average colour values for a 1mm slice of the core, ultimately produced from continuous measurement down the length of the core. Very low theoretical periods (Nyquist periods) can therefore be resolved in these data. The Nyquist period is defined as twice the maximum sample spacing, though in "non-ideal" situations such as a bioturbated core it may be more realistic to use 3-4 times the maximum sample spacing (Giosan et al. 2002). A table representing minimum period length that may be derived by various sampling resolutions at various rates of accumulation are shown below as Table 3.3.1.

Table 3.3.1 Nyquist periodicities at various sampling intervals and rates of accumulation.

Rate of sedimentation (cm/kyr)	Nyquist period (2 x maximum sampling period) in years	Modified for bioturbation/diagenesis (3-4 x sampling period) in years x 3	x4
For 1cm resolution			
0.01	200,000	300,000	400,000
0.1	20,000	30,000	400,00
1	2,000	3,000	4,000
5	400	600	800
10	200	300	400
15	133.3	200	266.7
20	100	150	200
25	80	120	160
50	40	60	80
100	20	30	40
For 1mm resolution			
0.01	20,000	30,000	40,000
0.1	2,000	3,000	4,000
1	200	300	400
5	40	60	80
10	20	30	40
15	13.3	20	26.7
20	10	15	20
25	8	12	16
50	4	6	8
100	2	3	4
For 100μm resolution			
0.01	2,000	3,000	4,000
0.1	200	300	400
1	20	30	40
5	4	6	8
10	2	3	4
15	1.3	2	2.7
20	1	1.5	2
25	0.8	1.2	1.6
50	0.4	0.6	0.8
100	0.2	0.3	0.4

The BOSCOR Minolta spectrophotometer was also used to define end members for the D13892 colour record in terms of their luminescence, chroma, hue and photo-spectra. To remove the effects of variable and unknown water content, samples were taken and oven dried for at least 24 hours. These were then crushed fine and full colour spectra measured from 400 to 700nm.

To remove environmental effects and machine error the measurements were made by filling a shallow well with the crushed sediment sample and flattening the top. The Spectrophotometer was then placed over the well, which has a diameter slightly larger than that of the device's aperture. The measurement was done three times and the output spectrum is the average of these three measured spectra. The spectrophotometer was calibrated to a reference white and to a "zero" before each measurement to remove internal measurement error and ensure reproducibility.

Sediment spectra are smooth and featureless, and are therefore usually pre-treated to increase their variance (Balsam and Deaton, 1996). According to the recommendation of Giosan (Giosan, 2002; Giosan et al., 2002)) the first derivative of the spectrum is used, as this has been successful in detecting mineralogical components in the past. Strong responses in the 400 – 520, 520-600 and 600-700nm wavelength ranges are ascribed to carbonate, oxidised iron minerals (esp. haematite) and non-mineralogical reduced iron (i.e. Fe^{2+}/Fe^{3+} in clays) respectively.

3.4 Grainsize

Samples were weighed wet, oven dried (50^0C) for at least 48 hours and then weighed again. The dry samples were then disaggregated in water and washed over a 63μm sieve. The fines (<63μm) were collected and oven heated (50^0C) until dry and for at least 24 hours before being weighed. The sand fraction (>63μm) was collected, oven dried (50^0C) until dry and for at least 12 hours before being sieved again at 125 and 150μm. The three fractions resulting from this (63 - 125, 125 - 150 and >150μm) were then weighed.

The salt content of the sample may be estimated from the loss of weight during drying and extracted from the weight of the filtrate (<63μm fraction) by the equation:-

$$Y = x\text{-}S(y\text{-}x)$$

Where:- Y = True dry weight.
y = Measured wet weight.
S = Salinity (~35g/kg).
x = Measured dry weight.

Data are presented as cumulative percentage weight of four grainsize fractions (<63μm, 63-125μm, 125-150μm and >150μm) for each sample.

3.5 Processing of Foraminiferal Samples

Faunal analyses were done on the fraction larger than 150μm. For planktonic assemblages, a sample splitter was used to produce samples of appropriate size, and every individual was taken from each split portion until more than 300 individuals had been identified. The fractional quantity of the sample that was used was also recorded. The identification of the planktonic foraminiferal species was based on Hemleben (1989). Assemblage data are reported as percentage of total planktonic tests and as individuals per gram, as appropriate.

In the absence of alteration by dissolution, the planktonic foraminiferal assemblage can be used as an estimator of Sea Surface Temperature (SST). During the course of this work, the transfer function method (F20 (Imbrie and Kipp, 1971)) and the Modern Analogue Technique (SIMMAX (Pflaumann et al., 1996)) were both used. However, these methods proved unstable as a result of the no-analogue problem, i.e. some assemblages were outside the range of the variability of the training set used to develop these methods.

The trained Artificial Neural Network (ANN) at Royal Holloway College (London University), was also made available, courtesy of Michal Kucera. This is a back-propagating neural network that searches for the network configuration that produces the lowest error of prediction. This method has significant advantages over those used previously as it can cope with non-linear relationships and to a certain extent can

overcome the no-analogue problem. Studies of ANN performance have indicated that it significantly out performs the transfer function and is at least as accurate as the Modern Analogue Technique (Malmgren et al., 2000). Within the Holocene the geographical bias that is fundamental to the SIMMAX method makes it the most accurate and precise technique. However, outside of the Holocene the ANN method is almost certainly the most widely applicable. Initial tests on data produced during this study indicated that the ANN method also satisfactorily overcame the no-analogue problem observed in the SIMMAX SST predictions. However, how the ANN copes with the mixed water masses in the Gulf of Cadiz, with Mediterranean, European and African water all contributing at various times, is unknown and difficult to test from such a small data set. Absolute SST values produced by this technique should therefore be considered with due caution.

Benthic foraminiferal assemblages were also determined for selected samples (>150μm fraction). All individuals were taken from the sample, and abundances are reported in percentage of total benthic tests and in number per gram of sediment.

3.6 Stable isotope analyses

Stable isotope measurements for oxygen and carbon were done on the Europa Geo 2020 mass spectrometer at SOC using the individual acid dosing method (S. Cooke p.c.). Each sample is dosed in turn with a small volume of orthophosphoric acid to dissolve the carbonate and liberate the carbon dioxide. The CO_2 is purged of water by passing the gas over a cold (-85^{0}C) water-trap and then concentrated by freezing down onto an internal cold finger. The frozen CO_2 is then warmed, ionised and accelerated before being passed through a strong magnetic field to split the various mass (i.e. isotopic) fractions into beams, the relative strength of which are determined by a Faraday cup.

Each sample is analysed six times, and subsequent to each sub-analysis a reference gas of known isotopic composition is measured. Calibration of the measured "beam strength" signals to the three major mass fractions of CO_2 (δ44, 45 and 46) is done by comparison to the reference gas, and the data are normalised to the Vienna Pee Dee Belemnite (vpdb) $\delta^{18}O$ standard by comparison to a set of internal standard carbonate samples (H1) run at the beginning and end of each automated analysis run. Processing

of the raw data to $\delta^{18}O$ vpdb was done by Steve Cooke (3/2001 to 3/2002), Matt Cooper (3/2002 to 11/2002) and Mike Bolshaw (11/2002 to 3/2003).

The samples from which individuals for analysis were to be taken were weighed wet and then dried overnight in an oven (50^0C) before being disaggregated in reverse osmosis water and washed over a 63μm sieve. The >63μm fraction was then returned to the oven (50^0C) and dried overnight.

Samples analysed comprised of 7-15 individuals of *Globigerina bulloides*, *Neogloboquadrina pachyderma* dextral or *Turborotalia quinqueloba*. Individuals of *T. quinqueloba* and *N. pachyderma* were selected from the 150 – 180μm and 180 - 212μm sieved grainsize fractions respectively to reduce size-related isotopic variability. *G. bulloides* is known to have more size–related variability and so individuals were selected from the 190-210μm diameter range by using a calibrated eyepiece.

After picking, the samples were washed with methanol and placed in an ultrasonic bath for 15-20 seconds. This removes any clay or organic material remaining on the surface of the tests. The methanol is then left to evaporate in the oven (50^0C) overnight and the sample is then placed in the oven of the mass spectrometer itself (70^0C) for a further 1-2 hours to ensure total dryness.

G. bulloides, though a species that is known to live in a variety of ecological niches, is a standard organism for the construction of stable isotope records in palaeoceanography as it is not temperature sensitive and is therefore often abundant throughout the record of the last glacial cycle. Other nearby records (eg. (Shackleton et al., 2000) have used *G. bulloides* and so the isotopic record for this species in this area is well described, making it important to use this as one of the major species worked on during this study. As *N. pachyderma* (d) is generally a species with predictable dwelling depth and ecology and is also common enough throughout the core records used in this study, it was selected as the main species for analysis for the development and correlation of age models and analysis of the palaeoceanography of the region.

As a result of the appearance of unexpected features in the assemblage data, a small number of samples of *T. quinqueloba* were analysed from D13898 in order to determine whether spikes in the abundance of this species were related to fresh water pulses.

3.7 Radiocarbon dating

The radiocarbon analyses for this project were undertaken with support from NERC Radiocarbon Laboratory (NERC-RCL).

Analyses were performed on samples of planktonic foraminifera picked from the >150μm of samples prepared for isotope analyses (see 4.7). For core D13892, these samples consisted of individuals of *G. bulloides* alone where abundance permitted and *G. bulloides, Globigerina falconensis, Globigerinoides ruber* and *Globigerinoides sacculifer* for other samples. The low abundance of tests in much of D13898 and D13686 (now known to be related to very high rates of sedimentation in these cores) meant that such a targeted approach was impossible. Therefore, all individuals of species thought to dwell at relatively shallow depths were used, with other taxa (eg. Genus *Globorotalia*, *Globigerina siphonifera* etc.) being rejected.

Carbonate in the foraminifera samples was quantitatively hydrolysed to CO_2 using 85% orthophosphoric acid by NERC-RCL. Acid hydrolysis was carried out in evacuated glass vessels overnight in a water bath at 25^0C. CO_2 was then cryogenically separated from other hydrolysis products. Aliquots of CO_2 were converted to an iron/graphite mix by Fe/Zn reduction (Slota et al., 1987). A sub-sample of CO_2 was used to measure $\delta^{13}C$ using a dual-inlet mass spectrometer (VG OPTIMA) in order to normalize ^{14}C data to -25 ‰ $\delta^{13}C$ PDB. The graphite prepared at the NERC Radiocarbon Lab was sent for AMS ^{14}C analysis to the NSF-AMS Facility University of Arizona (Donahue, 1990). In keeping with international practice (Stuiver and Polach, 1977) the results are reported as conventional radiocarbon years BP (relative to AD 1950) and % modern ^{14}C, both expressed at the ± 1sigma level for overall analytical confidence (C. Bryant p.c.).

Conversion of raw conventional radiocarbon ages into an age model during this project has been done in several ways as dictated by circumstance and the method for age model development for each record is discussed in the relevant chapter.

3.8 Sediment Chemistry

Elemental analyses were done on samples from D13900 by simultaneous inductively coupled plasma atomic emission spectroscopy (ICP-AES) at SOC. Samples were dried at 105°C and analysis was performed after total sample dissolution effected by a lithium metaborate fusion (Jarvis, 1992). This produces bulk sediment compositions of major and trace elements (Al, Si, Ca, Mg, Ba, Zr and Cr) which are presented in ratio, usually with aluminium, to avoid problems associated with the so called "closed sum problem".

3.9 XRF logging

An electron can be ejected from its atomic orbital by the absorption of an externally produced photon of sufficient energy. When an inner orbital electron is ejected from an atom, an electron from a higher energy level orbital will transfer into the vacant lower energy orbital, thus producing florescence. Atomic fluorescence can therefore be stimulated in a controlled way by subjecting a substance to an X-ray beam. This is called X-Ray Fluorescence, or XRF. When subjected to a suitably high energy X–ray beam, each atom in the sample will fluoresce at its characteristic wavelength. Therefore, by determining the wavelengths and intensities of the X-ray peaks in a sample's spectrum it is possible to qualitatively establish the elemental composition of the sample, and quantitatively establish the abundances of those elements excited by irradiation.

For this study, XRF analysis was done on core D13892 only (due to time restrictions) using the Cox Analytical Systems XRF logger at BOSCOR. This unique system uses capillary optics to focus an X-Ray beam produced from a molybdenum filament onto the surface of a split core. A stepper motor allows the core to be moved by 400μm increments, and at each increment the core is irradiated. The atomic fluorescences produced are collected by an analyser held close to the surface of the core on an automated arm. The intensity of fluorescence peaks at the characteristic wavelengths of elements of interest are recorded for each step, providing a 400μm resolution

record for those elements throughout the analysed section. These records are shown smoothed by a 3 point running average.

These data are complicated by the role that changes in sediment density and in the distance between the core surface and the analyser (i.e. the thickness of the section) have in regulating the amount of excitement produced, and therefore fluorescence measured. The Compton and Rayleigh peaks, found in all X-ray spectra, are produced by scattering from the core surface and thus are controlled by the density of the material but not by its composition. In this case, the intensities of these peaks may practically be used to compensate for changes in sediment density by normalising the intensity peaks so the Rayleigh and Compton peaks are constant, thus increasing the intensities of low density layers and vice versa. The analyser is also automatically moved relative to the surface to keep the distance between it and the surface constant to minimise the influence of the latter within any given section. This allows the fluorescence intensities within a single section to be considered quantitatively. Neither of these compensations can correct for edge effects however, and at the ends of sections at cracks within a section there will be apparent compositional changes that are not representative of the material under analysis. The analyser cannot return to exactly the same height between section runs, and so the fluorescence intensities produced by irradiation are also not comparable between sections. Ratios between intensities are not affected however, and very good comparability and reproducibility is found between ratios measured during different analysis runs. Data are therefore presented only in ratio, usually with calcium as aluminium is too light to be excited by a molybdenum filament. Events and transitions within a section are also reported as relative changes as these can also be compared between sections.

Chapter 4

The Azores Front Since the Last Glacial Maximum

Submitted to Earth and Planetary Science Letters (July 2003).

The Azores Front since the Last Glacial Maximum

M. Rogerson*, E.J. Rohling, P.P.E. Weaver and J.W. Murray

Southampton Oceanography Centre, European Way, Southampton, SO14 3ZH, UK

* Corresponding author *Email address:*- mr9@soc.soton.ac.uk

Abstract

The spatial distribution of warm surface water in the Atlantic Ocean reflects the state of the thermohaline circulation. The Azores Front, which is a recirculation of the Gulf Stream, marks the northeastern boundary of the North Atlantic sub-tropical gyre. Its position is therefore diagnostic of the width of the Atlantic warm water sphere. Here we report high resolution stable isotope and faunal abundance records of planktonic foraminifera in a sediment core from the Gulf of Cadiz (south-west Spain) which reflects shifting of the Azores Front since the Last Glacial Maximum (LGM). Today, the Azores Front does not penetrate into the Gulf of Cadiz, even though the front resides at the same latitude as the Gulf of Cadiz in the Atlantic. Our results indicate that the Azores Front is a robust feature of the Atlantic surface circulation, and that is present both in glacial and interglacial time at the same latitude. However, during the LGM prior to 16ka BP and during the Younger Dryas, the Azores Front did penetrate far into the Gulf of Cadiz.

Introduction

Close to the Azores Islands lies the Azores Front (AF) (see Fig. 1). It marks the boundary between the European and African surface water masses (Gould, 1985; Schiebel et al., 2002) and extends across the Atlantic between latitudes of 30° and 40°N from the Newfoundland Grand Banks to the coast of Morocco (Gould, 1985). South of the Azores, the AF coincides with the Azores Current, a strong eastward flow that is generated by water mass transformation in the Gulf of Cadiz (GoC), southwest of Spain (Jia, 2000). The AF marks a zone of strong hydrographic transition, in terms of both temperature (~4°C (Gould, 1985)) and water column structure (Fasham et al., 1985), and it is characterised by locally intense upwelling (Rudnick, 1996; Alves and DeVerdière, 1999). The plankton assemblage changes substantially across the AF, particularly below the seasonal thermocline, as a result of

Figure 1

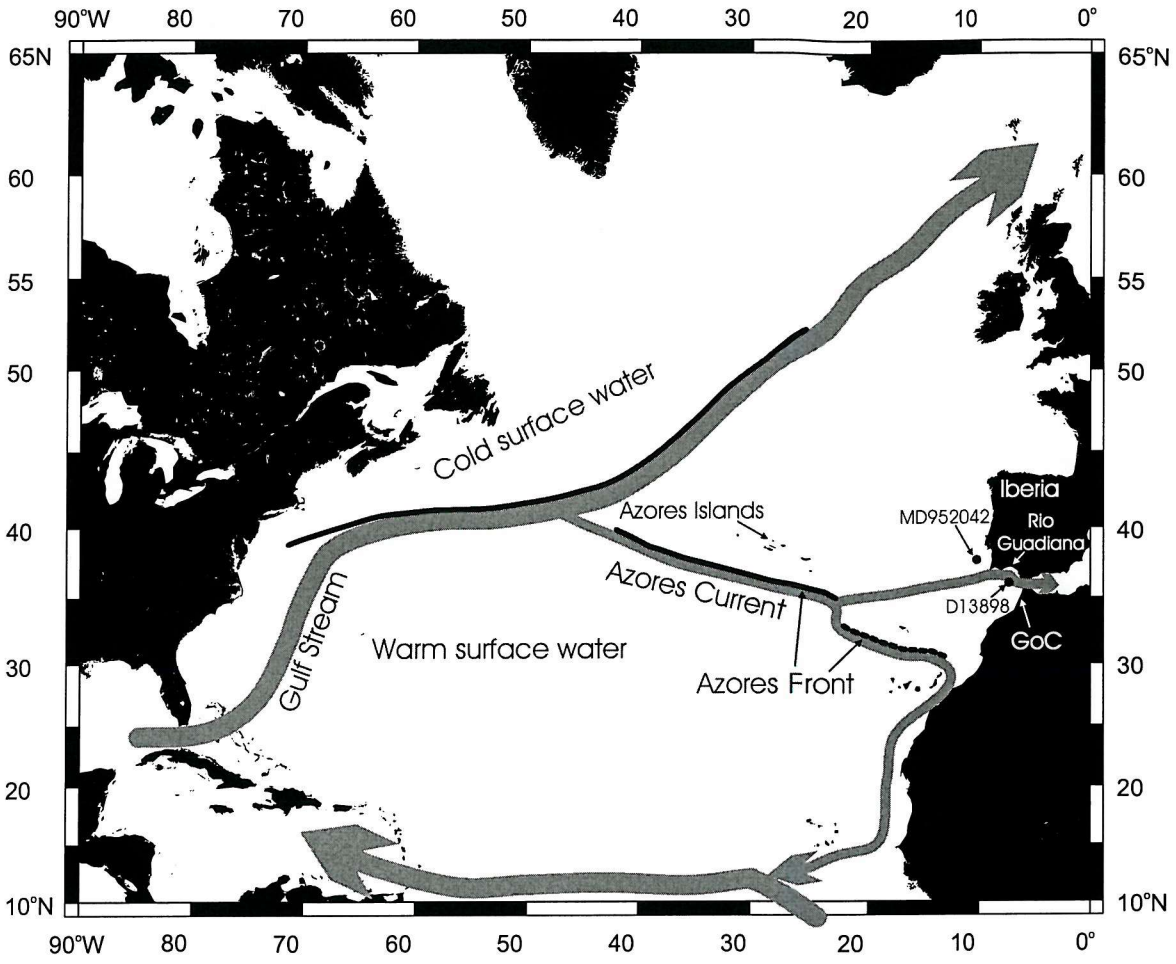

Figure 1. General surface circulation in the North Atlantic today. Core locations are shown.

higher overall productivity and a deeper Deep Chlorophyll Maximum north of the front (Fasham et al., 1985; Angel, 1989; Fernandez and Pingree, 1996; Schiebel et al., 2002). The local thermal and ecological signature of the AF/AC close to the Azores Islands allows evidence of its past behaviour to be preserved in the sediment record. The AC/AF is strongest in the spring (Alves and DeVerdière, 1999) and shows random variability in strength and position throughout the year as a result of meandering (Alves et al., 2002). The sediment record will therefore record the long-term average position of the AF meander belt, rather than that of the AF itself.

Towards the East Atlantic Margin, the geographic positions of the AC and AF are separated. The AC flows into the Gulf of Cadiz to replace water lost during water mass transformation. The AF resides further to the south, between the Canary Islands and Madeira (Kase et al., 1985). A high-resolution circulation model captures observations made during the CANIGO project and so offers comprehensive insight into the oceanography of the area between the Azores and the Strait of Gibraltar (Johnson and Stevens, 2000). The model shows the AC continuing eastwards from the Azores to the Strait of Gibraltar, while the AF (a sharp ~4°C transition at the Azores) degenerates into two weaker transitions, one lying to the west of the GoC but not penetrating into it (~1°) and one lying further to the south (~3°) (see Fig. 2). The southern branch coincides with a second zone of increased velocity, which turns south to flow between the Canary Islands and North Africa.

We here report stable isotope (C and O) and foraminiferal planktonic assemblage records for a core from the GoC in comparison with core MD952042 from offshore southern Portugal (Shackleton et al., 2000), to investigate the history of the Azores Current / Azores Front in the GoC region.

Material and Methods

We present high-resolution data for core D13898 from the GoC, to assess changes in the regional oceanography between the LGM and present. The chronostratigraphic framework for D13898 is based on 10 AMS radiocarbon dates performed on >6mg of shallow-dwelling planktonic foraminiferal tests picked from the >150μm fraction. The radiocarbon analyses were undertaken via the NERC Radiocarbon Laboratory (NERC-RCL), at the University of Arizona NSF-AMS facility. The datings have been

Figure 2a. Present day oceanographic setting from CANIGO regional model (Johnson et al., 2000).

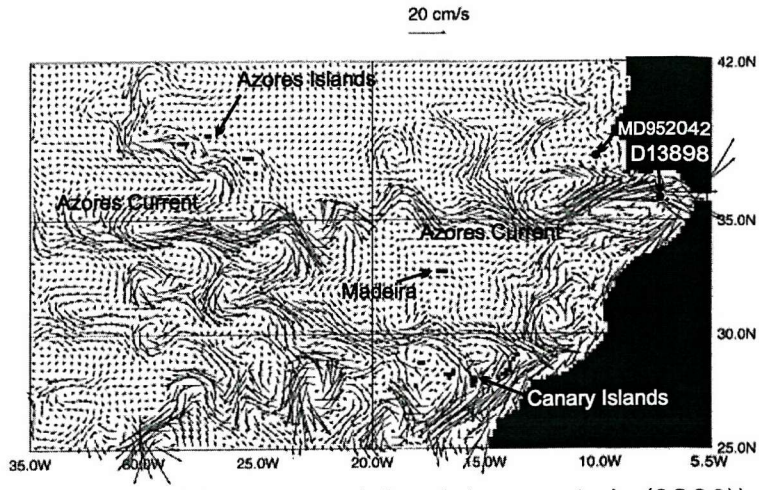

Velocity at 36.6m depth (after Johnson et al., (2000)).

Figure 2b.

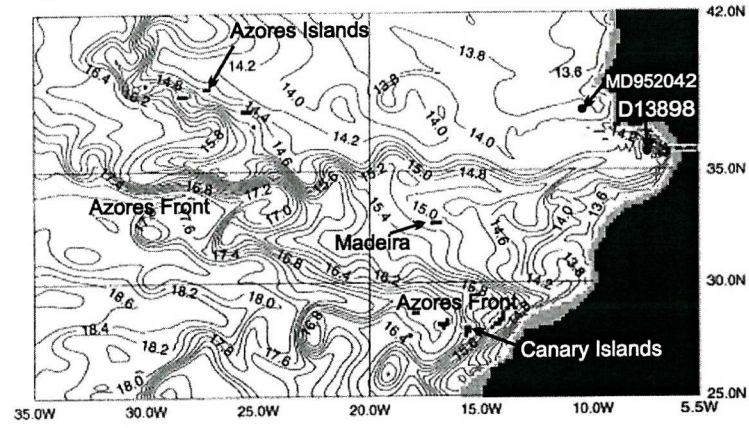

Temperature at 202m depth (after Johnson et al., (2000)).

calibrated using the Calib 4.3 program, and the Laj et al. (1996) correction model in the case of the oldest two (see table 2). As the aim of this study is to compare the Gulf of Cadiz records to that of MD952042, the chronostratigraphy is "tuned" to that of MD952042 by correlation of tie-points concerning global events such as the deglaciation and Heinrich Events. Five tie points were found to be sufficient to make those isotopic events recognisable in both $\delta^{18}O_{G.\ bulloides}$ records synchronous and addition of further tie points was found to make no significant improvement in the correlation between the $\delta^{18}O_{G.\ bulloides}$ records. Both termination 1a and 1b are marked by significant and rapid declines in $\delta^{18}O$ at both locations, and can be correlated with some confidence. A sharply defined $\delta^{18}O_{G.\ bulloides}$ maximum in D13898, which coincides with a maximum in $\delta^{18}O_{N.\ pachyderma\ (d)}$, is dated by ^{14}C to be comparable in age to Heinrich Event 2 (25ka), and was therefore correlated to this event in MD-952042 (identified in this case by a bloom in *N. pachyderma* (s) (Cayre et al., 1999)). These three events provide well-defined age constraints for the correlation at both limits of the glacial period recorded in D13898. A sharply defined isotopic maximum of smaller magnitude is noted in MD95-2042 at ~20ka and is preceded by a broad isotopic minimum, with peak values at ~21ka. A similar configuration is found in the $\delta^{18}O_{G.\ bulloides}$ for D13898 and a local minimum is also noted at the same depth in the $\delta^{18}O_{N.\ pachyderma\ (d)}$ record of D13898. The maximum and minimum values at these ages were therefore correlated between the $\delta^{18}O_{G.\ bulloides}$ records. The tie-points used are indicated in table 2.

For the planktonic foraminiferal abundance study, samples were disaggregated, washed and sieved to remove all material finer than 150μm. Where necessary, samples were split into suitable aliquots of at least 300 individuals. The data are presented as percentages of total planktonic foraminiferal number.

The specimens selected for stable isotope analyses were washed and sonicated in methanol to remove surface contamination. Stable isotope analyses were carried out on 7-15 individuals of *Neogloboquadrina pachyderma* (d) between sizes of 150 and 212μm or 6-15 individuals of *Globigerina bulloides* sized between 190 and 210μm. Stable isotope analyses were carried out using a Europa Geo 2020 mass spectrometer with individual acid-bath preparation. The carbon and oxygen isotope ratios are

expressed as δ values, in per mils (‰), relative to the Vienna Peedee Belemnite standard (Coplen, 1988, 1994).

Framework for interpretation of stable isotope data

Oxygen isotope records are dominated by changes in global ice volume, because the preferential sequestration of the lighter (^{16}O) isotope into ice sheets causes relative ^{18}O enrichment in the oceans. As the records discussed have been synchronised, global ice-volume effects will be equally represented at any given time.

Detailed comparisons are made only between records based on the same species, thus avoiding any bias from metabolic ("vital") effects so that offsets between records represent genuine differences in the environmental conditions. These differences concern the combined influences in changes in temperature and the freshwater cycle. Higher temperatures cause more light oxygen to be incorporated into calcite, giving negative $\delta^{18}O$ shifts. Fresh water has a light $\delta^{18}O$, and influxes of fresh water will be recorded as negative excursions in the oxygen isotope record. Conversely, evaporative loss causes the waters to become heavier in $\delta^{18}O$. It is unlikely that amounts of isotopically light fresh water large enough to cause more than transient excursions were supplied to the GoC in the past, as there are no major rivers to supply it and the GoC is open to the Atlantic in the west. This open setting also makes large offsets between cores due to evaporative loss unlikely. Large isotopic offsets between the records discussed in this study are therefore predominantly the result of spatial differences in temperature.

In today's western Mediterranean, *G. bulloides* is a spring-summer species that grows at the base of the photic zone feeding on phytoplankton produced during the spring bloom, and temperature is considered much less important than food availability (Pujol and Vergnaud-Grazzini, 1989). It is the dominant species in plankton tows at ~100m from Sicily to the westward edge of the GoC (Cifelli, 1974) and is reported in high abundances in core tops from the GoC (Sierro et al., 1999). East of the Azores, *G. bulloides* is found in high abundances at less than 100m depth during August and is absent in January, as is the case in the Mediterranean (Schiebel et al., 2002). Isotopic records for a species will be biased towards the season and environment of

maximum test production, and as this seems to be constant throughout the study area, *G. bulloides* can be considered to be a useful marker for conditions at relatively shallow levels in spring to summer.

Table 1. Dwelling depth of *Globigerina bulloides* in the region surrounding the GoC.

Location	Western Mediterranean	Transect from Sicily to western GoC	Azores Islands (S of AF)	Azores Islands (N of AF)	Azores Islands (E of Islands)	BIOTRANS (offshore Cape Finnisterre)
Dwelling depth range	"Base of Photic Zone" <100m	≤100m	Uncommon ~100m	Uncommon ~100m	<100m	<100m descending to ~100m
Source	(Pujol and Vergnaud-Grazzini, 1989)	(Cifelli, 1974)	(Schiebel et al., 2002)	(Schiebel et al., 2002)	(Schiebel et al., 2002)	(Schiebel et al., 2001)

Neogloboquadrina pachyderma (d) is found only in low abundances in the Mediterranean today, and is not present in significant numbers in plankton tows (Cifelli, 1974) or core tops (Sierro et al., 1999) from the GoC. It is found in high abundance further north in the adjacent North Atlantic (Schiebel and Hemleben, 2000; Schiebel et al., 2001), and has been widely described as a temperate to sub-polar species (e.g. (Hemleben et al., 1989; Hilbrecht, 1997)). *N. pachyderma* (d) is a dominant species during the last glaciation in both the Mediterranean and the GoC (Pujol and Vergnaud-Grazzini, 1989; Sierro et al., 1999). In the Mediterranean, *N. pachyderma* (d) is generally considered to be a mesopelagic species that thrives at the Deep Chlorophyll Maximum, and it typically reflects stable (deep) conditions that are "set" in winter (Pujol and Vergnaud-Grazzini, 1989; Rohling et al., 1993; Rohling et al., 2003b; Spero et al., 2003). Similar habitats at depth have been observed for *Neogloboquadrinids* (*N. pachyderma* (s and d) and *N. dutertrei*) in the Atlantic (Fairbanks and Wiebe, 1980; Fairbanks et al., 1980; Fairbanks et al., 1982; Ravelo and Fairbanks, 1992; Kohfeld et al., 1996), Pacific (Ortiz et al., 1995; Ortiz et al., 1996; Spero et al., 2003) and Southern Oceans (Mortyn and Charles, 2003).

Results

In the D13898 record, *N. pachyderma* (d) consistently shows heavier $\delta^{18}O$ than *G. bulloides* (Fig. 3A). This is consistent with *N. pachyderma* (d) dwelling at greater depth, and therefore lower temperature, and this isotopic configuration can be

Figure 3.

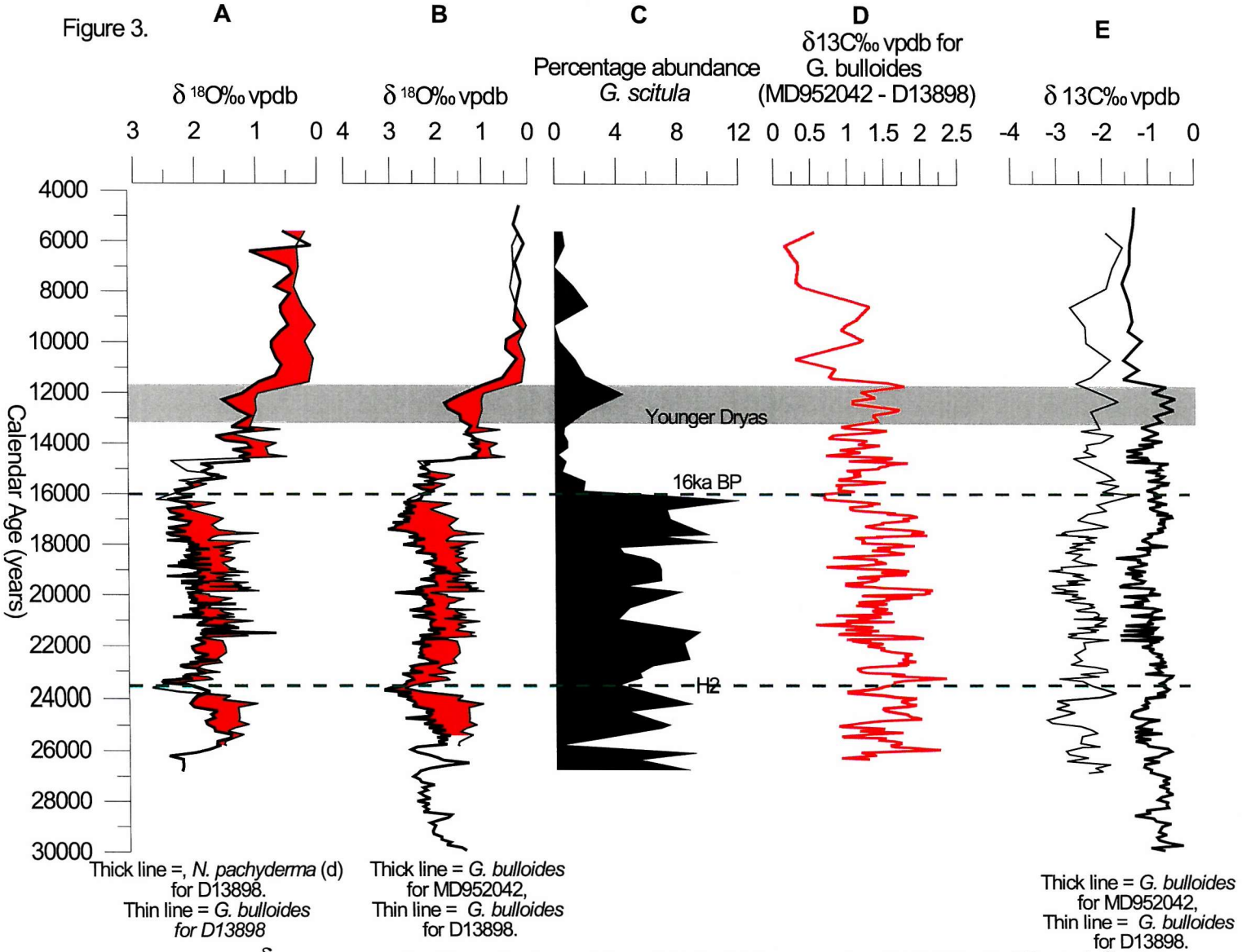

Figure 3. A; Offset of $\delta^{18}O$ between the *N. pachyderma* (d) and *G. bulloides* records of D13898. B; Offset of $\delta^{18}O$ between the *G. bulloides* record of D13898 and the *G. bulloides* record of MD952042. C; Percentage abundance of *G. scitula*. D; Offset of carbon isotope values between *G. bulloides* records of MD952042 and D13898. E; $\delta^{13}C$ for *G. bulloides* in D13898 and MD952042.

considered robust. At 23.5ka BP and during the deglaciation the *N. pachyderma* (d) and *G. bulloides* records show similar $\delta^{18}O$. The increase in $\delta^{18}O$ at 23.5ka BP is close in age to Heinrich Event 2 (H2; 24ka BP (Rohling et al., 2003a)) and probably represents this event in D13898. Strong cooling associated with the Heinrich Events has been found in alkenone records (which, like *G. bulloides*, are indicative of spring conditions) from the Alboran Sea (Cacho et al., 1999). It is likely that the stronger response of *G. bulloides* compared to *N. pachyderma* (d) during H2 is due to the latter being representative of different seasonal conditions (winter) and living at greater depth. H1 (17ka BP (Rohling et al., 2003a)) does not appear to be strongly represented in D13898.

In the period prior to 16ka, vertical stratification at D13898 is maintained, and the $\delta^{18}O_{G.\ bulloides}$ and $\delta^{18}O_{N.\ pachyderma\ (d)}$ records are parallel. During this period and during the Younger Dryas, $\delta^{18}O_{G.\ bulloides}$ for D13898 show lighter $\delta^{18}O$ values than $\delta^{18}O_{G.\ bulloides}$ for MD952042 (Fig. 3B). A strong isotopic gradient is thus identified between the $\delta^{18}O_{G.\ bulloides}$ records of MD952042 and D13898 prior to 16ka BP and during the Younger Dryas. $\delta^{18}O_{N.\ pachyderma\ (d)}$ in D13898 also shows highly similar, and often marginally lighter, values for these periods than $\delta^{18}O_{G.\ bulloides}$ for MD952042, despite the former being representative of conditions during the winter and at greater depth than *G. bulloides*. As $\delta^{18}O$ will reflect temperature in this instance, this indicates that the isotherms must dip to the south between the Portuguese margin and the GoC, and the isotopic anomaly noted in $\delta^{18}O_{G.\ bulloides}$ is therefore not confined to the surface, but is also reflected at greater depth.

Throughout the last 26kyr, D13898 shows significantly lighter $\delta^{13}C_{G.\ bulloides}$ than MD952042 (Fig. 3D, E). The records compared in Fig. 3D and E are for the same species, so that differences cannot be ascribed to "vital effects" and are unlikely to be due to differing seasons of growth. A significant reduction in the separation between the $\delta^{13}C_{G.\ bulloides}$ records is found at 16ka and is caused by a significant enrichment in $\delta^{13}C$ in D13898. The separation prior to 16ka could in principal have been caused either by increased resupply of ^{12}C in the GoC, or by significantly increased productivity on the Portuguese margin. However, were the differences between these records "driven" by productivity at MD952042, the collapse of the separation at 16ka

would be anticipated to coincide with an increase in ^{13}C depletion (i.e. reduced ^{12}C export) at MD952042, which is not recognised in figure 3E. The reduction in separation at 16ka is caused by a significant enrichment in D13898, further indicating that the separation between these records prior to 16ka was maintained by enhanced ^{12}C resupply in the GoC rather than by high productivity at the Portuguese margin. The high random variability in $\delta^{13}C_{G.\ bulloides}$ D13898 compared to that in MD952042 is also consistent with a highly dynamic environment in the GoC, and the relatively low variability at MD952042 is indicative of a rather stable ^{12}C balance at this location. The lighter values in D13898, relative to MD952042, therefore suggest a higher rate of ^{12}C resupply to surface waters in the Gulf of Cadiz compared to the Portuguese margin, and the separation appears to be "driven" by conditions in the GoC. In many records (eg. (Peeters et al., 1999) high resupply of light carbon to surface waters has been related to vertical mixing during coastal upwelling. Though coastal upwelling is known to occur along the Portuguese margin, it does not occur in the Gulf of Cadiz to the south of the Guadiana estuary (Fiuza, 1981; Fiuza et al., 1982). Though the two $\delta^{13}C_{G.\ bulloides}$ records are similar in shape, the offset between the records is very variable, with Holocene offsets of ~0.25‰ and glacial offsets up to 1.75‰ (Fig, 3D, E). In the absence of upwelling, the ^{12}C resupply to surface waters must have been provided by another mechanism, which has undergone significant variation throughout the last 26,000 years.

In our faunal abundance data, D13898 shows downcore variations consistent with the thermal history of the Last Glacial Maximum and the Last Deglaciation, in agreement with other records from the GoC (eg. (Sierro et al., 1999)). However, we concentrate specifically on the record for *Globorotalia scitula,* a deep dwelling species (100 – 700m water depth; (Schiebel et al., 2002)), whose abundance changes seem to be inadequately explained by temperature alone. It is common (~10%) prior to 16ka BP, but is rare throughout the rest of the core with the exception of the Younger Dryas and a small peak at ~9ka BP (Fig. 3C). The decrease in abundance at 16ka BP predates Termination 1a by ~2000 years. It does however coincide closely with the disappearance of the $\delta^{18}O_{G.\ bulloides}$ offset between D13898 and MD952042 (Fig. 3B). As argued before, offsets between two closely spaced records from an open ocean setting predominantly reflect temperature contrasts. Hence, we interpret the $\delta^{18}O_{G.}$

bulloides difference between D13898 and MD952942 as a temperature gradient. Its disappearance at 16ka BP seems to be mostly due to a cooling at D13898. If *G. scitula* is considered to be an indicator for cold conditions (Thunnell, 1978), it would be expected to increase in association with this cooling. Instead, a decrease is observed, and the collapse of the *G. scitula* population needs to be considered in view of changes in the regional hydrographic context.

Discussion and Conclusions

G. scitula reaches its maximum abundance in the modern North Atlantic around the Azores Islands (Prell et al., 1999). Plankton tows indicate that *G. scitula* is present in high abundances north of the Azores Front where frontal upwelling causes high productivity, but in very low abundances to the south (Schiebel et al., 2002). The abundance peak of *G. scitula* on the northern flank of the AF offers a useful indicator for the presence of the AF (Schiebel et al., 2002), and we consider the presence or absence of *G. scitula* in core D13898 as a marker for past presence or absence of the AF at this location.

The intervals with peak abundances of *G. scitula* coincide with times when the oxygen isotope offset between D13898 and MD952042 is persistent and of considerable magnitude (Fig. 3). This suggests that there was a large thermal gradient between the two locations. The magnitude of the isotopic offset between D13898 and MD952042 indicates that the site of D13898 was on average 4-5°C warmer than that of MD952042 during this time, using a value for changes in the oxygen isotope ratio of 0.23‰ $^{\circ}C^{-1}$ (Kim and O'Neill, 1997) and assuming that the isotopic contrast was entirely related to temperature. Such a contrast would be consistent with the magnitude of the thermal transition across the AF today (~4°C, see Fig. 2b). High abundances of *G. scitula* and relatively high (isotopic) temperatures in the D13898 record prior to 16,000 years and during the Younger Dryas therefore suggest that the AF resided close to the D13898 location at these times. Subsequent to the withdrawal of the AF at 16ka BP, the $\delta^{18}O$ offset between *N. pachyderma* (d) and *G. bulloides* in D13898 is absent, indicating a poorly stratified water column during the deglaciation.

The AF is known to be a location of vigorous upwelling (Alves et al., 2002) and if it resided near the location of core D13898, this should be represented in the carbon

isotope record. Greater resupply of light carbon to the surface waters would be expected to characterise the signals in D13898 prior to 16ka BP and during the Younger Dryas. The offset between the D13898 and MD952042 $\delta^{13}C$ records for *G. bulloides* is highly variable, but it is generally enhanced during the glacial period than relative to the Holocene (Fig. 3d). Just before 16ka BP, the offset declines significantly and then increases again toward glacial values in the Younger Dryas. This pattern supports our interpretation of the $\delta^{18}O$ differences and the *G. scitula* abundance data.

The presence of a large $\delta^{18}O$ offset between D13898 and MD952042 strongly suggests that an enhanced thermal gradient existed between the Gulf of Cadiz and the Portuguese margin prior to 16ka BP. At the same time, the Gulf of Cadiz shows high abundances of *G. scitula,* a species that peaks in abundance at the Azores Front and so offers an indicator for the presence or absence of the Azores Front in the study area. Furthermore, these times were also characterised by enhanced resupply of light carbon to surface waters in the Gulf of Cadiz, a likely reflection of frontal upwelling. During the Younger Dryas, the enhanced thermal gradient between the Gulf of Cadiz and the Portuguese margin returns. At this time, there is a marked increase in the abundance of *G. scitula* and a return of frontal upwelling in the Gulf of Cadiz. It is therefore proposed that prior to 16ka BP the Azores Front resided in the northern Gulf of Cadiz, and it briefly returned to this position during the Younger Dryas.

Acknowledgements

We thank S. Cooke, M. Cooper and M. Bolshaw for performing the stable isotope analyses, and A. Hogg and J. Marotzke for stimulating discussions and feedback. We would also like to thank B. Hoogakker for reading an early version of this manuscript. The radiocarbon datings were carried out as part of NERC-RCL project 949.1201.

Figure 4

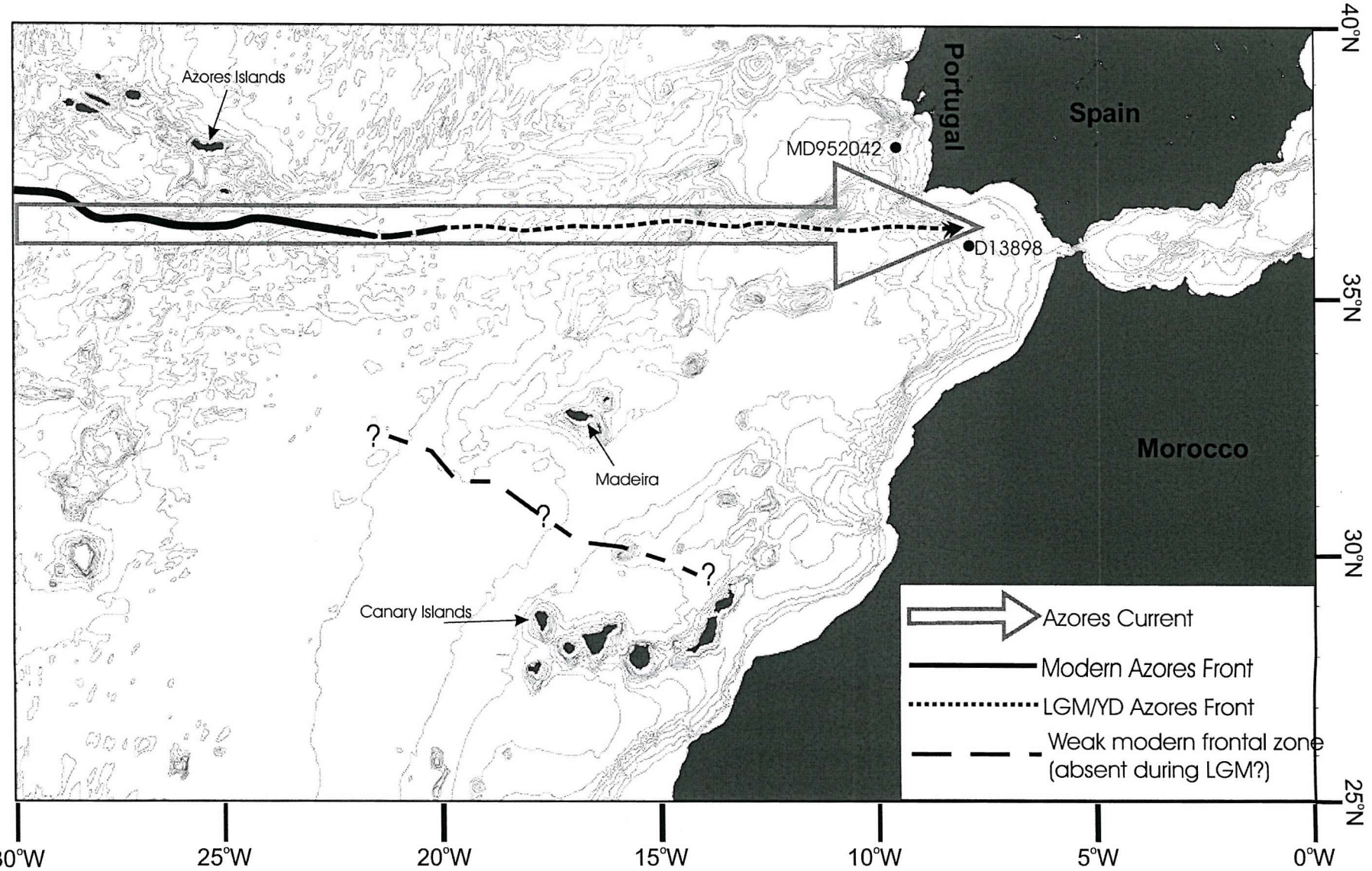

Figure 4. Mean position of Azores Front prior to 16ka and during the Younger Dryas. During these times, the Azores Front is interpreted as penetrating further east along the pathway of the Azores Current than is now the case, and resided in the northern Gulf of Cadiz. The weak, southern frontal zone noted in the modern setting is likely to be absent at these times.

Table 2. Stratigraphic position of radiocarbon datings. Conversion from conventional to calendar years is done with the Calib4.3 program. No reservoir correction has been used, as the record is subsequently tuned to MD952042, the chronostratigraphic framework for which was derived by correlation to the ^{14}C dated record of SU18-81, for which no reservoir adjustment was made (Bard et al., 1987).

Sample depth (cm)	**Conventional radiocarbon age**	**1σ**	**Mean calendar age**
0	5227	42	5597
100	8615	55	9317.5
220	11642	89	13303.5
300	12796	73	14927
380	14716	86	17039
480	16480	120	19068.5
608	17600	110	20358
834	19340	120	22360.5
1234	23010	180	26363.17*
1628	24040	200	27461.53*
Tie point depth (cm)	**Event**	**Calibrated radiocarbon age**	**Age in MD952042**
172	Termination 1b	11700	11800
318	Termination 1a	15200	14700
721	Sharp isotopic maximum	21200	20100
944	Peak of broad isotopic minimum	22600	21600
1152cm	H2	25200	23700

* Conversion done using Laj et al. (1996) curve.

Chapter 5:- Deeper Settling of the Mediterranean Outflow Plume in the Gulf of Cadiz during the Last Glacial Maximum

Abstract

Micropalaentological and grainsize records from a set of sediment cores recovered from the Gulf of Cadiz (south-west Spain) are presented, and reflect changes in the position and strength of the Mediterranean Outflow current. Radiocarbon (^{14}C) dating and analysis of the stable isotopic (^{13}C, ^{18}O) composition of planktonic foraminiferal tests provide age determination of changes in the behaviour of the Mediterranean Outflow plume and indicate that the flow was present, and probably stronger, on the Gil Eanes Drift during the Last Glacial Maximum. This observation is found to be consistent with the physical constraints on the Gibraltar Exchange and on the settling and spreading of the plume on the Iberian Margin. An altered position of the Mediterranean Outflow on the slope of the Gulf of Cadiz is found to explain the apparent paradox between the observations of decreased activity in the modern flow-path of the current during the last glacial maximum (Nelson et al., 1993) and the ongoing anti-estuarine circulation that is believed to have been present in the Mediterranean at this time (Myers et al., 1998). As the Mediterranean Outflow is a major source of salt transported to the northern North Atlantic, changes in the properties, flux and flow-path of the plume in the past has a potential to impact circulation in the Atlantic. Deeper settling of the plume would certainly have precluded the Mediterranean Outflow from supplying salt to the Nordic seas as has been proposed for the late Holocene (Reid, 1979), and this would be anticipated to retard the formation of North Atlantic Deep Water.

Introduction

The Gulf of Cadiz (GoC) embayment (southwest of Iberia) lies at the western end of the Strait of Gibraltar, where density driven exchange occurs between the Mediterranean Sea and the Atlantic. Here, dense Mediterranean waters flow west at depth to form the Mediterranean Outflow current (MO) and relatively fresh Atlantic water flows east at the surface to form the Atlantic Inflow current (AI). This is part of

an anti-estuarine circulation that is prevalent across the Mediterranean basin and driven by high net evaporation in the eastern Mediterranean (Bryden and Stommel, 1984). Having exited the strait, the MO flows down the slope of the GoC and passes out into the North Atlantic. Within the GoC the MO is complicated by branching (Iorga and Lozier, 1999; Borenas et al., 2002; Johnson et al., 2002), which causes the formation of two flow cores at 500-800m and 1000-1500m respectively (Iorga and Lozier, 1999).

The deeper branch of the current (MO2) forms a large plume of warm, saline water that reaches as far west as the Azores (Alves et al., 2002), and elevated salinities that may be attributed to it can be found at the Bahaman Bank (Armi and Bray, 1982). Some of this deeper water also follows the course of the shallower flow core into the northern North Atlantic (Iorga and Lozier, 1999) (see Fig. 1). The shallower, more onshore flow core (MO1) passes along the Portuguese margin (Iorga and Lozier, 1999) and eventually penetrates the Greenland-Iceland-Norwegian Sea (GIN) by passing over the Scotland-Iceland Ridge (Reid, 1979). The flow path and salinity field of the plume of Mediterranean water produced in the North Atlantic by this exchange are shown in Fig. 1.The Scotland-Iceland ridge is too shallow (750-1000m) for the northern component of MO2 to cross and it is thought to be recirculated into the deep North Atlantic (Reid, 1979; Schönfeld and Zahn, 2000). Salt supplied to surface waters in the GIN by the MO may promote the development of negative buoyancy in the nascent North Atlantic Deep Water (Reid, 1979; Schönfeld and Zahn, 2000). Influence of changed MO properties on the meridional flow in the North Atlantic analogous to those predicted by Reid have been observed in an Ocean Circulation model (Rahmstorf, 1998).

The purpose of this study is to use the sedimentary characteristics, microfossil abundance data and stable isotope records from sediment cores recovered from the Gulf of Cadiz to reconstruct the position, flux and influence of the MO during the Last Glacial Maximum (LGM).

Figure 1

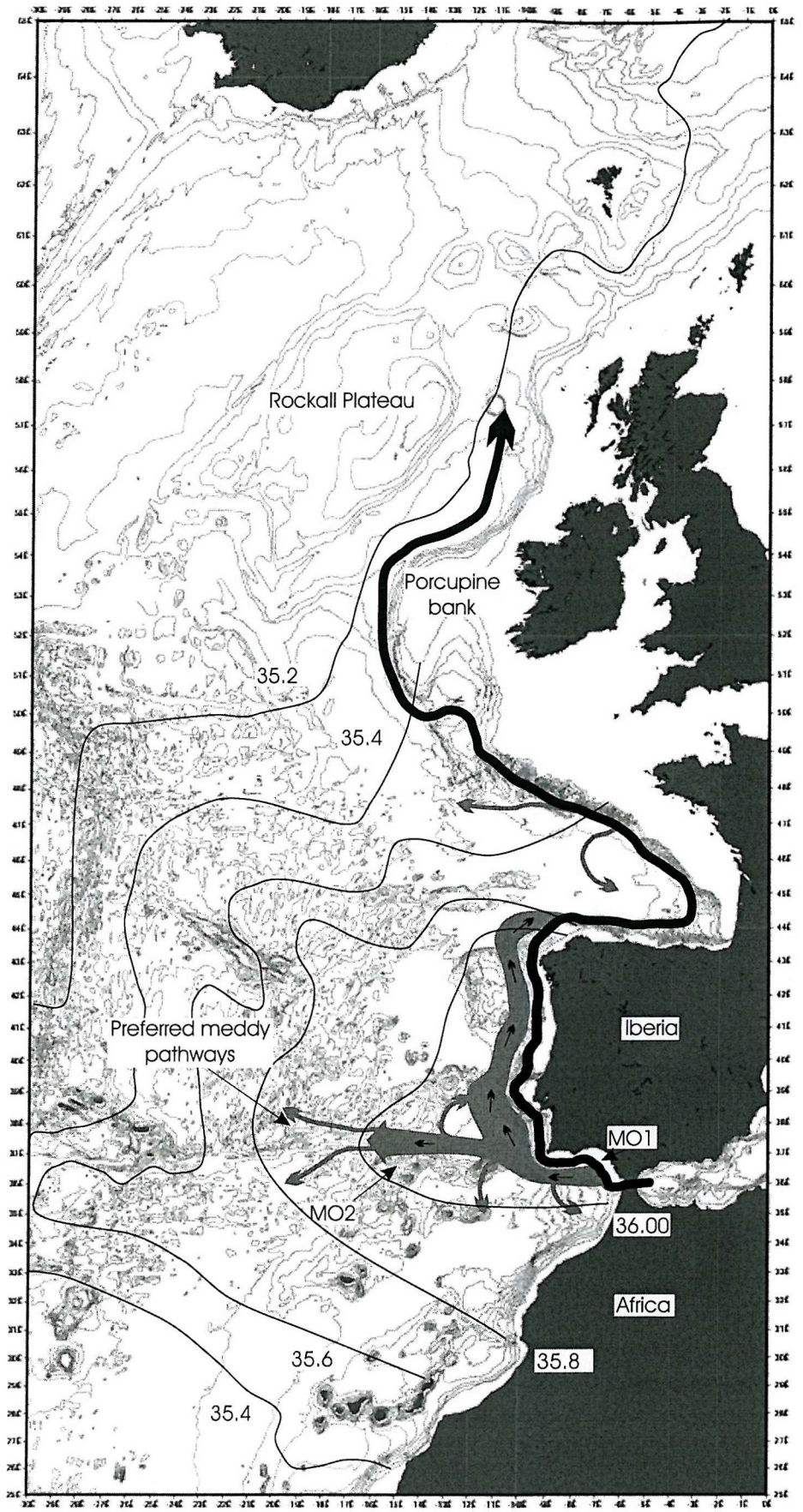

Figure 1. Summary of the Mediterranean Outflow in the eastern North Atlantic. The main flow paths of MO 1 and MO 2 are taken from Iorga and Lozier (1999). Contours show salinity of Mediterranean Outflow as defined by Reid, 1979, (in parts per mille).

Observations concerning the MO during the LGM

Seismic sections from the GoC contourite drift show an alternating series of highly reflective and acoustically transparent layers, shown by sediment core studies to represent paired layers of sand and mud (Nelson et al., 1993; Rodero et al., 1999). Radiocarbon dating of the most recent pair indicates that the start of sand deposition was at the beginning of the Younger Dryas, and the mud layer therefore represents a glacial age facies (Nelson et al., 1993). The onset of sand deposition in other core records are dated at the oldest to the last deglaciation (~16 kyr BP (Stow et al., 1986)). Each sand-mud pair is thus believed to represent one glacial cycle, indicating that during interglacials the MO plume is in a similar position to that observed today, whereas it is absent from the slope when sea level falls more than 50m below the present level, and it is postulated that this represents absence of water mass exchange at Gibraltar (Nelson et al., 1993). There is substantial complexity in this system which is not accounted for in this model however, as some evidence of flow has been observed within the flowpath of the MO that has conclusively been shown to date from the last glaciation (Caralp, 1988; Mulder et al., 2002). Though the evidence for altered MO flow during the LGM is strong, the simple on-off alternation envisaged by Nelson and others is therefore too simple. Evidence of reduced flow has also been reported from the Portuguese margin during the last glaciation, based on both sedimentological and chemical proxy data (Hall and McCave, 2000; Schönfeld and Zahn, 2000; Moreno et al., 2002b). However, it is also postulated that the flow deeper than 2000m may have been enhanced, suggesting that the lower flow core (MO2) was stronger in the past (Thomson et al., 1999; Schönfeld and Zahn, 2000).

Realistic numerical models (Bigg, 1995; Myers et al., 1998; Rohling, 1999; Myers, 2002) and oxygen isotope reconstructions (Thunnell and Williams, 1989; Rohling and De Rijk, 1999) indicate that for the last 30,000 years the Mediterranean has experienced anti-estuarine circulation similar to that of today, with the possible exception of the duration of the S1 sapropel in the early Holocene. It is therefore unlikely that the MO flow has switched on and off on glacial/interglacial timescales as proposed by Nelson et al, (1993) and therefore the absence of the MO flow from its present course in the GOC during sea level lowstands must be related to the flow changing its position on the continental slope.

Physical Oceanography of the Mediterranean Outflow

The Gibraltar Exchange

To understand the history of the MO plume, we first summarise the physical constraints on its behaviour. The shallow (284m) and narrow (12-15km) Strait of Gibraltar limits the amount of water-mass exchange between the Mediterranean and the Atlantic. The two-layer flow in the Strait has been shown to be critical (i.e. the two-layer Froude number exceeds 1) through most of the tidal cycle, and approximately half of the MO flux is achieved under critical flow during the falling tide (Bryden et al., 1988). The Gibraltar Exchange may thus practically be assumed to be maximal or very near maximal (Bryden et al., 1988; Bryden and Kinder, 1991). Under lower sea level conditions, as have existed in the past, the exchange must have been maximal throughout the tidal cycle (Rohling and Bryden, 1994).

Under maximal conditions, assuming the Camarinal sill (see Fig. 1) is triangular in cross section, the fluxes of the MO and AI can be considered as conforming to:

$$1) \qquad Q_{AI} - Q_{MO} = C\,(D_s\, b_s / 2)\,\sqrt{(g'\, D_s)}$$

Where Q_{AI} is the flux of the AI, Q_{MO} is the flux of the MO, b_s is the sill width, D_s is the water depth at the sill, g' is the reduced gravity ($g' = g\beta(S_{MO} - S_{AI})$ where S_{MO} and S_{AI} are the salinities of the Mediterranean and Atlantic waters respectively and β is determined from the equation of state for seawater (Bryden, 1993)) and C is a constant that depends on the physical configuration of the strait (~ 0.28 in this case (Bryden, 1993)). Combining this with the statements of salt and mass conservation, it is possible to show that the salinity contrast between the Mediterranean and Atlantic at Gibraltar is determined by net evaporation in the Mediterranean and the depth and width of the sill (Bryden, 1993):-

$$2) \qquad (S_{AI} - S_{MO})^{3/2} = C\,E\,/\,((b_s\, Ds)\,\sqrt{D_s})$$

Where E is the net evaporation over the Mediterranean basin. Lowering sea level will therefore decrease the exchange through the Strait of Gibraltar by decreasing both D_s and b_s, thereby reducing the flux and increasing the salinity of the MO.

The maximum flux of Mediterranean water able to be transported through the Strait of Gibraltar during the Last Glacial Maximum (LGM) has been calculated at 0.32 Sv (Rohling and Bryden, 1994), less than half that measured today (0.79 Sv (Bryden and Kinder, 1991)), assuming no change in net evaporation in the Mediterranean (termed $(E\text{-}P)_M$). This would be associated with more than a doubling in the salinity contrast across the Strait of Gibraltar ($S_1 - S_2$), which is 1.9 psu today (Bryden et al., 1988) and estimated at 4.1 psu during the LGM (Rohling and Bryden, 1994). The inference of increased Mediterranean salinity is supported by the observation of enriched $\delta^{18}O$ in the tests of planktonic foraminifera during the LGM, particularly in the Levantine basin, (Rohling, 1999; Rohling and De Rijk, 1999). Proportional changes in flux are found in a numerical model of the internal circulation of the Mediterranean (Myers et al., 1998), and basin average $(E\text{-}P)_M$ is expected to be similar to today, though its spatial distribution may be altered (Bigg, 1994, 1995; Myers et al., 1998), so LGM $S_1 - S_2$ will be close to the estimate of 4.1 psu. As the MO passes out of the Strait of Gibraltar, it rapidly descends the slope as a result of its high negative buoyancy and its downslope velocity is controlled by the reduced gravity (g'). Increased Mediterranean salinity will cause g' to be significantly increased, resulting in the MO plume passing into the GoC to settle to greater depths in the Atlantic during the LGM compared to today.

The MO in the Gulf of Cadiz

The MO entrains Atlantic water as it passes into the GoC, increasing in volume by a factor of 3-4 within the first 100km of the Strait of Gibraltar (O'Neill-Baringer and Price, 1999), which reduces its negative buoyancy and erodes the velocity of the plume. The final depth of settling of the MO plume is controlled by the final density of the MO product water (equal to $a\rho_{MO} + b\rho_{atl}$) where ρ_{MO} and ρ_{atl} are the densities of Mediterranean and Atlantic waters respectively and a and b are the fractions of Mediterranean and Atlantic water in the plume respectively ($a + b = 1$). Today b/a is of the order of 2 to 3 (O'Neill-Baringer and Price, 1999).

Since Mediterranean water ultimately is evaporated Atlantic water, so that ρ_{MO} is determined to a large extent by ρ_{atl} and $(E\text{-}P)_M$, the effects of variation in ρ_{atl} through

time virtually cancel out. However, there is a 2°C temperature range between the waters mixed into the upper and lower parts of the MO plume during the crucial period of high entrainment within 100km of Gibraltar, and the final density of the top of the plume is therefore lower than that of the bottom (O'Neill-Baringer and Price, 1999). The vertical range of Atlantic water densities incorporated into the MO plume can be termed $\Delta\rho_{atl}$ and causes some small lateral spreading within the plume that is exaggerated by the topography that exists on the GoC slope (Borenas et al., 2002).

A layer of almost pure Mediterranean water can be found at the base of the MO on the GoC slope, and the height of this layer is less than half of that of the height of frictional influence (Ekman layer) from the bottom (Johnson et al., 1994). In areas with a high ratio of height (H) over the thickness of the Ekman layer ($D = \pi(2A/f)^{1/2}$ where A is the eddy viscosity coefficient and f is the Coriolis force), the bottom layer will be laterally sheared to lie at an angle to the rest of the plume (up to 45° if H/D = ½ (Gammelsrod, 1975)) which tends to cause lateral spreading. As the plume thins into the GoC, H/D decreases and the angle of veering also decreases, reducing the tendency of the plume to spread as it passes into the North Atlantic. In addition to the direct influence of this shearing, which is termed Ekman veering, friction acts on the plume as a whole, generally causing the flow to spread laterally and descend the slope (O'Neill-Baringer and Price, 1999). The magnitude of the frictional force is largely dependent on bottom drag and plume height (Price and O'neill-Baringer, 1994).

The height of the MO plume (H) will be proportional to the flux. D will not vary significantly through time, so that the effect of reducing H will be to decrease the angle of veering, thus reducing the amount of spreading. Reduced H will also decrease $\Delta\rho_{atl}$, thus further reducing the tendency of the plume to spread laterally. Stream tube models have shown that the splitting behaviour is probably caused by the high topography of the GoC slope acting on the MO current as it spreads laterally (Borenas et al., 2002), and reduced spreading would thus diminish the capability of topography to induce flow splitting. The MO is therefore expected to form a more narrow, more coherent (single?) plume of water during the LGM compared to today.

The above is a schematic representation, which will be complicated by the fact that the proportion of mixing in the first 100km from the Strait of Gibraltar (b/a) may not be constant. A smaller MO flux would be expected to mix and lose its negative buoyancy faster, and b/a is therefore expected to be greater than today. If b/a is not constant, the final settling depth of the plume does not vary linearly with g', and therefore is not fully predictable from the MO salinity (S_{MO}). It is conceivable that the effects of increased relative entrainment could cause the MO to settle at shallower depths during the LGM, despite the increase of g'. To overcome this uncertainty, the LGM flow path of the MO must be found within the GoC, as this is diagnostic of the relative change in density the plume has experienced.

Sedimentary Processes under the modern MO

A large sediment body, the Gulf of Cadiz contourite, has formed as a result of the activity of the MO plume on the GoC slope. This extends from Cape Spartel in the southwest to Cape St. Vincent in the northwest and the sediment generally fines north-west and down slope as the current decelerates (Kenyon and Belderson, 1973). Figure 2 shows an interpretation of sidescan sonar data for the GoC contourite drift, which can be divided into 5 parts (Hernandez-Molina et al., 2003). Four of these chart the declining velocity of the MO across the GoC margin.

The south-east area (region 1 in Fig. 2), where the MO displays velocities of 1.4 m s^{-1} (O'Neill-Baringer and Price, 1999), is characterised by sand deposition, abrasion surfaces and erosional surfaces with rock outcrops (Kenyon and Belderson, 1973). On the downslope flank of the drift in region 1, a high levee of sand marks the lower edge of the drift where the velocity of the MO decreases (Hernandez-Molina et al., 2003). Current meter studies show that some water spills over the levee, passing further downslope to contribute to the lower (MO2) flow (O'Neill-Baringer and Price, 1999). Offshore of Cadiz between regions 1 and 3, the flow becomes complicated by the high topography. The Cadiz and Guadalquivir Ridges deflect the MO for a short distance downslope in the area north of the Gil Eanes channel (Fig. 2).

Regions 3 and 4 (Fig. 2) are characterised by branching and anastomosing channels, and include the areas of maximum contourite deposition (eg. the Faro drift). Though the MO is forced to spread and split by the ridges it passes over in this region, most of

Figure 2

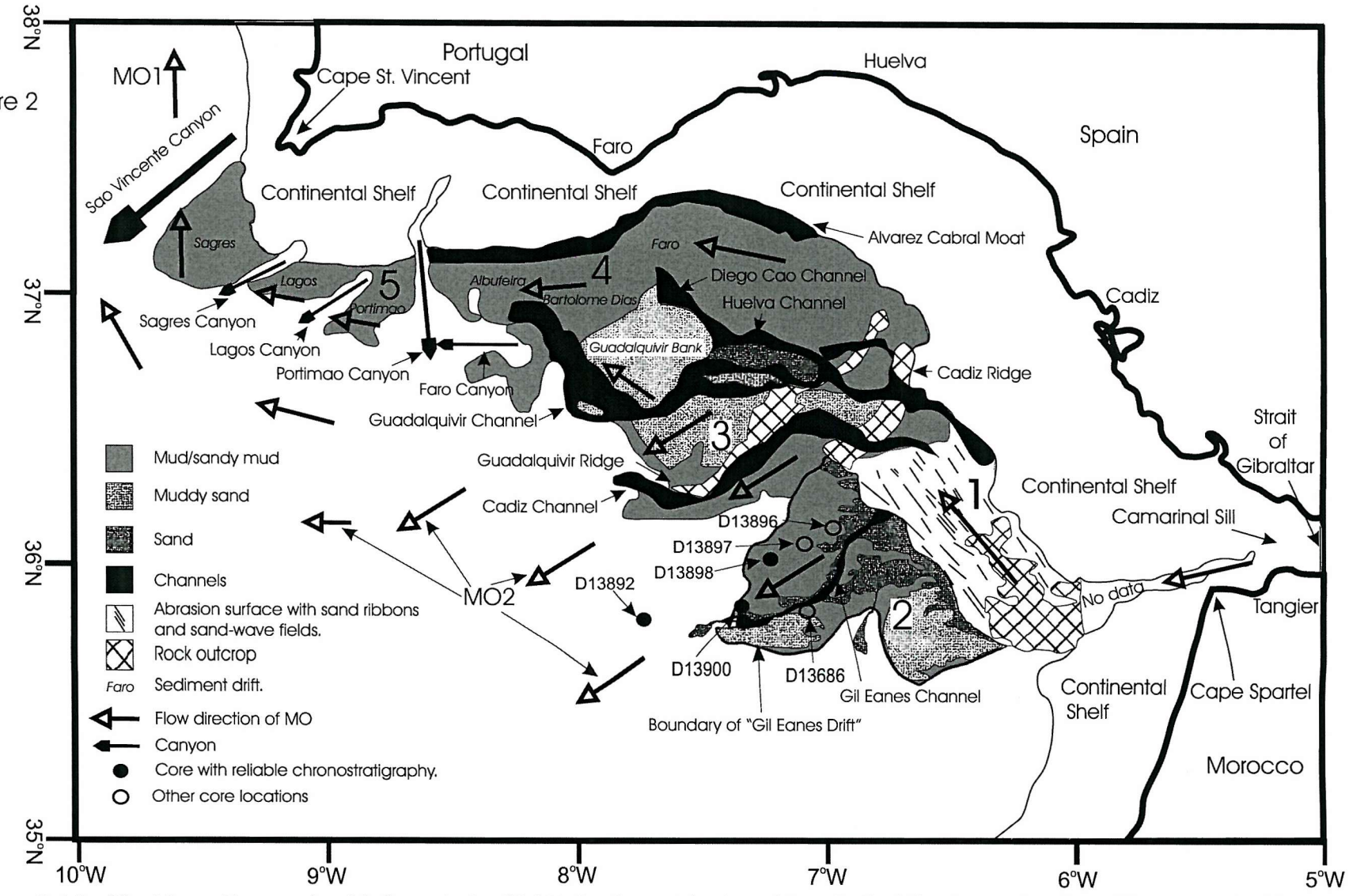

Figure 2. Modified from Hernandez-Molina et al., (2003). Sediment facies of the Gulf of Cadiz contourite drift as revealed by sidescan sonar data. Core locations are indicated.

the flow coalesces before it rounds Cape St. Vincent and it is this water that constitutes MO1 (Iorga and Lozier, 1999). Region 5 (Fig. 2) is the most distal, and much of the MO here has lifted off the sediment surface. The velocity has also dropped low enough for mud-dominated deposition to occur (0.3-0.6ms^{-1} (O'Neill-Baringer and Price, 1999)). This area is characterised by muddy sediment drifts dissected by large canyons.

The overspill lobe sector (region 2 in Fig. 2), called the Gil Eanes Drift hereafter and of which the Gil Eanes channel is part, is different in character. The Gil Eanes channel is a downslope channel between 1.5 and 3km wide that extends 40km downslope between 900 and 1500m water depth. MO water that has spilt over the levee of the main sediment drift (region 1) slowly descends the slope in this area (<0.5ms^{-1}, (O'Neill-Baringer and Price, 1999)) to form the deepest parts of MO2 (Iorga and Lozier, 1999). Though some sand is transported down the axis of the Gil Eanes channel to form an irregular sand body at its termination today, most of the Gil Eanes Drift is the site of muddy sediment deposition (Habgood et al., 2003; Hernandez-Molina et al., 2003).

Material and Methods

The chronostratigraphic framework for D13898 is based on 10 AMS radiocarbon dates performed on >6mg of clean handpicked planktonic foraminifera from the >150μm fraction. The radiocarbon analyses were undertaken via the NERC Radiocarbon Laboratory (NERC-RCL), at the University of Arizona NSF-AMS facility (Table 1). The datings have been calibrated using the OXCAL program, and the point of maximum probability is used as the age determination in each case (Fig. 3a). In the case of the oldest two dates, the Laj et al (1996) correction has been used. A 400 year reservoir age correction (ΔR) has been used in all cases. The same method was used to calibrate 4 radiocarbon dates from D13686, with the latter three being done using the Laj et al (1996) correction (Table 1).

Core D13898 was taken from the distal part of the Gil Eanes Drift (Fig. 2) and consists of mud that is visually homogeneous throughout. There is no evidence of turbidite activity in the core, nor on the entire Gil Eanes Drift (Habgood, et al., 2003). D13900 was recovered 13km to the SW of D13898 (Fig. 3) and consists of similar

Figure 3a

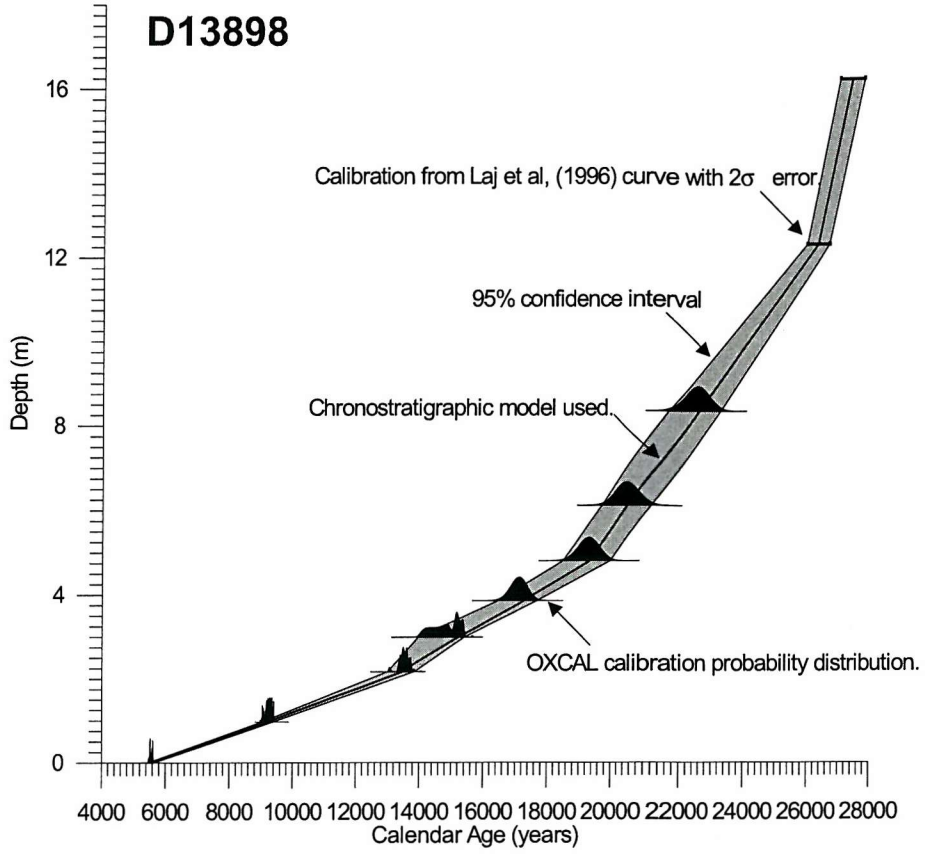

Figure 3b

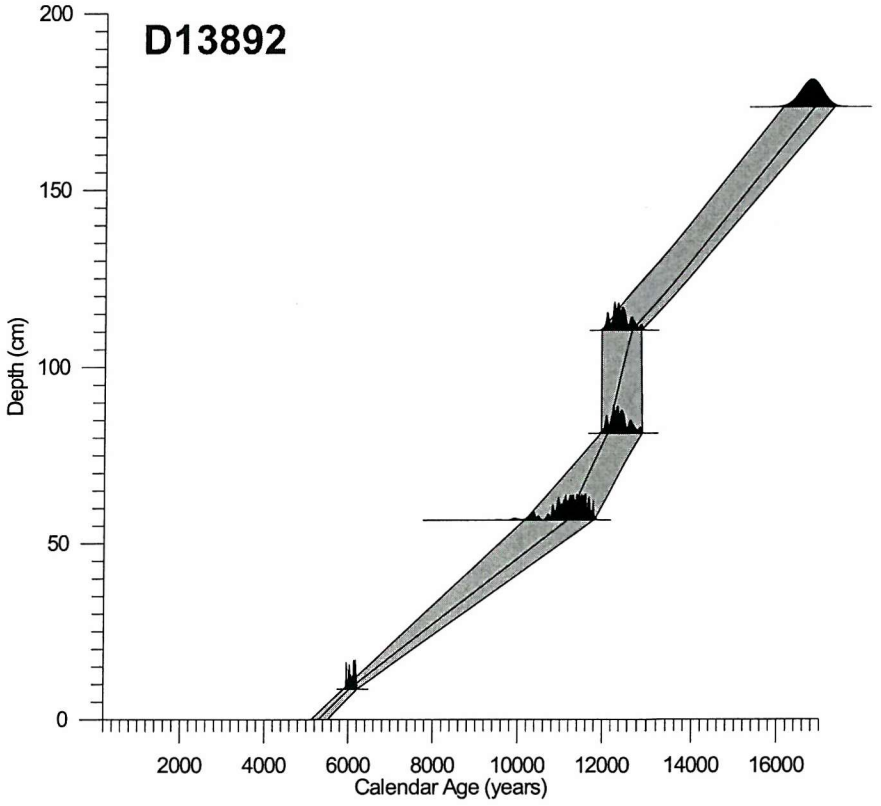

Figure 3. Accumulation rate in D13898 and D13892 derived from radiocarbon age determinations.

muddy material, except for an interval of very fine sand between ~2m and ~4m depth. The chronostratigraphic framework for D13900 has been constructed by correlation of the oxygen and carbon isotope records with D13898. This age model is further supported by planktonic foraminiferal assemblages records (Figs. 4 and 5). As this record contains a sand layer with evidence of reworked grains the age model shown is approximate before the last deglaciation, which is expressed as a strong and synchronous event in the D13900 records. Significant markers during the latter part of the last glaciation in D13898 are the disappearance and recovery of *Globigerinoides ruber* during the LGM (~16 - 20kyrs), which are also well expressed in D13900.

Core D13892 is a 2m long kasten core taken from the GoC, west of the region of MO interaction with the sea floor. The chronostratigraphic framework for this core is based on 5 radiocarbon dates (Table 1) prepared and processed in the same manner as those for D13898 (Fig. 3b). There is no evidence of the presence of turbidites or hiatus within this core.

For the planktonic foraminiferal abundance study, samples were disaggregated, washed and sieved to remove all material finer than 150μm using demineralised water. Where necessary, samples were then split into suitable aliquots of at least 300 individuals for identification according to the taxonomy of Hemleben et al., (1989). The data are presented as percentages of total planktonic foraminiferal number. The foraminiferal sample preparations were used to also obtain rough grain-size information. Data are presented as percentage weight of four grainsize fractions (<63 μm, 63-125 μm, 125-150 μm and >150 μm) for each sample. The specimens selected for stable isotope analyses were washed and sonicated in methanol to remove surface contamination. Analyses were carried out on 7-15 individuals of *N. pachyderma* (d) between sizes of 150 and 212μm or 6-15 individuals of *Globigerina bulloides* from a 190 to 210μm size window. Stable isotope analyses were carried out using a Europa Geo 2020 mass spectrometer with individual acid dosing. The stable carbon and oxygen isotope ratios are expressed as δ values, in per mil (‰), relative to the Vienna Peedee Belemnite standard (Coplen, 1988, 1994).

Results

Figure 4 shows the oxygen isotope records for *G. bulloides* and *N. pachyderma* (d) for D13898. Also shown is the oxygen isotope record for *N. pachyderma* (d) for D13900 and abundance of *G. ruber* and *N. pachyderma* for both records. There is some complexity in the thermal history of this area, and $\delta^{18}O_{N.\ pachyderma}$ for D13900 resembles that of $\delta^{18}O_{G.\ bulloides}$ for D13898 and $\delta^{18}O_{N.\ pachyderma}$ in D13898 displays slightly heavier isotope values. This is related to the past presence of the Azores Front in the GOC, which caused strong horizontal thermal gradients to be present in this area (Chapter 4). Figure 5 shows the abundance records of the abundant planktic foraminiferal species in D13898, D13900 and D13892.

The 63-125 μm fraction is similar in all samples from D13898 and D13900 and also in other sandy samples on the Gil Eanes Drift (see Fig. 2). It is siliceous with a high content of quartz and lithic fragments. There is much black, oxidised wood and in some samples there is also some soft, brown plant material. Benthic foraminifera become very abundant in the most sandy samples of D13900, and include many species characteristic of the shelf such as *Planorbulina mediterranensis*, *Elphidium crispum* and *Ammonia beccarii*. The benthic foraminiferal assemblage and petrology are similar to that found in sandy sediments deposited at the termination of the Gil Eanes channel today, indicating that they originate from the same source. The 63-125μm fraction of D13898 is almost exclusively made up of siliciclastic sand, whereas the >150 μm fraction almost exclusively consists of planktonic foraminiferal tests. Both cores show a significant decrease in grainsize occurs at the last glacial termination (1a) (Fig. 6). In D13900 this is very sharp, dropping from ~90% >63 μm to ~10% >63 μm. In both records, the Younger Dryas is also marked by a relatively sandy layer.

The accumulation rate of D13898 shows a decline up core (Fig. 3a). This indicates a reduction in the sedimentation rate by a factor of five for the Holocene compared to the sediment older than 25,000 years. Variable accumulation rate has resulted in increased dilution of the planktonic tests in the lower part of the core, causing the >150μm in D13898 to appear to decline during periods of high accumulation. This fraction is thus not fully representative of local energy, and this core is best

Figure 4

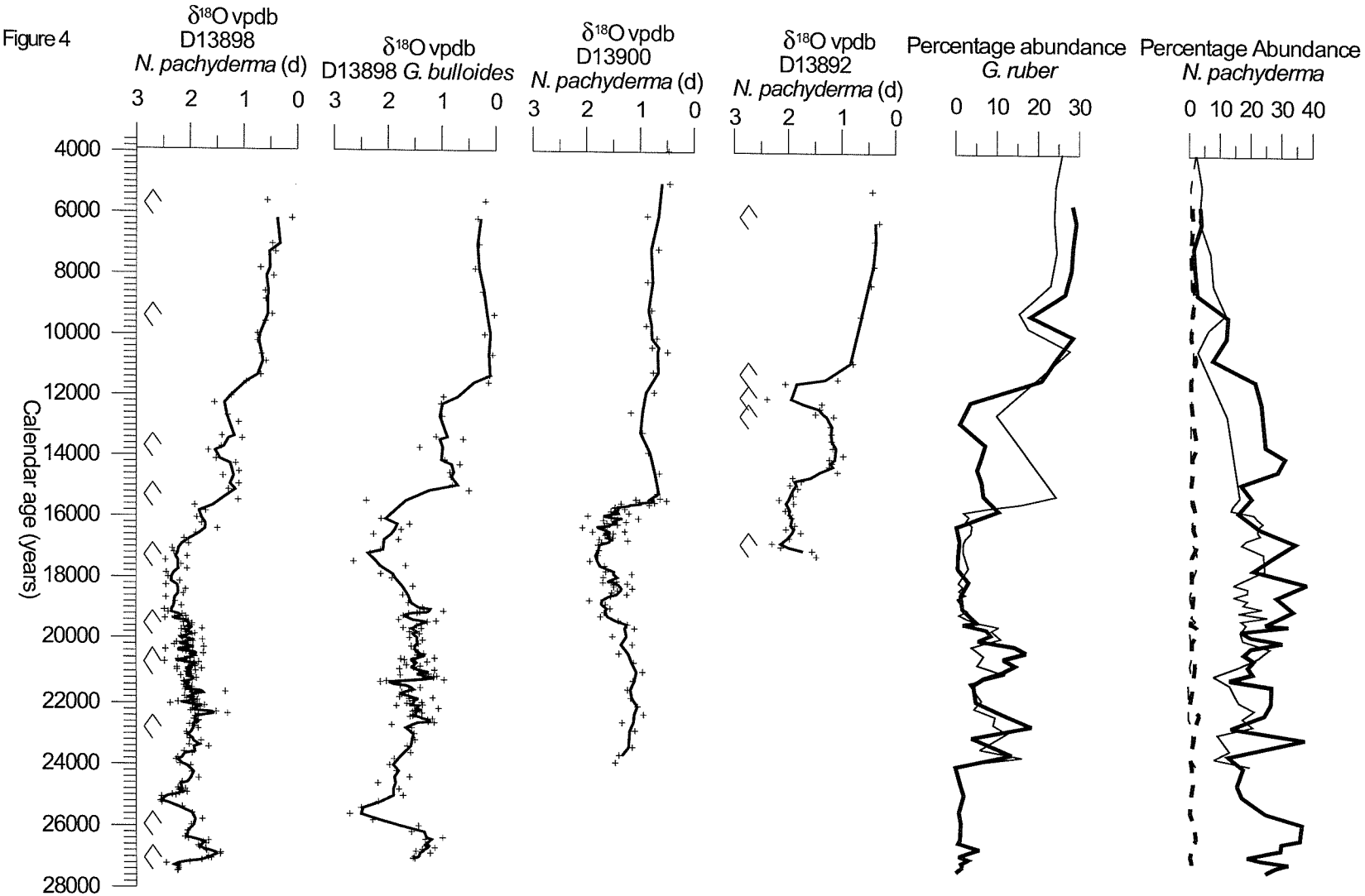

Figure 4. $\delta^{18}O$ and abundance records of *G. ruber* and *N. pachyderma* for D13900 and D13898. In $\delta^{18}O$ plots, 3 point moving averages are shown Diamonds represent ^{14}C age determinations in D13898 and D13892. In abundance plots, thick lines represent D13898 and thin represent D13900. For *N. pachyderma* broken and continuous lines represent sinsitral and dextral respectively.

Figure 5.

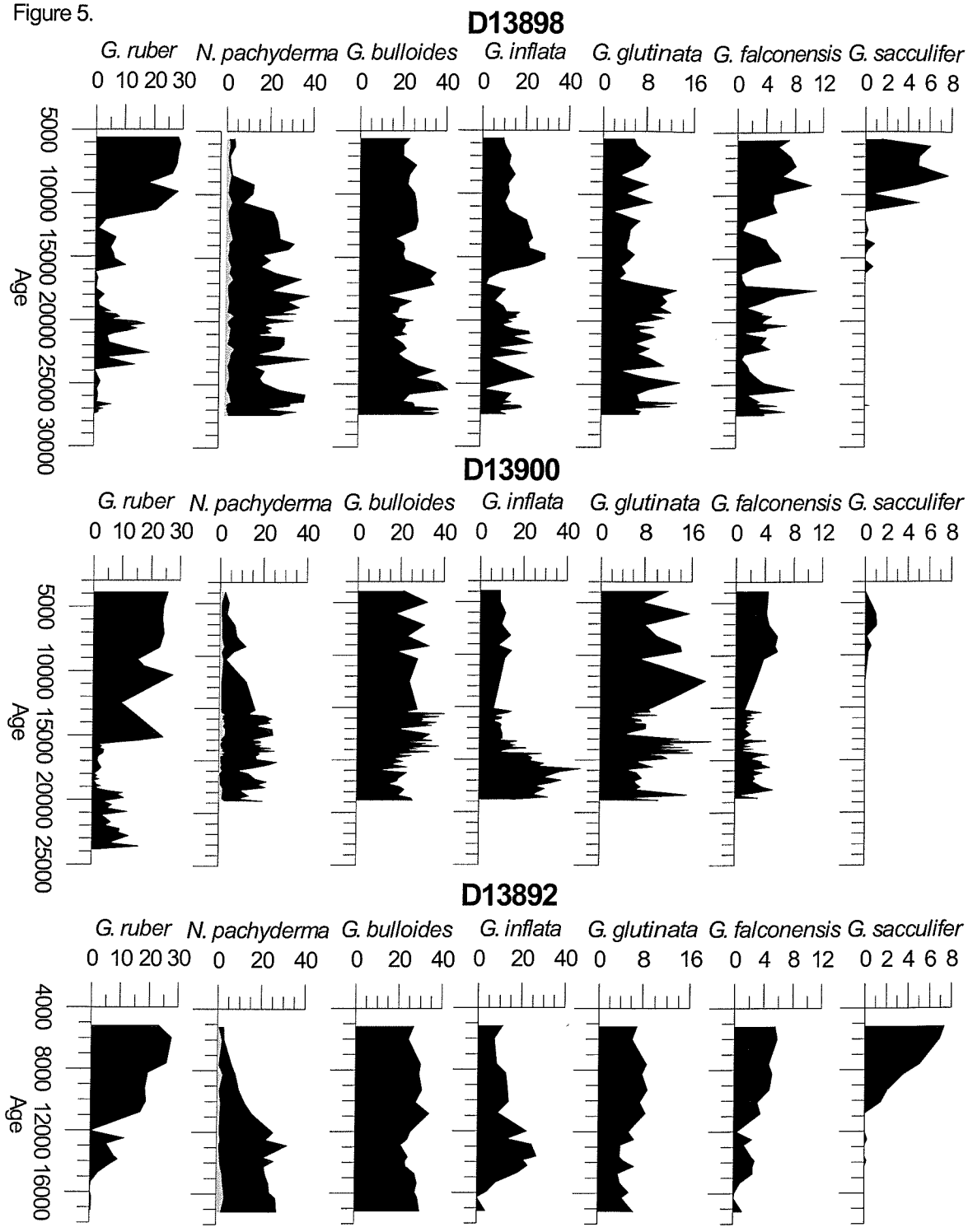

Figure5. Abundance records of major planktonic foraminiferal species in D13898, D13892 and D13900. For *N. pachyderma*, black represents dextral and grey represents sinistral. Ages are in calendar years.

considered without this fraction (Fig. 6c) The upper parts of giant piston cores may be stretched during recovery, often by as much as a factor of 2 (Thomson et al., 2000; Thouveny et al., 2000). If this is the case here, the true rate of sedimentation may have reduced by as much as an order of magnitude during the last deglaciation.

Discussion

Accumulation was slower in D13898 during the Holocene compared to the glacial (see Fig. 3a), indicating that more sediment was being supplied to the Gil Eanes Drift and that less was being trapped further upslope than it is today. This is consistent with the interpretation that the current was less active in its present course during the LGM compared to today (Nelson et al., 1993). The presence of increased sand in D13898 during the last glaciation is diagnostic of increased flow velocity at this location at that time. Though they lack definite age determination, other giant piston cores (e.g. D13897) from this flank of the Gil Eanes Drift have similar downcore grainsize trends as D13898. This observation supports the inference of generally increased current velocity on the Gil Eanes Drift during the past.

Core D13900 is located at the termination of the Gil Eanes channel and hence its composition is controlled by the rate of sediment transport down the axis of the channel. There is little evidence of turbidite activity in this location. Moreover, the deposit formed by the Gil Eanes channel thickens basinward, the channel does not branch and it has symmetrical sediment waves on its levees. These observations are inconsistent with a gravity-flow origin of these deposits, and the downslope channels in this area are consequently thought to be formed solely from downslope flow of the MO (Habgood et al., 2003). The upward coarsening of the sandy layer in D13900 after 20ka BP (Fig. 6) years is indicative of a prograding sediment lobe. The dramatic decline in the amount of sand transported down the axis of the Gil Eanes channel, recorded as a rapid switch from sand to mud deposition in core D13900 (Fig. 6), suggests that this lobe was abandoned rapidly during the deglaciation.

The increased energy of the MO flow on the Gil Eanes Drift during the LGM confirms the hypothesis that the MO plume should be settling to greater depths made on the basis of the physical constraints of the system. The inference of strong flow on the Portuguese margin at 2000m during the LGM (Schönfeld and Zahn, 2000) is also

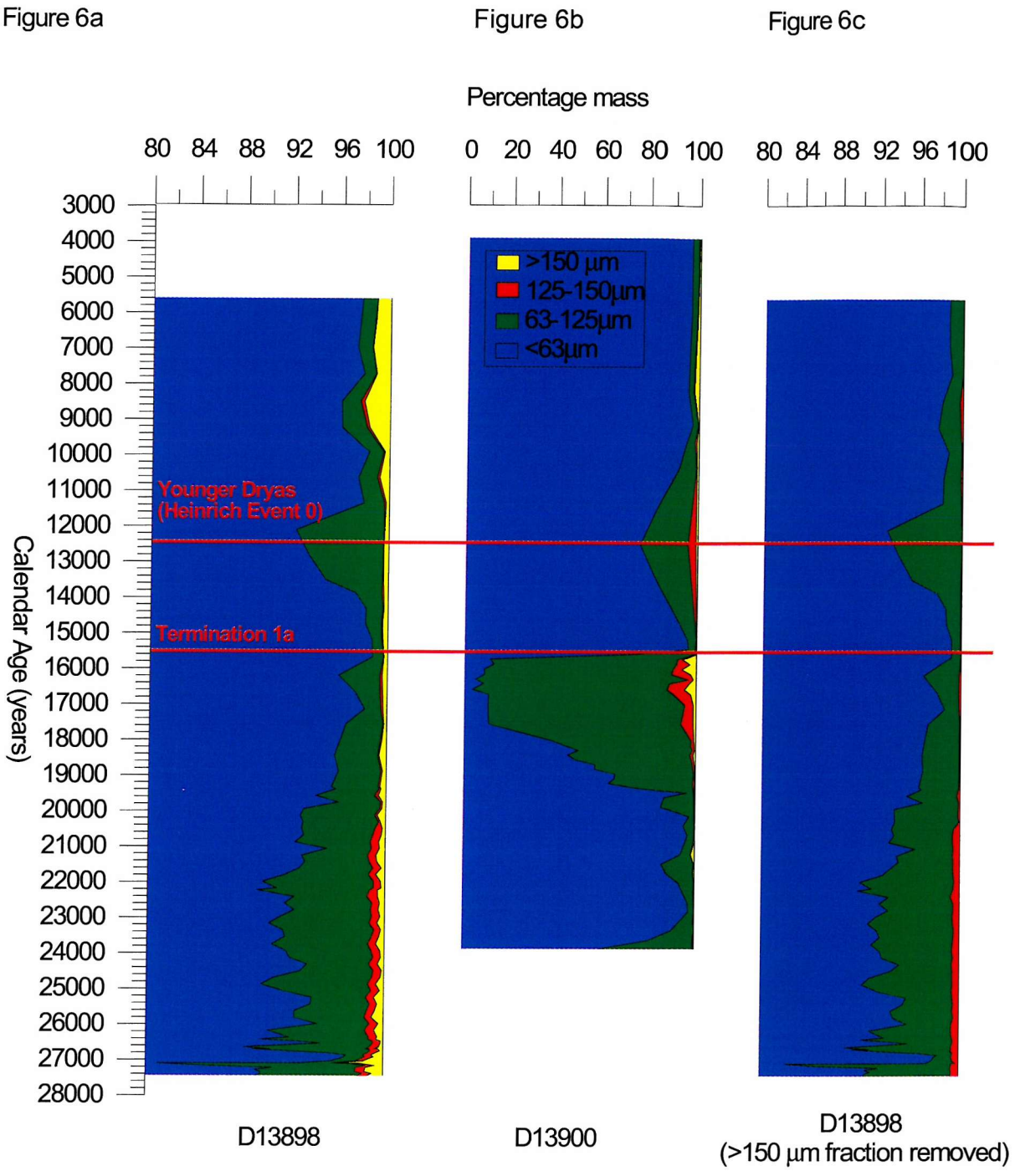

Figure 6a and 6b show Grainsize data for D13898 and D13900. Each of the four grainsize fractions are represented as percentage of total dry mass. The >150 µm fraction of D13898 is excluded in Fig. 6c, which is shown as percentage of dry mass finer than 150µm.

consistent with this reconstruction. This suggests that the settling depth of the main MO flow core has changed from ~800m today (Iorga and Lozier, 1999), to ~2000m at the LGM, indicating that the MO was settling to greater depths by roughly a factor of 2.5 compared to today. This change is similar to the change in g', which is predicted to have increased by a factor of at least 2.46 by the hydraulics of the Gibraltar exchange (Rohling and Bryden, 1994). The past behaviour of the MO therefore can be assumed to be dominated primarily by the hydraulics of the Strait of Gibraltar and not by changes in the amount of mixing in the GoC.

Radiocarbon and isotopic investigation of a sandy core from the Gil Eanes Drift (D13686) shows a thin (20-30cm), layer of Holocene age (4150 – 4525 calendar years in D13686) that is discoloured and overlies un-discoloured sand with cold water planktonic fauna similar to the glacial assemblages in D13898, D13900 and other records from the area (eg. (Sierro et al., 1999)) and heavy oxygen isotope signatures (~1 to 1.5‰). Three radiocarbon dates from this part of D13686 indicate calendar ages of ~27903, ~29560 and ~29970 years bp. Individuals of *N. pachyderma* (d) with glacial oxygen isotope signatures are found in the Holocene layer along side characteristic Holocene species such as *Globigerinoides sacculifer*, indicating that much of the sand deposited at this time has been reworked from the glacial deposits. The core top of D13896 shows a similar mixed planktonic foraminiferal assemblage as in the core top of D13686 and again individuals of *N. pachyderma* (d) with oxygen isotope signatures typical of glacial conditions (~1.5‰) extend to the core top, indicating significant reworking of glacial age material. Below the core top, the D13896 record is characterised by glacial assemblages and heavy oxygen isotopes ratios (1.5 – 2.5‰). This indicates that at both locations sand was being supplied during the last glaciation, confirming that the MO current was active at this location at this time, but there has been no significant supply of sand during the Holocene. This has allowed only the deposition of a thin, condensed layer that has been chemically altered in D13686. Cores recovered from channels on the northern margin of the Gil Eanes Drift (close to D13896) show that these are now the sites of muddy deposition, and the sand is buried (Habgood et al., 2003). There is little evidence for the transportation of sand during the Holocene outside of the axis of the Gil Eanes channel itself. The Gil Eanes Drift can therefore be considered as being a glacial age sandy drift that is now becoming draped by Holocene mud or that is the site of little

deposition. If the Gil Eanes Drift were interpreted as the LGM Mediterranean Outflow sediment drift, this would be consistent with the prediction that the current should interact with a greatly reduced area of sea floor, as a result of reduced spreading. This interpretation is shown in Figure 7.

The sand found in both D13898 and D13900 during the Younger Dryas cannot be ascribed to the influence of lower sea level, as sea level was roughly static through this period and rising during the preceding Bølling-Allerød. This indicates that the MO has been influenced by some other mechanism at this time. Particularly intense MO activity has been recognised on the GoC slope elsewhere than the Gil Eanes Drift during the Younger Dryas, and it is at this time that the MO returns to its modern position on the slope (Faugères et al., 1986; Nelson et al., 1993). A large export of fine material from the drift region during the Younger Dryas is inferred from core D13892, which shows very rapid accumulation (~50cm kyr^{-1} see Fig. 3b) of terrigenous material (mainly clay and silt with some very fine sand) comparable to that found on the Gil Eanes Drift. This layer stands in contrast to the Holocene in this core, which shows slower accumulation (<10cm kyr^{-1}) of carbonate rich mud with no terrigenous fine sand grains.

Increased deep flow during the Younger Dryas may be explained by 1, increased buoyancy loss due to cold SST; 2, increased buoyancy loss due to increased aridity / net evaporation (Gasse and vonCampo, 1994; Grousset et al., 1998; Cacho et al., 2000; Bateman and Diez-Herrero, 2001; Roucoux et al., 2001); 3, purging of highly dense deep waters formed in the basin under glacial conditions (Myers et al., 1998). The onset of increased flow in D13898 coincides well with meltwater pulse 1a (Bard et al., 1996). As the Mediterranean does not turn over instantaneously (100 years today, probably more during the LGM (Rohling and Bryden, 1994)), a rapid sea level rise of 10's of metres would place ΔS_{gib} out of equilibrium with that calculated from equation 3. A rise of ~20m from ~-100m relative to today (Bard et al., 1996) would cause a disequilibrium in ΔS_{gib} ~0.47psu. This would enhance any buoyancy loss caused by the reasons outlined above, and would decline until equilibrium is re-established

Figure 7

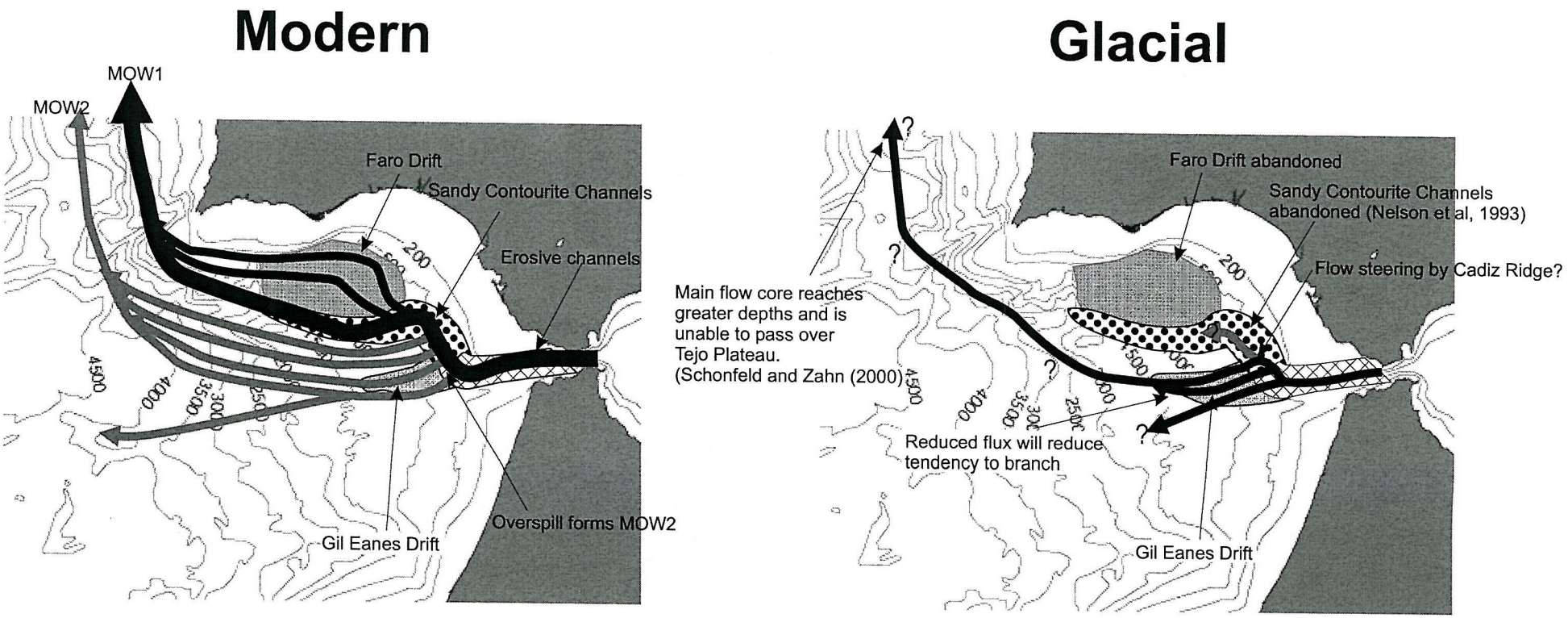

Figure 7. Position of the MO flow pathway today, and interpretation of the pathway of the MO during the LGM.

Conclusions

The observation of reduced flow in the flow path of MO1 during the last glacial maximum (Nelson et al., 1993) and the synchronous deposition of significant sand under the flow path of MO2 indicates that most of the flux of the MO followed the course of the latter at that time. The Gil Eanes Drift was therefore within the flow path of the MO on the GoC slope during the last Glaciation and this repositioning of the MO during the LGM away from its modern pathway to the Gil Eanes Drift is consistent with the behaviour of the MO being dominated by the hydraulics of the Strait of Gibraltar. The behaviour of the MO plume in the Atlantic is therefore regulated by sea level. That the Gil Eanes Drift was the flow path of the LGM plume is also consistent with the observation of Schönfeld and Zahn (2000) that the MO settled to greater depths during the LGM, the main axis of the flow probably lying close to 2000m. This change of settling depth is proportional to the predicted change in g' at the western end of the Strait of Gibraltar, and so there appears to be relatively little influence from altered net evaporation in the Mediterranean basin or changes in the relative volume of mixing as the MO passes into the Atlantic at this time. This does not indicate that there was no change in these two systems, but their influence was certainly relatively small. At a depth of 2000m, the MO plume would be unable to supply any salt to the GIN and if the assertion of Reid (1979) is correct, this would significantly retard the formation of NADW, thus slowing the global thermohaline circulation.

The Younger Dryas is a time of generally enhanced flow on the GoC sediment drift, but cannot be related to the direct effect of sea level on the Gibraltar Exchange. It is probable that enhanced flow is related to the response of the exchange to meltwater pulse 1a and increased buoyancy loss over the Mediterranean due to low temperatures and high aridity at this time.

Table 1. Stratigraphic position of radiocarbon datings. Conversion from conventional to calendar years is done with the OxCal program. A 400 year reservoir correction has been used.

Sample depth (cm)	Conventional radiocarbon age	1σ	Predicted calendar age
D13898			
0	5227	42	5500
100	8615	55	9270
220	11642	89	13480
300	12796	73	15190
380	14716	86	17200
480	16480	120	19390
608	17600	110	20600
834	19340	120	22600
1234	23010	180	25963.17*
1628	24040	200	27061.53*
D13892			
8	5647	45	6010
56.7	10429	56	11210
71	10868	59	12040
110	10868	58	12660
173	14353	76	16800
D13686			
17	4336	66	4450
42.2	24455	193	27903*
74	26488	123	29970*
83.6	26074	125	29560*

* Conversion done using Laj et al. (1996) curve.

Chapter 6:- Colour Logging as a Tool in High Resolution Palaeoceanography.

Abstract

Colour and diffuse reflectance records have been proposed as a means of developing astronomically tuned age models for long sediment cores (Ortiz et al., 1999; Grutzner et al., 2002). Here, we present high resolution (1mm) colour records from a sediment core (D13892) spanning the last deglaciation that are shown to correlate with stable isotope (^{18}O) and Sea Surface Temperature proxy data. An age model developed from AMS radiocarbon dating is also presented. Comparison between the colour record of D13892 and the GISP2 oxygen isotope series is reasonable ($R^2 = 0.81$) and confirms that sediment colour reflects the state of the climate. Use of colour to develop initial age models for sediment cores records by astronomical tuning or correlation to a well constrained climatic record is therefore considered valid.

The causes of the colour variability in D13892 are also considered, and related to changes in the local particle flux. The colour of sediment has also been shown to be diagnostic of its mineralogical / chemical composition (Giosan et al., 2002). The colour records in D13892 indicate that the last glaciation and Younger Dryas were characterised by increased supply of terrigenous detritus to the western Gulf of Cadiz (southwest Spain) and this is supported by evidence from XRF-logging. This terrigenous detritus is probably supplied by the Mediterranean Outflow, and the source of the detritus seems to be southwestern Iberia.

Introduction

Colour has been considered to be diagnostic of sediment composition for some time (Mix et al., 1992 and references therein), though this concept was first applied to soils (Goddard et al., 1948). Geochemical investigation of sediment core material has shown that components of colour are reliable indicators of the important sedimentological components such as carbonate, free and bound iron, many Fe minerals (e.g. haematite, pyrite, goethite) and clay (Mix et al., 1992; Nagao and Nakashima, 1992; Mix et al., 1995; Balsam and Deaton, 1996; Giosan et al., 2002).

The dominant redox state of the iron present, both within minerals and as ions (particularly within the lattice of clay minerals), can also be reliably estimated from colour (Mix et al., 1992; Nagao and Nakashima, 1992; Mix et al., 1995; Balsam and Deaton, 1996; Giosan et al., 2002). Greyscale has been used for initial chronostratigraphic model development within long (esp. ODP) sediment cores (Ortiz et al., 1999; Grutzner et al., 2002), as it is rapidly and easily measured and dominantly controlled by the carbonate content, which is thought to be regulated by orbitally modulated insolation (Hays and Peruzza, 1972; Volat et al., 1980; Ortiz et al., 1999). Recently, a combined investigation of geochemistry and sediment colour has shown systematic variability in mineralogical and carbonate content, both predicted by colour, on Milankovitch and sub-Milankovitch (1.5kyr) wavelengths (Grutzner et al., 2002). There is therefore potential for colour to be used as a means of developing initial chronostratigraphic models for high resolution records from the late Quaternary, and even the Holocene. Here, we present sediment colour, geochemical and palaeoceanographic (planktonic foraminiferal assemblage and stable isotope) records for a sediment core from the western Gulf of Cadiz (southwest Spain) with an independent age model derived from radiocarbon age determination in order to investigate this potential.

The Gulf of Cadiz (GoC) is the large embayment to the southwest of Iberia, south of Portugal and west of the Strait of Gibraltar (see fig. 1). This location is characterised by a number of strong oceanic currents at various depths formed by the exchange of water between the Mediterranean Sea and Atlantic Ocean (Bryden et al., 1988). The exchange and the currents derived from it have wide ranging implications for circulation in both basins (Bethoux, 1979; Reid, 1979; Bryden and Stommel, 1984; Iorga and Lozier, 1999; Jia, 2000), making the palaeoceanography of the GoC highly important. The most suitable location for the development of quantitative palaeoceanographic reconstructions is the western GoC where there is a high rate of sediment supply and no current reworking, which is significant on the northern and eastern margin (Nelson et al., 1993), or significant turbidite deposition (Habgood et al., 2003). This report also aims to give an initial assessment of sediment supply to the western GoC over the last deglaciation and into the Holocene; and the implications of this supply for palaeocurrent reconstruction by means of sediment colour and sediment composition records.

Figure 1

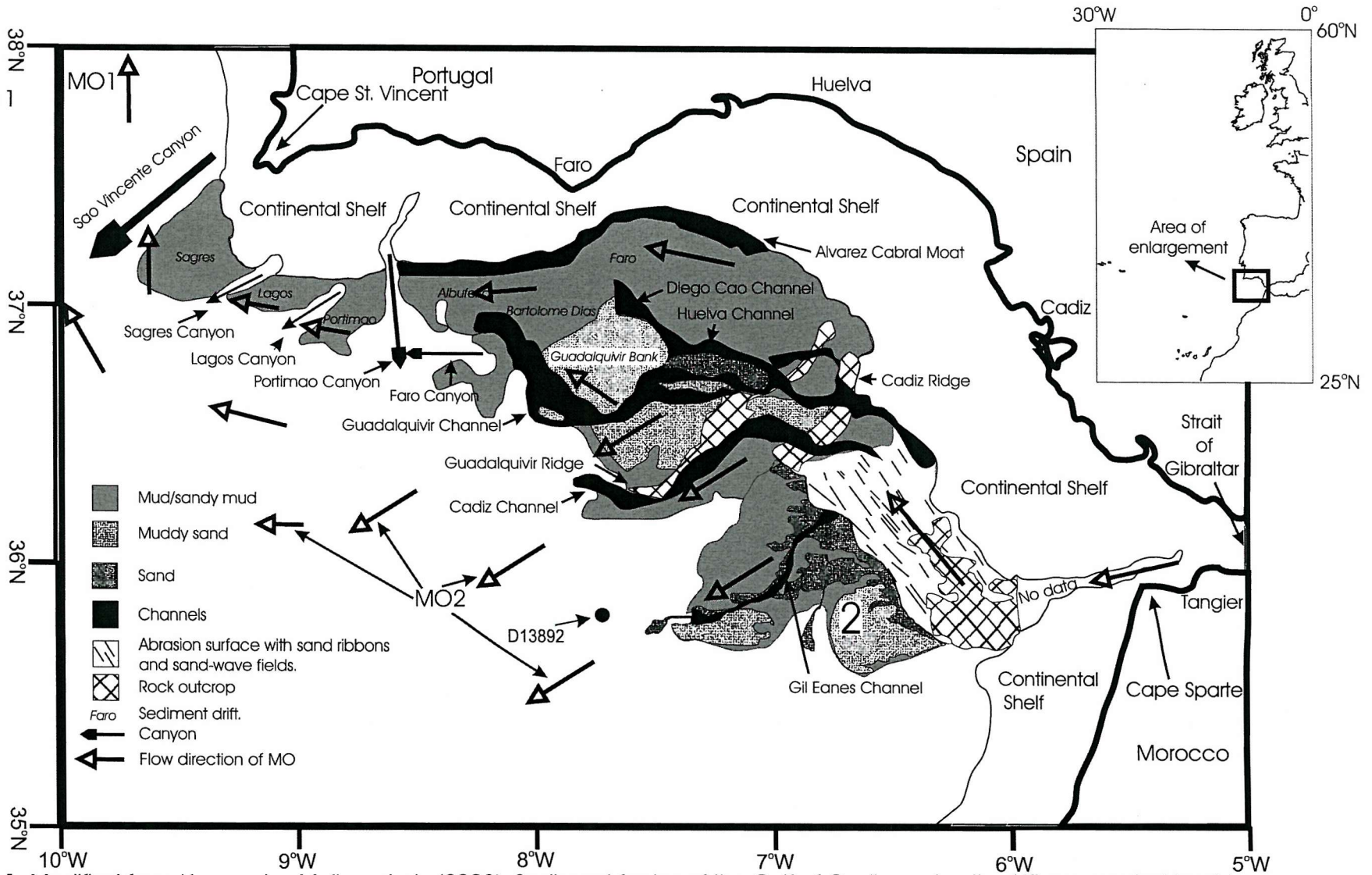

Figure 1. Modified from Hernandez-Molina et al., (2003). Sediment facies of the Gulf of Cadiz contourite drift as revealed by sidescan sonar data. Location of D13892 is indicated.

The exchange of Mediterranean and Atlantic water at Gibraltar, which lies at the eastern edge of the GoC, drives the formations of two currents (Bryden et al., 1988). The Atlantic Inflow is a shallow eastward flowing current at Gibraltar which replaces water lost from the Mediterranean by evaporation and as a deep, westward flowing component in the Gibraltar Exchange (the Mediterranean Outflow). The Atlantic Inflow current flows along the shelf from northwest to southeast and has elongated the sedimentary deposits formed at the mouths of the Iberian rivers along the northern and eastern margins of the GoC (Bryden et al., 1988; Lopez-Galindo et al., 1999). The abundant sediment supplied by the Iberian rivers (particularly the Guadalquivir but also the Guadiana, Tinto-Odiel and Huelva) is also reworked along the shelf from northwest to southeast and down onto the slope, and on the shelf sediment accumulation is rather slow (6-12cm kyr^{-1} (Nelson et al., 1999)).

The Mediterranean Outflow (MO) is a plume of warm, dense water that flows out of the Strait of Gibraltar and passes along slope between 500 and 1500m water depth interacting with the sea floor of the GoC from Cape Spartel in the south-east to Cape St. Vincent in the north-west (Kenyon and Belderson, 1973; Ambar and Howe, 1979; Iorga and Lozier, 1999). Where the Mediterranean Outflow interacts with the sea floor it profoundly influences the nature of sedimentation, transporting material along the slope from southeast to northwest (Kenyon and Belderson, 1973). In the southeast, where the flow is strongest, the path of the current is characterised by abrasion surfaces and sand ribbons and these fine northwestwards, as the flow decelerates, to become sandy and then muddy sediment drifts. Material is also transported in suspension out into the western GoC, where the MO no longer interacts with the sea floor (Ambar et al., 2002).

On the upper slope where the flow is at least partially in contact with the sea floor, the MO plume is characterised by significantly higher suspended particulate matter (SPM) content than the Atlantic water it is passing through (Ambar et al., 2002). This SPM comprises both mineral and biogenic grains, the biogenic component being dominantly calcareous. Offshore, the SPM content of water in the MO plume is significantly decreased, and more comparable to Atlantic water than the Mediterranean water found close to the shelf (Ambar et al., 2002). SPM is found in

less abundance, is generally <10μm in diameter and the biogenic component is dominantly siliceous (Ambar et al., 2002). This indicates that the majority of the SPM transported by the Mediterranean Outflow is deposited close to the region of supply and where the plume interacts with the sea floor and relatively little is transported into the western GoC today.

Material and Methods

Core D13892 is a 2m long kasten core recovered from the western Gulf of Cadiz, from a water depth of 1500m, during RRS *Discovery* cruise 249. This location is beyond where the Mediterranean Outflow interacts with the sea floor, and there is no indication of either current or turbidite activity in this core. Five radiocarbon age determinations have been performed. Analyses were performed on >6mg of planktonic foraminiferal tests picked from the >150μm fraction. The radiocarbon analyses were undertaken via the NERC Radiocarbon Laboratory (NERC-RCL), at the University of Arizona NSF-AMS facility (Bryant, pers. com, 2003).

For the planktonic foraminiferal abundance study, samples were disaggregated, washed and sieved to remove all material finer than 150μm. Where necessary, samples were then split into suitable aliquots of at least 300 individuals for identification according to the taxonomy of Hemleben et al., (1989). The data are presented as percentages of total planktonic foraminiferal number.

Planktonic foraminifera assemblages were analysed by Artificial Neural Network (ANN) to produce estimates of summer and winter sea surface temperature (Malmgren et al., 2000). The training set used was based on core tops from both the North Atlantic and the Mediterranean, as the GOC lies between these two basins (A. Hayes, personal communication).

The specimens selected for stable isotope analyses were washed and sonicated in methanol to remove surface contamination. For each sample stable isotope analyses were carried out on 7-15 individuals of *N. pachyderma* (d) between sizes of 150 and 212μm. Stable isotope analyses were carried out using a Europa Geo 2020 mass spectrometer with individual acid dosing method. The carbon and oxygen isotope

ratios are expressed as δ values, in per mils (‰), relative to the Vienna Peedee Belemnite standard, (Coplen, 1988, 1994).

Colour analysis

The surfaces of core sections to be imaged are first scraped clean with a glass slide to produce a surface that clearly shows core structure and has minimum unevenness. The core is then imaged using a GEOSCAN colour line scan camera. This is a 3 CCD device using 3 x 1024 pixel CCD (charge-coupled device) arrays that measure absolute red green and blue (RGB) colour intensities to produce a finely pixelated image of the sediment surface. Data are produced as continuous curves both down and across core, which are then averaged for each pixel area ($14\mu m^2$) to produce RGB values. These pixels are then combined into a series of bitmap files for each core, into which section number and section depth are encrypted.

A panel of the image covering a whole core, core section or part of a section may be selected visually. This allows areas of disturbed core or with poor focussing (due to very uneven surfaces or large height variation within sections) to be omitted from the final data. Downcore resolution can be set at any level up to a maximum of 100μm. Averaging pixel values down and across each depth interval then produces the final RGB curves, which shows the average red, green and blue colour intensity across the width of the selected panel for each depth interval. Data can be expressed as absolute intensity or relative intensity.

Ultimately the values are produced from continuous measurement down the length of the core, though these are averaged over depths of 1cm to 100μm. Very low theoretical periods (Nyquist periods) can therefore be resolved in these data. Data for D13892 have been produced at a 1mm resolution.

Additional analysis was done using a Minolta Spectrophotometer. Samples were taken from the core, oven dried and ground to a fine powder. This powder was poured into a well cut into a sheet of cardboard and the surface smoothed before the analysis was performed, to remove error derived from changes in water content and surface unevenness.

Several systems have been used for parameterisation of sediment colour in the visible wavelengths. The most commonly used is the L*a*b* system, which is a three dimensional Cartesian system that defines the position of a particular colour spatially. The space defined by this system approximates a cylinder, with L* (which is the lightness of the sediment) defining the length of the axis and a* and b* defining the position of a point within a quasi-circular normal section. The position in this normal section can be more naturally approximated by considering a radius (termed *chroma* (C), an estimation of the deviation from a grey of given lightness) and H, an angle from east (termed *hue*) (Giosan et al., 2002). Lightness (L) and hue (H) have been shown in numerous studies to be sensitive to the carbonate composition and the content and redox state of iron respectively (Mix et al., 1992; Nagao and Nakashima, 1992; Mix et al., 1995; Giosan et al., 2002). However, the response of colour to chemical and mineralogical changes is non-linear, and quantitative estimation of sediment composition is difficult. Here, colour data are supported by chemical data produced by X-ray fluorescence (XRF) analysis.

Chemical analysis was done with the Cox Analytical Systems XRF logger at Southampton Oceanography Centre. This unique system uses capillary optics to focus an X-Ray beam produced from a molybdenum filament onto the surface of a split core. A stepper motor allows the core to be moved by 400μm increments, and at each increment the core is irradiated. The atomic fluorescences produced are collected by an analyser held close to the surface of the core on an automated arm. The intensity of fluorescence peaks at the characteristic wavelengths of elements of interest are recorded for each step, providing a 400μm resolution record for that element throughout the analysed section. These records are shown smoothed by a 5 point running average.

Chronostratigraphic Framework

The radiocarbon dates were calibrated to calendar ages using the OXCAL program (www.rlaha.ox.ac.uk/orau/oxcal.html), assuming a 400 year reservoir age. OXCAL calibrates ^{14}C in the same manner as the Calib method (Stuiver, 1986). However, while the latter gives only the highest probability point and standard error for the calibrated value, OXCAL gives a complete probability breakdown for the calibration.

Figure 2.

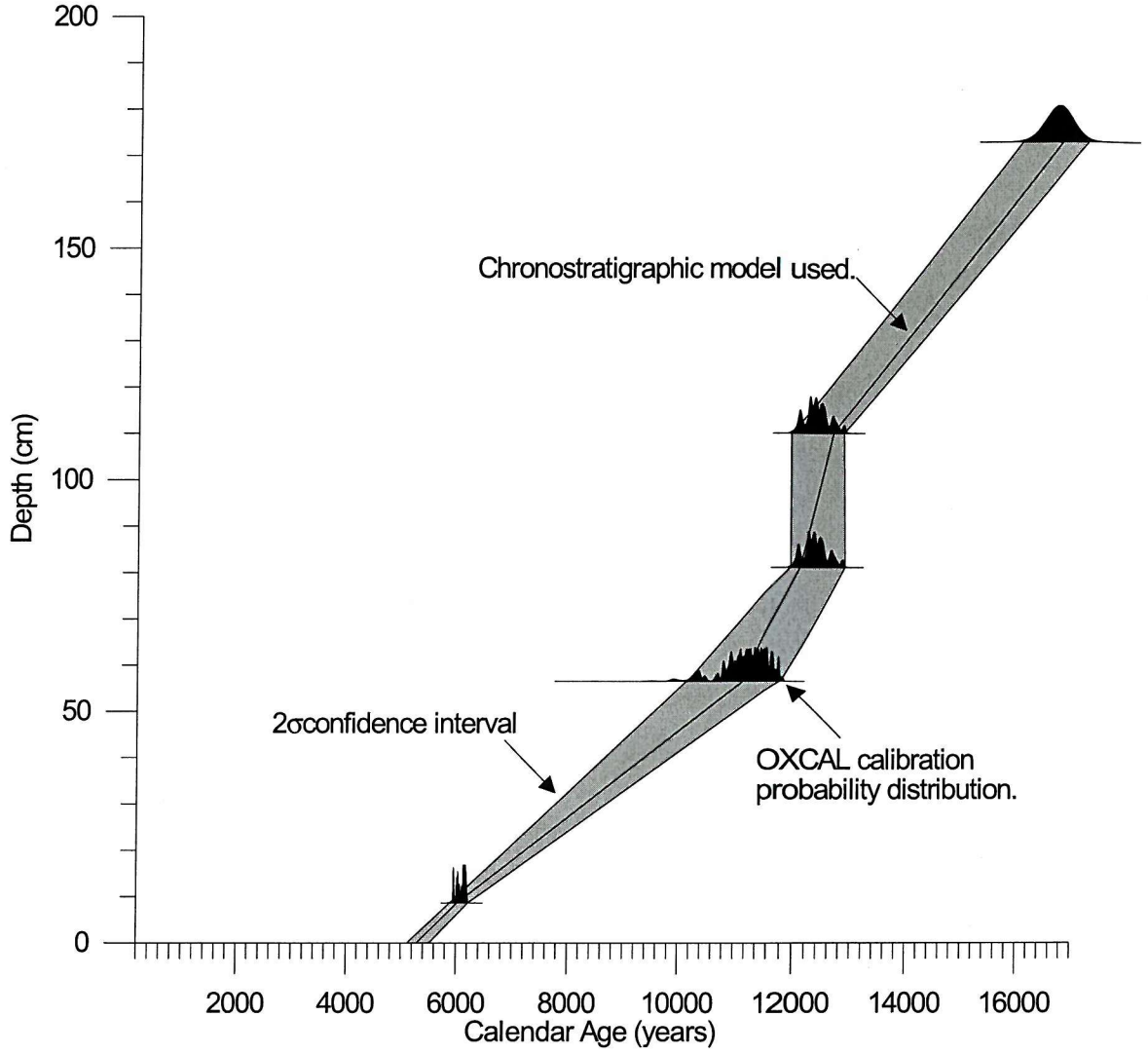

Figure 2. Initial chronostratigraphy for D13892

Figure 2 shows the position of the calibrated radiocarbon dates, the probability distribution of their calibrations to calendar age and the 95% confidence interval of possible age-depth correlations. This approach provides 1) a chronostratigraphic "envelope" through which the final chronostratigraphic model must fit and 2) information regarding not only the age of maximum probability of each ^{14}C measurement, but the ages and relative probabilities of the secondary and tertiary probability peaks. An initial chronostratigraphic model is developed from this plot (shown in black), and represents the smoothest line of best fit between peaks of high probability. It is assumed that major events, such as the warming at the termination of the last glaciation and the start and end of the Younger Dryas are synchronous between this location in the North Atlantic and Greenland. The chronostratigraphic model for D13892 can therefore be confirmed and fine-tuned by correlating these events in the D13892 $\delta^{18}O$ record to the GISP2 series. Further support can be gained by comparison with the lower resolution SST record. Figure 3 shows the SST and oxygen isotope data on this final chronostratigraphic model relative to the GISP2 isotope series, with the correlation points marked.

The adjustment made to the chronostratigraphic framework during the fine-tuning process is small (individual corrections were <500years (see table 1)) and correlations were rejected that caused the model to fall out of the 2σ confidence interval defined by the ^{14}C determinations. Terminations 1a and 1b are well recognised in both the $\delta^{18}O_{N.\ pachyderma\ (d)}$ and ANN summer SST records in D13892, and these were corrected to the GISP2 chronology by +411 and +184 years respectively. A strong cooling is noted in the D13892 records just prior to Termination 1b, and this is interpreted as the Younger Dryas. A further tie point (at 13000 years) is therefore included at the position of the last "warm" (ANN summer SST > 18°C; $\delta^{18}O_{N.\ pachyderma\ (d)}$ <1.25‰) data point prior to this. Although an alternative correlation for this point exists (at the point marked with the letter "A" on figure 3), the correlation used above is preferred as the latter would cause this part of the age model to fall outside of the ^{14}C 2σ envelope. In addition, the cooling represented in the D13892 proxy curves subsequent to the tie-point used probably represents the termination of the Bölling-Allerød, which would be displaced by 600 years relative to the GISP2 record if the alternative correlation were used. Prior to Termination 1a, a number of oscillations are noted both in $\delta^{18}O_{N.}$

Figure 3

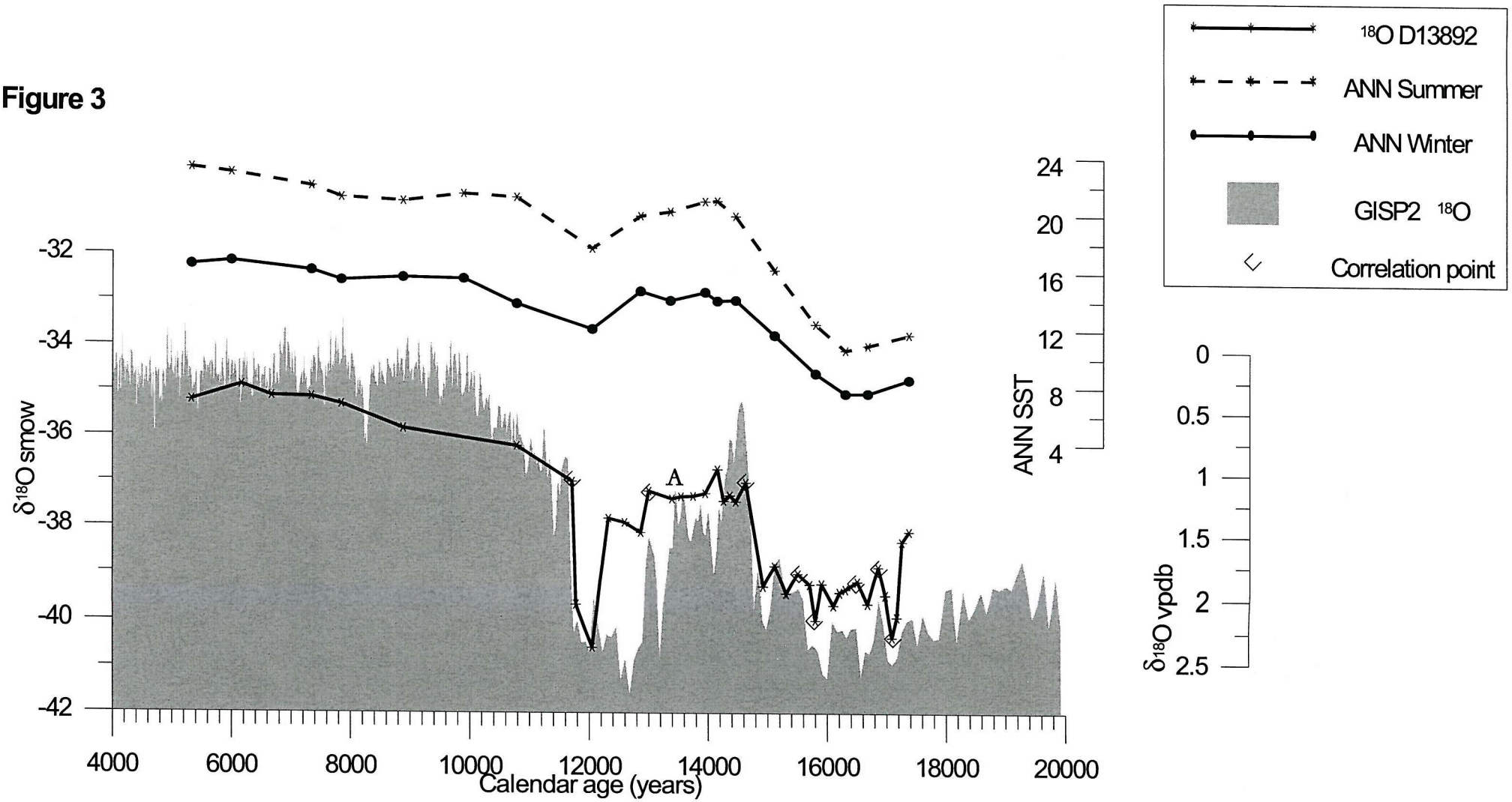

Fig 3. ANN SST and $\delta^{18}O_{N.\ pachyderma\ (d)}$ records for D13892 relative to GISP2 $\delta^{18}O$ record. Correlation points are shown. A indicates alternative tie point (see text).

pachyderma (d) for D13982 and $\delta^{18}O$ for GISP2, which crudely correlate in the ^{14}C derived chronology for D13892. The maxima and minima of these have been corrected to align in the final chronostratigraphic framework.

Results

Figure 4 shows RGB and $\delta^{18}O_{N.\ pachyderma\ (d)}$ plots for D13892. As the red, green and blue plots track, the colour variation is mainly related to lightness, and therefore directly comparable to diffuse reflectance and a proxy for carbonate content. Spectrophotometry (Fig. 5) confirms that the major change in reflectance between the glacial and Holocene parts of this core is in the wavelength band associated with carbonate (Giosan et al., 2002). The bulk colour changes in the core therefore represent the ratio of carbonate and detrital material supplied to this location, which lies at 1500m and is therefore unlikely to have experienced conditions that promote substantial carbonate dissolution. The relative intensity of each of the wavelengths varies along core (Fig. 4), indicating that the colour variation is not simple grey scale, but has a hue/chroma component. Green shows the most stable relative intensity, and therefore most accurately represents the grey scale (carbonate) variability.

The correspondence of changes in $\delta^{18}O_{N.\ pachyderma\ (d)}$ with changes in colour is strong, with increasing $\delta^{18}O_{N.\ pachyderma\ (d)}$ generally correlating with a relative darkening in colour. This indicates that the history of supply of sediment grains to this location is dominated by changes in global and/or local climate. The colour intensity and GISP2 records are similar, and correlate on millennial to centennial timescales locally. Relatively subtle climatic events such at the 8.2kyr cooling (Alley et al., 1997) are registered within the colour record. Though the correlation between the green intensity and GISP2 curves is not perfect, it has an R^2 of 0.81 indicating that it is significant. Sediment colour records have previously been shown to have spectral peaks at Milankovitch and sub-Milankovitch (1.5kyr) wavelengths (Giosan et al., 2002) and the D13892 record confirms that colour logging may be of potential use for the development of initial sediment core chronostratigraphies. One discrepancy between the records is the expression of the warmest part of the Bölling – Allerød, as recognised in the GISP2 record. This is very weakly expressed in the colour record of

Figure 4

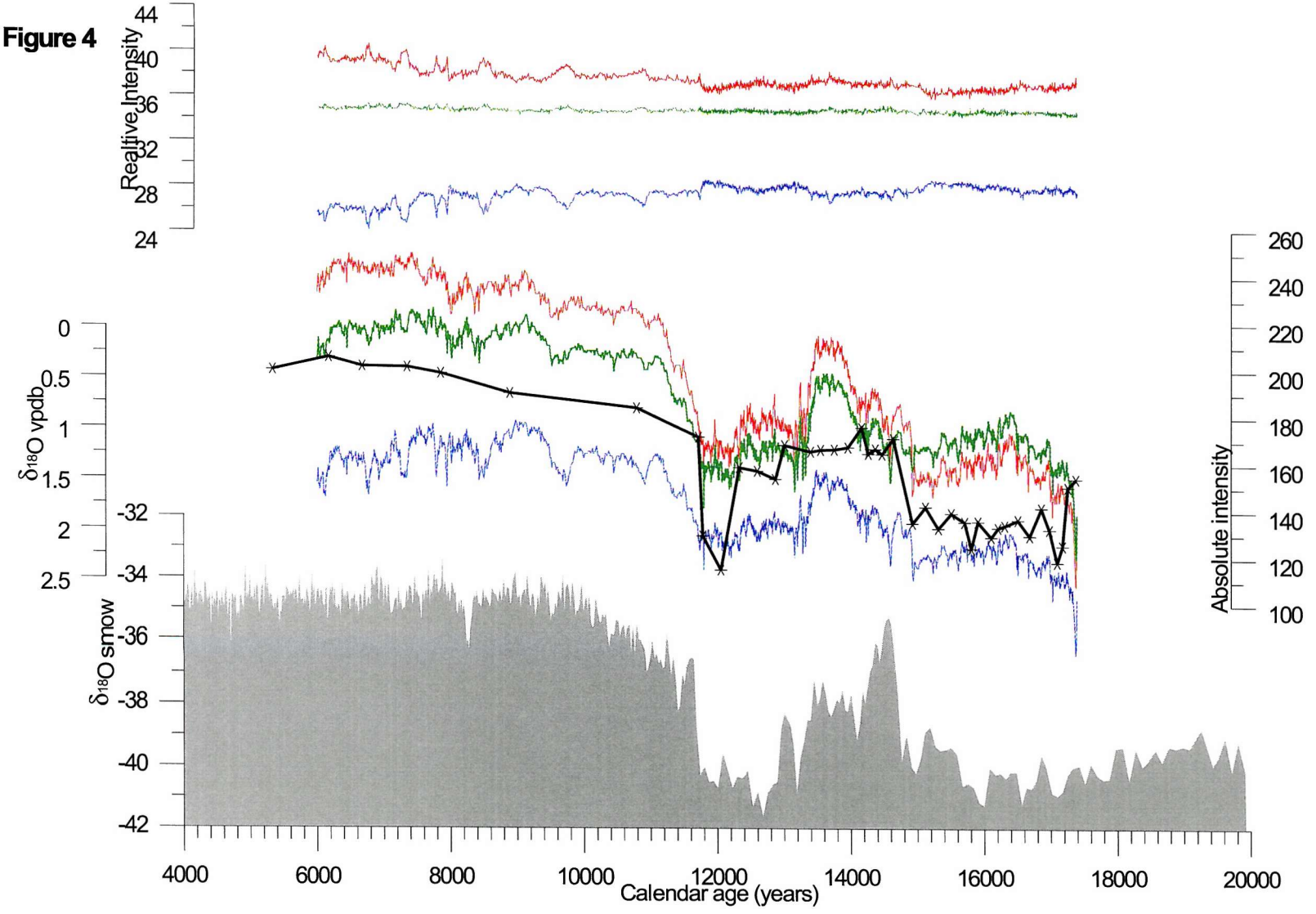

Figure 4. Grey represents GISP2 $\delta^{18}O$, black represents $\delta^{18}O_{N.\ pachyderma\ (d)}$ for D13892. Coloured lines represent red-green-blue intensities, with upper curves indicating relative contribution to colour and lower curves indicating absolute intensity.

Figure 5

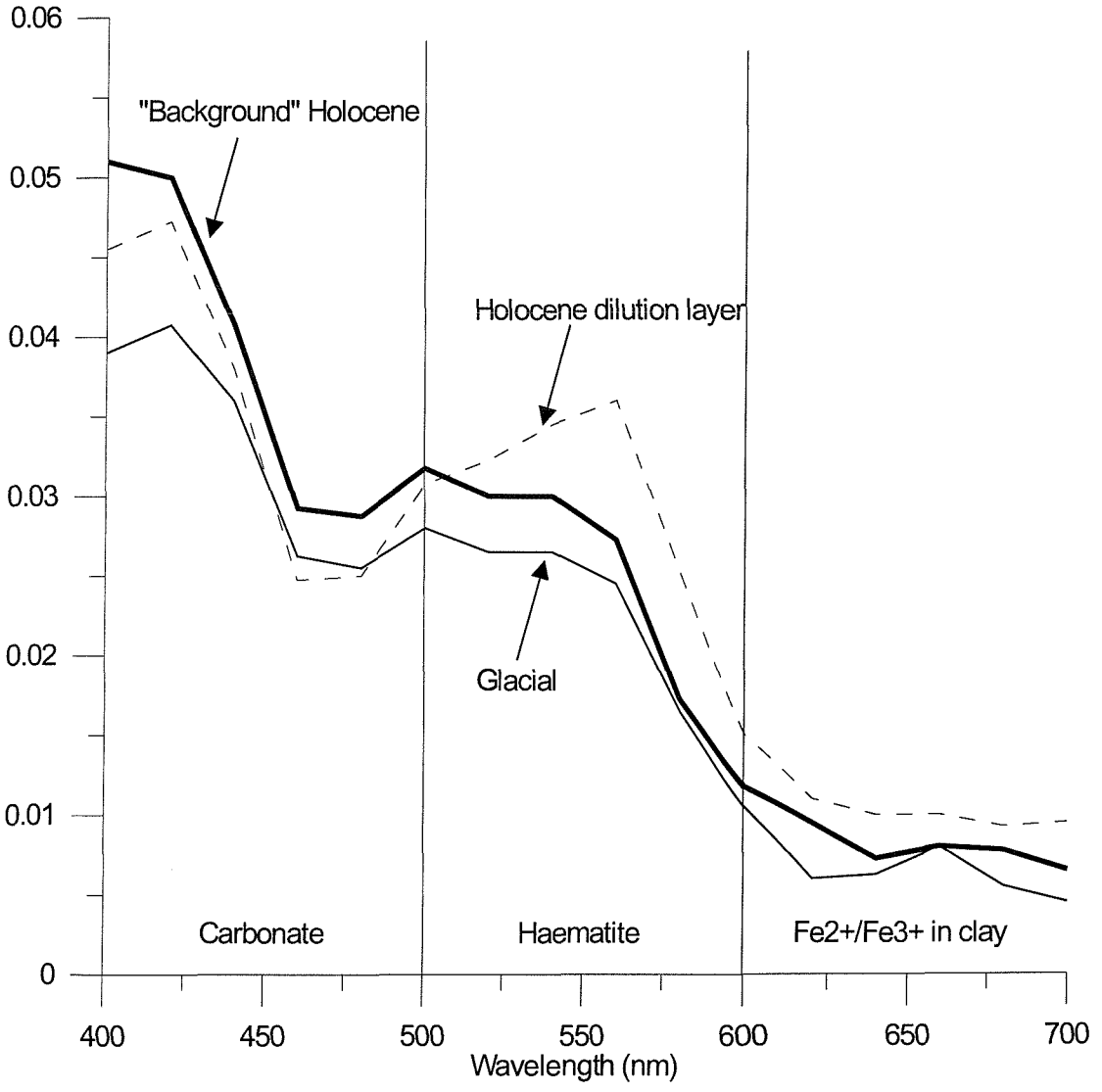

Figure 5. First differential of reflectance from spectrophotometry of representative samples from D13892. Interpretation of primary controls on reflectance intensities follows Giosan *et al.*, 2002.

Figure 6

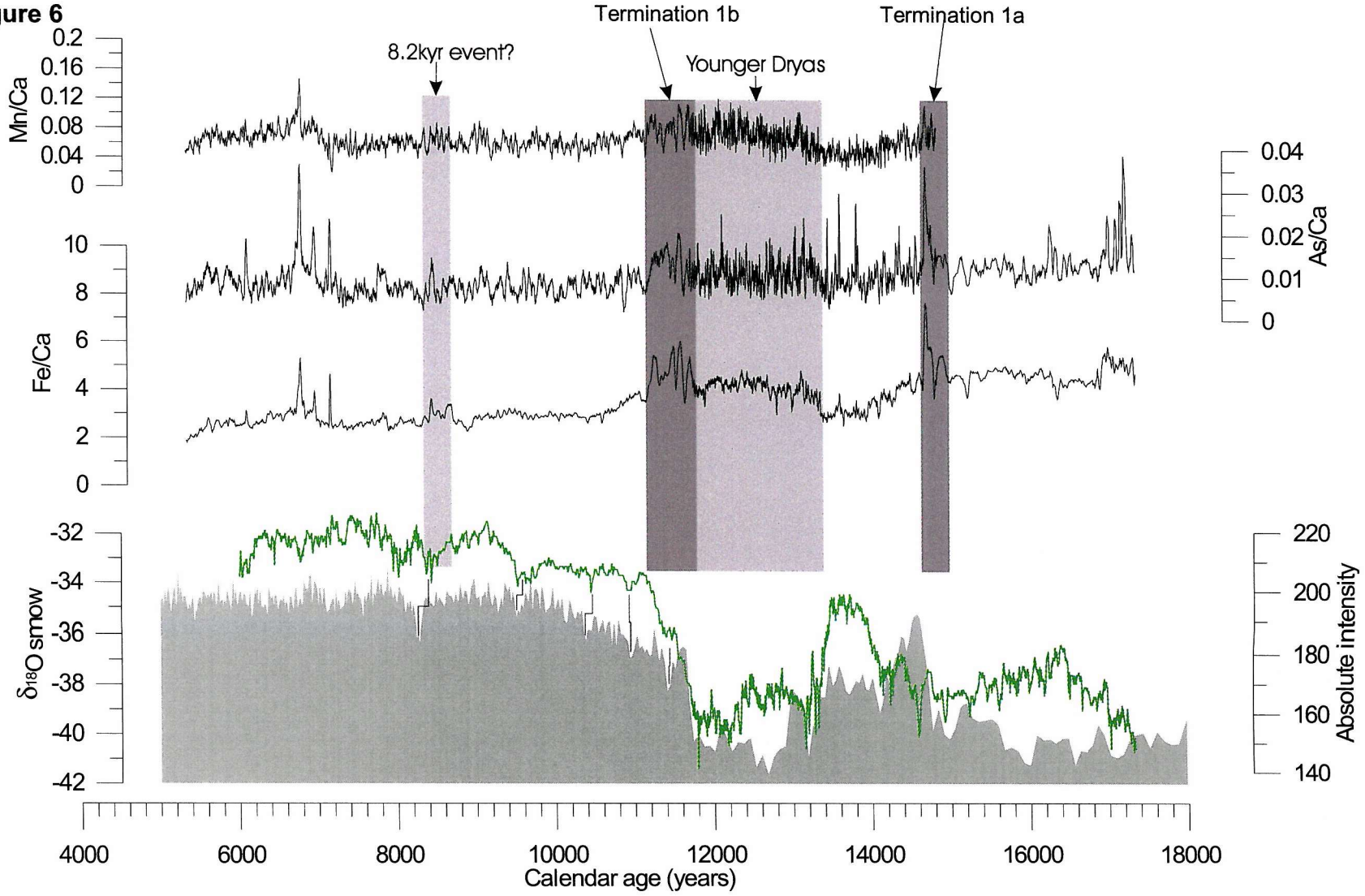

Figure 6. Colour and geochemical data for D13892 relative to the GISP2 isotope series.

D13892, and Termination 1a appears to arrive slightly later in the colour record than in the isotope record (see below).

The Holocene parts of D13892 exhibit a series of lightness minima, which often closely compare in age to temperature minima in GISP2 (Fig. 4) and are quasi-cyclic. These represent short duration (~100-500 years) periods of either increased supply of mineral detritus, or decreased carbonate productivity. The relative colour records show the cyclicity well and indicate that these dilution events are generally redder in hue than the background Holocene. Spectrophotometry indicates that they have increased reflectance in the wavelengths associated with haematite (Fig 5).

Figure 6 shows the green absolute intensity for D13892, GISP2 isotope series and chemical data produced by XRF logging for D13892 (Fe/Ca, Mn/Ca and As/Ca). Fe/Ca can be viewed as the detrital : carbonate ratio, and is high when the lightness is low. Several Holocene lightness minima coincide with local maxima in Fe/Ca confirming that these represent diluted layers, but the increases are not proportional and the cyclicity is not so evident in this record. The largest maxima in the Holocene parts of the chemical records are not coincident with significant cooling in the GISP2 record, and therefore are unlikely to be primarily related to climatic variability. Very high Fe/Ca also occurs at the times of Terminations 1a and 1b, and its it probably the high rate of detrital supply during Termination 1a that causes the apparent delay of this event in the colour record relative to $\delta^{18}O$. The number of planktonic foraminiferal tests per gram (dry weight) decreases during those periods with the highest rate of accumulation. In the Holocene the number of tests per gram is in the region of 1000-1600, whereas during the latter part of the Younger Dryas when deposition was most rapid (Fig. 2) this is found to be as low as 201 tests $gram^{-1}$. This is consistent with the variability being related to dilution.

Discussion

The Younger Dryas and glacial parts of the D13892 record exhibit lower lightness, higher Fe : Ca and significantly higher accumulation rates than the Holocene. The Bölling-Allerød is characterised by greater lightness, reduced Fe : Ca and slightly reduced accumulation rate relative to the over- and under-lying layers. This is most consistent with a variable rate of supply of detrital grains to this location through

time, with cold periods exhibiting significantly increased supply of detritus. Some variation in the rate of carbonate production cannot be ruled out, however on the Portuguese margin the rate of carbonate supply is not thought to have greatly varied over the past 140kyr (Thomson et al., 1999) and reduced carbonate production would tend to slightly reduce the rate of accumulation during the darker intervals.

During the Holocene the >150μm fraction almost exclusively comprises the tests of planktonic foraminifera. Before the Holocene, and particularly during the Younger Dryas, terrigenous grains are found in this fraction. These are mainly quartz and lithic clasts, some of them with dark coatings, with abundant mica and some black, oxidised wood. Similar grain assemblages have been observed in samples from the Gil Eanes drift (see preceding chapter). This is strong evidence that much of the diluting material found in this core is being supplied by the Mediterranean Outflow plume. As the SPM in the MO declines rapidly offshore (Ambar et al., 2002) this is more likely to be related to increased turbulence in the plume than to increased sediment loading though very large increases in loading cannot be discounted.

The Mn/Fe data for D13892 show a linear enrichment in manganese relative to iron up core, and is consistent with post-depositional diffusion without the presence of major diagenetic fronts (Thomson et al., 1996). There are synchronous enrichments in Fe/Ca, Mn/Ca and As/Ca, indicating that these elements are all found within the dilutant (i.e. detrital) material. Arsenic is not a major component of sediment and is generally only found in association with diagenetic pyrite, which seems to be of minor importance here. In this case the arsenic is probably contained either within lithic grains derived from an arsenic rich source rock or in oxyhydroxide complexes in grain coatings. Absolute enrichment data (i.e. not in ratio with Ca) indicate that some of the Holocene iron rich layers are enriched in arsenic by a factor of two or more, which is proportional to the enrichment in iron. This high arsenic content of the detrital phase strongly indicates that it is at least partially sourced from a region that is unusually rich in this element. Figure 7 shows the region around the GoC that may be the source of the detritus found in D13892, with the drainage basins of the major rivers marked. Close to the northeast margin of the GoC is the large iron ore deposit named the Iberian Pyrite Belt. This is a massive sulphide deposit of hydrothermal

Fig. 7

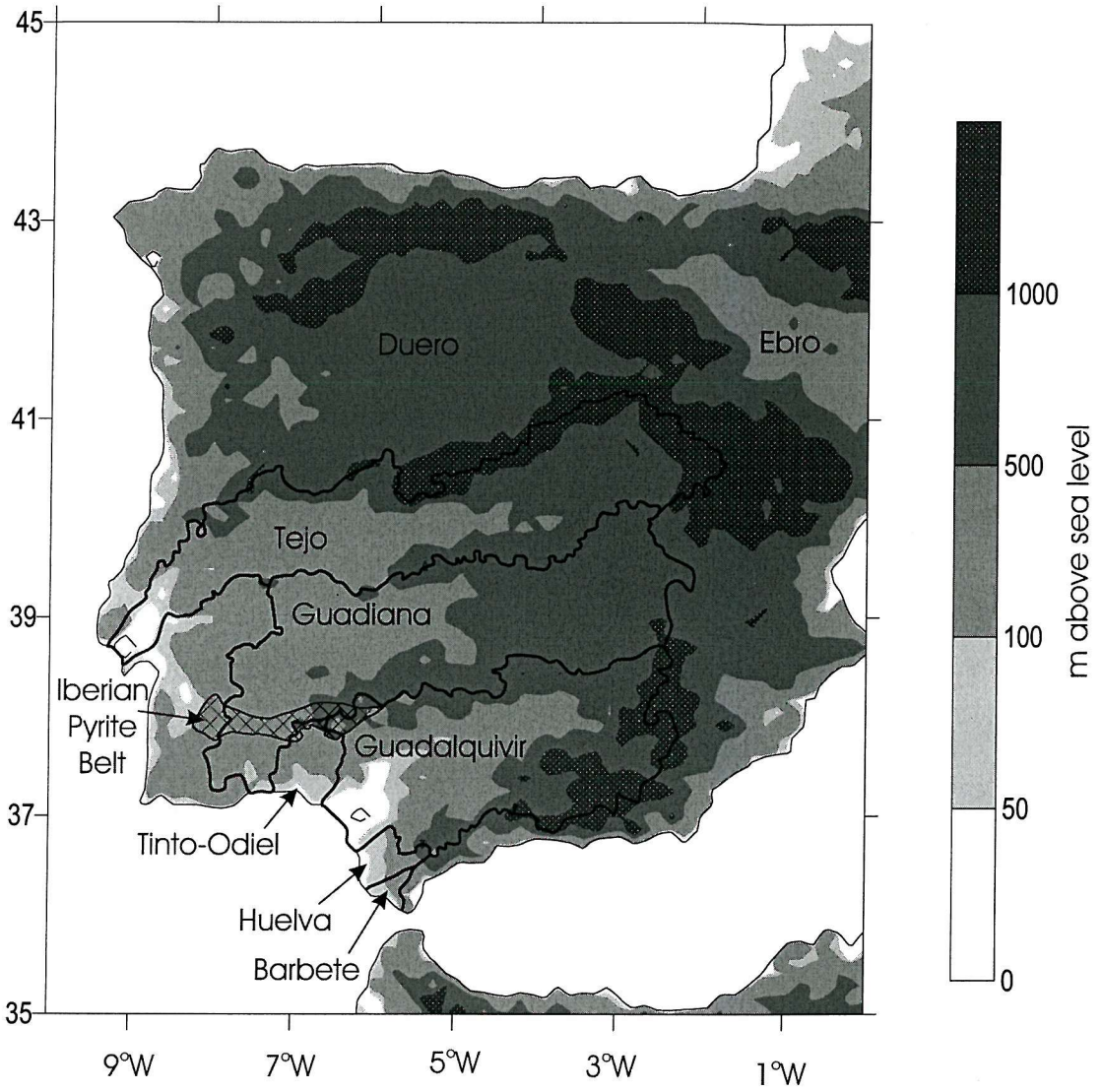

Figure 7. Drainage basins in southwest Iberia and the position of the Iberian Pyrite Belt. Elevation data from GLOBE DEM (www.ngdc.noaa.gov/seg/topo/globe), position of watersheds from separate DEM stream delineation (http://www.ce.utexas.edu/prof/olivera/Iberia/), position of outcrop from van Geen et al, (1997).

origin that outcrops over a region roughly 30km wide and 250km long, and relative to continental crust is enriched in iron (x120) and arsenic (x2200) (vanGeen et al., 1997). Arsenic is not mobile is normal surface conditions, though it becomes soluble in water with very low pH and is highly enriched in acidic mine waste (AMW) (Alpers et al., 1994). It is generally considered similar to iron in terms of its mobility (vanGeen et al., 1997), and indeed is often found in association (Fukushi et al., 2003). As the extreme pH of AMW is attenuated rapidly away from the source, the mobility of arsenic is also attenuated and this is accelerated by the activity of microorganisms (Duquesne et al., 2003). It is therefore a common feature of many mining areas for narrow dispersion haloes of arsenic to develop round the tailing dams (Alpers et al., 1994; Fukushi et al., 2003; Garcia-Sandchez and Alvarez-Ayuso, 2003; Hammarstrom et al., 2003; Wang et al., 2003). In Salamanca province (north of the IPB), this halo is found to be <500m in diameter (Garcia-Sandchez and Alvarez-Ayuso, 2003). Arsenic precipitates preferentially in association with metastable iron minerals such as schwertmannite (Fukushi et al., 2003) and are found to be retained in association with iron oxyhydroxides in the soil, with groundwater only rarely showing enhanced levels, even in highly polluted regions (Fukushi et al., 2003; Garcia-Sandchez and Alvarez-Ayuso, 2003). Without the presence of water with very low pH, arsenic liberated from the IBP by weathering will therefore remain available for transportation as a detrital phase and will tend to be enriched in iron bearing detrital grains. As the Iberian Pyrite Belt lies almost entirely within the drainage basins of rivers debouching into the GoC, that part of the erosion product of the Iberian Pyrite belt exported by rivers will entirely be supplied to this area, giving good potential for arsenic enriched grains to contribute to the SPM in the MO. Muddy sediment and suspended sediment from the Rio Tinto estuary have been found to contain 800-1600 ppm of arsenic, which is highly enriched relative to the background level (50-100ppm) (Nelson and Lamothe, 1993).

The origin of the manganese is not adequately explained by an Iberian Pyrite belt source, as the ore body is depleted relative to continental crust in this element (vanGeen et al., 1997). It is likely that the manganese is largely present as grain coatings, and it is a significant component of the desert varnish coatings typical of many arid regions (McKeown and Post, 2001). As all the surrounding area is arid, including Andalusia which is a highly arid semi-desert, and has been shown to be

more arid during the Younger Dryas and last glaciation relative to today (Grousset et al., 1998; Sanchez-Goni et al., 2000; Bateman and Diez-Herrero, 2001; Moreno et al., 2002; Sanchez-Goni et al., 2002) varnished grains could be supplied from either margin, and either by riverine or aeolian inputs.

In the case of the detrital pulses noted during the Holocene, and during Terminations 1a and 1b it is not easy to be certain about the relative roles of transport by winds and the MO. Neither the large accumulation rate increase or characteristic mineral assemblage noted in the Younger Dryas that have been ascribed to the MO have been observed. The region is arid and characterised by strong and stable winds, especially the easterly Levanter and northerly trade winds (Dorman et al., 1995) (see Fig. 7). Today, Levanter winds trap air pollution and dust close to the ground and cause visibility to decrease by as much as 30%. During the summer, the trade winds are strong, stable and active >50% of the time at the city of Cadiz (Fiuza et al., 1982). It is therefore possible that some of the detrital material has an aeolian origin. Some of the Holocene pulses are probably related to local changes in the sedimentary system as they do not appear to correlate to events outside of the GoC, but the lightness record indicates dilution variability which is potentially related to low amplitude climatic oscillations known to have occurred during the Holocene (e.g. (Alley et al., 1997; Meeker and Mayewski, 2002). Spectophotometry on samples taken from periods of high dilution in the Holocene indicate that there is an increase in the abundance of haematite relative to background conditions, which is often related to enhanced aeolian activity (Balsam et al., 1995). The 8.2kyr cold outbreak in the Holocene has been demonstrated to coincide with reduced precipitation in North Africa (Gasse and vonCampo, 1994) and Europe (vonGrafenstein et al., 1998) and increased trade wind strength (Hughen et al., 1996). Increased aridity will increase the availability of material for aeolian transport in Iberia, and intensified trade winds would enhance the potential for transport from the region of the Iberian Pyrite Belt and Extremadura. Alternatively, enhanced aridity and low temperatures in the Mediterranean have been shown to increase the buoyancy loss on the northern margin and enhance the strength of the Mediterranean's internal circulation (Rohling et al., 1998; Cacho et al., 2000). This could potentially affect the local energy of the Mediterranean Outflow as far afield as the western GoC.

Conclusions

1) Colour logging is a useful tool that may be used for producing high-resolution chronostratigraphic frameworks by correlation with well-constrained climatic records. It has potential to be particularly useful as a method of developing initial chronostratigraphic information for a sediment core in order to develop a sampling strategy for more conventional analyses, as continuous colour logging is a cheap, rapid, non-destructive method of producing very high-resolution data for sediment cores. Colour data are also independent of conventional palaeoclimatic tools, such as stable isotope analysis, as they are a measure of whole sediment fabric rather than of the properties of individual grains within the sediment itself.

2) The western Gulf of Cadiz experienced an enhanced supply of detrital grains during the Younger Dryas and the latter part of the last glaciation. The detritus was largely sourced from southwestern Iberia and was probably transported by the Mediterranean Outflow plume, and thus ultimately is derived from a riverine source. As SPM content decreases rapidly in the MO plume away from the continental margin today (Ambar et al., 2002), such a change in supply to D13892 is unlikely to be related to increased debouchment of detritus at the coast, but rather increased transport of SPM by the MO plume itself. As it is turbulence that keeps material suspended in a fluid, this increase in transport is most likely to reflect an increase in the turbulence (and by implication velocity) of the plume between the coast and D13892. Increased sediment supply by the MO plume is therefore diagnostic of increased velocity of the plume passing over the Gil Eanes Drift. This supports independent palaeocurrent reconstructions for this area (see preceding chapter).

3) Enhanced detrital supply is also found in the western GoC during the glacial Terminations (1a and 1b) and during periods within the Holocene, which potentially correlate to transient cold periods (e.g. 8.2 kyr event). This detritus is also probably derived from southwestern Iberia, but may have been transported either by the Mediterranean Outflow or by wind, or both.

Haematite enrichments in the Holocene layers imply that enhanced aeolian supply may be important at these times.

Table1. Radiocarbon datings and tie-points used in development of D13892 chronology. The OXCAL calibration system was used for conversion of conventional radiocarbon dates to calendar years.

Sample depth (cm)	**Conventional radiocarbon age**	**1σ**	**Predicted calendar age**
8	5647	45	6010
56.7	10429	56	11210
71	10868	59	12040
110	10868	58	12660
173	14353	76	16800
Tie point depth (cm)	**Event**	**Calibrated radiocarbon age**	**Age in GISP2 chronology**
61.7	Termination1b	11349	11700
100	Termination of Bölling-Allerød	12594	13000
136.7	Termination 1a	14416	14600
146	Local $\delta^{18}O$ minimum	14971	15400
152	Local $\delta^{18}O$ maximum	15333	15800
166	Local $\delta^{18}O$ minimum	16171	16500
170	Local $\delta^{18}O$ minimum	16419	16850
176.3	Local $\delta^{18}O$ maximum	16799	17100

Chapter 7:- Supply of Continental Shelf Sands to the Gulf of Cadiz Sediment Drift

Abstract

The slope of the Gulf of Cadiz (southwest Iberia) is characterised by a sediment drift deposited by the Mediterranean Outflow. This is a strong bottom current that passes along the slope from southeast to northwest decelerating along slope (north) and down the slope (west). The tests of benthic foraminifera typical of the continental shelf have been observed within samples taken from a variety of sedimentary environments on the Gil Eanes Drift, the part of the Gulf of Cadiz sediment drift positioned lowest on the continental slope. That sand deposited by the Mediterranean Outflow is derived from sediment previously deposited on the shelf is confirmed by the presence of other bioclasts typical of the continental shelf and sediment chemistry. The reworked tests are found to show a distinct succession from those that are largest and heaviest to those that are most easily transported along the declining energy gradient found on the Gil Eanes Drift. This is interpreted as reflecting energetic sorting of the test population by the Mediterranean Outflow current as it decelerates.

Introduction

The northern and eastern continental slope of the Gulf of Cadiz (GoC), southeast of Iberia (Fig. 1), is the site of significant sediment drift development as a result of the strong bottom current derived from dense Mediterranean water exported westward by the Strait of Gibraltar exchange (Ambar and Howe, 1979; O'Neill-Baringer and Price, 1997). The current, named the Mediterranean Outflow (MO), impinges on the slope between 500m and 1500m from Cape Spartel in the southeast to Cape St. Vincent in the northwest, decelerating and slowly descending the continental slope as it entrains Atlantic water and is slowed and spread by friction (O'Neill-Baringer and Price, 1997, 1999). The sedimentary characteristics of the sediment drift reflect this gradual deceleration. Close to the Strait of Gibraltar, the path of the Mediterranean Outflow is characterised by rock outcrops, abrasion surfaces and longitudinal sand dunes (Kenyon and Belderson, 1973), which grade into muddy drifts along slope (to the

Figure 1

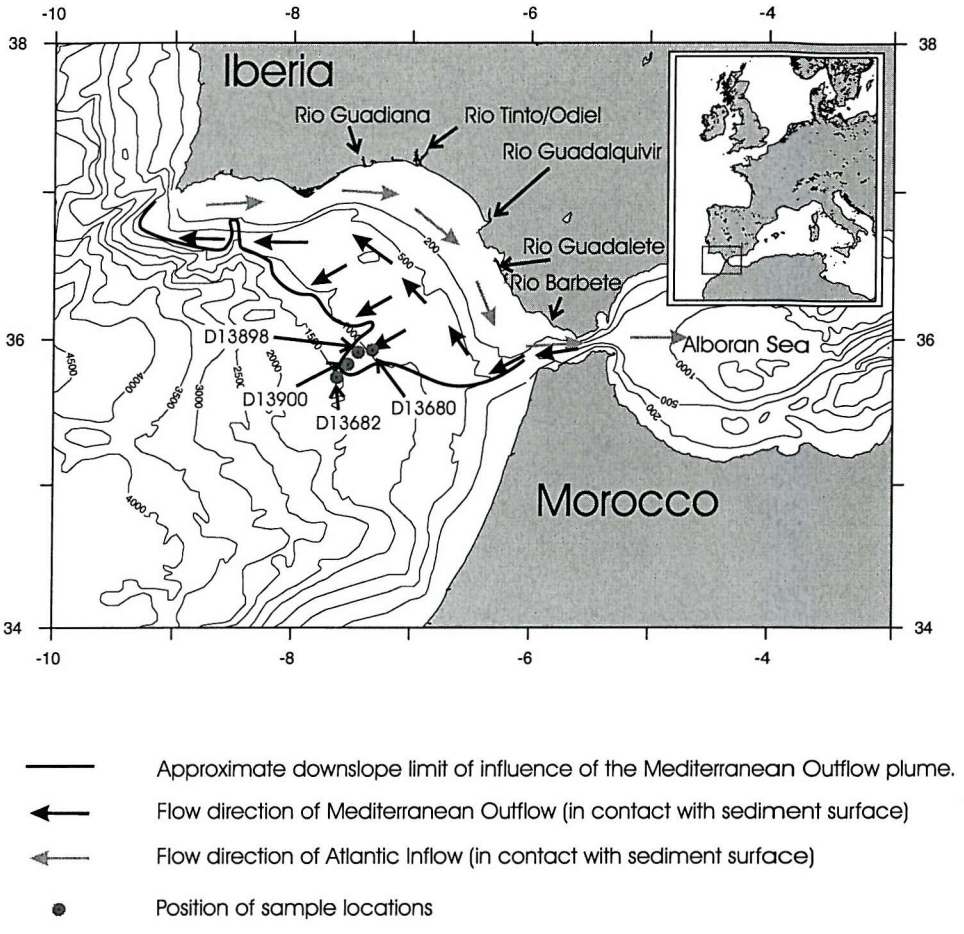

Figure 1. Location of study area and position of major rivers and currents in the GoC. Location of samples are shown.

north) and downslope (to the west) (Hernandez-Molina et al., 2003; Kenyon and Belderson, 1973).

On the continental shelf of the GoC the Atlantic Inflow current flows in the reverse sense to the MO (Lopez-Galindo et al., 1999) (Fig. 1). This is the eastward and surface component of the Gibraltar Exchange which accelerates towards the southeast as it nears Gibraltar, and as a result the grainsize of the surface sediment increases towards the southeast (Lopez-Galindo et al., 1999). It is widely believed that the sediment deposited on the GoC slope is derived from material debouched from the rivers along the Iberian coastline (Guadalquivir, Guadiana, Tinto-Odiel, Barbete) (Lopez-Galindo et al., 1999; Nelson et al., 1999; Nelson and Lamothe, 1993). In this scenario, sediment is initially deposited on the continental shelf by the Atlantic Inflow and then transported down onto the upper slope, entrained into the MO and deposited on the sediment drift. Evidence supporting this hypothesis is presented here.

A number of downslope oriented channels can be found on the lower edge of the Gulf of Cadiz sediment drift (Fig. 2), which are formed by the lower part of the Mediterranean Outflow plume as it descends the slope (Habgood et al., 2003). They are believed to be formed almost exclusively by current activity, and little evidence for gravity-flows has been found associated with these channels (Habgood et al., 2003). The largest of the freestanding channels, the Gil Eanes Channel, is flanked by a muddy sediment drift termed herein the Gil Eanes Drift. The Gil Eanes Channel itself is between 1.5 and 3km wide and extends 40km downslope between 900 and 1500m water depth, connecting up-slope to the main sand drift (Habgood et al., 2003). The channel has steep walls, which rise from the flat bottom to levee-like flanks that are ~50-100m high (Habgood et al., 2003). Close to the termination of the Gil Eanes Channel, at a depth of ~1200m, the Mediterranean Outflow water lifts off the sea floor to form a plume that can be observed at intermediate depths in the Atlantic (Kenyon and Belderson, 1973).

At the termination of the Gil Eanes Channel there is a sandy deposit which shows a very irregular surface in side-scan sonar images (Habgood et al., 2003), Fig. 2). The unevenness of the surface is mainly caused by the presence of numerous small gravity-flow scarps, and material from this sand body is funnelled downslope to form

Figure 2

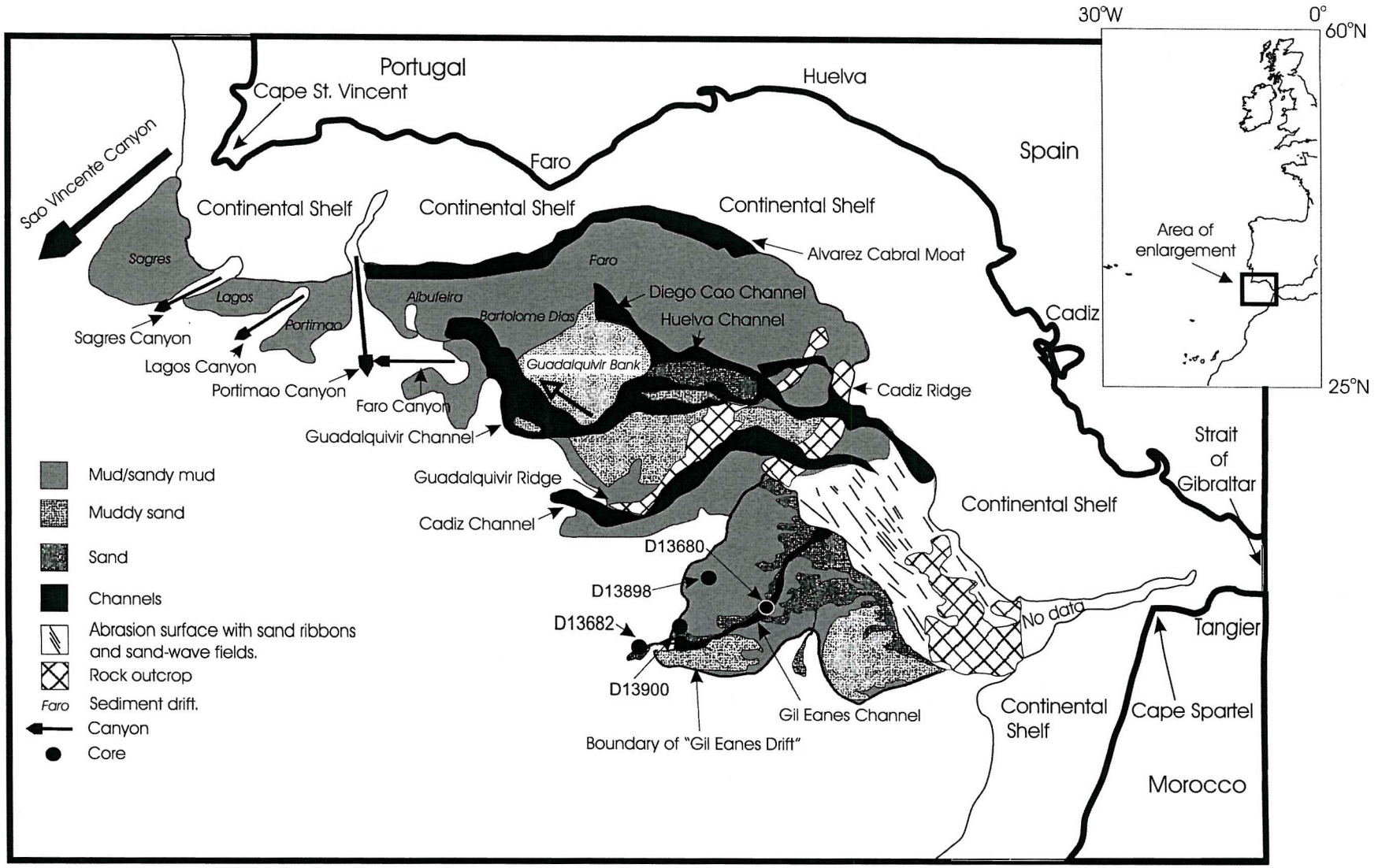

Figure 2. Modified from Hernandez-Molina et al., (2003). Sediment facies of the Gulf of Cadiz contourite drift as revealed by sidescan sonar data. Core locations are indicated.

a small but complex sandy lobe below (N. Kenyon, personal communication). There are a number of these small lobes elsewhere, all of which occur below the sediment drift and are of similar size and geometry to the one below the Gil Eanes Channel (Habgood et al., 2003). The material discussed in this report are taken from the flank, axis and termination of the Gil Eanes channel and from the sandy lobe deposited below the termination of the channel.

Material and Methods

Samples for grain size analyses were dried at 50°C, weighed and then disaggregated in tap water. They were then wet sieved at 63μm and the filtrate was collected. The >63μm fraction was dried at 50°C and dry sieved at 125 and 150μm. The masses of these three fractions were then measured. The filtrate was left to settle for at least 3 days before the connate water was poured off. The filtrate was then dried at 50°C and weighed. Data are presented as percentage weight of four grainsize fractions (<63 μm, 63-125 μm, 125-150 μm and >150 μm) for each sample.

The >150μm fraction was removed for the benthic foraminiferal abundance study and where necessary, samples were then split into suitable aliquots of at least 300 individuals for identification. The data are presented as percentages of total number of benthic foraminiferal tests. The mineralogical and bioclastic composition of the >150μm fraction of samples were also observed.

Elemental analyses were done on samples from D13900 by simultaneous inductively coupled plasma atomic emission spectroscopy (ICP-AES) at SOC. Samples were dried at 105°C and analysis was performed after total sample dissolution effected by a lithium metaborate fusion (Jarvis, 1992). This produces bulk sediment compositions of major and trace elements (Al, Si, Ca, Mg, Ba, Zr and Cr), which are presented in ratio.

Results

Core D13900 contains a layer of fine to very fine sand between depths of ~2 and ~4m (See fig 3). This layer has a sharp top overlain by clay rich mud and coarsens upward from an underlying layer of mud. The sand is very fine (mainly in the 63-125μm

Figure 3

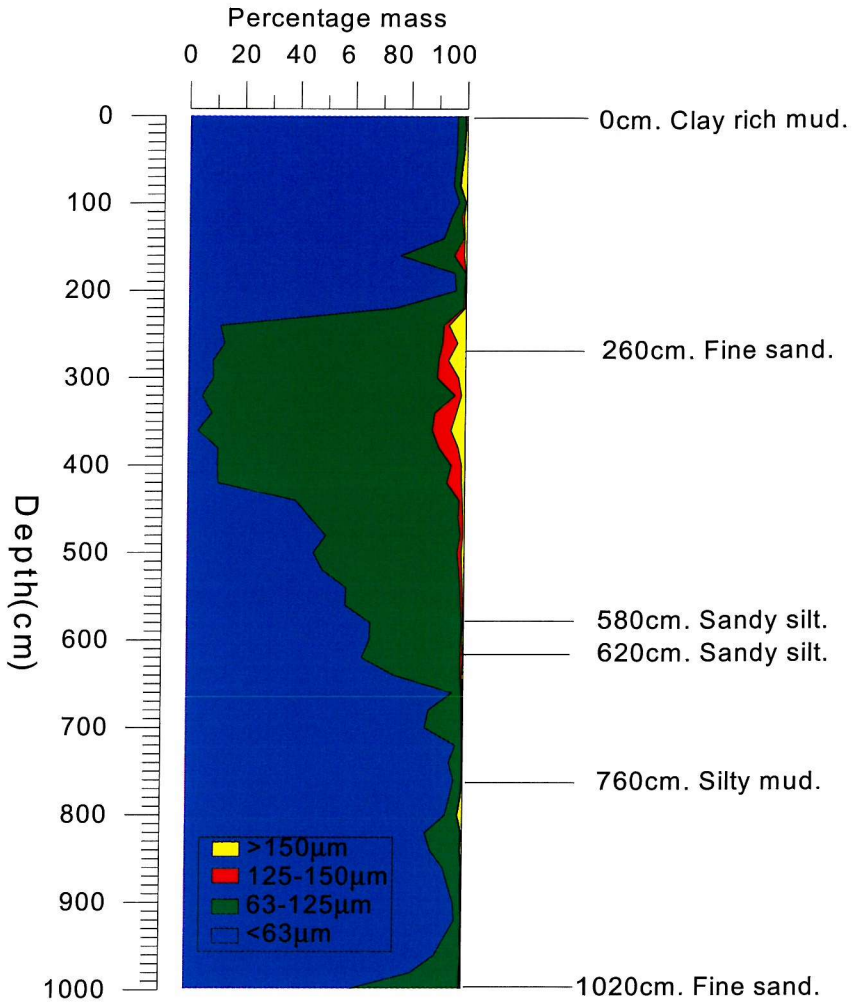

Figure 3. Grainsize data for D13900. Each of the four grainsize fractions are represented as percentage of total dry mass. Positions of described samples are shown.

Figure 4

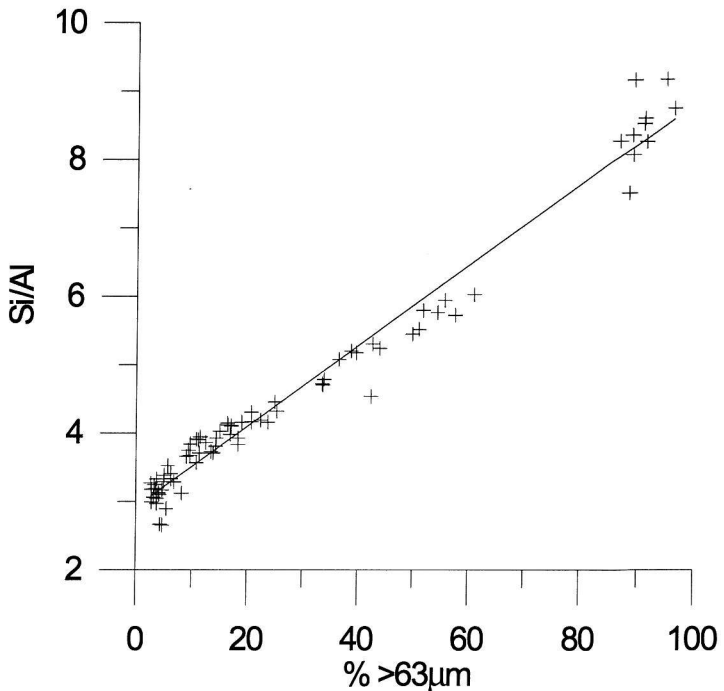

Figure 4. Correlation of grainsize and chemical data for D13900. A linear fit is shown ($r^2 = 0.97$).

grainsize fraction), though in its coarsest parts contains more than 10% in the >150μm fraction by mass. The coarsest (>150 and 125-150μm) fractions contain abundant bioclasts, including broken and whole echinoderm spines, pteropod fragments, coralline algae fragments, dinoflagellate cysts of *Lingulodinium machaerophorum,* sponge spicules, black oxidised wood, brown unoxidised plant material, rare whole gastropods and the broken and whole tests of both benthic and planktonic foraminifera.

The 63-125μm fraction is very dark, and contains some bioclastic carbonate and abundant mineral grains, some of which display a dark coating which contributes to its characteristically dark appearance. The mineral grains are mainly quartz, dark coloured lithic clasts and mica. The sandy material is very silica rich and the coarsest parts are also enriched in zirconium, iron and titanium, all of which are characteristic of the heavy minerals found in terrestrial derived sands (e.g. zircon and rutile). Figure 4 shows the relationship between the Si/Al and the percentage weight of the >63μm component (sand). This indicates that D13900 can be considered as a mixture of two end members, one a marine clay (Si/Al of 3) and the other a fine/very fine terrigenous sand (Si/Al of 8.5).

Ten samples which span the range of sediment types found on the Gil Eanes Drift are described here. Six of these are taken from core D13900, and these are indicated in Figure 3. Two further samples are taken from D13898 at 60cm and 260cm respectively. This is a core from the flank of the Gil Eanes Drift which is generally massive and muddy, comprising mainly clay at the core top and becoming siltier below 200cm. The benthic foraminiferal assemblage of muddy material in D13900 and from D13898, which is massive and fine-grained throughout, is typical of the upper continental slope (See Table 1). Tests are not highly abundant (~20 tests/g) and are dominated by species such as *Uvigerina peregrina*, *Melonis affinis* and various *Cibicidoides* species. The sandy material contains a far more diverse assemblage (>60 species, compared to ~25 in the muddy samples) and benthic tests are also several times more abundant in the sandy material (115 tests/g). Several species found in these samples are thought to be shelf-dwelling (Table 1), e.g. *Planorbulina mediterranensis*, *Elphidium macellum, Hyalinea balthica, Astrononion stelligerum*,

juvenile *Elphidium crispum* (defined as lacking a complete whorl) and *Ammonia beccarii*. *E. crispum* is only found in small numbers, and is not found in the silty part of the sand in D13900. Conversely, *P. mediterranensis* reaches its maximum abundance in these samples. Common species in all the sandy samples are *Cibicides lobatulus* and *Cassidulina laevigata,* and these are also found in lower abundances in the muddy samples from on the flanks of the Gil Eanes Drift (Table 1). Sand taken from the top of the lobe beyond the termination of the Gil Eanes channel (top of core D13682) is similar to the sand in D13900 in terms of the mineralogical and bioclastic assemblage. It also has a very similar benthic foraminiferal assemblage (Table 1), with abundant and diverse species, several of which are characteristic of the shelf. As in D13900, *C. lobatulus* and *C. laevigata* are amongst the most abundant species.

A core top sample from the axis of the Gil Eanes channel was also inspected (D13680). This is a medium to coarse bioclastic sand with less of the small (<150μm) lithic grains found in D13900 and D13682, but abundant well rounded near-spherical quartz grains that are often >200μm in diameter. The benthic tests are generally significantly larger than in any other sample (up to 1.5mm, whereas the largest tests in other samples are ~500μm (~700μm for *P. mediterranensis*)). The dominant species, again *C. lobatulus* which contributes almost 20% of the tests, shows a greater size range than the other abundant species within the D13680 sample, and tests as small as 150μm (the mesh size) are found. The median test size for *C. lobatulus* is ~500μm which is also smaller than those of the other common species (~650μm for *Textularia*, ~700μm for *D. coronata* and ~750μm for *E. crispum*) due to the large number of relatively small tests. Other common taxa in D13680 include adult *E. crispum,* various *Cibicidoides, Discamomalina coronata, Triloculinella obliquinodus, Elphidium advenum,* a large species of *Textularia* and a species of *Loeblichopsis*. No *P. mediterranensis* or juvenile *E. crispum* were found. *C. laevigata* was also rarer than in D13900 and D13892 (<2% compared to >10%). In all the sandy samples many broken tests were observed and in D13680 many tests were found to have evidence of abrasion. One *E. crispum* test had been badly worn, and its ornamentation was barely visible.

Discussion

As noted above, the chemical data for D13900 indicate that this core can be considered as a mixture of two end members, one a marine clay and the other a sand (see Fig. 4). Extrapolation of the regression indicates intersection with the Y axis at ~3. This is due to the fine end member (0% >63μm) having Si/Al of 3 rather than of 0. The presence of only two end members also indicates that the sand in this core was supplied from a single source and transported by one process. The silica and heavy mineral rich composition of this sand is consistent with material deposited on the shelf (Turekian and Wedepohl, 1961), as is its bioclastic assemblage. This sand is petrologically similar to those described from higher on the slope (the "bioclastic sands" of (Habgood et al., 2003; Nelson et al., 1993; Nelson et al., 1999)) and similar sands described in (Faugères et al., 1984; Gonthier et al., 1984; Stow et al., 1986)) and on the eastern shelf of the GoC (Lopez-Galindo et al., 1999; Nelson et al., 1999). It is likely that this sand is transported downslope by the flow of the MO, and that at least a significant part of it is derived from the eastern shelf region. The muddy samples described here can be considered as representative of the low sand end-member of this mixture (with mainly indigenous benthic foraminifera) and the channel axis sample (D13680) as a coarse lag deposit derived form the most dense parts of the shelf derived sand. One implication of this continuity is that the reworked grain assemblages within these samples (including the shelf-dwelling benthic foraminifera) should be comparable, and differences within the assemblage are caused only by processes occurring during transportation and deposition.

Origin of the sand described on the Gil Eanes Drift from the GoC shelf is further supported by the presence of a number of characteristically shelf-dwelling benthic foraminifera species in these samples. *Elphidium crispum* is a species with a heavy and large test and which lives within the photic zone by retention of chloroplasts (Lee et al., 1988; Murray, 1971, 1991). The tests of this species are thus almost certainly derived from the uppermost shelf. Living examples of this species have not been reported in the literature from the Gulf of Cadiz as yet, though this probably reflects a general lack of investigation of the very near shore (epiphytic) environment preferred by this species elsewhere (Lee et al., 1988; Murray, 1971, 1991). Other species of Genus *Elphidium* (most frequently *macellum* and *gerthi*), which is almost exclusively

restricted to the shelf during life (Murray, 1971, 1991), are also found within these samples. *Hyalinea balthica* has been found to be a shelf-edge species on the Portuguese and GoC margins (Schönfeld, 2002b; Villanueva-Guimerans and Cervera-Currado, 1999), and is absent from the living assemblage at greater depths (Schönfeld, 1997, 2002b) indicating that these tests have also experienced significant post mortem downslope transport. *Planorbulina mediterranensis* secretes a wide, flat, thin walled test that it attaches to the fronds of marine plants and hard, elevated substrates during life (Murray, 1971, 1991). This species has been reported living on the northern shelf of the Gulf of Cadiz (Villanueva-Guimerans and Cervera-Currado, 1999), is found to be absent from the assemblage at greater depths throughout the GoC (Schönfeld, 2002b) and thus the tests recovered from the Gil Eanes Drift are almost certainly derived from the shelf.

There is strong indication of size-sorting within the population of the reworked tests, which is consistent with the flow waning in strength as it passes down the slope. A good example of this sorting is found in *E. crispum,* the large and heavy tests of which are relatively difficult to transport. The adults of *E. crispum* are found only in the channel axis and the juveniles are found only in the coarsest samples from the channel termination and are absent from sandy silt and silty mud samples from the same location. The light, flat tests of *P. mediterraniensis* are far more easily transported post mortem. This species is rare in the channel axis but is found in higher abundance in the coarser deposits at the channel termination, though abundance is still low (1-5%). Highest abundance of this species is found within the sandy silt sample of D13900, where its contributes ~8.7% of the total assemblage. Sorting is further indicated by the populations of other species, as there is a clear distinction in size between the test population in the channel axis and termination. The light tests of *E. macellum, H. balthica* and *A. stelligerum* are rare in the channel axis, whereas the heavy and robust tests of *Cibicidoides robertsonianus, D. coronata, T, obliquinodus* and *Textularia* are common only in the channel axis.

The association of specific test populations within samples of varying grainsize allows a theoretical succession of assemblages to be defined along a declining velocity field (Fig. 5). It is highly likely that any deposit derived from a spatially or temporally waning flow would show a similar energetic partitioning of an initial grain

Figure 5

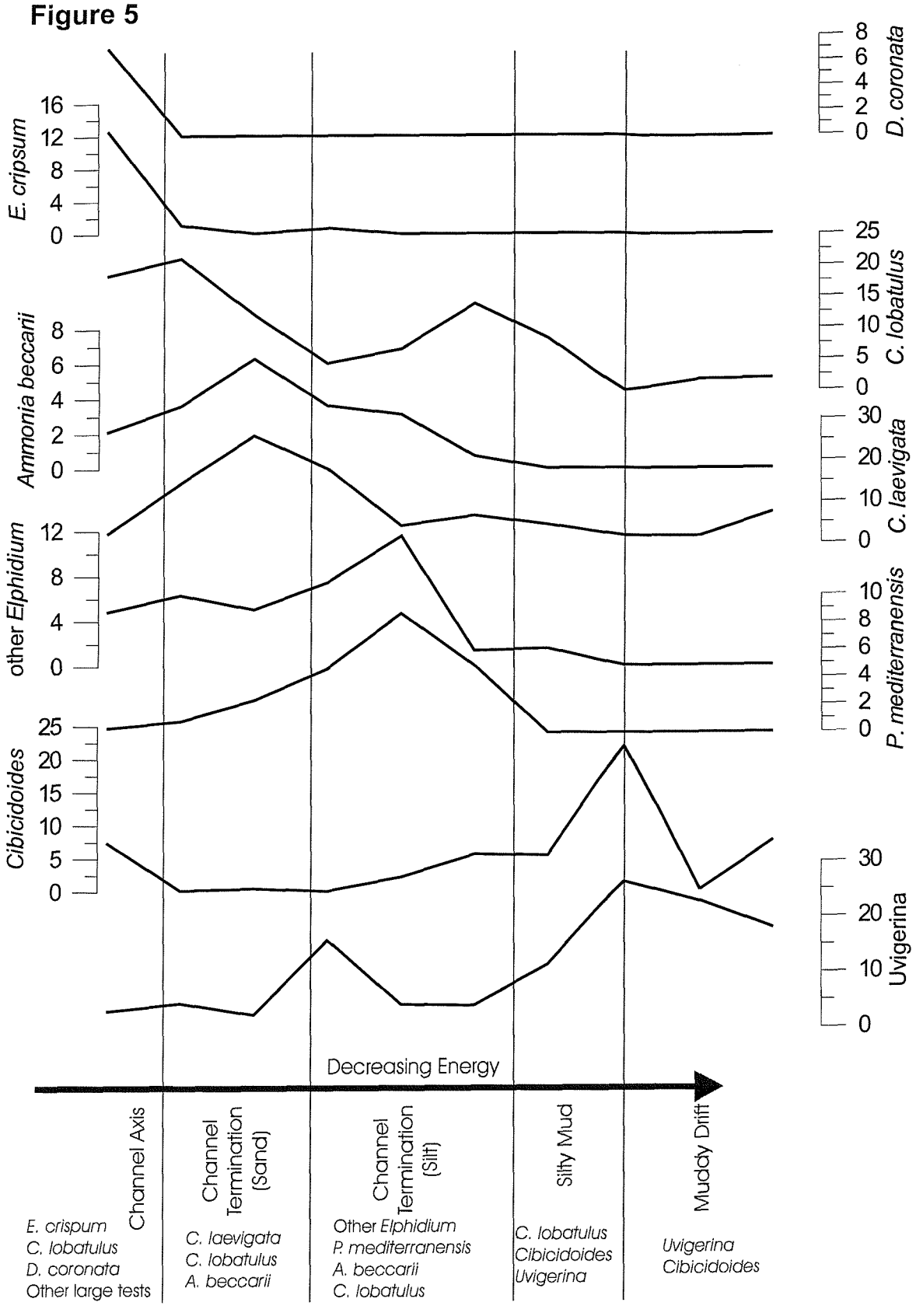

Figure 5. Environmental succession of benthic foraminiferal species on the Gil Eanes Drift. Indicator species for each environment are shown. Taxa represented are from top down, *D. coronata, E. cripsum, C. lobatulus, A. beccarii, C. laevigata, other Elphidium, P. mediterranensis, Cibicidoides and Uvigerina.*

population, and this would thus be expected in other bottom current or turbidite deposits.

Cibicides lobatulus is found in high abundance in all the sandy samples, and there are several very small (150μm) specimens in D13680 which are not found in those species believed to have been derived from the shelf. This indicates that this is probably an indigenous species in D13680. High abundance of this species, which is an important member of the "elevated epifauna" group, has been strongly linked to the presence of strong bottom-currents (Schönfeld, 1997, 2002a, b). The presence of an indigenous population of *C. lobatulus* within an assemblage that shows clear evidence of transportation is therefore consistent with the environment in which this sample was taken (i.e. with a permanent current) but would be inconsistent with a setting within a similar gravity-flow channel. A slope canyon would be identical in terms of subtrate, reworking of material from higher on the slope and position on the slope but has no permanent current and there would therefore be anticipated to be no large indigenous population of *C. lobatulus*. Such an association found in a fossil deposit would therefore provide supportive evidence for identification of the deposit as of the "contourite facies" rather than any other deep-sea sand, particularly where a spatially waning flow could be shown to be present.

Conclusion

The transportation of sands from the continental shelf onto the Gulf of Cadiz sediment drift is confirmed by the presence of abundant shelf dwelling benthic foraminifera and other bioclasts typical of the shelf. There is clear evidence of size-sorting in these transported tests, with the largest and densest tests deposited as part of a coarse lag in the axis of the Gil Eanes channel and lighter tests transported beyond the cannel to be deposited as part of increasingly fine deposits at the termination of the channel.

The presence of a probably indigenous population of the elevated epifaunal species *Cibicides lobatulus* within this assemblage is consistent with the hypothesis that high abundance of this species is indicative of strong near-bottom currents (Schönfeld, 2003). Where high populations of similar filter-feeding species can be found in association with reworked and sorted populations of species not believed to be indigenous in fossil deep-sea sands, this should be considered as indicative of a

permanent and spatially or temporally waning flow. This would be strong evidence supporting a hypothesis of a contourite origin for this sand developed from independent sedimentological characteristics. As recognition of fossil contourites is still controversial, evidence of this nature could be significant in increasing our understanding of these complex depositional systems.

Table 1. Abundance of important benthic foraminiferal species from the Gil Eanes Drift.

			D13900						D13898	
Species	Channel Axis (D13680)	Sandy Lobe (D13682)	Sand (260)	Silty Sand (1020)	Sandy silt (580cm)	Sandy silt (620cm)	Silty mud (760cm)	Clay-rich mud (0cm)	Clay-rich mud (60cm)	Silty mud (260cm)
C. lobatulus‡	18.4	21.2	12.2	4.4	13.9	6.7	8.4	0	1.8	2
C. laevigata	2.5	14.7	26.2	18.2	6.8	4.4	4.6	1.9	1.8	7.5
*P. mediterranensis**	0.4	0.9	2.4	4.7	4.9	8.7	0	0	0	0
E. crispum (of which juvenile)†	12.6 (0)	1.1 (1.1)	0.1 (0.1)	0.7 (0.7)	0	0	0	0	0	0
Other *Elphidium*†	4.8	6.3	5.0	7.4	1.3	11.5	1.5	0	0	0
*H. balthica**	1.2	2.8	1.3	0.3	6.1	3.3	1.5	0	0	0
*A. stelligerum**	0	0.3	0.3	8.2	4.2	0	0.8	0	0	0
*Ammonia beccarii**	2.1	3.6	6.3	3.6	0.7	3.1	0	0	0	0
D. coronata ‡	7.0	0	0	0	0	0	0	0	0	0
Large *Textularia*	5.8	0	0	0	0	0	0	0	0	0
Uvigerina	3.3	4.7	2.6	16	4.2	4.4	11.5	26.4	22.8	18
Cibicidoides	7.4	0.13	0.4	0	5.5	2.1	5.3	21.7	0	7.5

† - Generally shelf dwelling species (Murray, 1991).

‡ - "Elevated Epifauna" species (Schönfeld, 2002a)

* - Species reported living on shelf of GoC (Schönfeld, 1997, 2002b; Villanueva-Guimerans, 2000; Villanueva-Guimerans et al., 1999; Villanueva-Guimerans and Cervera-Currado, 1999)

8 Synthesis

A suite of sediment cores recovered from the Gil Eanes Drift (lower slope of the Gulf of Cadiz, Southwest Iberia) have been presented which give significant insight into the history of the major currents and hydrographic features and the sedimentology of this complex region. In contrast to previous observations made elsewhere in the Gulf of Cadiz (GoC), evidence is presented (Chapter 5) for the presence of the Mediterranean Outflow current during the Last Glaciation (sand in D13900, D13896, D13897 and D13686) and for locally increased current velocity (increased fine sand content in D13898 and D13897, increased sediment supply to D13892). This alteration in the flow path of the Mediterranean Outflow (MO) strongly suggests that the plume settled to greater depths during this period, and is consistent with observations of increased current activity below 1000m on the Portuguese margin (Schönfeld and Zahn, 2000). The behaviour of the MO current over the last 30ka is found to be consistent with predictions made from the physical constraints on the system; this observation has several implications:-

1) Sea level is the dominant control over the behaviour of the Mediterranean Outflow plume.
2) During the last glaciation, the Mediterranean Sea experienced anti-estuarine circulation comparable to that observed today.
3) During the last glaciation, the basin average net evaporation of the Mediterranean Sea was comparable to today.
4) Atlantic water was entrained into the Mediterranean Outflow plume in the past in a similar way to that observed today, and in similar proportion.
5) Mass transformation was therefore ongoing during the last glaciation, and the Azores Current is therefore expected to have been present.
6) Less salt may have been supplied to the Nordic Seas during the last glaciation, and this may have suppressed the formation of North Atlantic Deep Water.

Enhanced flow is found during the Younger Dryas when sea level was at an intermediate level (Chapter 5). Enhanced flow is observed both on the Gil Eanes Drift and in the modern flow path of the MO. Increased current activity may be related in

part to the impact on the circulation of the Mediterranean of melt water pulse 1a but increased buoyancy loss in the Mediterranean by increased net evaporation and cooling is also implicated.

Evidence for the presence of the Azores Front in the northern Gulf of Cadiz (the modern position of the Azores Current) is also presented (Chapter 4). As noted above, the Azores Current is expected to be present throughout the last 30,000 years as a result of export of water from the GoC. The Azores Front would therefore also be anticipated to be present, as velocity and temperature are intimately linked in ocean circulation. That the Azores Front penetrated into the northern GoC is indicated by enhanced thermal gradient between the GoC and the Iberian margin synchronous with increased vertical mixing. High abundances of the deep-living planktonic foraminiferan *Globorotalia scitula,* which is found in high abundances at the Azores Front today, confirms that this is the cause of the above. The Azores Front penetrates to ~1000m today, and would probably have done so in the past. Today, the top of the Mediterranean Outflow lies at 500m, and it may be the interaction between this plume and the Azores Front that prevents the latter penetrating into the GoC. A model of the transport of the Azores Current / Front has been shown to be strongly affected by the presence / absence of the Mediterranean Outflow (Alves and DeVerdière, 1999). The deeper settling of the plume in the past (probably to twice the modern depth during the last glacial maximum) may have allowed the AF to penetrate directly into the GoC.

The observation of the Azores Front in the palaeoceanographic record of the GoC has implications both for the practice of palaeoceanography and for the state of the ocean circulation in the past:-

1) A similar multi-proxy approach is likely to be valid in the investigation of other oceanic fronts. Oceanic circulation during the Last Glacial Maximum is beginning to be mapped and evidence of the presence / absence and position of major frontal systems (e.g. Gulf Stream, Sub-Arctic Polar Front etc.) provides vital constraint on models of palaeocirculation.
2) The behaviour of frontal zones can significantly influence proxy records.

3) The Azores Front lay at similar latitude to today during the last glaciation. The warm water sphere therefore was of similar extent.
4) It is likely that low latitude circulation in the North Atlantic was similar to today.

The Gil Eanes Drift itself has proven to have a complex sedimentary history (Chapters 5, 6, and 7). At present, it is the location of either muddy deposition or no net deposition as a result of sediment entrapment in the main flow path of the MO further up the slope. On the flanks of the drift, this is expressed as a light coloured clay rich mud which is rich in the tests of planktonic foramininfera and has accumulated relatively slowly (<10cm kyr^{-1}) under weak current conditions. Close to the lower parts of the Gil Eanes Channel (D13900) this clay overlies sand that is indicative of significantly increased energy conditions. On the uppermost Gil Eanes Drift this is expressed as a complex of thin layers of various composition (similar clay to that described above and clean, fine sand are both represented) separated by unconformities. This area is now the location of barchan-like dunes with erosional troughs. On the levees of the Gil Eanes Channel the Holocene is represented by a thin (30cm) layer of sand that has been strongly discoloured by diagenesis. This discolouration is probably diagenetic manganese.

Sediment deposited in the region of the Gil Eanes Drift is ultimately sourced from south-western Iberia (Chapter 6), and therefore supplied by the rivers that line the northern and eastern margins of the GoC as previously proposed by Nelson and others. It is initially deposited on the shelf where it probably remains for some time, as a wide range of characteristically shelfal bioclasts contribute to the sediment found on the slope. This sediment is reworked down slope, probably by mass flows, entrained into the MO and transported northwest along the slope to be deposited as the current wanes. Energetic sorting of these grains is observed in the reworked benthic foraminiferal tests (Chapter 7), which show a distinct succession from the least to the most transportable across the Gil Eanes Drift. This observation has some potential as a means of testing hypotheses regarding the origin of deep-sea sands.

High-resolution colour records are proposed as a means of developing initial chronostratigraphic frameworks for sediment cores. Correlations made on the basis of

colour may be particularly useful for developing sampling strategies for more conventional methods, such as stable isotope analysis. The origin of the colour variability found in the western GoC is found to be dilution of carbonate by terrigenous detritus. The detritus is petrologically similar to that found on the Gil Eanes Drift and so is probably derived from particulate matter suspended within the MO plume. Supply of detritus was high during the last glaciation relative to today, indicating that the turbulence of the plume was greater. This is consistent with the MO plume having a higher velocity during the LGM. Colour variability on a ~1.5kyr cycle in the Holocene, with dilution maxima coinciding with cool climatic periods is found. Increased haematite content is found within these layers, and it is proposed that this represents changes in atmospheric circulation at this location.

9 Future Work

Though significant light has been shed on the response of the Gulf of Cadiz to climate change, a number of observations and processes that deserve further investigation have also been found. These are described below.

Modelling of the LGM Mediterranean Outflow

The obvious continuation of this work is to attempt to model the settling of the MO plume in the GoC and its export into the North Atlantic. As the behaviour of the MO plume in the GoC seems to be simple and there appears to be no fundamental change in the mode of mixing and entrainment of Atlantic water it should be possible to modify a model that accurately simulates the settling of the plume today. Such a model exists, and is sufficiently accurate to produce both meddies off Cape St. Vincent and splitting of the plume, without any explicit attempt to make it do so (Johnson et al., 2002). As Mediterranean water is ultimately modified Atlantic water, an accurate settling trajectory may be achieved by modification of the properties of the water exported from Gibraltar to those calculated from the hydraulic constraints exerted by its sill and narrows configuration.

The Gibraltar Exchange and MO during the Younger Dryas

The anomalously strong current noted throughout the GoC during the Younger Dryas suggests a significant change in the state of the Gibraltar Exchange, and a simple model of the exchange and the Mediterranean Circulation is the best way of assessing which of the many possible causes is most likely. A model of this nature could give significant insight into the response of the circulation of the Mediterranean to rising sea level and millennial scale climatic variability. It would also be a tool by which the likely causes of the current oscillations found on the southern levee of the Gil Eanes Channel (Chapter 7) could be assessed.

Quantitative estimation of deep export from the GoC

A suite of long sediment cores taken perpendicular to the axis of the Gil Eanes Channel and extending beyond the limit of the Gil Eanes Drift on both sides would allow quantitative estimation of the flux of the MO as it lifts off the sea floor. A variety of proxy measurements could be used in order to achieve this, including temperature and velocity. If locations at which the two end-members of the mixed

MO plume water (Mediterranean and Atlantic) could be assessed were found, a wide range of geochemical measurements of conservative tracers (^{13}C, ^{18}O, ^{87}Sr and the ratios of Ba, B, Sr, Mg, and others to Ca) could be made on epibenthic foraminiferal tests. A full assessment of the behaviour of the MO current from its formation in the Alboran Sea out into the open Atlantic could be made. This would be a very powerful tool in assessment of the palaeo-circulation of the western Mediterranean and at intermediate depths in the Atlantic.

The expression of the deglaciation in the Gulf of Cadiz

In Chapter 4 it is noted that during the deglaciation, subsequent to the withdrawal of the Azores Front, the surface stratification at D13898 seems to collapse. Coincident with this, the planktonic foraminiferan *Globigerina quinqueloba* becomes abundant (~15%) for the first time in this record. A similar feature is found coincident with the termination of the Younger Dryas, which is also immediately subsequent to a withdrawal of the Azores Front. Coincident peaks in *G. quinqueloba* are found in D13892. It is likely that these features represent a systematic change in the surface circulation as a response to rapid sea level rise or the melting of terrigenous ice and snow. Further investigation of a suite of cores more widely spread through the GoC might produce significant insight into the influence of the deglaciations on the circulation of the GoC and surrounding region.

Oceanic Fronts

Fronts are an important part of the ocean circulation, and are largely still an unknown quantity in terms of their behaviour as a response to climate change. The approach used in Chapter 4 should be applicable both as a means of tracing the Azores Front across the Atlantic and for identification and mapping of fronts in other locations and at other times.

10 References

Aksu, A. E., D. Yasar, P. J. Mudie, and H. Gillespie, 1995, Late Glacial-Holocene paleoclimatic and paleoceanographic evolution of the Aegean Sea - micropaleontological and stable isotopic evidence: Marine Micropalaeontology, v. 25, p. 1-28.

Allen, J. R. M., U. Brandt, A. Brauer, H.-W. Hubberten, B. Huntley, J. Keller, M. Kraml, M. Mackensen, J. Mingram, J. F. W. Negendank, N. R. Nowaczyk, H. Oberhansli, W. A. Watts, S. Wulf, and B. Zolitschka, 1999, Rapid environmental changes in southern Europe during the Last Glacial Cycle: Nature, v. 400, p. 740-742.

Allen, J. R. M., and B. Huntley, 1996, The vegetation and climate of north-west Iberia over the last 14,000 years.: Journal of Quaternary Science, v. 11, p. 125-147.

Alley, R. B., 1998, Icing the North Atlantic: Nature, v. 392, p. 335-336.

Alley, R. B., S. Anandakrishnan, and P. Jung, 2001, Stochastic resonance in the North Atlantic: Paleoceanography, v. 16, p. 190-198.

Alley, R. B., and P. U. Clark, 1999, The deglaciation of the northern hemisphere: a global perspective: Annual Review of Earth and Planetary Science, v. 27, p. 149-182.

Alley, R. B., P. A. Mayewski, T. Sowers, M. Stuiver, K. C. Taylor, and P. U. Clark, 1997, Holocene climatic instability: A prominent, widespread event 8200 yr ago: Geology, v. 25, p. 483-486.

Alpers, C. N., D. W. Blowes, D. K. Nordstrom, and J. L. Jambor, 1994, Secondary minerals and acid mine-water chemistry, *in* J. L. Jambor, and D. W. Blowes, eds., Short Course Handbook on Environmental Geochemistry of Sulfide Mine-Wastes., Mineralogical Association of Canada, p. 247–270.

Alves, M., F. Gaillard, M. Sparrow, M. Knoll, and S. Giraud, 2002, Circulation patterns and transport of the Azores front-current system: Deep-Sea Research II, v. 49, p. 3983-4002.

Alves, M. L. G. R., and A. C. DeVerdière, 1999, Instability dynamics of a subtropical jet and applications to the Azores Front current system: Eddy-driven mean flow: Journal of Physical Oceanography, v. 29, p. 837-864.

Ambar, I., and M. R. Howe, 1979, Observations of the Mediterranean Outflow II - The deep circulation in the vaicinity of the Gulf of Cadiz: Deep-Sea Research, v. 26A, p. 555-568.

Ambar, I., N. Serra, M. J. Brogueira, G. Cabecadas, F. Abrantes, P. Freitas, C. Goncalves, and N. Gonzalez, 2002, Physical, chemical and sedimentological aspects of the Mediterranean outflow off Iberia: Deep-Sea Research II, v. 49, p. 4163-4177.

An, Z. H., G. J. Kukla, S. C. Porter, and J. L. Xiao, 1991, Magnetic susceptibility evidence of monsoon variation on the loess plateau of central China during the last 130,000 yaers: Quaternary Research, v. 36, p. 29-36.

Angel, M. V., 1989, Vertical profiles of pelagic communities in the vicinity of the Azores Front and their implications to deep ocean ecology: Progress in Oceanography, v. 22, p. 1-46.

Anklin, M., J. Schwander, B. Stauffer, J. Tschumi, A. Fuchs, J. M. Barnola, and D. Raynaud, 1997, CO2 record between 40 and 8 kyr BP from the Greenland Ice

Core Project ice core: Journal of Geophysical Research - Oceans, v. 102, p. 26539-26545.

Antonov, J. I., S. Levitus, T. P. Boyer, M. E. Conkright, T. D. O'Brien, and C. Stephens, 1998, Temperature of the Atlantic Oceans: World Ocean Atlas 1998, v. 1: Silver Spring, MD, U.S. Department of Commerce.

Arhan, M., 1990, The North Atlantic Current and Subarctic Intermediate Water: Journal of Marine Research, v. 48, p. 109-144.

Armi, L., and N. A. Bray, 1982, A standard analytical curve of potential temperature versus salinity for the western North Atlantic: Journal of Physical Oceanography, v. 24, p. 1295-1316.

Armi, L., and D. M. Farmer, 1986, Maximal two-layer exchange through a contraction with barotropic flow: Journal of Fluid Mechanics, v. 164, p. 27-51.

Armi, L., and D. M. Farmer, 1988, The flow of Mediterranean water through the Srait of Gibraltar: Progress in Oceanography, v. 21, p. 1-105.

Arnold, A. J., and W. C. Parker, 1999, Biogeography of planktonic foraminifera, *in* B. K. SenGupta, ed., Modern Foraminifera: Great Britain, Kluwer Academic Press, p. 103-122.

Azanon, J. M., A. Crespo-Blanc, V. Garcia-Duenas, and M. Sanchez-Gomez, 1996, Folding of metamorphic isograde in the Adra extensional unit (Alpujarride complex, Central Betics): Compte Rendus de l'Academie des Sciences; Serie II Fascicule A - Sciences de la Terre et des Planets, v. 323, p. 949-956.

Balsam, W. L., and B. C. Deaton, 1996, Determining the composition of late Quaternary marie sediments from NUV, VIS and NIR diffuse reflectance spectra.: Marine Geology, v. 134, p. 31-55.

Balsam, W. L., B. L. Ottobleisner, and B. C. Deaton, 1995, Modern and last glacial maximum eolian sedimentation patterns in the Atlantic-ocean interpreted from sediment iron-oxide content: Paleoceanography, v. 10, p. 493-507.

Barber, D. C., A. Dyke, C. Hillaire-Marcel, A. E. Jennings, J. T. Andrews, M. W. Kerwin, G. Bilodeau, R. McNeely, J. Southon, M. D. Morehead, and J.-M. Gagnon, 1999, Forcing of the cold event of 8,200 years ago by catastrophic drainage of Laurentide lakes: Nature, v. 400, p. 344-348.

Bard, E., A. J. Arnold, P. Maurice, J. Duprat, J. Moyes, and J. C. Duplessy, 1987, Retreat velocity of the North Atlantic polar front during the last deglaciation determined by ^{14}C accelerator mass spectrometry: Nature, v. 328, p. 791-794.

Bard, E., B. Hamelin, M. Arnold, L. Montaggioni, G. Cambioch, G. Faure, and F. Rougerie, 1996, Deglacial sea-level record from Tahiti corals and the timing of global meltwater discharge: Nature, v. 382, p. 241-244.

Bar-Matthews, M., A. Ayalon, A. Kaufman, and G. J. Wasserburg, 1999, The Eastern Mediterranean paleoclimate as a reflection of regional events: Soreq cave, Israel: Earth and Planetary Science Letters, v. 166, p. 85-95.

Bateman, M. D., and A. Diez-Herrero, 2001, The timing and relation of aeolian sand deposition in central Spain to the aeolian sand record of NW Europe: Quaternary Science Reviews, v. 20, p. 779-782.

Behl, R. J., and J. P. Kennett, 1996, Brief interstadial events in the Santa Barbara Basin, NE Pacific, during the last 60kyr.: Nature, v. 379, p. 243-246.

Bemis, B. E., H. J. Spero, J. Bijma, and D. W. Lea, 1998, Reevaluation of the oxygen composition of planktonic foraminifera: experimental results and revised paleotemperature equations: Paleoceanography, v. 13, p. 150-160.

Bemis, B. E., H. J. Spero, D. W. Lea, and J. Bijma, 2000, Temperature influence on the carbon isotopic composition of *Globigerina bulloides* and *Orbulina*

universa (planktonic foraminifera): Marine Micropalaeontology, v. 38, p. 213-228.

Bemis, B. E., H. J. Spero, and R. C. Thunnell, 2002, Using species-specific paleotemperature equations with foraminifera: a case study in the Southern California Bight: Marine Micropalaeontology, v. 46, p. 405-430.

Berger, A., T. Fichefet, H. Gallee, I. Marsiat, C. Tricot, and J. P. Vanypersele, 1990, Physical Interactions within a Coupled Climate Model over the Last Glacial Interglacial Cycle: Transactions of the Royal Society of Edinburgh-Earth Sciences, v. 81, p. 357-369.

Berger, A. L., 1978, Long-term variations of daily insolation and Quaternary climatic changes: Journal of Atmospheric Science, v. 35, p. 2362-2367.

Berger, A. L., 1979, Insolation signatures of Quaternary climatic chnages.: Il nuovo Cimento, v. 2, p. 63-87.

Berger, A. L., and M. F. Loutre, 1988, Insolation values for the climate of the last 10 million years: Quaternary Science Reviews, v. 10, p. 297-317.

Berger, W. H., 1981, Oxygen and carbon isotopes in foraminifera - an introduction: Palaeogeography, Palaeoclimatology, Palaeoecology, v. 33, p. 3-7.

Bethoux, J. P., 1979, Budgets of the Mediterranean Sea. Thier dependance on the local climate and on the characteristics of the Atlantic waters: Oceanologica Acta, v. 2, p. 157-163.

Bigg, G. R., 1994, An ocean general circulation model of the glacial Mediterranean thermohaline circulation: Paleoceanography, v. 9, p. 705-722.

Bigg, G. R., 1995, Aridity of the Mediterranean Sea at the Last Glacial Maximum: A reinterpretation of the $\delta^{18}O$ record.: Paleoceanography, v. 10, p. 283-290.

Bintanja, R., R. S. W. van de Wal, and J. Oerlemans, 2002, Global ice volume variations through the last glacial cycle simulated by a 3-D ice-dynamical model: Quaternary International, v. 95-6, p. 11-23.

Bond, G., W. Broecker, S. Johnsen, J. McManus, L. Labeyrie, J. Jouzel, and G. Bonami, 1993, Correlations between climate records from north Atlantic sediments and Greenland ice: Nature, v. 365, p. 143-147.

Borenas, K. M., A. K. Wahlin, I. Ambar, and N. Serra, 2002, The Mediterranean outflow splitting - a comparison between theoretical models and CANIGO data: Deep-Sea Research II, v. 49, p. 4195-4205.

Bormans, M., C. Garrett, and K. R. Thompson, 1986, Seasonal variability of the surface inflow through the Straits of Gibraltar: Oceanologica Acta, v. 9, p. 403-414.

Borrego, J., F. Ruiz, M. L. Gonzalez-Regalado, J. G. Pendon, and J. A. Morales, 1999, The Holocene transgression into the estuarine central basin of the Odiel River mouth (Cadiz gulf, SW, Spain): lithology and faunal assemblages: Quaternary Science Reviews, v. 18, p. 769-788.

Bouvier-Soumagnac, Y., and J. C. Duplessy, 1985, Carbon and oxygen isotopic composition of planktonic foraminifera from laboratory culture, plankton tows and recent sediment: implications for the reconstruction of paleoclimatic conditions and of the global carbon cycle.: Journal of Foraminiferal Research, v. 15, p. 302-320.

Broecker, W., 1991, The Great Ocean Conveyor.: Oceanography, v. 4, p. 79-89.

Broecker, W., 1994, Massive iceberg discharges as triggers for global climate change: Nature, v. 372, p. 421-424.

Broecker, W., 1997, Mountain glaciers: Recorders of atmospheric water vapor content?: Global Biogeochemical Cycles, v. 11, p. 589-597.

Broecker, W., D. M. Peteet, and D. Rind, 1985, Does the ocean-atmosphere system have more than one stable mode of operation.: Nature, v. 315, p. 21-26.

Broecker, W. S., 2000, Abrupt climate change: causal constraints provided by the paleoclimate record: Earth-Science reviews, v. 51, p. 137-154.

Brovkin, V., 2002, Climate-vegetation interaction: Journal De Physique Iv, v. 12, p. 57-72.

Bryden, H. L., 1993, Sill exchange to and from enclosed seas, *in* N. F. R. D. Croce, ed., Symposium Mediterranean Symposium., Instituto Scienze Ambientali Marine, p. 17-41.

Bryden, H. L., E. C. Brady, and R. D. Pillsbury, 1988, Flow through the strait of Gibraltar, *in* J. L. Almazan, H. L. Bryden, T. Kinder, and G. Parilla, eds., Seminario sobre la Oceanografia fisica del Estracho de Gibraltar: Madrid, SECEG.

Bryden, H. L., J. Candela, and T. Kinder, 1994, Exchange through the Strait of Gibraltar: Progress in Oceanography, v. 33, p. 201-248.

Bryden, H. L., and T. Kinder, 1991, Steady two-layer exchange through the Strait of Gibraltar: Deep-Sea Research, v. 38, p. S445-463.

Bryden, H. L., and H. M. Stommel, 1982, Origins of the Mediterranean Outflow: Journal of Marine Research, v. 40, p. 55-71.

Bryden, H. L., and H. M. Stommel, 1984, Limiting processes that determine basic features of the circulation in the Mediterranean Sea: Oceanologica Acta, v. 7, p. 289-196.

Cacho, I., J. O. Grimalt, M. Canals, L. Sbaffi, N. J. Shackleton, J. Schönfeld, and R. Zahn, 2001, Variability of the western Mediterranean Sea surface temperature during the last 25,000 years and its connection with the northern hemisphere climatic changes: Paleoceanography, v. 16, p. 40-52.

Cacho, I., J. O. Grimalt, C. Pelejero, M. Canals, F. J. Sierro, J. A. Flores, and N. Shackleton, 1999, Dansgaard-Oesschger and Heinrich event imprints in Alboran Sea palaeotemperatures: Paleoceanography, v. 14, p. 698-705.

Cacho, I., J. O. Grimalt, F. J. Sierro, N. J. Shackleton, and M. Canals, 2000, Evidence for enhanced Mediterranean thermohaline circulation during rapid climatic coolings: Earth and Planetary Science Letters, v. 183, p. 417-429.

Calvert, A., l. E. Sandvo, D. Seber, M. Barazangi, F. Vidal, G. Alguacil, and N. Jabour, 2000, Propagation of regional seismic phases (Lg and Sn) and Pn velocity structure along the Africa-Iberia plate boundary zone: tectonic implications: Geophysical Journal International, v. 142, p. 384-408.

Candela, J., C. D. Winant, and H. L. Bryden, 1989, Meteorologically forced subinertial flows through the Strait of Gibraltar: Journal of Geophysical Research, v. 94, p. 12667-12679.

Caralp, M. H., 1988, Late Glacial to recent deep-sea benthic foraminifera from the Northeastern Atlantic (Cadiz Gulf) and Western Mediterranean (alboran Sea): Palaeoceanographic results: Marine Micropalaeontology, v. 13, p. 265-289.

Casford, J. S. L., E. J. Rohling, R. Abu-Reid, S. Cooke, C. Fontanier, M. Leng, and V. Lykousis, 2002, Circulation changes and nutrient concentrations in the late Quaternary Aegean Sea: A nonsteady state concept for sapropel formation: Paleoceanography, v. 17.

Cayre, O., Y. Lancelot, E. Vincent, and M. A. Hall, 1999, Palaeoceanographic reconstructions from planktonic foraminifera off the Iberian Margin: temperature, salinity and Heinrich events: Paleoceanography, v. 14, p. 384-396.

Chapman, M. R., N. J. Shackleton, and J. C. Duplessy, 2000, Sea surface temperature variability during the last glacial-interglacial cycle: assessing the magnitude and pattern of climate change in the North Atlantic: Palaeogeography, Palaeoclimatology, Palaeoecology, v. 157, p. 1-25.

Cifelli, R., 1974, Planktonic foraminifera from Mediterranean and adjacent Atlantic waters (cruise 49 of the Atlantis II, 1969): Journal of Foraminiferal Research, v. 4, p. 171-183.

Clague, J. J., and T. S. James, 2002, History and isostatic effects of the last ice sheet in southern British Columbia: Quaternary Science Reviews, v. 21, p. 71-87.

Clark, P. U., and P. J. Bartlein, 1995, Correlation of late-Pleistocene glaciation in the western United States with North Atlantic Heinrich events: Geology, v. 23, p. 483-486.

CLIMAP, 1976, The surface of the ice-age earth: Science, v. 191, p. 1131-1137.

Coplen, T. B., 1988, Normalization of oxygen and hydrogen isotope data.: Chemical Geology (Isotope Geoscience Section), v. 72, p. 293-297.

Coplen, T. B., 1994, Reporting of stable hydrogen, carbon, and oxygen isotopic abundances.: Pure and Applied Chemistry, v. 66, p. 273-276.

Dansgaard, W., S. Johnsen, H. B. Clausen, D. Dahl-Jensen, N. S. Gundestrup, C. U. Hammer, C. S. Hvidberg, J. P. Steffensen, A. E. Sveinbjornsdottir, J. Jouzel, and G. Bond, 1993, Evidence for general instability of past climate from a 250-kyr ice-core record: Nature, p. 218-220.

Deuser, W. G., 1987, Seasonal variations in isotopic composition and deep-water fluxes of the tests of perennially abundant planktonic foraminifera of the Sargasso Sea - results from sediment-trp collections and thier paleoceanographic significance: Journal of Foraminiferal Research, v. 17, p. 14-27.

Donahue, D. J., 1990, Radiocarbon analysis by accelerator mass spectrometry.: International J. Mass Spectrometry and Ion Processes, v. 143, p. 235-245.

Dorman, C. E., R. C. Beardsley, and R. Limeburner, 1995, Winds in the Strait of Gibraltar: Quarterly Journal of the Meteorological Society, v. 121, p. 1903-1921.

Doval, D. D., X. A. Alvarez-Salgado, and F. F. Perez, 2001, Organic matter distributions in the Eastern North Atlantic-Azores Front region: Journal of Marine Systems, v. 30, p. 33-49.

Duplessy, J. C., P. L. Blanc, and A. W. H. Be, 1981, O-18 enrichment of planktonic foraminifera due to gametogenetic calcification below the euphotic zone: Science, v. 213, p. 1247-1250.

Duplessy, J. C., N. J. Shackleton, R. G. Fairbanks, L. Labeyrie, D. Oppo, and N. Kallel, 1988, Deepwater source variations during the last climatic cycle and thier impact on the global deepwater circulation: Paleoceanography, v. 3, p. 343-360.

Duprat, J., 1983, Les foraminifères planktoniques du Quaternaire terminal d'un domaine pericontinental (Golfe de Gascoigne, Côtes ouest-Iberiques, Mer d'Alboran): écologie - biostratigraphique: Bulletin Institue Géologique Bassin d'Aquitaine, v. 33, p. 71-150.

Duquesne, K., S. Lebrun, C. Casiot, O. Bruneel, J. C. Personne, M. Leblanc, F. Elbaz-Poulichet, G. Morin, and V. Bonnefoy, 2003, Immobilization of arsenite and ferric iron by acidithiobacillus ferrooxidans and its relevance to acid mine drainage: Applied Environmental Microbiology, v. 69, p. 6165-6173.

Dutkiewicz, S., L. Rothstein, and T. Rossby, 2001, Pathways of cross-frontal exchange in the North Atlantic Current: Journal of Geophysical Research - Oceans, v. 106, p. 26917-26928.

Emiliani, C., 1955, Pleistocene temperatures: Journal of Geology, v. 63, p. 538-587.

Fairbanks, R. G., 1990, The age and origin of the "Younger Dryas event" in Greenland ice cores.: Paleoceanography, v. 5, p. 937-948.

Fairbanks, R. G., M. S. Sverdlove, R. Free, P. H. Wiebe, and A. W. H. Be, 1982, Vertical distribution and isotopic fractionation of living planktonic foraminifera: Nature, v. 298, p. 841-844.

Fairbanks, R. G., and P. H. Wiebe, 1980, Foraminifera and chrolophyll maximum: vertical distribution, seasonal succession and paleoceanographic significance: Science, v. 209, p. 1524-1526.

Fairbanks, R. G., P. H. Wiebe, and A. W. H. Be, 1980, Vertical distribution and isotopic composition of living foraminifera in the western North Atlantic: Science, v. 207, p. 61-63.

Farmer, D. M., and L. Armi, 1986, Maximal two-layer exchange over a sill and contraction with barotropic flow.: Journal of Fluid Mechanics, v. 164, p. 53-76.

Farmer, D. M., and L. Armi, 1988, The flow of Atlantic water through the Strait of Gibraltar: Progress in Oceanography, v. 21, p. 1-105.

Fasham, M. J. R., T. Platt, B. Irwin, and K. Jones, 1985, Factors affecting the spatial pattern of the Deep Chrolophyll Maximum in the region of the Azores Front, *in* J. Crease, W. J. Gould, and P. M. Saunders, eds., Essays on Oceanography: A tribute to John Swallow: Progress in Oceanography, v. 14: Oxford, Pergamon Press, p. 129-166.

Faugères, J. C., E. Gonthier, J. P. Peypouquet, C. Pujol, and C. Vergnaud-Grazzini, 1986, Distribution et variations des courants de fond sur la ride, de Faro (Golfe de Cadiz), temoins des modifications de échanges Mediterranee Atlantique au Quaternaire Recent: Bulletin Société Géologique de France, v. 2, p. 423-432.

Faugères, J. C., E. Gonthier, and D. A. V. Stow, 1984, Contourite drift remolded by deep Mediterranean outflow.: Geology, v. 12, p. 296-300.

Faugères, J. C., and D. A. V. Stow, 1993, Bottom-current-controlled sedimentation: a synthesis of the contourite problem: Sedimentary geology, v. 82, p. 287-297.

Fernandez, W., and R. D. Pingree, 1996, Coupling between physical and biological fields in the North Atlantic subtropical front southeast of the Azores: Deep-sea research I, v. 43, p. 1369-1393.

Fiuza, A. F. G., 1981, Upwelling off Portugal, *in* E. Suess, and J. Thiede, eds., Coastal Upwelling: NATO Conference Series: Series IV: Marine Sciences, v. A: New York, Plenum Press, p. 85-98.

Fiuza, A. F. G., M. E. Macedo, and M. R. Guerreiro, 1982, Climatological space and time variation of the Portuguese coastal upwelling: Oceanologica Acta, v. 5, p. 31-40.

Fratantoni, D. M., 2001, North Atlantic surface circulation during the 1990's observed with satellite-tracked drifters: Journal of Geophysical Research - Oceans, v. 106, p. 2067-22093.

Fukushi, K., M. Sasaki, T. Sato, N. Yanase, H. Amano, and H. Ikeda, 2003, A natural attenuation of arsenic in drainage from an abandoned arsenic mine dump: Applied Geochemistry, v. 18, p. 1267-1278.

Gammelsrod, T., 1975, Instability of Couette flow in a rotating fluid and origin of Langmuir circulations: Journal of Geophysical Research, v. 80, p. 5069-5075.

Ganssen, G., and M. Sarnthein, 1983, Stable isotope composition of foraminifers: the surface and bottom water record of coastal upwelling, *in* E. Suess, and J. Thiede, eds., Coastal Upwelling: its sediment record: NATO conference series:- series IV Marine Sciences, v. Part A: New York, Plenum Press, p. 604.

Garcia-Sandchez, A., and E. Alvarez-Ayuso, 2003, Arsenic in soils and waters and its relation to geology and mining activities (Salamanca Province, Spain): Journal of Geochemical Exploration, v. 80, p. 69-79.

Garrett, C. M., M. Bormans, and K. Thompson, 1990, Is the exchange through the Straits of Gibraltar maximal or sub-maximal, *in* L. J. Pratt, ed., The Physical oceanogrpahy of sea straits: Boston, Kluwer, p. 271-194.

Gasse, F., and E. vonCampo, 1994, Abrupt post-glacial climate events in west Asia and north Africa monsoon domains: Earth and Planetary Science Letters, v. 126, p. 435-456.

Giosan, L., 2002, On the use of spectrophotometry on old sediment material.

Giosan, L., R. D. Flood, and R. C. Aller, 2002, Palaeoceanographic significance of seidment color on western North Atlantic drifts: I, Origin of color: Marine Geology, v. 189, p. 25-41.

Girton, J. B., T. B. Sanford, and R. H. Kase, 2001, Synoptic sections of the Denmark Strait Overflow: Geophysical Research Letters, v. 28, p. 1619-1622.

Goddard, M. B., R. M. Overbeck, O. N. Rove, J. T. Singewald, and P. D. Trask, 1948, Rock-Color Chart: Washington D.C., National Research Council, 6 p.

Gonthier, E., J. C. Faugères, and D. A. V. Stow, 1984, Contourite facies of the Faro Drift, Gulf of Cadiz, *in* D. A. V. Stow, and D. J. Piper, eds., Fine-grained sediments: Deep-water processes and facies, v. 15: London, Geological Society Special Publication, p. 275-292.

Gould, W. J., 1985, Physical Oceanography of the Azores Front, *in* J. Crease, W. J. Gould, and P. M. Saunders, eds., Essays in Oceanography: A tribute to John Swallow: Progress in oceanography: Oxford, Pergamon Press, p. 167-190.

Grimm, E. C., G. L. Jacobson, W. A. Watts, B. C. Hansen, and K. A. Maasch, 1993, A 50,000-year record of climatic oscillations from Florida and its temporal correlation with the Heinrich Events: Science, v. 261, p. 198-200.

GRIP_Members, 1993, Climate instability during the last interglacial period recorded in the GRIP ice core: Nature, v. 364, p. 203-218.

Grootes, P., M. Stuiver, J. W. C. White, S. Johnsen, and J. Jouzel, 1993, Comparison of the oxygen isotope curves of GISP2 and GRIP Greenland ice cores: Nature, v. 366, p. 552-554.

Grossman, E. L., 1984, Carbon isotopic fractionation in live benthic foraminifera - comparison with inorganic precipitate studies: Geochimica et Cosmochimica Acta, v. 48, p. 1505-1512.

Grousset, F. E., E. Cortijo, S. Huon, L. Herve, T. Richter, D. Burdloff, J. Duprat, and O. Weber, 2001, Zooming in on Heinrich layers: Paleoceanography, v. 16, p. 240-259.

Grousset, F. E., M. Parra, A. Bory, P. Martinez, P. Bertrand, G. Shimmield, and R. M. Ellam, 1998, Saharan wind regimes traced by the Sr-Nd isotopic composition of subtropical Atlantic sediments: Last Glacial Maximum and Today: Quaternary Science Reviews, v. 17, p. 395-409.

Grousset, F. E., C. Pujol, L. Labeyrie, G. Auffret, and A. Boelaert, 2000, Were the North Atlantic Heinrich events triggered by the behaviour of the European ice sheets?: Geology, v. 28, p. 123-126.

Grutzner, J., L. Giosan, S. O. Franz, R. Tiedemann, E. Cortijo, W. P. Chaisson, R. D. Flood, S. Hagen, L. D. Keigwin, S. Poli, D. Rio, and T. Williams, 2002, Astonomical age models for Pleistocene drift sediments from the western North Atlantic (ODP Sites 1055-1063). Marine Geology, v. 189, p. 5-23.

Habgood, E., N. H. Kenyon, D. G. Masson, A. Akhmetzhanov, P. P. E. Weaver, J. Gardner, and T. Mulder, 2003, Deep-water sediment wave fields, bottom current sand channels and gravity flow channel-lobe systems: Gulf of Cadiz, NE Atlantic: Sedimentology, v. 50, p. 1-27.

Hall, I. R., and I. N. McCave, 2000, Palaeocurrent reconstruction, sediment and thorium focussing on the Iberian margin over the last 140ka: Earth and Planetary Science Letters, v. 178, p. 151-164.

Hammarstrom, J. M., R. R. Seal, A. L. Meier, and J. C. Jackson, 2003, Weathering of sulfidic shale and copper mine waste: secondary minerals and metal cycling in Great Smoky Mountains National Park, Tennessee, and North Carolina, USA: Environmental Geology, v. 45, p. 35-57.

Harland, R., 1983, Distribution maps of recent dinoflagellate cycts in bottom sediments from the north Atlantic Ocean and adjacent seas.: Palaeontology, v. 26, p. 321-387.

Hastings, D. W., A. D. Russell, and S. R. Emerson, 1998, Foraminiferal magnesium in Globeriginoides sacculifer as a paleotemperature proxy: Paleoceanography, v. 13, p. 161-169.

Hays, J. D., and A. Peruzza, 1972, The significance of calcium carbonate oscillations in the eastern equatorial Atlantic deep-sea sediments for the end of the Holocene warm interval: Quaternary Research, v. 2, p. 355-362.

Healy-Williams, N., 1992, Stable isotope differences among morphotypes of *Neogloboquadrina pachyderma* (Ehrenburg): implications for high-latitude palaeoceanographic studies: Terra Nova, v. 4, p. 693-700.

Heilemann, K., 2000, Hydrodynamische Anderungen des Mittelmeersausstromwassers und deren Abbildung in der Sedimenten des iberischen Kontinentalhangs, Christian-Albrechts-Universitat, Kiel.

Heinrich, H., 1988, Origin and consequences of cyclic ice rafting in the northeast Atlantic Ocean during the Past 130,000 years.: Quaternary Research, v. 29, p. 142-152.

Hemleben, C., D. Meischner, R. Zahn, A. AlmogiLabin, H. Erlenkeuser, and B. Hiller, 1996, Three hundred eighty thousand year long stable isotope and faunal records from the Red Sea: Influence of global sea level change on hydrography: Paleoceanography, v. 11, p. 147-156.

Hemleben, C., and M. Spindler, 1983, Recent advances in research on living planktonic foraminifera: Utrecht. Micropalaeontol. Bull., v. 30, p. 141-170.

Hemleben, C., M. Spindler, and O. R. Anderson, 1989, Modern Planktonic Foraminifera, Springer-Verlag, 363 p.

Hernandez-Molina, J., E. Llave, L. Somoza, M. C. Fernandez-Puga, A. Maestro, R. Leon, T. Medialdea, A. Barnolas, M. Garcia, V. D. d. Rio, L. M. Fernandez-Salas, J. T. Vazquez, F. Lobo, J. M. Alverinho-Dias, J. Rodero, and J. Gardner, 2003, looking for clues to palaeoceanogrpahic imprints: A diagnosis of the Gulf of Cadiz contourite depositional systems: Geology, v. 31, p. 19-22.

Heuser, A., 2002, Variations in calcium isotopes (δ44C) in Foraminifers over the past 24Ma, Christian Albrechts Universitat, Kiel, 97 p.

Hilbrecht, H., 1997, morphologic gradation and ecology in *Neogloboquadrina pachyderma* and *Neogloboquadrina dutertrei* (planktic foraminifera) from core top sediments.: Marine Micropalaeontology, v. 31, p. 31-43.

Hostetler, S. W., P. U. Clark, P. J. Bartlein, A. C. Mix, and N. J. Pisias, 1999, Atmospheric transmission of North Atlantic Heinrich events: Journal of Geophysical Research, v. 104, p. 3947-3952.

Hughen, K. A., J. T. Overpeck, L. C. Peterson, and S. Trumbore, 1996, Rapid climate changes in the tropical Atlantic region during the last deglaciation: Nature, v. 380, p. 51-54.

Hutson, W. H., 1980, The Agulhas current during the Late Pleistocene. Analysis of modern faunal analogs: Science, v. 207, p. 64-66.

Imbrie, J., A. L. Berger, E. A. Boyle, S. C. Clemens, A. Duffy, W. R. Howard, G. Kukla, J. Kutzbach, D. Martinson, A. McIntyre, A. Mix, B. Molfino, J. J. Morley, L. C. Peterson, N. G. Pisias, W. Prell, M. E. Raymo, N. J. Shackleton, and J. R. Toggweiler, 1993, On the structure and origin of major glaciation cycles, 2. The 100,000-year cycle: Paleoceanography, v. 8, p. 699-735.

Imbrie, J., E. A. Boyle, S. C. Clemens, A. Duffy, W. R. Howard, G. Kukla, J. Kutzbach, D. Martinson, A. McIntyre, A. Mix, B. Molfino, J. J. Morley, L. C. Peterson, N. G. Pisias, W. Prell, M. E. Raymo, N. Shackleton, and J. R. Toggweiler, 1992, On the structure and origin of major glaciation cycles 1. Liner responses to Milankovitch forcing: Paleoceanography, v. 7, p. 701-738.

Imbrie, J., and J. Z. Imbrie, 1980: Science, v. 207, p. 943.

Imbrie, J., and N. G. Kipp, 1971, A new micropalaeontological method for quantitative palaeoclimatology: Application to a late Pleistocene Caribbean core, *in* K. K. Turekian, ed., Late Cenozoic glacial ages: New Haven, Yale University Press, p. 77-181.

Iorga, M. C., and M. S. Lozier, 1999, Signatures of the Mediterranean outflow from a North Atlantic climatology 1. Salinity and density fields: Journal of Geophysical Research, v. 104, p. 25,985-26,009.

Jarvis, I., 1992, Sample preparation for ICP-MS, *in* K. E. Jarvis, A. L. Gray, and R. S. Houk, eds., Handbook of inductively coupled mass spectrometry: Glasgow, Blackie.

Jia, Y., 2000, Formation of an Azores current due ot the Mediterranean Overflow in a modelling study of the North Atlantic: Journal of Physical Oceanography, v. 30, p. 2342-2358.

Jimenez-Munt, I., P. Bird, and M. Fernandez, 2001, Thin-shell modeling of neotectonics in the Azores-Gibraltar region.: Geophysical Research Letters, v. 28, p. 1083-1086.

Johnson, G. C., R. G. Lueck, and T. B. Sanford, 1994, Stress on the Mediteranean Outflow Plume: Part II. Turbulent Dissipation and shear measurements: Journal of Physical Oceanography, v. 24, p. 2084-2092.

Johnson, J., I. Ambar, N. Serra, and I. Stevens, 2002, Comparative studies of the spreading of the Mediterranean water through the Gulf of Cadiz: Deep-Sea Research II, v. 49, p. 4179-4193.

Johnson, J., and I. Stevens, 2000, A fine resolution model of the eastern North Atlantic between the Azores, the Canary Islands and the Gibraltar Strait: Deep-sea research I, v. 47, p. 875-899.

Jouzel, J., R. B. Alley, K. M. Cuffey, W. Dansgaard, P. Grootes, G. Hoffmann, S. J. Johnsen, R. D. Koster, D. Peel, C. A. Shuman, M. Stievenard, M. Stuiver, and J. White, 1997, Validity of the temperautre reconstruction from water isotopes in ice cores: Journal of Geophysical Research, v. 102, p. 26471-26487.

Kalis, A. J., J. Merkt, and J. Wunderlich, 2003, Environmental changes during the Holocene climatic optimum in central Europe - human impact and natural causes.: Quaternary Science Reviews, v. 22, p. 33-79.

Kase, R. H., W. Zenk, T. B. Sanford, and W. Hillier, 1985, Currents, fronts and eddy fluxes in the Canary Basin: Progress in Oceanography, v. 14, p. 231-257.

Kenyon, N. H., and R. H. Belderson, 1973, Bed forms of the Mediterranean Undercurrent Observed with Side-Scan sonar: Sedimentary geology, v. 9, p. 77-99.

Kim, S. T., and J. R. O'Neill, 1997, Equilibrium and nonequilibrium oxygen isotope effects in synthetic calcites: Geochimica et Cosmochimica Acta, v. 61, p. 3461-3475.

Kinder, T. H., and G. Parilla, 1987, Yes, some of the Mediterranean outflow does come from great depth.: Geophysical Research, v. 93, p. 2901-2906.

Kinder, T. H., G. Parilla, N. A. Bray, and D. A. Burns, 1988, The hydrographic structure of the Strait of Gibraltar, *in* J. L. Almazan, H. L. Bryden, T. H. Kinder, and G. Parilla, eds., Seminario sobre la oceanografia fisica del Estrecho de Girbraltar: Madrid, SECEG, p. 55-67.

Knoll, M., A. Hernandez-Guerra, B. Lenz, F. Lopez-Laatzen, F. Machin, T. J. Muller, and G. Siedler, 2002, The eastern boundary current system between the Canary Islands and the African coast: Deep-Sea Research II, v. 49, p. 3427-3440.

Kohfeld, K. E., R. G. Fairbanks, S. L. Smith, and I. D. Walsh, 1996, *Neogloboquadrina pachyderma* (sinistral coiling) as paleoceanographic tracers in polar oceans: Evidence from Northeast Water Polyna plankton tows, sediment traps and surface sediments: Paleoceanography, v. 11, p. 679-699.

Kudrass, H. R., 1973, Sedimentation am Kontinentalhang vor Portugal und Marokko im Spatpleistozan und Holozan.: "Meteor" Forsch.-Ergebn., v. C(13), p. 1-63.

Lacombe, H., and C. Richez, 1982, The regime of the Strait of Gibraltar, Harvard University Division of Applied Sciences, Reports in Meteorology and Oceanography,, p. 57-114.

Lamb, H. H., 1966, The changing climate.: London, Methuen & Co. Ltd., 236 p.

Larsen, J. C., 1992, Transport and heat-flox of the Florida Current at 27-degrees-N derived from cross-stream voltages and profiling data - theory and observations: Philosophical Transactions of the Royal Society of London (Series A:- Mathematical and Engineering Sciences), v. 338, p. 169-236.

Lebreiro, S. M., J. C. Moreno, F. F. Abrantes, and U. Pflaumann, 1997, Productivity and paleoceanography on the Tore seamount (Iberian margin) during the last 225 kyr: Foraminiferal evidence: Paleoceanography, v. 12, p. 718-272.

Lee, J. J., E. Lanners, and B. Terkuile, 1988, The retention of chloroplasts by the foraminifer *Elphidium crispum*: Symbiosis, v. 5, p. 45-59.

Lobo, F. J., F. J. Fernandez-Molina, L. Somoza, and V. D. d. Rio, 2001, the sedimentary record of the post-glacial transgression on the Gulf of Cadiz continental shelf (Southwest Spain): Marine Geology, v. 178, p. 171-195.

Lopez-Galindo, A., J. Rodero, and A. Maldonado, 1999, Subsurface facies and sediment dispersal patterns: southeastern Gulf of Cadiz, Spanish continental margin: Marine Geology, v. 155, p. 83-98.

Lowe, J. J., H. H. Birks, S. J. Brooks, G. R. Cope, D. D. Harkness, F. E. Mayle, C. Sheldrick, C. S. M. Turney, and M. J. C. Walker, 1999, The chronology of palaeoenvironmental changes during the Last Glacial-Holocene transition: towards an event stratigraphy for the British Isles: Journal of the Geological Society, London, v. 156, p. 397-410.

Lund, D. C., and A. Mix, 1998, Millenial-scale deep water oscillations: Refelctions of the North Atlantic in the deep Pacific from 10-60ka: Paleoceanography, v. 13, p. 1-19.

MacAyeal, D. R., 1993, Growth / purge oscillations of the Laurentide ice sheet as a cause of the North Atlantic's Heinrich Events: Paleoceanography, v. 8, p. 775-784.

Majoube, M., 1971, Fractionnement en oxygene 18 et deuterium entre l'eau et sa vapeur: Journal of Chemical Physics, v. 10, p. 1423-1436.

Malmgren, B. A., M. Kucera, J. Nyberg, and C. Waelbrock, 2000, Comparison of statistical and artificial neural network techniques for estimating past sea surface temperatures from planktonic foraminifera census data: Paleoceanography, v. 16, p. 520-530.

Martinez, J. I., 1994, Late Pleistocene paleoceanography of thr Tasman Sea - implications for the dynamics of the warm pool in the Western Pacific.: Palaeogeography, Palaeoclimatology, Palaeoecology, v. 112, p. 19-62.

Martins, C. S., M. Hamann, and A. F. G. Fiuza, 2002, Surface circulation in the eastern North Atlantic, from drifters and altimetry: Journal of Geophysical Research - Oceans, v. 107, p. Art. No. 3217.

Martinson, D. G., N. S. Pisias, J. D. Hays, J. Imbrie, T. C. Moore, and N. J. Shackleton, 1987, Age dating and orbital theory of the Ice Ages: development of a High-resolution 0 to 300,000 - year chronostratigraphy: Quaternary Research, v. 27, p. 1-29.

Mayewski, P. A., L. D. Meeker, S. Whitlow, M. S. Twickler, M. C. Morrisson, P. Bloomfield, G. Bond, R. B. Alley, A. J. Gow, P. M. Grootes, D. A. Meese, M. Ram, K. Taylor, and W. Wumkes, 1994a, Changes in atmospheric circulation and ocean ice cover over the north Atlantic during the last 41,000 years: Science, v. 263, p. 1747-1751.

Mayewski, P. A., L. D. Meeker, S. Whitlow, M. S. Twickler, M. C. Morrisson, P. Grootes, G. Bond, R. B. Alley, D. A. Meese, A. J. Gow, K. Taylor, M. Ram, and M. Wumkes, 1994b, Polar atmospheric cell and ocean ice cover variability over the North Atlantic region during the last 41,000 years.: Science, v. 263, p. 1747-1751.

McCartney, M. S., and C. Mauritzen, 2001, On the origin of the warm inflow to the Nordic Seas: Progress in Oceanography, v. 51, p. 125-214.

McConnaughey, T., 1989, C-13 and O-18 isotopic disequilibrium in biological carbonates. 2. Invitro simulation of kinetic effects: Geochimica et Cosmochimica Acta, v. 53, p. 163-171.

McKeown, D. A., and J. E. Post, 2001, Characterization of manganese oxide mineralogy in rock varnish and dendrites using X-ray absorption spectroscopy: American Mineralogist, v. 86, p. 701-713.

McManus, J., G. Bond, W. Broecker, S. Johnsen, L. Labeyrie, and S. Higgins, 1994, High-resolution climate records from the North Atlantic during the last interglacial: Nature, v. 371, p. 326-329.

Meeker, L. D., and P. A. Mayewski, 2002, A 1400-year high-resolution record of atmospheric circulation over the North Atlantic and Asia: The Holocene, v. 12, p. 257-266.

Mikolajewicz, U., T. J. Crowley, A. Schiller, and R. Voss, 1997, Modelling teleconnections between the North Atlantic and North Pacific during the Younger Dryas: Nature, v. 387, p. 384-387.

Mix, A., S. Harris, and T. R. Janecek, 1995, Estimating lithology from nonintrusive reflectance spectra: Leg 138: Proceedings of the Ocean Drilling Program, Scientific results, v. 138, p. 413-427.

Mix, A. C., E. Bard, and R. Schneider, 2001, Environmental Processes of the ice age: land, oceans, glaciers (EPILOG): Quaternary Science Reviews, v. 20, p. XXXXX.

Mix, A. C., W. Rugh, N. G. Pisias, S. Veirs, and L. S. Party, 1992, Color reflectance spectroscopy: A tool for rapid characterization of Deep-Sea sediments: Proceedings of the Ocean Drilling Program, Initial Reports 1, v. 138, p. 67-76.

Morales, J. A., 1997, Evolution and facies architecture of the mesotidal Guadiana River delta (S.W. Spain-Portugal): Marine Geology, v. 138, p. 127-148.

Moreno, A., I. Cacho, M. Canals, M. A. Prins, M. F. Sanchez-Goni, J. O. Grimalt, and G. J. Weltje, 2002a, Saharan dust transport and high-latitude glacial climatic variability: The Alboran Sea Record: Quaternary Research, v. 58, p. 318-328.

Moreno, E., N. Thouveny, D. Delanghe, I. N. McCave, and N. Shackleton, 2002b, Climatic and oceanographic changes in the Northeast Atlantic reflected by magnetic properties of sediments deposited on the Portuguese margin during the last 340ka.: Earth and Planetary Science Letters, v. 202, p. 465-480.

Mortyn, P. G., and C. D. Charles, 2003, Planktonic foraminiferal depth habitat and d18O calibration: Plankton tow results from the Atlantic sector of the Southern Ocean: Paleoceanography, v. 18, p. 1037-1051.

Mulder, T., P. Lecroart, M. Voisset, J. Schönfeld, E. LeDrezen, E. Gonthier, V. Hanquiez, R. Zahn, J. C. Faugères, J. Hernandez-Molina, E. Llave-Barranco, and A. Gervais, 2002, Studying past Deep-ocean circulation and the Palaeoclimate record in the Gulf of Cadiz: EOS, v. 83, p. 481-488.

Mulder, T., S. Migeon, B. Savoye, and J. C. Faugères, 2001, Inversely graded turbidite sequences in the Deep Mediterranean: a record of deposits from flood-generated turbidity currents: Geo-Marine Letters, v. 21, p. 86-93.

Murray, J. W., 1971, An Atlas of British Recent Foraminiferids: London, Heinemann Educational Books, 244 p.

Murray, J. W., 1991, Ecology and distribution of benthic foraminifera, *in* Lee, and Anderson, eds., Biology of foraminifera: London, Academic press, p. 221-253.

Myers, P. G., 2002, Flux-forced simulations of the palaeocirculation of the Mediterranean: Paleoceanography, v. 17, p. 613-620.

Myers, P. G., K. Haines, and E. J. Rohling, 1998, Modeling the paleocirculation of the Mediterranean: The last glacial maximum and the Holocene with emphasis on the formation of sapropel S_1: Paleoceanography, v. 13, p. 586-606.

Nagao, S., and S. Nakashima, 1992, The factors controlling vertical color variations of North Atlantic Madeira Abyssal Plain sediments: Marine Geology, v. 109, p. 83-94.

Nelson, C. H., J. Baraza, and A. Maldonado, 1993, Mediterranean undercurrent sandy contourites, Gulf of Cadiz, Spain: Sedimentary geology, v. 82, p. 103-131.

Nelson, C. H., J. Baraza, A. Maldonado, J. Rodero, C. Escutia, and J. H. Barber, 1999, Influence of the Atlantic Inflow and Mediterranean outflow currents on

Late Quaternary sedimentary facies of the Gulf of Cadiz continental margin: Marine Geology, v. 155, p. 99-129.

Nelson, C. H., and P. J. Lamothe, 1993, Heavy metal anomalies in the Tinto and Odiel river and estuary system, Spain: Estuaries, v. 16, p. 496-511.

Nicolau, J. M., A. Solé-Benet, J. Puigdefábregas, and L. Gutiérrez, 1996, Effects of soil and vegetation on runoff along a catena in semi-arid Spain.: Geomorphology, v. 14, p. 297-309.

O'Neil, J. R., R. N. Clayton, and T. K. Mayeda, 1969, Oxygen isotope fractionation on divalent metal carbonates: Journal of Chemical Physics, v. 51, p. 5547-5558.

O'Neill-Baringer, M., and J. F. Price, 1997, Mixing and spreading of the Mediterranean outflow: Journal of Physical Oceanography, v. 27, p. 1654-1677.

O'Neill-Baringer, M., and J. F. Price, 1999, A review of the physical oceanography of the Mediterranean outflow: Marine Geology, v. 155, p. 63-82.

Ortiz, J., A. Mix, and R. W. Collier, 1995, Environmental control of living symbiotic and asymbiotic foraminifera of the California Current: Paleoceanography, v. 10, p. 987-1009.

Ortiz, J., A. Mix, S. Harris, and S. O'Connell, 1999, Diffuse spectral reflectance as a proxy for percent carbonate content in North Atlantic sediments: Paleoceanography, v. 14, p. 171-186.

Ortiz, J. D., A. Mix, W. Rugh, J. M. Watkins, and R. W. Collier, 1996, Deep-dwelling planktonic foraminifera of the northeastern Pacific ocean reveal environmental control of oxygen and carbon isotopic disequilibria: Geochimica et Cosmochimica Acta, v. 60, p. 4509-4523.

Orvik, K. A., and O. Skagseth, 2003, The impact of the wind stress curl in the North Atlantic on the Atlantic inflow to the Norwegian Sea towards the Arctic.: Geophysical Research Letters, v. 30, p. art. no. -1884.

Paillet, J., and H. Mercier, 1997, An inverse model of the eastern North Atlantic general circulation and thermocline ventilation: Deep-sea research I, v. 44, p. 1293-1328.

Park, J., and K. A. Maasch, 1993, Plio-Pleistocene time evolution of the 100-kyr cycle in marine paleoclimate records: Journal of Geolphysical Research - Solid Earth, v. 98, p. 447-461.

Peeters, F. J. C., G. Ganssen, and G. J. A. Brummer, 1999, The stable isotope composition of living planktic foraminifera in the upwelling area off Oman/Yemen, *in* E. Ivanova, ed., Late Quaternary monsoon history and palaeoproductivity of the western Arabian Sea: Amsterdam, Academisch proefschrift Vrije Universiteit, p. 123-151.

Pettigrew, N. R., 1989, Direct measurements of the flow of Western Mediterranean Deep Water over the Gibraltar sill.: Journal of Geophysical Research, v. 94, p. 18089-18093.

Pflaumann, U., J. Duprat, C. Pujol, and L. Labeyrie, 1996, SIMMAX: A modern analog technique to deduce Atlantic sea surface temperatures from planktonic foraminifera in deep-sea sediments: Paleoceanography, v. 11, p. 15-35.

Pickard, G. L., and W. J. Emery, 1990, Descriptive physical oceanography: an introduction.: Oford, Pergamon Press, 320 p.

Porter, S. C., and Z. H. An, 1995, Correlation between climate events in the North Atlantic and China during the last Glaciation: Nature, v. 375, p. 305-308.

Prell, W., A. Martin, J. Cullen, and M. Trend, 1999, The Brown University Foraminiferal Database, IGBP PAGES/World Data Centre-A for Palaeoclimatology, Data Contribution Series 1999-2027, NOAA/NGDC Palaeoclimatology Program, Boulder CO, USA.

Price, J. F., and M. O'neill-Baringer, 1994, Outflows and deep water production by marginal seas: Progress in Oceanography, v. 33, p. 161-200.

Price, J. F., M. O'neill-Baringer, R. G. Lueck, G. C. Johnson, I. Ambar, G. Parilla, A. Cantos, M. A. Kenelly, and T. B. Sanford, 1993, Mediterranean Outflow Mixing and Dynamics: Science, v. 259, p. 1277-1282.

Pujol, C., and C. Vergnaud-Grazzini, 1989, Palaeoceanography of the last Deglaciation in the Alboran Sea (Western Mediterranean). Stable isotopes and planktonic foraminiferal records: Marine Micropalaeontology, v. 15, p. 153-179.

Rahmstorf, S., 1998, Influence of Mediterranean Outflow on Climate: EOS, v. 79, p. 281-282.

Rasmusson, E. M., 1985, El-Nino and variations in climate: American Scientist.

Ravelo, A. C., and R. G. Fairbanks, 1992, Oxygen isotopic composition of multiple species of planktonic foraminifera: recorders of the modern photic zone temperature gradient: Paleoceanography, v. 7, p. 815-831.

Ravelo, A. C., and R. G. Fairbanks, 1995, Carbon isotopic fractionation in multiple species of planktonic foraiminifera from core-tops in the Tropical Atlantic: Journal of Foraminiferal Research, v. 25, p. 53-74.

Reguera, M. I., 2001, Paleoceanografia y setratigrafia de alta resolucion en el golfo de Cadiz en los ultimos 40,000 anos mediante el estudio de foraminiferos planctonicos: Ms. thesis, Universidad de Salamanca, Salamanca.

Reid, J. L., 1979, On the contribution of the Merditerranean Sea outflow to the Norwegian-Greenland Sea: Deep-Sea Research, v. 26A, p. 1199-1223.

Renssen, H., B. vanGeel, J. vanderPlicht, and M. Magny, 2000, Reduced solar activity as a trigger for the start of the Younger Dryas?: Quaternary International, v. 68-71, p. 373-383.

Riverdin, G., P. P. Niiler, and H. Valdimarsson, 2003, North Atlantic Ocean surface currents: Journal of Geophysical Research, v. 108, p. 3002-3026.

Robinson, S. G., and I. N. McCave, 1994, Orbital forcing of bottom-current enhanced sedimentation on Feni Drift, NE Atlantic, during the Mid-Pleistocene: Paleoceanography, v. 9, p. 943-972.

Rodero, J., L. Pallares, and A. Maldonado, 1999, Late Quaternary seismic facies of the Gulf of Cadiz Spanish margin: depositional processes influenced by sea-level change and tectonic controls: Marine Geology, v. 155, p. 131-156.

Roemmich, D., and C. Wunsch, 1985, Two transatlantic sections: meridional circulation and heat flux in the subtropical North Atlantic Ocean: Deep-Sea Research, v. 32, p. 619-664.

Rohling, E. J., 1999, Environmental control on Mediterranean salinity and $\delta^{18}O$: Paleoceanography, v. 14, p. 706-715.

Rohling, E. J., and H. L. Bryden, 1994, Estimating past changes in the Eastern Mediterranean freshwater budget, using reconstructions of sea level and hydrography: Proceedings Koninklije Akademie van Wetenschappen, v. 97, p. 201-217.

Rohling, E. J., and S. Cooke, 1999, Stable oxygen and carbon isotopes in foraminferal carbonate shells, *in* B. K. SenGupta, ed., Modern Foraminifera: Great Britain, Kluwer Academic Press, p. 239-258.

Rohling, E. J., and S. De Rijk, 1999, Holocene Climate Optimum and Last Glacial Maximum in the Mediterranean: the marine oxygen isotope record: Marine Geology, v. 153, p. 57-75.

Rohling, E. J., M. DenDulk, C. Pujol, and C. Vernaud-Grazzini, 1995, Abrupt hydrographic change in the Alboran Sea (western Mediterranean) around 8000 yrs BP: Deep-sea research I, v. 42, p. 1609-1619.

Rohling, E. J., M. Fenton, F. J. Jorissen, P. Bertrand, G. Ganssen, and J. P. Caulet, 1998a, Magnitudes of sea-level lowstands of the past 500,000 years: Nature, v. 394, p. 162-165.

Rohling, E. J., A. Hayes, S. DeRijk, D. Kroon, W. J. Zachariasse, and D. Eisma, 1998b, Abrupt cold spells in the northwest Mediterranean: Paleoceanography, v. 13, p. 316-322.

Rohling, E. J., F. J. Jorissen, C. Vergnaud-Grazzini, and W. J. Zachariasse, 1993, Northern Levantine and Adriatic Quaternary planktic foraminifera; Reconstruction of paleoenvironmental gradients: Marine Micropalaeontology, v. 21, p. 191-218.

Rohling, E. J., P. A. Mayewski, and P. Challenor, 2003a, On the timing and mechanism of millennial-scale climate variability during the last glacial cycle: Climate Dynamics, v. 20, p. 257-267.

Rohling, E. J., M. Sprovieri, T. Cane, J. S. L. Casford, S. Cooke, I. Bouloubassi, K. C. Emeis, R. Schiebel, M. Rogerson, A. Hayes, F. J. Jorissen, and D. Kroon, 2003b, Reconstructing past planktic foraminiferal habitats using stable isotope data: a case history for Mediterranean sapropel S5: Marine Micropalaeontology, v. in press.

Rossignol-Strick, M., 1999, The Holocene climatic optimum and pollen records of sapropel 1 in the eastern Mediterranean, 9000-6000 BP: Quaternary Science Reviews, v. 18, p. 515-530.

Roucoux, K. H., N. J. Shackleton, L. deAbreu, J. Schönfeld, and P. C. Tzedakis, 2001, Combined proxy and pollen analyses reveal rapid Iberian vegetation response to North Atlantic millenial-scale climate oscillations: Quaternary Research, v. 56, p. 128-132.

Rudnick, D. L., 1996, Intensive surveys of the Azores Front. 2. Inferring the geostrophic and vertical velocity fields: Journal of Geophysical Research, v. 101, p. 16,291-16,303.

Ryall, D. B., R. G. Derwent, A. J. Manning, A. L. Redington, J. Corden, W. Millington, P. G. Simmonds, S. O'Doherty, N. Carslaw, and G. W. Fuller, 2002, The origin of high particulate concentrations over the United Kingdom, March 2000: Atmospheric Environment, v. 36, p. 1363-1378.

Sanchez-Goni, M. F., I. Cacho, J. L. Turon, J. Guiot, F. J. Sierro, J. P. Peypouquet, J. O. Grimalt, and N. Shackleton, 2002, Sychroneity between marine and terrestrial responses to millennial scale climatic variability during the last glacial period in the Mediterranean region: Climate Dynamics, v. 19, p. 95-105.

Sanchez-Goni, M. F., J. L. Turon, F. Eynaud, and S. Gendreau, 2000, European climatic repsonse to milennial scale changes in the atmosphere-ocean system during the last glacial period: Quaternary Research, v. 54, p. 394-403.

Sarnthein, M., K. Stattegger, D. Dreger, H. Erlenkeuser, P. Grootes, B. Haupt, S. Jung, T. Kiefer, W. Kuhnt, U. Pflaumann, C. Schafer-Neth, H. Schulz, M. Schulz, D. Seidov, J. Simstich, S. vanKreveld, E. Vogelsang, A. Volker, and M. Weinelt, 1999, Fundamental modes and abrupt changes in North Atlantic

circulation and climate over the last 60ky - concepts, reconstruction and numerical modeling, *in* P. Scafer, W. Ritzrau, M. Schluter, and J. Thiede, eds., The Northern North Atlantic: a changing environment: Berlin, Springer, p. 45-66.

Schiebel, R., and C. Hemleben, 2000, Interannual variability of planktonic foraminiferal populations and test flux in the eastern North Atlantic ocean (JGOFS): Deep-Sea Research II, v. 47, p. 1809-1852.

Schiebel, R., J. Waniek, M. Bork, and C. Hemleben, 2001, Planktic foraminiferal production stimulated by chlorophyll redistribution and entrainment of nutrients: Deep-sea research I, v. 48, p. 721-740.

Schiebel, R., J. Waniek, A. Zeltner, and M. Alves, 2002, Impact of the Azores Front on the Distribution of planktic foraminifers, shelled gastropods and coccolithophorids: Deep-Sea Research II, v. 49, p. 4035-4050.

Schmitz, W. J., and M. S. McCartney, 1993, On the North-Atlantic Circulation: Reviews of Geophysics, v. 31, p. 29-49.

Schönfeld, J., 1997, The impact of the mediterranean outflow water (MOW) on benthic foraminiferal assemblages and surface sediments at the southern Portugese continental margin: Marine Micropalaeontology, v. 29, p. 211-236.

Schönfeld, J., 2002a, A new benthic foraminiferal proxy for near-bottom current velocities in the Gulf of Cadiz, northeastern Atlantic Ocean.: Deep-sea research I, v. 49, p. 1853-1875.

Schönfeld, J., 2002b, Recent benthic foraminiferal assemblages in deep high-energy environments from the Gulf of Cadiz (Spain): Marine Micropalaeontology, v. 853, p. 1-22.

Schönfeld, J., and R. Zahn, 2000, Late glacial to holocene history of the Mediterranean Outflow. Evidence from benthic foraminiferal assemblages and stable isotopes at the Portugese margin: Palaeogeogrpahy, Palaeoclimatology, Palaeoecology, v. 159, p. 85-111.

Seidov, D., and M. Maslin, 1999, North Atlantic deep water circulation collapse during Heinrich events: Geology, v. 27, p. 23-26.

Shackleton, N., 1987, Oxygen isotopes, ice volume and sea level.: Quaternary Science Reviews, v. 6, p. 183-190.

Shackleton, N., 2001, Climate across the hemispheres: Science, v. 291, p. 58-59.

Shackleton, N., M. A. Hall, and E. Vincent, 2000, Phase relationships between millennial-scale events 64,000-24,000 years ago: Paleoceanography, v. 15, p. 565-569.

Shackleton, N. J., 2000, The 100,000-year ice-age cycle identified and found to lag temperature, carbon dioxide and orbital eccentricity: Science, v. 289, p. 1897-1903.

Shackleton, N. J., and N. D. Opdyke, 1973, Oxygen isotope and paleomagnetic stratigraphy of equatorial Pacific core V28-238: oxygen isotope temperatures and ice volumes on a 105 and 106 year timescale: Quaternary Research, v. 3, p. 39-55.

Shanmugam, G., 2000, 50 years of the turbidite paradigm (1950s-1990s): deep-water processes and facies models - a critical perspective: Marine and Petroleum geology, v. 17, p. 285-342.

Sheng, J. Y., and K. R. Thompson, 1996, Summer surface circulation on the Newfoundalnd shelf and grand banks: The roles of local density gradients and remote forcing.: Atmosphere - Ocean, v. 34, p. 257-284.

Short, D. A., J. G. Mengel, T. J. Crowley, W. T. Hyde, and G. R. North, 1989, Filtering of Milankovitch Cycles by Earths Geography: Quaternary Research, v. 35, p. 157-173.

Sierro, F. J., J. A. Flores, and J. Baraza, 1999, Late glacial to recent palaeoenvironmental changes in the Gulf of Cadiz and formation of sandy contourite layers: Marine Geology, v. 155, p. 157-172.

Sierro, F. J., J. A. Gonzalez-Delgado, C. J. Dabrio, J. A. Flores, and J. Civis, 1996, Late Neogene depositional sequences in the foreland basin of Guadalquivir (SW Spain), *in* P. F. Friend, and C. J. Dabrio, eds., Tertiary basins of Spain: World and Regional Geology, v. 6: Cambridge, Cambridge University Press, p. 339-345.

Slota, P. J., A. J. T. Jull, T. W. Linick, and L. J. Toolin, 1987, Preparation of small samples for 14C accelerator targets by catalytic reduction of CO.: Radiocarbon, v. 29, p. 303-306.

Spero, H. J., J. Bijma, D. W. Lea, and B. E. Bemis, 1997, Effect of seawater carbonate concentration on foraminiferal carbon and oxygen isotopes: Nature, v. 390, p. 497-500.

Spero, H. J., and D. W. Lea, 1993, Intra specific stable-isotope variability in the planktic foraminifera *Globgerinoides sacculifer* - results from laboratory experiments: Marine Micropalaeontology, v. 22, p. 221-234.

Spero, H. J., and D. W. Lea, 1996, Experimental determination of stable isotope variability in *Globigerina bulloides*: implications for paleoceanographic reconstructions: Marine Micropalaeontology, v. 28, p. 231-246.

Spero, H. J., K. M. Mielke, E. M. Kalve, D. W. Lea, and D. K. Pak, 2003, Multispecies approach to reconstructing eastern equatorial Pacific thermocline hydrography during the past 360ky.

Spero, H. J., and S. L. Parker, 1985, Photosynthesis in the symbiotic planktonic foraminifer *Orbulina universa*, and its potential contribution to oceanic primary productivity: Journal of Foraminiferal Research, v. 15, p. 273-281.

Stommel, H. M., 1972, Deep winter-time convection in the western Mediterranean Sea, *in* A. L. Gordon, ed., Studies in Physical Oceanography, v. 2: New York, Gordon and Breach, p. 232.

Stommel, H. M., H. L. Bryden, and P. Mangelsdorf, 1973, Does some of the Mediterranean outflow come from great depth?: Pure Appl. Geophysics, v. 105, p. 879-889.

Stow, D. A. V., J. C. Faugères, and E. Gonthier, 1986, Facies distribution and textural variation in Faro Drift contourites: velocity fluctuation and drift growth: Marine Geology, v. 72, p. 71-100.

Stow, D. A. V., J. C. Faugeres, A. Viana, and E. Gonthier, 1998, Fossil contourites: a critical review.: Sedimentary Geology, v. 115, p. 3-31.

Stow, D. A. V., and J. P. B. Lovell, 1979, Contourites: thier recognition in modern and ancient sediments: Earth-Science reviews, v. 14, p. 251-291.

Stow, D. A. V., and M. Mayall, 2000, Deep-water sedimentary systems: New models for the 21st centuary: Marine and Petroleum geology, v. 17, p. 125-135.

Stuiver, M., 1986, Radiocarbon age calibration of marine samples back to 9000 calendar years B.P.: Radiocarbon, v. 28, p. 980-1021.

Stuiver, M., and H. A. Polach, 1977, Discussion: Reporting of 14C data.: Radiocarbon, v. 19, p. 355 - 363.

Sturges, W., and B. G. Hong, 2001, Gulf Stream transport variability at periods of decades: Journal of Physical Oceanography, v. 31, p. 1304-1312.

Talley, L., and M. S. McCartney, 1982, Distribution and circulation of Labrador Sea Water: Journal of Physical Oceanography, v. 12, p. 1189-1205.

Thomson, J., L. Brown, S. Nixon, G. T. Cook, and A. B. MacKenzie, 2000, Bioturbation and Holocene sediment accumulation fluxes in the north-east Atlantic Ocean (Benthic Boundary Layer experiment sites). Marine Geology, v. 169, p. 21-39.

Thomson, J., N. C. Higgs, and T. Clayton, 1995, A geochemical criterion for the recognition of Heinrich events and estimation of thier depositional fluxes by the $(^{230}Th_{excess})_0$ profiling method: Earth and Planetary Science Letters, v. 135, p. 41-56.

Thomson, J., N. C. Higgs, and S. Colley, 1996, Diagentic redistributions of redox-sensitive elements in northeast Atlantic glacial / interglacial transition sediments: Earth and Planetary Science Letters, v. 139, p. 365-377.

Thomson, J., S. Nixon, C. P. Summerhayes, J. Schönfeld, R. Zahn, and P. Grootes, 1999, Impications for sedimentation changes on the Iberian margin over the last two glacial/interglacial transitions from $(^{230}TH_{excess})_0$ systematics: Earth and Planetary Science Letters, v. 165, p. 255-270.

Thorpe, S. A., 1976, Variability of the Mediterranean undercurrent in the Gulf of Cadiz: Deep-Sea Research, v. 23, p. 711-727.

Thouveny, N., E. Moreno, D. Delanghe, L. Candon, Y. Lancelot, and N. Shackleton, 2000, Rock magnetic detection of distal ice-rafted debris: clue for the identification of Heinrich layers on the Portuguese margin: Earth and Planetary Science Letters, v. 180, p. 61-75.

Thunnell, R. C., 1978, Distribution of recent planktonic forminifera in surface seidments of the Mediterranean Sea: Marine Micropalaeontology, v. 3, p. 147-173.

Thunnell, R. C., and D. F. Williams, 1989, Glacial-Holocene salinity changes in the Mediterranean Sea: Hydrographic and depositional effects: Nature, v. 338, p. 493-496.

Tsuchiya, M., L. D. Talley, and M. S. McCartney, 1992, An eastern Atlantic section from Iceland southward across the equator: Deep-Sea Research, v. 39, p. 1885-1917.

Turekian, K. K., and K. H. Wedepohl, 1961, Distruibution of the Elements in some major units of the Earths Crust: G.S.A. Bulletin, v. 72, p. 175-192.

Uppenbrink, J., 1999, Climate variability - The North Atlantic oscillation: Science, v. 283, p. 948-949.

vanAken, H. M., 2000, The hydrography of the mid-latitude Northeast Atlantic Ocean II: The intermediate water masses: Deep-Sea Research I, v. 47, p. 789-824.

vanGeen, A., J. F. Adkins, E. A. Boyle, C. H. Nelson, and A. Palanques, 1997, A 120yr record of widespread contamination from mining of the Iberian pyrite belt: Geology, v. 25, p. 291-294.

vanKreveld, S. A., M. Knappertsbusch, J. Ottens, G. M. Ganssen, and J. E. vanHinte, 1996, Biogenic carbonate and ice-rafted debris (Heinrich layer) accumulation in deep-sea sediments from a Northeastern Atlantic piston core: Marine Geology, v. 131, p. 21-46.

Veiga-Pires, C. C., and C. Hillaire-Marcel, 1999, U and Th isotope constraints on the duration of Heinrich events H0-H4 in the southeastern Labrador Sea: Paleoceanography, v. 14, p. 187-199.

Vergnaud-Grazzini, C., 1974, Les foraminifères planctoniques de la mer Ligure. Distribution saisonnière et caractéristiques thermiques.: Union Océanogr. France., v. VI, p. 30-35.

Vidal, L., R. R. Schneider, O. Marchal, T. Bickert, T. F. Stocker, and G. Wefer, 1999, Link between the north and south Atlantic during the Heinrich events of the last glacial period: Climate Dynamics, v. 15, p. 909-919.

Villanueva-Guimerans, P., 2000, Bolivinidae y Buliminidae (foraminíferos bentónicos) del margen septentrional del Golfo de Cádiz (España): Revista Espanola de Micropalaeontologia, v. 32, p. 131-141.

Villanueva-Guimerans, P., J. I. Canudo-Sanagustin, and J. L. Cervera-Currado, 1999, Los foraminíferos bentónicos recientes de la superfamilia Miliolacea Ehrenberg, 1839 en los sedimentos superficiales del margen septentrional del Golfo de Cádiz.: Revista Espanola de Micropalaeontologia, v. 31, p. 99-122.

Villanueva-Guimerans, P., and J. L. Cervera-Currado, 1999, Distribution of Planorbulinacea (benthic foraminifera) assemblages in surface sediments on the northern margin of the Gulf of Cadiz.: Boletín. Instituto Español de Oceanografía, v. 15, p. 181-190.

Volat, J.-L., L. Pastouret, and C. Vergnaud-Grazzini, 1980, Dissolution and carbonate fluctuations in Pleistocene deep-sea cores: a review: Marine Geology, v. 34, p. 1-28.

vonGrafenstein, U., H. Erlenkeuser, J. Muller, J. Jouzel, and S. Johnsen, 1998, The cold event 8200 years ago documented in oxygen isotope records of precipitation in Europe and Greenland: Climate Dynamics, v. 14, p. 73-81.

Waelbroeck, C., L. Labeyrie, J. C. Duplessy, J. Guiot, M. Labracherie, H. Leclaire, and J. Duprat, 1998, Improving past sea surface temperature estimates based on planktonic fossil faunas: Paleoceanography, v. 13, p. 272-283.

Wang, J. W., D. Bejan, and N. J. Bunce, 2003, Removal of arsenic from synthetic acid mine drainage by electrochemical pH adjustment and coprecipitation with iron hydroxide: Environmental Science and Technology, v. 37, p. 4500-4506.

Watts, W. A., J. R. M. Allen, B. Huntley, and S. C. Fritz, 1996, Vegetation history and climate of the last 15,000 years at Laghi di Monticchio, southern Italy: Quaternary Science Reviews, v. 15, p. 113-132.

Weaver, A. J., M. Eby, F. F. Augustus, and E. C. Wiebe, 1998, Simulated influence of carbon dioxide, orbital forcing and ice sheets on the climate of the Last Glacial Maximum: Nature, v. 394, p. 847-853.

Weaver, P. P. E., 2000, RRS Discovery Cruise 249: History of sedimentation in the Gulf of Cadiz: investigations with the SOC Giant Piston Corer, Southampton, SOC, p. 19.

Weaver, P. P. E., M. R. Chapman, G. Eglinton, M. Zhao, D. Rutledge, and G. Read, 1999, Combined coccolith, foraminiferal and biomarker reconstruction of paleoceanographic conditions over the past 120kyr in the northern North Atlantic: Paleoceanography, v. 14, p. 336-349.

Weaver, P. P. E., and P. J. Schultheiss, 1982, Detection of repenetration and sediment disturbance in open-barrel gravity cores: Journal of Sedimentary Petrology, v. 53, p. 649-678.

Wefer, G., and W. H. Berger, 1991, Isotope paleontology - growth and composition of extant calcareous species: Marine Geology, v. 100, p. 207-248.

Williams, D. F., R. Ehrlich, H. J. Spero, N. Healy-Williams, and A. C. Gary, 1988, Shape and isotopic differences bwteen conspecific foraminiferal morphotypes

and resolution of paleoceanogrpahic events: Palaeogeography, Palaeoclimatology, Palaeoecology, v. 64, p. 153-162.

Zahn, R., and A. C. Mix, 1991, Benthic foraminiferal $\delta^{18}O$ in the oceans temperature-salinity flield: constraints on ice age thermohaline circulation: Paleoceanography, v. 6, p. 1-20.

Zangger, E., and I. N. McCave, 1990, A redesigned kasten core barrel and sampling technique: Marine Geology, v. 94, p. 165-171.

1947-1948, Swedish Deep-Sea Expedition Reports.

1994, Geological map of the world. Scale 1:30 000 000: Open University.

Appendix 1:-

Reconstructing past foraminiferal habitats using stable isotope data: a case study history for Mediterranean sapropel S5.

E.J. Rohling, M. Sprovieri, T. Cane, J.S.L Casford, S.Cooke, I. Bouloubassi, K.C. Emeis, R. Schiebel, **M. Rogerson**, A. Hayes, F.J. Jorissen, D. Kroon.

In the judgement of the first author, M. Rogerson contributed ~5% of this work. Specifically, this concerned the details regarding the so-called "vital effects" on the stable isotopic composition of foraminiferal tests,

Reconstructing past planktic foraminiferal habitats using stable isotope data: a case history for Mediterranean sapropel S5

Rohling, E.J.[1], Sprovieri, M.[2], Cane, T.[3], Casford, J.S.L.[4], Cooke, S.[5], Bouloubassi, I.[6], Emeis, K.C.[7], Schiebel, R.[8], Rogerson, M.[1], Hayes, A.[9], Jorissen, F.J.[10], and Kroon, D.[11]

[1] School of Ocean and Earth Science, Southampton Oceanography Centre, European Way, Southampton, SO14 3ZH, UK

[2] Institute for Coastal Marine Environment-CNR, Geomare Section, Calata Porta di Massa, 80, Porto di Napoli, 80100 Naples, Italy.

[3] School of Chemistry, Physics and Environmental Science, University of Sussex, Falmer, Brighton, BN1 9QJ, UK.

[4] Dept. of Geography, Science Site, South Road, Durham, DH1 3LE, UK

[5] Department of Earth Sciences, University of Waikato, Hamilton, New Zealand

[6] Laboratoire de Physique et Chimie Marines, Université P. et M. Curie, 4 place Jussieu, 75252 Paris Cedex 05, France

[7] Inst. für Biogeochemie und Meereschemie, Universität Hamburg, Bundesstr. 55, D-20146 Hamburg, Germany

[8] Geological Institute, ETHZ, Sonneggstrasse 5, NOG 32.2, 8092 Zürich, Switzerland

[9] Department of Geology, Royal Holloway, University of London, Egham, Surrey TW20 0EX, UK

[10] Laboratoire de Géologie, Faculté Sciences, Université d'Angers, 2 Boulevard Lavoisier, 49045 Angers Cedex, France

[11] Faculty of Earth Sciences, De Boelelaan 1085, 1081 HV Amsterdam, The Netherlands

Abstract. A high-resolution stable O and C isotope study is undertaken on all planktic foraminiferal species that are reasonably continuous through an Eemian sapropel S5 from the western side of the eastern Mediterranean. The data are considered within a context of high-resolution isotope records for two further S5 sapropels from the central and easternmost sectors of the basin, alkenone-based sea surface temperature records for all three sapropels, and planktic foraminiferal abundance records for the same sample sets through all three sapropels. Results are compared with similar data for Holocene sapropel S1. The adopted approach allows distinction between species that are most suitable to assess overall changes in the climatic/ hydrographic state of the basin, including depth-related differentiations and the main seasonal developments, and species that are most affected by variable biological controls or local/regional and transient physico-chemical forcings. It is found that *a-priori* assumptions about certain species' palaeohabitats, based on modern habitat observations, may become biassed when non-analogue conditions

develop. In the case of Mediterranean sapropel S5, these consisted of enhanced freshwater dilution, elevated productivity, shoaling of the pycnocline between intermediate and surface waters, and stagnation of the subsurface circulation. Under these conditions, some species are found to "shift" into habitat settings that differ considerably from those occupied today. The present multiple-species approach can identify such "anomalous responses", and thus offers a sound background for further shell-chemistry investigations and quantitative interpretation of the isotopic profiles. We capitalise on the latter potential, and offer the first quantitative estimates of monsoon flooding into the Mediterranean during the deposition of Eemian sapropel S5.
Keywords: *Planktonic foraminifera, isotopes, Mediterranean, sapropel, palaeohabitats*

1. Introduction

Palaeoceanographic interpretations of past planktic foraminiferal assemblages commonly assume that the various species' past habitat characteristics in the past were similar to those observed today. Often, a basic distinction is applied between 'mixed-layer' and 'thermocline' dwellers to characterise past water-column gradients and their variability. Some studies go into more detail. Regarding the major species in the Quaternary of the Mediterranean, there has been particular interest in: *G. ruber* (w) to reflect summer mixed-layer conditions; *N. pachyderma* (dextral) as a marker for Intermediate Water shoaling into the base of the euphotic layer, fuelling a distinct Deep Chlorophyll Maximum; and *G. inflata* and/or *G. scitula* to reflect the cool, deep, homogeneous and relatively eutrophic winter mixed layer. These habitat characterisitics were inferred from habitat studies inside and outside the Mediterranean (e.g., Fairbanks et al., 1982; Hemleben and Spindler, 1983; Thunell and Reynolds, 1984; Bé et al., 1985; Hemleben et al., 1989; Pujol and Vergnaud-Grazzini, 1989; Reynolds and Thunell, 1989; Rohling and Gieskes, 1989; Rohling et al., 1993, 1995; Pujol and Vergnaud-Grazzini, 1995; Reiss et al., 1999; Schiebel and Hemleben, 2000).

The assumption of 'stable' habitat characteristics has developed into an almost fundamental principle to studies that involve chemical analyses of species-specific foraminiferal shells to reconstruct past water-column property gradients (e.g., $\delta^{18}O$, $\delta^{13}C$, $\delta^{11}B$, Mg/Ca, Sr/Ca, Ba/Ca, and Cd/Ca), with increasingly far-reaching interpretations.

Oxygen isotope values have been used, after accounting for temperature and ice-volume effects, to estimate past salinities and even palaeodensity gradients (e.g., Thunell and Williams, 1989; Duplessy et al. 1991; Rostek et al., 1993; Maslin et al., 1995; Hemleben et al., 1996; Labeyrie et al., 1996; Kallel et al., 1997a, b). Records of $\delta^{13}C$, $\delta^{11}B$, Ba/Ca, and Cd/Ca provide proxies for sea-water pH and nutrient concentrations, which in association with other proxy data have been used to reconstruct past pCO_2 and large-scale ocean circulation changes (e.g., Palmer et al., 1998; Pearson & Palmer, 1999, 2000; Boyle & Keigwin, 1982, 1985/86, 1987).

The underlying assumption that habitat characteristics of planktic foraminifera are 'stable' through time remains largely unchallenged. It can be tested by deriving past foraminiferal habitat structures from paired O and C stable isotope analyses. The procedure requires that all (major) species are analysed, and that reasonable – preferably quantitative – concepts and expectations for the analysed signals are developed. We here present a Mediterranean case-history along these lines, focussed on the strongly developed anoxic interval known as sapropel S5 in Vicomed core KS205, from the NW Ionian Sea (eastern Mediterranean). S5 dates from the Eemian, Marine Isotope Stage (MIS) 5e, roughly between 124 and 119 ka BP (Cane et al., 2002; Rohling et al., 2002) (Fig. 1). Our work expands on previous studies that pioneered the multiple-species approach in lower resolutions (Ganssen and Troelstra, 1987; Tang and Stott, 1993).

A Mediterranean record is selected because: (1) the modern foraminiferal distribution in this basin is well studied (Pujol and Vergnaud-Grazzini, 1995; Reiss et al., 1999; and references therein); (2) the basin has a relatively small volume and is semi-isolated from the open ocean, so that it shows very rapid and amplified responses to climatic forcings; (3) it is relatively easy to calculate equilibrium calcite $\delta^{18}O$ values for the various water masses in this basin (e.g., Rohling and De Rijk, 1999; Rohling, 1999); (4) there are no problems with diagenetic calcite dissolution or foraminiferal preservation; (5) there is sufficient palaeoceanographic background knowledge to allow the evaluation of new results within a basin-wide context (Fig. 1).

We concentrate on sapropel S5 because the anoxic bottom-water conditions during its deposition prevented bioturbation, so that the resolution of records is constrained only by foraminiferal availability per unit volume of sediment. Also, the Mediterranean

circulation regime at times of sapropel deposition was radically different from the present, due to a basin-wide reduction of surface buoyancy loss, while biological productivity was elevated throughout the basin (e.g., Rossignol-Strick et al., 1982; Jenkins and Williams, 1983; Rossignol-Strick, 1983, 1985, 1987; Vergnaud-Grazzini, 1985; Parisi, 1987; Rohling and Gieskes, 1989; De Lange et al., 1990; Rohling and Hilgen, 1991; Castradori, 1993; Rohling et al., 1993, 2000; Rohling, 1994; Thomson et al., 1995; Myers et al., 1998; Cramp and O'Sullivan, 1999; Rohling and De Rijk, 1999; Struck et al., 2001; Casford et al., 2002). The combination of a different circulation regime and elevated productivity offers an ideal 'non-analogue' environment for testing the assumption that habitats remain stable through time.

We present high-resolution stable isotope records for all major planktic foraminiferal species through S5, along with complementing alkenone sea-surface temperature (SST) records. Detailed faunal abundance data on the same samples and the development of a high-resolution (± 1cm) basin-wide correlation context for S5 may be found in Cane et al. (2002) and Rohling et al. (2002).

The central aims of this study are: to qualitatively and quantitatively assess the habitat characteristics of the investigated species at the time of S5 deposition; to compare those conclusions with the apparent habitats at the time of Holocene sapropel S1 (~9-6 ka BP); and – in particular – to compare the inferred palaeohabitats with the same species' modern observed habitats. This approach identifies which species reflect the general state of circulation, which species are prone to record transient 'anomalies' in the environment and so are of only local relevance, and which species give non-systematic records that contribute little palaeo-environmental understanding. The applied $\delta^{18}O$ box model further offers new insight into the environmental conditions associated with sapropel S5 – notably the severity of monsoon flooding.

2. Material and Methods

The three S5 sapropels reported here are found at 482.5-506.0 cm in Vicomed core KS205 (38°11.86' N; 18°08.04' E; 2384 m), 40.2-63.0 cm in section 1H-3 of ODP Hole 971A (24°41' N; 33°43' E; 2026 m), and 74.5-103 cm in section 1H-5 of ODP Hole 967C (34°04.27' N; 32°43.53' E; 2554 m) (Fig. 1). A previous correlation study (Cane et al.,

2002) allows the records to be plotted with ±1 cm accuracy along a single depth scale: the 971A-equivalent units (cm) used throughout this paper. Average sediment accumulation rates through the studied sapropels are 4.7, 4.6, and 5.7 cm kyr^{-1}, respectively, based on a 5 kyr duration of S5 deposition (Bar-Matthews et al., 2000; Cane et al., 2002).

S5 presents itself as a dark grey to black sedimentary interval bound by homogeneous pale brown to grey sediments. Persistent bottom-water anoxia during its deposition led to complete absence of benthic foraminifera, starting abruptly at the onset of the dark colour (Cane et al., 2002). The S5 sapropels in KS205 and 971A were sampled in continuous 0.5cm intervals. In 967C the interval was 1cm. Cane et al. (2002) presented full planktic foraminiferal abundance records for all three S5 sapropels along with stable isotope records for *Globigerinoides ruber* (white) and *Neogloboquadrina pachyderma* (dextral). We add records for *Globorotalia scitula* in both 971A and KS205 (Fig. 1), and establish a full-faunal perspective for KS205 by adding data for *Globigerinoides ruber* (pink), *Orbulina universa*, *Globigerinoides sacculifer*, *Globigerinoides sacculifer* (*trilobus* type), *Globigerinella siphonifera* (wide open-coiled morphotype), *Globigerina bulloides*, *Globigerinita glutinata*, and *Hastigerina pelagica* (Fig. 2). We follow the taxonomic concepts presented by Hemleben et al. (1989) to which we refer for details.

All foraminiferal samples were wet sieved (demineralised water) into several size fractions, and random splits from the 150-600 μm fraction were used for faunal abundance studies (Cane et al., 2002). The remaining residue was used to pick adult specimens for stable isotope analyses, using a measurement eyepiece to constrain size-windows of ~50 μm (abundant species) to ~100 μm (rare species) around each species' mean size through the sapropel. Selected specimens were cleaned, where necessary using ultrasound, and dried. The stable isotope analyses were performed on batches of 3-10 specimens, using a PDZ Europa Geo 20-20 mass spectrometer with individual acid-bath carbonate preparation (reaction with orthophosphoric acid at 70°C). Isotope ratios are reported as $\delta^{13}C$ and $\delta^{18}O$, in ‰ values relative to Vienna Peedee Belemnite (VPDB). External precision is better than 0.06 ‰ for both $\delta^{13}C$ and $\delta^{18}O$. Any ice-volume effects would equally affect all species investigated, and so cannot account for different trends between species. Comparisons between temperature and $\delta^{18}O$ values rely on a conversion of 0.23‰ $°C^{-1}$ (O'Neil et al., 1969; Kim and O'Neil, 1997).

For the alkenone SST records, freeze-dried sediments from cores KS205 and 967C were solvent extracted by ultrasonication. Samples from core 971A were extracted in a Dionex ASE 200 Accelerated Solvent Extractor after adding 1 μg cholestane and n-C_{36}, and 0.5 μg nonadecanone as internal standards (extraction pressure N_2 80 bar, temperature 75°C, solvent 100% dichloromethane). Extraction vessels were packed at base with 2 cm extraction-grade silica gel (modified diatomaceous earth). Alkenone fractions were isolated by silica gel column chromatography (core KS205), or by high pressure liquid chromatography (HPLC) (core 967C), and analysed by capillary gas chromatography (GC). Extracts from core 971A were analysed without prior clean up. Alkenones were identified based on their retention times and those of standards. The alkenone unsaturation index $U^{k'}_{37} = C_{37:2}/(C_{37:2} + C_{37:3})$ was calculated from peak areas and translated into temperatures using the global calibration derived by Müller et al. (1998): SST (°C)$=(U^{k'}_{37} - 0.044)/0.033$. Emeis et al. (1998; 2000) and Rohling et al. (2002) provide further details on the alkenone SST determinations and the calibration.

The temporal resolution in the analytical series through S5 for *G. ruber* (w), *G. ruber* (p), *G. siphonifera*, *O. universa*, and *G. bulloides* is ~100 years for an S5 duration of ~5 kyrs. Results for *N. pachyderma*, *G. scitula*, *G. sacculifer* (with sac-like final chamber), *G. sacculifer* (*trilobus* type), *G. glutinata*, and *H. pelagica* are wider spaced, limited by variations in the availability of suitable specimens (Fig. 2). The alkenone SST record for S5 in KS205 has an average temporal resolution of ~160 years. Note that the applied 5-kyr duration for S5 substantially exceeds the radiocarbon-dated 3 kyrs for Holocene sapropel S1 (Stanley and Maldonado, 1979; Vergnaud-Grazzini, 1985; Troelstra et al., 1991; Perissoratis and Piper, 1992; Jorissen et al., 1993; Mercone et al., 2000).

3. Concept / Working Hypothesis

3.1. Identifying water masses

The warm summer mixed layer is thinner, hence less voluminous, than the deep and cool winter mixed layer. Any runoff event or heating anomaly would therefore leave a signal of considerably larger magnitude in summer than a similar-scale event in winter. The effects of a runoff event would be particularly noticeable in a thin layer/ lenses, stabilised at the surface by a transient halocline. Considerable $\delta^{18}O$ variability is therefore

expected in the summer mixed layer, and especially in association with any narrow top-layers/lenses. In the Mediterranean, such lenses are expected due to the seasonal monsoon flooding (today concentrated via the Nile), which peaks in NE Africa over a period of ~2 months centred on August (Maynard et al., 2002). In freshwater-diluted layers/lenses, the low freshwater $\delta^{18}O$ anomaly remains concentrated until the halocline breaks down and the anomaly gets mixed through the more extensive mixed layer. Lenses of freshwater-diluted mixed-layer water are known to survive for extended periods of time and large distances with distinct nutrient/mixing characteristics, creating potential habitats that differ greatly from those in adjacent surface waters (e.g., Zaire and Amazon/Orinoco plumes: Ryther et al., 1967; Calef and Grice, 1967; Nof, 1981; Ufkes et al., 1998; Schmuker, 2000; Schmuker and Schiebel, 2002). Concerning stable carbon isotopes, the summer mixed layer should theoretically show the heaviest (most ^{13}C enriched) $\delta^{13}C$ values in the water column, as ^{12}C is preferentially sequestered during photosynthesis within the euphotic layer and removed from the surface layers by export production ('biological pump'). If extensive freshwater addition takes place, however, surface waters could record ^{12}C enrichment: fresh water not only contains dissolved inorganic carbon with $\delta^{13}C$ values of –5 to –10 ‰, but in addition carries dissolved and suspended organic carbon (e.g., humics) with $\delta^{13}C$ values as low as –27 ‰ (Fontugne and Calvert, 1992).

Waters below the summer mixed layer, i.e. below the seasonal thermocline, are very similar in temperature (T) and salinity (S) to the winter mixed layer, since the summer mixed layer 'grows' in the previous winter mixed layer by warming progressively from the surface downwards, aided by reduced wind-driven mixing in the calmer summer season. The subthermocline part of the surface system in summer therefore remains dominated by winter-typical properties. These winter-typical properties evolve in the deep winter mixed layer, whose great homogenised volume restricts the amplitude of isotopic anomalies in response to hydrological events. The $\delta^{18}O_{calcite}$ records for winter-type waters will therefore be characterised by reduced variability and, due to the lower temperatures, by a distinct offset to heavier values relative to $\delta^{18}O_{calcite}$ records for the summer mixed layer.

The relatively shallow (150-600 m) intermediate waters in the eastern Mediterranean in essence represent winter waters from the region with highest surface densities. Today, this condition is achieved between Cyprus and Rhodes (e.g., Wüst, 1961; POEM group, 1992; Roether and Well, 2001), and at times of sapropel formation it likely occurred in the Adriatic Sea (Myers et al., 1998; Rohling et al., 2000; Casford et al., 2002). Away from those areas, therefore, the intermediate water reflects a long-term mixture of intense winter conditions in a relatively remote region, which would by virtue of long-term (decadal-scale) homogenisation have lost almost all short-term variability in T, S, and $\delta^{18}O$. Basically, it acts like a giant capacitor that eliminates high-frequency noise, generating a stable long-term averaged signal.

Records of $\delta^{18}O_{calcite}$ cannot further distinguish between the main winter-water types (winter mixed-layer, summer subthermocline, and intermediate waters), except possibly for heavier mean values in species living in the somewhat colder and/or more evaporated intermediate water. Helpful contrasts are expected in the $\delta^{13}C_{calcite}$ records. While both the summer and winter mixed layers equilibrate with the atmosphere, the summer subthermocline (winter-type) waters remain seasonally isolated, awaiting the next deep winter mixing and building up a ^{12}C excess due to respiration. The resultant (light) $\delta^{13}C$ anomaly depends on the vigour of export production and respiration. However, it would remain smaller than the anomaly in the intermediate water: the relatively remote nature of the intermediate water, combined with its depth range that coincides with the mid-depth remineralisation maximum, determines that it becomes even more enriched in respiration products (cf. Pierre, 1999). Today, with very active intermediate water ventilation and oligotrophic conditions throughout the eastern Mediterranean, the surface to intermediate water $\delta^{13}C_{\Sigma CO2}$ gradient in the western Levantine and Ionian Basins is typically of the order of 0.3 ‰ (Pierre et al., 1999). It would be enhanced at times with elevated productivity and reduced ventilation.

The above suggests that the O and C isotope ratios in the various planktic foraminiferal species should distinguish up to five different water masses in the upper water column (Table 1). Specimens living in or very near to the thin top-layer/lenses of warm surface waters affected by freshwater floods from the (late) summer monsoon will display light and highly variable $\delta^{18}O$ values, along with variable $\delta^{13}C$ compositions between rather

heavy (productivity effect) and very light values (terrestrial carbon influence). Those living in the more extensive warm summer mixed layer can be distinguished on the basis of light $\delta^{18}O$ values, although not as light and variable as those in the thin freshwater-affected layer, and a less variable and likely heavier $\delta^{13}C$ values. Specimens living in cold winter-type waters will display $\delta^{18}O$ records with generally heavy mean values and suppressed variability. Those from the winter mixed layer proper will combine these characteristics with rather constant $\delta^{13}C$ values, although light values may be introduced when deep turbulence 'erodes' the underlying nutricline. Foraminifera from summer subthermocline waters are likely to record winter-type $\delta^{18}O$ values combined with light $\delta^{13}C$ values. Specimens from intermediate waters are likely to record winter-type $\delta^{18}O$ values (possibly somewhat heavier and with less short-term variability) accompanied by the lightest $\delta^{13}C$ values.

Finally, some species may show very little systematic behaviour in their $\delta^{18}O$ and $\delta^{13}C$ records. This would be characteristic of species that live by preference during seasonal 'transitions' of intensive mixing (e.g. the autumn breakdown of stratification) or early water-mass separation (e.g. spring build-up of seasonal stratification). Considering the 'identified' water masses as 'mixing end-members', such species would be expected to show strong variability between the end-member extremes. Another possible cause for non-systematic behaviour in foraminiferal $\delta^{18}O$ and $\delta^{13}C$ records relates to the unknown potential of the various species to experience a shift of their optimum shell-production conditions through the seasonal cycle, or in the vertical through the water column, in response to changes in overlooked (biological?) controls on their abundance distribution. One would then expect inexplicable variability independent of other signals when viewed over the whole record, although it may covary with other signals over parts of the record.

3.2. Vital effects

Most species secrete their calcite tests out of isotopic equilibium for $\delta^{18}O$ and $\delta^{13}C$, due to so-called 'vital effects' (Table 2) (e.g., Williams et al., 1981; Bouvier-Soumagnac and Duplessy, 1985; Spero and Williams, 1988; Ortiz et al., 1996; Bemis et al., 1998; Peeters, 2000; Simstich et al., 2003; Spero et al., 2003). General overviews can be found in Grossman (1987), Ravelo and Fairbanks (1995), Spero et al. (1991), and Rohling and

Cooke (1999). Palaeoceanographic studies allow for such processes by considering that the vital-effect offset from equilibrium is a constant through time for each species. The relative trends and variability in isotopic records are independent of such systematic disequilibria, which only affect the absolute values.

There is no *a-priori* "correction" for vital effect offsets in this study, because no values are yet available for specimens originating from the Mediterranean. In view of the extensive genetic differentiation within planktonic foraminiferal morpho-species (e.g., Darling et al., 2000; Stewart et al., 2001; Kucera and Darling, 2002; Pawlowski and Holzmann, 2002), we consider that the Mediterranean's quasi-isolation over at least 5 million years may well have fostered a fauna of endemic genotypes with vital-effect offsets that differ from those in their open oceanic morphological counterparts. In view of this uncertainty, it is more sensible to work with actually measured values than with values derived from a potentially erroneous "correction". For completeness, the most commonly reported (extra-Mediterranean) vital-effect values are listed in Table 2. Note that this table illustrates that straightforward "corrections" would also be difficult: (a) because the offsets for several of the species investigated here have not yet been determined; and (b) since – when determined – the offsets appear to be sensitive to SST. Our stable oxygen isotope model offers some crude insight into (dis)equilibrium values of the various species within the Mediterranean setting, for comparison with values in Table 2.

3.2. Modelling $\delta^{18}O$ variations

The implications for $\delta^{18}O$ of equilibrium calcite within the water masses discussed above are modelled using a previous Mediterranean $\delta^{18}O$ box model (Rohling, 1999). It is modified by separation of its single surface box into a succession of a winter mixed-layer box, a summer mixed-layer box, a summer-subthermocline box, and a monsoon-affected top-layer box within the summer mixed layer (Fig. 3). It calculates $\delta^{18}O_{water}$, salinity, and $\delta^{18}O_{calcite}$ for the various endmember water masses. Values of $\delta^{18}O_{calcite}$ in between those of the endmembers may result from (a) mixtures between endmember water masses, or (b) initial stages of temperature change. An example of (a) would be a partial breakdown of the halocline that separates freshwater lenses (monsoon box) from the rest of the

summer mixed layer. The $\delta^{18}O$ signals of foraminifera secreting shells under such conditions would score in between the values calculated for the monsoon box and the summer mixed-layer box. An example of (b) concerns the initial warming in the winter mixed layer at the early stages of seasonal stratification in spring. The $\delta^{18}O$ values of foraminifera living under such conditions would range in between those modelled for the winter mixed-layer box and the summer mixed-layer box.

The model contains a primitive annual cycle that consists of a 6-month summer and a 6-month winter. Precipitation onto the sea at any time is taken according to its present-day proportion relative to evaporation (40%: Garrett et al., 1993). The portion of runoff that equals the present-day runoff into the basin ('normal' runoff) is apportioned equally over the year. During periods of sapropel formation, late summer monsoon-sourced runoff into the basin was strongly enhanced (Adamson et al., 1980; Rossignol-Strick et al., 1982; Rossignol-Strick, 1983, 1985, 1987; Rohling et al., 2002). This influence is approximated by imposing a monsoon-affected box at the very surface of the summer mixed layer over a period of two months. This box is assigned a depth of 5 m over the entire basin, to primitively simulate considerably diluted conditions in response to the monsoon flooding, which in reality would be found concentrated in lenses or patches. This simplification is justified as we only aim to approximate relationships between the main trends in the various $\delta^{18}O$ records, not to realistically simulate circulation, and it is evaluated using sensitivity tests. The monsoon box allows assessment of the potential affinity of foraminiferal species with freshwater-diluted layers/lenses.

Inflow into the Mediterranean is regulated using a simplified version of the Bryden and Kinder (1991) model for exchange transport through the Strait of Gibraltar (cf. Rohling, 1999). Sea level for the time of S5 is taken constant and similar to the present, so that exchange transport through the Strait of Gibraltar only depends on changes in excess evaporation, according to $Q_A/Q_A^p = (X/X^p)^{1/3}$ where Q_A is the inflow from the Atlantic into the Mediterranean, X is excess of evaporation over total freshwater influx, and p indicates present-day values. Inflow is proportionally separated into the mixed-layer and subthermocline boxes according to the thickness of these boxes relative to the total surface-system depth. For non-sapropel times, the total surface-system depth is taken as 150 m, which then equals the total depth of the winter mixed layer, and which in summer

separates into a 50 m mixed-layer box and a 100 m thick subthermocline box. A basin-wide shoaling of the interface between surface and intermediate waters is well-documented for times of sapropel formation (Rohling and Gieskes, 1989; Castradori, 1993; Rohling, 1994; Myers et al., 1998). Consequently, the surface system for those times is set to a (winter mixed-layer) depth of 100 m, which in summer separates into 50 m for the mixed layer box and 50 m for the subthermocline box.

The hydrological cycle affects boxes exposed at the surface. Evaporation is calculated as outlined in Rohling (1999) with respect to the temperature of the box exposed at the surface (T_s for the summer mixed-layer and monsoon boxes, T_w for the winter mixed-layer box). Relative humidity, sea-air temperature contrast, and wind speed are kept constant at annual mean values of 70%, 0.5°C and 7.5 m s^{-1} (cf. Rohling, 1999). Seasonal temperatures are calculated using alkenone SSTs as an approximation of annual average SST (Rohling et al., 2002), and allowing seasonal deviations from the mean of +3°C in summer to –3°C in winter (Stanev et al., 1989). Since the alkenone SSTs are determined for the eastern Mediterranean, whereas the model concerns the entire basin, alkenone SSTs were first adjusted by –2°C to compensate for the difference between mean SST in the eastern basin only and mean SST in the entire Mediterranean.

We have performed preliminary SST reconstructions using an Artificial Neural Network approach (Hayes et al., 2003) on the planktonic foramninferal abundance data through S5 in core KS205 as given in Cane et al. (2000). The results broadly corroborate the schematic mean and seasonal change in SST used in the model calculations, although we may be underestimating seasonal variability by up to 2°C (Fig. 4). It also appears that the fauna-based SST values are considerably higher than alkenone-based estimates in the "pre-S5" and "base lower lobe" intervals (cf. Table 3), suggsting that our derived monsoon flooding values for that interval could be exaggerated and in fact may have been more similar to those in the "upper lobe" of S5. It remains to be established whether the difference in SST estimates relects a change in the dominant bloom season of alkenone producing phytoplankton, or some problem with the ANN method like a productivity overprint. ICP-AES based Mg/Ca analyses on foraminiferal calcite from S5 in KS205 (*G. ruber* w and *N. pachyderma* d) proved inconclusive because of erratic large-amplitude variability in the ratios (between 2 and 8 mmol/mol). Similarly erratic

results were obtained from benthic foraminiferal calcite from eastern Mediterranean sapropel S1, using laser-sampling ICP-MS (Reichart, pers. comm. Nice, April 2003).

The model calculates mean residence times in the surface system and then iterates over the appropriate number of annual cycles (Fig. 3). Winter mixing homogenises all summer boxes over the entire depth of the surface system (150 m in non-sapropel times, 100 m in sapropel times). Winter evaporation is calculated at temperature T_w. Precipitation is taken at 40% of evaporation, and runoff into the (6-month) winter mixed-layer box is $^6/_{12}$ of the 'normal' (= present-day) annual runoff. Next, the surface-most 50 m is separated (summer mixed layer). It undergoes evaporation at temperature T_s and receives a proportional amount (40%) of precipitation. The summer mixed-layer box is exposed to the hydrological cycle for 4 months, and so receives $^4/_{12}$ of the annual 'normal' runoff. The summer subthermocline box, which makes up the rest of the total depth of the surface system (50-150 m in non-sapropel times and 50-100 m in sapropel times), is not exposed and 'preserves' the properties achieved at the end of the previous winter mixed-layer episode. During two months at the end of summer in periods with specified monsoon intensification (Table 3), a 5 m thick layer is separated from the summer mixed-layer box at the very surface, to form the 'monsoon box'. Over these two months, the monsoon box sustains the effects of evaporation (at T_s), and receives a proportional amount of precipitation as well as $^2/_{12}$ of the 'normal' annual runoff. The monsoon box also receives the entire excess monsoon flooding imposed on the model. Monsoon intensification is quantified by a ratio, M, between the volume of the monsoon flood and that of the annual 'normal' (= present-day) runoff. A new 'year' is started in the model's iterative sequence with the homogenisation of all water masses to give the next winter's mixed-layer conditions. After completion of the iterative sequence, the final salinity and $\delta^{18}O$ values are noted for all boxes. End-product winter waters are used to represent the properties of intermediate water, which sustains the outflow from the basin through the Strait of Gibraltar (Fig. 3).

Environmental controls on $\delta^{18}O$ in the various boxes are treated as in Rohling (1999), except that we here keep the $\delta^{18}O$ of 'normal' runoff continuously at –6‰, rather than variable between –6‰ (non-sapropel times) and –8‰ (sapropel times) as in the earlier study. The present model allows the monsoon floods to enter the 2-month monsoon box

with isotopic values between –8 and –10‰, in agreement with the isotopic conditions reconstructed for monsoon floods (Sonntag et al., 1979; McKenzie, 1993; Rozanski, 1985; Hoelzmann et al., 2000; Gasse, 2000).

After determination of salinity and $\delta^{18}O_{water}$ in all boxes, the appropriate temperature for each box (T_s or T_w) is used to calculate equilibrium calcite $\delta^{18}O_{calcite}$ by means of the equations of O'Neil (1969), Coplen et al. (1983), and NIST (1992) (see elaboration in Rohling, 1999). The $\delta^{18}O_{calcite}$ value for intermediate waters considers an extra 1°C cooling. Although a rough approximation, this gives a useful confidence margin to the identification of species that reflect extreme winter-water conditions.

4. Results and Discussion

4.1. Qualitative habitat assessment

The isotope results for S5 in KS205 are consistent with those for S5 in ODP 971A and in ODP 967C (Fig. 1). The alkenone SST records show stable high values through all three S5 sapropels, although the high 'plateau' is reached considerably after the onset of the sapropel (Fig. 1). The $\delta^{18}O_{G.ruber\ (w)}$ records of KS205 and 971A show a general shift to light values within S5 that is interrupted by a brief enrichment. Neither of the two independently sampled and analysed $\delta^{18}O_{G.ruber\ (w)}$ records for 967C shows this 'interruption'. Overall, the lightest $\delta^{18}O_{G.ruber\ (w)}$ values are found in 971A (Fig. 1), similar to observations of lightest $\delta^{18}O$ values in the easternmost Ionian Sea / westernmost Levantine Sea for other sapropels (Fontugne et al., 1994; Emeis et al. 2002). The implications of this spatial $\delta^{18}O$ distribution pattern were elaborated previously (Rohling et al., 2002). Here, we emphasise that, despite local/regional differences, the general faunal and isotope patterns in KS205 are representative of S5 on a basin-wide scale (see also Corselli et al., 2002).

Figs. 2 and 5 present the isotope data through S5 in core KS205, along with means and $\pm 1\sigma$ bounds for six key intervals (means for S5 as a whole are listed in Table 4). The key intervals (Table 3) have been selected to capture the main 'states' in the records, avoiding the inclusion of strong shifts. The alkenone SST data are presented in Fig. 1, and means and $\pm 1\sigma$ bounds for the KS205 alkenone SST values in the six key intervals are shown in Fig. 5, after conversion to equivalent shifts in equilibrium calcite $\delta^{18}O$.

We are primarily concerned with differences between the general trends (mean values) in the various species' $\delta^{18}O$ records, and also consider the level of short-term variability/noise around those trends. The $\delta^{18}O$ signals of *G. scitula* and *N. pachyderma* (d) are very stable, with little short-term variability (Fig. 2). In fact, changes in $\delta^{18}O_{N.pachyderma\ (d)}$ and $\delta^{18}O_{G.scitula}$ are so limited to general trends that they show a highly significant positive covariation with one another from the top of MIS-6 through S5 (N = 36; $R^2 = 0.92$; $\delta^{18}O_{Gsc} = 0.85\ \delta^{18}O_{Np} + 0.39$). In view of the statistical nature of specimen selection for isotope analysis, one would expect considerable 'random' variability between individual analyses, and especially between series for two different species, unless these species (a) derived from a water mass with remarkable stability, displaying only long-term trends and no short-term 'noise', and (b) strictly adhered to one and the same, narrowly-constrained habitat. We also note that the $\delta^{18}O_{G.scitula}$ and $\delta^{18}O_{N.pachyderma\ (d)}$ data show a significant positive correlation with the alkenone SST estimates (N = 16; $R^2 = 0.42$, and N = 19; $R^2 = 0.67$, respectively). This suggests a close adherence to the general temperature developments in the basin with little interference from short-term environmental variability, which again implies a habitat in a water mass with remarkable temporal stability.

The $\delta^{18}O$ records of *G. ruber* (w), *G. ruber* (p), *G. glutinata*, *O. universa*, and *G. sacculifer* (*trilobus* type) instead show strong short-term variability around the mean trends, and no significant relationship with the alkenone SST trends (Fig. 2). Since the actual $\delta^{18}O$ values through S5 for the two *G. sacculifer* morphotypes are significantly correlated (N = 23; $R^2 = 0.58$), the *G. sacculifer* types with sac-like final chamber also belong in this group. Whatever additional forcing was associated with S5, it must have been small enough to have virtually no impact on some species (*N. pachyderma* (d) and *G. scitula*), yet at times strong/concentrated enough to seriously influence others (most notably white *G. ruber*).

The main additional control on foraminiferal $\delta^{18}O$ at times of sapropel formation was freshwater addition, mostly associated with to monsoon intensification during the precession-related insolation maxima (for overviews, see Rossignol-Strick et al., 1982; Rossignol-Strick, 1983, 1985; Jenkins and Williams, 1984; Rohling, 1994, 1999; Rohling and De Rijk, 1999; Cramp and O'Sullivan, 1999; Rohling et al., 2002; Emeis et al., 1998,

2000, 2003). Especially the trends in $\delta^{18}O$ of *G. ruber* (w), a shallow-dwelling species in the present-day Mediterranean (Hemleben et al., 1989; Pujol and Vernaud-Grazzini, 1995; Reiss et al., 1999), show high-amplitude variability through S5 that suggest an important impact of freshwater dilution (Figs. 2,5). Resistance of *G. ruber* (w) to freshwater disturbances at the very surface might also explain its shift to anomalously low $\delta^{13}C$ values within S5, as a consequence of the light terrestrial values in runoff (Figs. 2,5). It is one of the most euryhaline species (Hemleben et al., 1989), and so may achieve a competitive advantage in freshwater-disturbed surface ecosystems. *G. ruber* (w) has been observed in the Caribbean as the only species to inhabit freshwater-diluted lenses from the Amazon/Orinoco (Schmuker, 2000; Schmuker and Schiebel, 2002).

There is a significant positive correlation ($N = 55$; $R^2 = 0.41$; $\delta^{18}O_{Ou} = 0.58\ \delta^{18}O_{Gr} + 0.63$) between the actual $\delta^{18}O$ values of *G. ruber* (w) and *O. universa* within S5, which suggests a similar but roughly half-amplitude response in $\delta^{18}O_{O.universa}$ relative to $\delta^{18}O_{G.ruber\ (w)}$ (Figs. 2,5). A muted impact of freshwater anomalies on $\delta^{18}O_{O.universa}$ seems supported by its weak $\delta^{13}C$ change through the sapropel (Figs. 2,5). As the peak monsoon flooding occurs in late summer, we 'place' both species mostly within the summer mixed layer, in agreement with their present-day peak season in the basin (Pujol and Vergnaud-Grazzini, 1995; Reiss et al., 1999). During the monsoon runoff peak, the 'normal' summer mixed-layer conditions became disturbed by freshwater-diluted layers/lenses, creating habitats that were particularly favoured by *G. ruber* (w). *O. universa* on the contrary appears to have favoured more 'normal' summer mixed-layer conditions outside the flooding season and/or below the lenses, which would agree with its preference for deeper waters in the mixed layer during part of its life cycle (e.g., Hemleben et al., 1989)

The discontinuous presence of *G. sacculifer* morphotypes through S5 makes interpretations less straightforward, but its $\delta^{18}O$ and $\delta^{13}C$ trends (Figs. 2,5) essentially suggest rather similar living conditions to those of *O. universa*. Note that the low $\delta^{18}O$ value for *G. sacculifer* (*trilobus* type) in the interval within S5 where *O. universa* shows heavy values is based on one possible analysis only. With no significant distinction between the isotope records of the two *G. sacculifer* morphotypes, we envisage that both are typical of the 'normal' summer mixed layer conditions, similar to *O. universa*, possibly spending (part of) the lifecycle at some depth within that layer. This would agree

with observed habitats in other regions (e.g., Hemleben et al., 1989; Bijma and Hemleben, 1994).

A strengthening of the 'biological pump' should theoretically result in heavier $\delta^{13}C$ values in shallow waters (*O. universa*, *G. sacculifer*), but we observe no shift in the $\delta^{13}C$ values of these species with the onset of S5, or even the opposite – a weak shift to lighter values (Figs. 2,5). In view of the considerable amounts of isotopically light terrestrial runoff (white *G. ruber*), however, the absence of an enrichment in $\delta^{13}C$ values through S5 does not necessarily imply that there was no increase in export production. Averaged over the whole thickness of the summer mixed layer, to affect *O. universa* and *G. sacculifer*, the freshwater-related anomaly may have caused a moderate shift to lighter values that offset any enrichment due to strengthening of the biological pump. Alternatively, the monsoon flooding may have affected light penetration sufficiently to reduce the photosynthetic activity of symbionts, allowing shell formation from a carbon pool with lighter $\delta^{13}C$ values (Spero and Williams, 1988; Spero, 1992; Spero and Lea, 1993). Symbiont-bearing species more affected by the freshwater discharge (*G. ruber* (w)) would then show a stronger shift to low $\delta^{13}C$ values, while species that were less affected (*O. universa*, *G. sacculifer*) show negligible effects. In any case, it is apparent that the carbon isotopes cannot be used in a straightforward manner to assess the strength of the biological pump associated with S5; a comprehensive carbon box model would be needed.

The $\delta^{13}C$ record of *G. siphonifera* is virtually featureless. The values within S5 are weakly lighter than above and below the sapropel, but within S5 the various mean values cannot be statistically distinguished from one another (Figs. 2,5). The $\delta^{18}O$ values are generally heavy, with a shift to lighter values within the sapropel, similar to the records of *N. pachyderma* (d) and *G. scitula*. The $\delta^{18}O_{G.siphonifera}$ record is featureless through S5, apart from slightly more depleted and more variable values in the early part relative to the rest. Variability in both the $\delta^{18}O$ and $\delta^{13}C$ records is identical when calculated for raw values over the entire S5 interval and when calculated after means-subtraction (Table 4), which highlights the absence of significant longer-term trends. The species therefore appears to have been continuously secreting its test in the same type of conditions. The water mass in which *G. siphonifera* lived does not appear to have become isolated for any

significant period of time during sapropel formation, as there is only a moderate shift to lighter $\delta^{13}C$ values associated with S5, and no trend to increasingly depleted values (Figs. 2,5).

The low variability in both the C and O isotope records of *G. siphonifera* suggests that it inhabited a well-mixed water mass of considerable volume. This is particularly exemplified by the visible but muted expression of the freshwater-related $\delta^{18}O$ anomalies seen in *G. ruber* (w). In fact, the $\delta^{18}O_{G.siphonifera}$ values show significant positive correlations with both $\delta^{18}O_{G.ruber\ (w)}$ and $\delta^{18}O_{O.universa}$ (with N = 55, $R^2 = 0.23$, $\delta^{18}O_{Gsi} = 0.35\ \delta^{18}O_{Gr} + 1.05$; and N = 57, $R^2 = 0.35$, $\delta^{18}O_{Gsi} = 0.47\ \delta^{18}O_{Ou} + 0.71$ respectively). These relationships crudely demonstrate that where $\delta^{18}O_{O.universa}$ responded with a similar fluctuation but of reduced amplitude to an environmental (freshwater) forcing that drove strong shifts in $\delta^{18}O_{G.ruber\ (w)}$, the same is true for $\delta^{18}O_{G.siphonifera}$ but with an even further reduced amplitude. The amplitude reduction from $\delta^{18}O_{G.ruber\ (w)}$ to $\delta^{18}O_{O.universa}$ was related to mixing of an initially concentrated signal over the larger volume of the summer mixed layer. The further amplitude reduction to that in $\delta^{18}O_{G.siphonifera}$ then suggests a further dilution of the initial signal, which immediately hints at the impact of deep homogenisation in the winter mixed layer. Overall, it appears that *G. siphonifera* thrived in a well ventilated (not isolated) and rather eutrophic (^{12}C enriched, possibly because of turbulent nutricline erosion) water mass that may have been relatively cold, based on the species' heavy $\delta^{18}O$ signature: the winter mixed layer.

Winter-water conditions are also reflected in the $\delta^{18}O$ records of *G. scitula* and *N. pachyderma* (d), with low-amplitude variability around very heavy mean values (Figs. 2,5). Their $\delta^{13}C$ values, however, place these species in a totally different environment than *G. siphonifera* (Figs. 2,5; Table 4). Both *G. scitula* and *N. pachyderma* (d) show shifts to extremely light $\delta^{13}C$ values, with trends of increasing depletion, through sapropel S5. The combined data suggest habitats within a winter-type water mass that was isolated for extended periods of time, allowing long-term build-up of ^{12}C-rich remineralisation products. We infer, therefore, that these two species lived at considerable depth in winter-type waters, near/in the nutricline. This places them possibly in a summer subthermocline setting, but more likely in close association with the more persistently isolated intermediate waters. As argued above, the great 'stability' in the

$\delta^{18}O_{G.scitula}$ and $\delta^{18}O_{N.pachyderma\ (d)}$ implies that their signals have been processed through a 'giant capacitor', which systematically removed all high-frequency variability to leave only the main trends. This supports a main habitat in the intermediate water.

Finally, there are three species that lack any systematic behaviour in their oxygen and carbon isotope records: *G. ruber* (pink), *G. bulloides*, and *G. glutinata*. *G. ruber* (pink) consistently shows the lightest $\delta^{18}O$ values of all species investigated (Figs. 5), which would suggest the warmest/freshest habitat. However, it shows relatively small amplitudes of change between the various mean values (Figs. 2,5). This is not what would be expected anywhere in the summer mixed-layer (e.g. *O. universa, G. sacculifer*), or indeed in the very surface levels with impact of monsoon runoff (*G. ruber* (w)). Instead, the pattern of shifts between the mean $\delta^{18}O$ and $\delta^{13}C$ values for *G. ruber* (p) is very similar to that for *G. bulloides*, except that it seems to be offset by –1 to –1.5‰ ($\delta^{18}O$) and +1.5 to +2‰ ($\delta^{13}C$) relative to *G. bulloides*. The short-term variability, in contrast, is much lower in *G. ruber* (p) than in *G. bulloides* (Figs. 2,5; Table 4). Evidently, they are not simply systematically offset from one another, which precludes a conclusion that both lived under similar conditions but with different deviations from equilibrium. *G. glutinata* shows very similar signals to those of *G. bulloides* (Figs. 2,5; Table 4).

As discussed before, a lack of systematic signal such as observed in *G. bulloides*, *G. glutinata*, and *G. ruber* (p), should be expected for species that prefer seasonal 'transitions', e.g. the autumn breakdown of stratification, or the build-up of stratification in spring. This is a proxy relationship, since *G. bulloides* and *G. glutinata* in reality depend less on radiation than on deep nutrient entrainment by to storms (both spring and fall; Schiebel et al., 2001). The insensitivity of these species' $\delta^{18}O$ records to the freshwater-related anomalies witnessed by *G. ruber* (w) (Figs.2,5) then suggests that they are not from the autumn, which follows shortly after the peak monsoon flooding, but instead were associated predominantly with the spring 'bloom'. Possibly, their erratic $\delta^{18}O$ signatures reflect variable depth habitats and the early development of (thermal) differentiation within the mixed layer. The observed differences in short-term variability between $\delta^{18}O_{G.bulloides}$, $\delta^{18}O_{G.glutinata}$, and $\delta^{18}O_{G.ruber\ (p)}$ then suggest growth conditions over

more extensive depth ranges for *G. bulloides* and *G. glutinata*, and a more narrowly constrained range (towards the surface?) for *G. ruber* (p).

An inferred spring-bloom habitat for *G. bulloides* and *G. glutinata* would be consistent with modern observations of cosmopolitan and eutrophic/opportunistic preferences (cf. Hemleben et al., 1989; Pujol and Vergnaud-Grazzini, 1995; Reiss et al., 1999; Schiebel and Hemleben, 2000). However, it is a controversial suggestion for *G. ruber* (p). It would imply that *G. ruber* (pink) secretes its shell in great disequilibrium, which may not be supported by observations (Deuser and Ross, 1989; Table 2). It appears that we cannot deduce a realistic palaeohabitat for this species on the basis of the available data.

4.2. Model-based habitat assessment

Fig. 6 shows the modelled equilibrium calcite $\delta^{18}O$ values for the various boxes. Two lines are displayed for each box. The lighter values represent the solution using a monsoon runoff $\delta^{18}O$ composition of –10‰, and the heavier values represent a scenario that uses –8‰. The lower 'lobe' of S5 was set to have a monsoon intensification factor M = 3, and the upper 'lobe' was set with M = 2 (Table 3). A complete collapse of the monsoon intensification was prescribed for the interval with heavy $\delta^{18}O_{G.ruber\,(w)}$ and $\delta^{18}O_{O.universa}$ values (Figs. 1,2,5). The specified range of monsoon intensity values is chosen: (a) to offer a range of simulations that portrays the model's sensitivity to strong extremes in M; and (b) so that the general underlying trends in the simulations are in basic agreement with the records. Sensitivity tests are discussed in section 4.5.

The dominant impact of a monsoon flood of isotopically light fresh water is observed in the small-volume monsoon box. Note, however, that this box also sustains all evaporation during its two-month life span (a high flux at the high T_s values). This considerably counteracts the salinity and $\delta^{18}O$ impacts of the flood. Mixed over the more voluminous summer mixed-layer box, the isotopic anomaly becomes strongly muted. The winter mixed-layer and summer subthermocline boxes, as expected, show virtually identical $\delta^{18}O_{calcite}$ values, and there is a systematic (1°C-equivalent) enrichment in the intermediate-water values relative to the winter boxes.

We next compare the modelled traces with the various species' mean values in the six key intervals. The model approaches the same intervals, since it relies on the seasonal

temperature values derived from the mean alkenone-SST values for the same intervals (Fig. 6). The analytical series are shifted until, in order of priority, best visual fits are obtained: (1) in the pre-sapropel interval; and (2) over the entire trace. This procedure offers a first-order insight into the (dis-)equilibrium state of the foraminiferal calcite, which is more extensively discussed in section 4.3. Figure 7 compares the actual data with the modelled traces, using the offsets determined in Fig. 6.

The data for *G. ruber* (w), *G. scitula*, and *N. pachyderma* (d) agree well with the modelled traces, with the simulated contrast between winter and summer/monsoon-box conditions close to that observed between the *N. pachyderma* (d)–*G. scitula* pair and *G. ruber* (w). The modelled long-term variability also agrees well with that in the observations for the winter-water species, but for *G. ruber* (w) the amplitude is underestimated. We were not able to drive the model simulations to the very heavy values indicated by $\delta^{18}O_{G.ruber\,(w)}$ in the 'interruption' without disturbing the close agreement in the other boxes with the analytical series of *N. pachyderma* (d), *G. scitula*, *O. universa*, and *G. siphonifera* (Figs. 6,7). Moreover, comparison of the modelled traces with $\delta^{18}O_{G.ruber\,(w)}$ variability through S5 in ODP sites 971A and 967C suggests that the main run yields a satisfactory trace for this species (971A), or even overestimates the enrichment (967C) (Fig. 8). We infer that the model reasonably approximates the actual changes in $\delta^{18}O_{G.ruber\,(w)}$ on a basin-wide scale, and that other (not included) influences caused regional deviations.

O. universa shows considerable longer-term variability, and it would appear to fit best 'in between' the modelled summer mixed-layer and monsoon box conditions (Figs. 6,7). This would imply that *O. universa* occupied the more 'normal' summer mixed-layer conditions in between and/or below, but for part of its life cycle affected by, freshwater-dilution at the very surface.

G. siphonifera shows a virtually in-equilibrium match with the modelled $\delta^{18}O_{calcite}$ record for winter-type waters (Figs. 6,7). The good results from the model for this species, as well as *N. pachyderma* (d), *G. scitula*, and also *O. universa*, inspire considerable confidence in the model's basic underlying assumptions such as the rough estimates for the monsoon-box thickness and the monsoon intensification factor. Note, for example, that an increase in the thickness of the monsoon box would necessitate an

increase in the monsoon floods to obtain the same isotopic anomalies in *G. ruber* (w) (and *O. universa*). However, that signal then becomes too dominant in the winter-water boxes, upsetting the good correspondence observed in the main run for *G. siphonifera*, *O. universa*, *N. pachyderma* (d) and *G. scitula* in KS205 as well as sites 971A and 967C.

The data for *G. ruber* (p), *G. bulloides*, and *G. glutinata* remain difficult to place (cf. section 4.1.). We proposed that *G. ruber* (p), *G. bulloides* and *G. glutinata* thrived in spring, reflecting the transition from winter-type conditions to summer-type conditions. Their isotopic (dis-) equilibrium states may then be tentatively estimated by shifting the records so that the bulk of values falls between the winter and summer 'extremes' (Figs. 6,7).

4.3. Assessment of the model-inferred offsets from equilibrium $\delta^{18}O$

The model does not allow for such processes as entrainment and mixing between the separate boxes, and also has simply prescribed, basin-averaged seasonal temperature and air humidity conditions. Comparisons between the simulated and analysed $\delta^{18}O$ values (Figs. 6-8) are therefore most reliable where relative trends and offsets are concerned. Although the simulated absolute $\delta^{18}O_{calcite}$ values deserve more caution, the inferred isotopic disequilibria for the various species still provide a useful criterion for gauging the general quality of the model-based reconstructions. Note that 1σ ranges around the analysed means used to evaluate the disequilibria amount to $\pm$ 0.2 to 0.6‰ (Table 4), and that additional bias may occur due to deviations of the species' actual growth temperatures from the applied schematic seasonal temperature variations.

For *G. ruber* (w), *N. pachyderma* (d), and *G. scitula*, the best fit to modelled $\delta^{18}O_{calcite}$ invokes an offset of roughly –0.6‰, which is within the 1σ range from values observed in culture experiments with *G. ruber* (w) and *N. pachyderma* at ~20°C or in plankton tow samples of *G. scitula* (Table 2). For *G. bulloides*, the tentatively inferred offset is roughly –0.3‰, which would be around 1‰ heavier than suggested by cluture experiments at 20°C (Table 2). The model-suggested offset of –0.3‰ for *G. siphonifera* is in reasonable agreement with warm-water plankton tow results of –0.55‰ (Table 2). Culture experiments suggest that *O. universa* secretes its test at –1.0 to –0.7‰ relative from equilibrium at ~20°C (Table 2). The difference between these values and our inferred

offset of +0.7‰ is rather large, but we note that Spero and Williams (1988) reported very different $\delta^{18}O_{O.universa}$ values near equilibrium (±0.2 to 0.4‰), which would be within our 1σ limits. The inferred offsets from equilibrium for *G. ruber* (p) is around –1.5‰, which exceeds some observations (Deuser and Ross, 1989) but may find some support from warm-water plankton tow results that show an offset of 0.0 to –0.4 ‰ relative to *G. ruber* (w) (Table 2), giving *G. ruber* (p) a total offset between –0.6 and –1.0‰ that approaches the 1σ limit (Table 4) around our model-estimated value of –1.5‰.

4.4. Model-based insight into the Salinity:$\delta^{18}O$ relationship

The model simultaneously resolves for salinity, $\delta^{18}O_{water}$, and $\delta^{18}O_{calcite}$. It therefore determines the seawater S:$\delta^{18}O_{water}$ relationship for the various boxes. With the monsoon intensification factor (*M*) set to values of 3 and 2 for the lower and upper lobes of S5, respectively (Table 3), two sets of solutions were obtained: one using a $\delta^{18}O$ of monsoon runoff of –8‰, and the other using –10‰ (Fig. 9). For salinity, both solutions are identical, but the simulated $\delta^{18}O$ records differ considerably. The right-hand panels of Fig. 9 illustrate the S:$\delta^{18}O_{water}$ relationships in the various boxes. The use of a different isotopic ratio for the monsoon runoff considerably alters the temporal S:$\delta^{18}O_{water}$ slopes. There also is a considerable difference between the temporal S:$\delta^{18}O_{water}$ slope of the monsoon box and the other boxes, within any single simulation experiment. If this were overlooked, then reconstructions based on $\delta^{18}O_{G.ruber\,(w)}$ would strongly overestimate the amount of change in the basin's hydrological forcing. It is further evident that $\delta^{18}O_{G.bulloides}$, $\delta^{18}O_{G.ruber\,(p)}$ and $\delta^{18}O_{G.glutinata}$ are also unsuitable for reconstructions of the basin's overall circulation state – in these cases because of a lack of firm affinity with any of the endmember water masses.

The most useful $\delta^{18}O$ records for establishing the overall circulation state are those for *G. siphonifera*, *N. pachyderma*, and *G. scitula*, since the winter-water conditions represent the most homogenised, least variable, long-term integrated response to the entire suite of possible environmental perturbations. However, even when using such representative records, and even if season/species-specific SST control were established, the fundamental problem remains that spatial and temporal S:$\delta^{18}O_{water}$ relationships are not normally the same (see also Rohling and Bigg, 1998; Rohling and De Rijk, 1999;

Rohling, 1999, 2000; Schmidt, 1999a,b). We expect more profound advances from palaeocirculation models of increasing complexity with embedded $\delta^{18}O$ calculations, validated against whole-faunal isotope data.

4.5. Sensitivity tests and monsoon intensification estimates

General sensitivity tests with the presented type of model have been reported previously (Rohling, 1999). The essential modification to be evaluated here involves the somewhat arbitrarily chosen thickness of the monsoon box. In the main run, its thickness is set at 5 m over the entire surface area of the basin. This may be an overestimate, since even at $M = 3$, the equivalent of just under 1 m of total runoff is specified into the basin. The lower limit for the monsoon-box thickness can be estimated at ~1.5 m. Mixture of that much marine water at a salinity of ~38 p.s.u. with 1 m of fresh water yields an endproduct with a salinity of ~22 p.s.u., the absolute minimum for survival of planktic foraminifera (Hemleben et al., 1989). For a reduction in the monsoon-box volume, less monsoon intensification would be needed to achieve roughly the same low $\delta^{18}O$ (and salinity) values in that box as found in the main run. To maintain the main run's values for the lower lobe of S5, the required monsoon intensification factor is related to the change (∂z_{mon}) in the thickness of the monsoon box as $M \approx M_0 (1 + 0.12\ \partial z_{mon})$, where M_0 is the value used in the main run (Table 3). For a 1.5 m thick monsoon box, this gives M = ~1.6 (lower lobe) and M = ~1.2 (upper lobe). Although this would not alter the temporal S:$\delta^{18}O$ ratio in the monsoon box (z_{mon} and M were changed proportionally), great shifts would result in the ratios for the other boxes (compare Figs. 9 and 10).

By defining a relatively thick (5 m) monsoon box in the main run, the model minimises the contrasts between the various boxes, in good agreement with the total range of foraminiferal $\delta^{18}O$ values. The total spread of the data spans 2.2‰ between the heaviest and lightest (consistent) mean values within S5 (Fig. 5), which is closely captured by the difference between extremes in the main run of the model (Figs. 6,7). Also, *G. siphonifera* shows some long-term fluctuations (Fig. 7) that agree better with the simulated patterns from the main run than with those from the experiment with a monsoon box of 1.5 m (Fig. 11). Although these are hints that the main run may be more realistic, the differences between the two experiments (Fig. 11) are mostly smaller than

the short-term variability in the data. Therefore, the full range of monsoon intensifications suggested by the two experiments should be considered: during the formation of the lower (upper) lobe of S5, monsoon flooding introduced an extra 160 to 300% (120 to 200%) of runoff into the basin, compared to the present. Although these are wide ranges, they offer the first quantitative indication of the order of magnitude of the freshwater disturbances when S5 developed.

4.6. Comparison of habitats during S5 and those during Holocene S1 and the Present

Here, we compare our stable isotope records through S5 with similar data through Holocene sapropel S1 in SE Aegean core LC21 (Fig. 12). The faunal and geochemical signals in LC21 are representative of developments in the wider Aegean Sea, and also resemble those observed in the Adriatic Sea and northern Levantine Basin (e.g., De Rijk et al., 1999; Mercone et al., 2000, 2001; Casford et al., 2001, 2002). The Holocene record adds an evaluation of *Globorotalia inflata* within the full-faunal context. This species was extremely rare through S5 (see also Corselli et al., 2002). Figure 12 shows a Late Glacial to Holocene $\delta^{18}O$ profile for *G. inflata* that overlaps with $\delta^{18}O_{N.pachyderma\ (d)}$, whereas $\delta^{13}C_{G.inflata}$ resembles $\delta^{13}C_{G.ruber\ (w)}$. The trends and position of the *G. inflata* records relative to those of the other major species show a strong similarity to those of *G. siphonifera* through S5 (Fig. 12). We infer that *G. inflata* also inhabited the well-ventilated, deeply homogenised winter mixed layer.

The comparison between S5 and S1 (Fig. 12) further shows that the strong depletions in S5, ascribed to freshwater dilution, are much less evident in S1. As a result, there is a much smaller difference between $\delta^{18}O_{G.ruber\ (w)}$ and $\delta^{18}O_{G.\ inflata}$ in S1 than between $\delta^{18}O_{G.ruber\ (w)}$ and $\delta^{18}O_{G.\ siphonifera}$ in S5. Moreover, the apparent summer species *G.ruber* (w), *O. universa*, and *G. sacculifer* (*trilobus* type) show much reduced spread between one another in S1 of core LC21. This suggests that the impact of discrete freshwater-diluted lenses in the summer mixed layer was virtually negligible during the deposition of S1 in the SE Aegean Sea.

Changes in the carbon isotope records are highly comparable between S5 and S1, except where *N. pachyderma* (d) is concerned. $\delta^{13}C_{N.pachyderma\ (d)}$ reaches very low values through S5, but there is no such strong trend in S1 of core LC21. In the central Aegean

Sea, stronger shifts were found through S1 for this species, reaching −1.5‰ (Casford et al. 2002, 2003). In Aegean core LC21, some low-oxygen tolerant benthic foraminifera (*Chilostomella mediterranensis*) survived through S1, and their values are indicated as well (Fig. 12). Their presence suggests intermittent availability of low concentrations of oxygen in bottom waters, and a more intensive phase of ventilation is thought to be responsible for the division of S1 into two discrete units. (cf. De Rijk et al., 1999; Myers and Rohling, 2000; Mercone et al., 2001). It is apparent that the very negative $\delta^{13}C$ values found in the planktic species *N. pachyderma* (d) and *G. scitula* in S5 approximate the S1 values for the benthic species *Chilostomella mediterranensis*, which lived at ~1500 m depth. Overall, the isotope gradients in S5 and S1 show comparable general developments, but the gradients are much stronger in S5 than in S1, while the freshwater dilution also appears much stronger in S5 than in S1. We infer that both sapropels reflect a similar hydrographic configuration, but that S5 represents a more 'intense' version of this configuration. The greater 'intensity' would agree with the fact that S5 commonly contains 4-10 %(wt.) of organic carbon, versus 1-3 %(wt.) for S1 (e.g. Murat, 1984; Fontugne and Calvert, 1992).

The inferred habitat characteristics for the various species during the deposition of S5, including the additional information for *G. inflata* from S1, can now be compared with the extensive (plankton tow) study of present-day foraminiferal distribution patterns in the Mediterranean presented by Pujol and Vergnaud-Grazzini (1995), and their distribution in core tops as synthesised by Thunell (1978). Both studies show that *G. ruber* is the most ubiquitous species in the eastern Mediterranean. Although present in detectable numbers also in winter, it dominates in summer, and occupies especially the upper 50 m of the water column. Both in the living assemblages and in surface sediments, *G. ruber* is particularly dominant (>60%) in extreme eastern locations. The diagrams for summer presented by Pujol and Vergnaud-Grazzini (1995) suggest a west-east increase in the dominance of pink types within *G. ruber*, but they emphasise that to the east of 18°E, total faunal abundances are extremely low, with domination by *G. ruber* (w). Pujol and Vergnaud-Grazzini (1995) find strong abundance maxima of spinose predatory species (notably *G. ruber* (p)) at the seasonal thermocline. In the eastern Mediterranean, *G. sacculifer* (*trilobus*) and *O. universa* prevail only in summer, and these species actually

control the standing stocks in the summer mixed layer in the western basin (Pujol and Vergnaud-Grazzini, 1995). The non-spinose species *G. inflata* and *G. truncatulinoides* (not found in the present study) were found to prevail to great depth in the western basin during winter, and are also among the more important species in winter in the eastern basin. Where present, notably in the Levantine basin, *G. siphonifera* displays peak abundances in winter. The studies of Pujol and Vergnaud-Grazzini (1995) and Rohling et al. (1995) furthermore illustrate that density fronts or density gradients within the photic layer can support year-round persistence of grazing species such as *G. inflata*, *G. truncatulinoides*, *N. pachyderma* (d).

It is tempting to ascribe the strong dominance of *G. ruber* in the easternmost sector of the basin to the impact of (pre-Aswan) Nile outflow, which under peak flood conditions caused salinities in the plume to drop to values as low as 28 p.s.u. (Reiss et al., 1999). In core GA-112 from the slope in the Ashdod area (S Israel; 31°56.41'N, 34°22.13'E, 472 m), Reiss et al. (1999) report a major abundance minimum of *G. ruber* between ~1700 (dated) and ~1000 (estimated) radiocarbon convention years BP, which appears to form the abrupt culmination of a very gradual reduction since ~2600 years BP. Its timing is remarkably coincident with an episode of low Nile flood conditions (Hassan, 1997). However convenient these observations might seem in relation to the affinity of *G. ruber* (w) for freshwater-diluted conditions inferred here and in Rohling et al. (2002), they are suggestive only. We feel supported, however, by recent Caribbean plankton tow results from freshwater-diluted lenses that originate from the Amazon/Orinoco, which show sustained populations dominated by *G. ruber* (w) (Schmuker, 2000; Schmuker and Schiebel, 2002).

Modern observations do not link *G. ruber* (p) with spring, as suggested in the present study. However, the unfortunate absence of a sampling in the spring season may be complicating the correct identification of the most important abundance season for many species. Alternative interpretations of *G. ruber* (p) may be possible in view of the data presented by Pujol and Vergnaud-Grazzini (1995). Possibly, the $\delta^{18}O$ record of this species is noisy because it reflects a range of temperature values resulting from its apparent living positions in both the very warm shallowest levels (upper 20 m) and in association with the considerably cooler summer thermocline. Some stations (especially

15B, south of Cyprus) even show an apparent bimodal depth distribution of *G. ruber* (p) between these two habitats (Pujol and Vergnaud-Grazzini, 1995). This would cause similar levels of 'noise' in the $\delta^{18}O$ record as the inferred spring habitat, and we conclude that there would be little hope to better constrain the palaeohabitat of species with such bi-(or multi-)modal abundance distributions.

O. universa and both morphotypes of *G. sacculifer* today appear as typical summer mixed-layer dwellers (Pujol and Vergnaud-Grazzini, 1995). The isotope reconstructions for S5 and S1 presented here suggest similar behaviour in the past. In other areas, these species show a tendency to secrete part of the shell at deeper levels within the summer mixed layer (e.g., Hemleben et al., 1989; Bijma and Hemleben, 1994), which would agree with our observation that they recorded much less of the freshwater dilution at S5 times than *G. ruber* (w). *G. glutinata*'s modern habitat in the Mediterranean was not well resolved, but a main preference for spring, as inferred here, would not be incompatible with its very low abundances in the summer and winter tows. The same holds true for *G. bulloides*, for which Pujol and Vergnaud-Grazzini (1995) actually report peak abundances in spring in the Alboran Sea (westernmost Mediterranean). *H. pelagica* remains enigmatic, and no definite conclusions can be formulated on the basis of its sparse occurrences. *G. siphonifera* today appears to be a winter mixed-layer species, which agrees with our reconstruction of its habitat during deposition of S5. The modern abundance distribution of *N. pachyderma* (d) is complex, as there seems to be no strict seasonal preference. In the Mediterranean today, it is a mesopelagic species, associated with density/nutrient gradients at depth (Pujol and Vergnaud-Grazzini,1995; Rohling et al. 1995), which agrees with the isotopic results for both S5 and S1 presented here. The mesopelagic habitat of *G. scitula* inferred from the stable isotope study in this paper cannot be compared with the present, since no living *G. scitula* have yet been observed in the Mediterranean basin, while it is also absent from core-top samples. The habitat reconstruction for *G. inflata* during S1 deposition is compatible with its modern preferences as well.

Table 5 summarises the inferred palaeohabitats for the various species investigated within especially S5 and also S1, in comparison with modern observations. It is apparent that there is a broad agreement between modern and inferred (S5-time) palaeohabitats,

which is reassuring for the purposes of environmental reconstructions based on shell chemistry. However, some species, such as *G. ruber* (w), do not appear to show their full environmental range in the Mediterranean today, but can adapt to anomalies such as excess freshwater input in accordance with their observed preferences/tolerances outside the Mediterranean. This observation offers a strong argument that detailed shell-chemistry work should rely on reconstruction methods such as presented here to diagnose palaeohabitats, rather than infer them simply in terms of the niches occupied today.

5. Concluding Remarks

Whole-faunal stable isotope studies elucidate which species in a specific study interval/area are best to assess overall changes in the climatic/hydrographic state of a basin, including depth-related differentiations and the main seasonal developments, and which species in contrast were most affected by variable biological controls or local/regional and transient physico-chemical forcings. Even when performed within a whole-fauna context, palaeoenvironmental interpretations based on multiple-specimen shell chemistry will be limited by the fact that the observed signals represent multi-annual weighted averages of a wide range of possible peak shell-production seasons, the relative importances of which may shift through the annual cycle in a species-specific manner (shell chemistry depends as much on biology as on physico-chemical conditions). A single-shell analytical approach seems essential before any biologically constrained habitat shifting, and/or the impact of transient features, can be addressed in earnest. Impacts of transient features and/or biological controls on habitat may result in signal amplitudes that rival those of the 'general' underlying trends, and – if overlooked – would seriously bias the palaeoenvironmental reconstructions. The present study finds that, at times of sapropel deposition, *G. ruber* (w) records tend to be compromised by concentrated signals from such a transient feature, namely freshwater-diluted lenses. Application of this species' isotope ratios to characterise the 'main state' of the basin will severely overestimate the magnitude of the freshwater influx. In other settings, one could envisage that transient eddies act as foci of shell production, which would bias shell-chemistry-based reconstructions since temperature, nutrient, and salinity distributions in transient eddies generally differ from those in abient waters.

Once the nature of the faunal responses (here in the Mediterranean) to a particular type of environmental perturbation (here enhanced freshwater influx) is understood, intensity differences between different sites or events can be evaluated. Our three records through S5 show considerable similarities – suggesting a general change in the basin-wide conditions – as well as distinct local/regional differences in the signal responses and intensities that are related to superimposed local/regional influences. We also find great similarities between the signals through sapropels S5 and S1, although the intensities of change are considerably higher in S5.

Although labour intensive and analytically expensive, a quantitatively interpreted full-faunal stable-isotope data set offers crucial advances in the understanding of temporal changes, differences between separate events, and spatial contrasts for individual events. The thus diagnosed (rather than "imposed") past habitat structures may be used to target further shell chemistry investigations that focus on specific reconstructions such as vertical property gradients. We also suggest that, to eliminate bias originating from the statistical nature of the specimen selection for analysis, shell-chemistry techniques should strive towards multiple-replicate single-shell analyses per species per sample. These underlying principles apply to all palaeoceanographic problems, not just those concerning Mediterranean sapropels.

Acknowledgements. We thank A. Almogi-Labin, W. Broecker, J. Erez, G. Ganssen, C. Hemleben, A. Kemp, M. Kucera, J. McManus, M. Palmer, G. Schmiedl, A. Scrivner, H. Spero, J. Thomson, D. Vance, and P. Wilson for stimulating discussions, feedback, and suggestions on various aspects of this study. M. Cooper kindly performed the foraminiferal Mg/Ca analyses. This paper contributes to NERC projects NER/B/S/2000/00288 and NER/B/S/2002/00268, and Leverhulme project F/07537/I.

References

Adamson, D.A., Gasse, F., Street, F.A., Williams, M.A.J., 1980. Late Quaternary history of the Nile. Nature, 288, 50-55.

Bar-Matthews, M., Ayalon, A., Kaufman, A., 2000.Timing and hydrological conditions of Sapropel events in the Eastern Mediterranean, as evident from speleothems, Soreq cave, Israel, Chemical Geology 169, 145-156.

Bauch, D. J. C., and Wefer, G., 1997. Oxygen isotope composition of living *Neogloboquadrina pachyderma* (s) in the Arctic ocean. Earth and Planetary Science Letters 146, 47-58.

Bé, A.W.H., Bishop, J.K.B., Sverdlove, M.S., Gardner, W.D., 1985. Standing stock, vertical distribution and flux of planktonic foraminifera in Panama Basin. Marine Micropaleontology 9, 307-333.

Bemis, B.E., Spero, H.J., Bijma, J., and Lea, D.W., 1998. Re-evaluation of the oxygen composition of planktonic foraminifera: experimental results and revised paleotemperature equations. Paleoceanography 13, 150-160.

Bijma, J., and Hemleben, C., 1994. Population dynamics of the planktic foraminifer *Globigerinoides sacculifer* (Brady) from the central Red Sea. Deep-Sea Res. I, 41, 485-510.

Bouvier-Soumagnac Y. and Duplessy J. C., 1985. Carbon and oxygen isotopic composition of planktonic foraminifera from laboratory culture, plankton tows and recent sediment: implications for the reconstruction of paleoclimatic conditions and of the global carbon cycle. J. Foram. Res., 15, 302-320.

Boyle, E.A., Keigwin, L., 1982. Deep circulation of the North Atlantic over the last 200,000 years: geochemical evidence. Science 218, 784-787.

Boyle, E.A., Keigwin, L., 1985/86. Comparison of Atlantic and Pacific paleochemical records for the last 215,000 years: changes in deep ocean circulation and chemical inventories. Earth and Planetary Science Letters 76, 135-150.

Boyle, E.A., Keigwin, L., 1987. North Atlantic thermohaline circulation during the past 20,000 years linked to high-latitude surface temperatures. Nature 330, 35-40.

Brovkin, V., Claussen, M., Petoukhov, V., Ganopolski, A., 1998. On the stability of the atmosphere-vegetation system in the Sahara/Sahel region. J. Geophys. Res. 103, 31613-31624.

Bryden, H.L., Kinder, T.H., 1991. Steady two-layer exchange through the Strait of Gibraltar. Deep-Sea Research 38 (Supplement 1), S445-S463.

Calef, G.W., Grice, G.D., 1967. Influecne of the Amazon River Outflow on the ecology of the western Tropical Atlantic II. Zooplankton abundance, copepod distribution, with remarks on the fauna of low-salinity areas. Journal of Marine Research 25, 84-xx.

Cane, T., Rohling, E.J., Kemp, A.E.S., Cooke, S., Pearce, R.B., 2002. High-resolution stratigraphic framework for Mediterranean sapropel S5: defining temporal relationships between records of Eemian climate variability. Palaeogeography, Palaeoclimatology, Palaeoecology 183, 87-101.

Casford, J.S.L., Abu-Zied, R., Rohling, E.J., Cooke, S., Boessenkool, K.P., Brinkhuis, H., De Vries, C., Wefer, G., Geraga, M., Papatheodorou, G., Croudace, I., Thomson, J., Wells, N.C., and Lykousis, V., 2001. Mediterranean climate variability during the Holocene. Mediterranean Marine Science 2, 45-55.

Casford, J.S.L., Rohling, E.J., Abu-Zied,R., Cooke, S., Fontanier, C., Leng, M., Lykousis,V., 2002. Circulation changes and nutrient concentrations in the Late Quaternary Aegean Sea: A non-steady state concept for sapropel formation, Paleoceanography, 17, DOI 0.1029/ 2000PA000601.

Casford, J.S.L., Rohling, E.J., Abu-Zied, R.H.., Jorissen, F.J., Leng, M., and Thomson, J., 2003. A dynamic concept for eastern Mediterranean circulation and oxygenation during sapropel formation, Palaeogeography, Palaeoclimatology, Palaeoecology 190, 103-119.

Castradori, D., 1993. Calcareous nannofossils and the origin of eastern Mediterranean sapropels. Paleoceanography 8, 459-471.

Claussen, M., Brovkin, V., Ganopolski, A., Kubatski, C., Petoukhov, V., 1998. Modelling global terrestrial vegetation-climate interaction. Phil. Trans. Roy. Soc. London 353, 53-63.

Coplen, T.B., Kendall, C., Hopple, J., 1983. Comparison of stable isotope reference samples. Nature 302, 236-238.

Corselli, C., Principato, M.S., Maffioli, P., and Crudeli, D., 2002. Changes in planktonic assemblages during sapropel S5 deposition : Evidence from Urania Basin area, eastern Mediterranean. Paleoceanography 17(3), pp 1.1-1.30 (DOI 10.1029/2000PA000536)

Cramp, A., O'Sullivan, G., 1999. Neogene sapropels in the Mediterranean: a review. Marine Geology 153, 11-28.

Darling, K.F., Wade, C.M., Stewart, I.A., Kroon, D., Dingle, R., and Brown, A.J.L., 2000. Molecular evidence for genetic mixing of Arctic and Antarctic subpolar populations of planktonic foraminifers. Nature 405, 43-47.

De Lange, G.J., Middelburg, J.J., Van der Weijden, C.H., Catalano, G., Luther III, G.W., Hydes, D.J., Woittiez, J.R.W., Klinkhammer, G.P., 1990. Composition of anoxic hypersaline brines in the Tyro and Bannock Basin, eastern Mediterranean. Marine Chemistry 31, 63-88.

De Rijk, S., Rohling, E.J., Hayes, A., 1999. Onset of climatic deterioration in the eastern Mediterranean around 7 ky BP; micropalaeontological data from Mediterranean sapropel interruptions. Marine Geology 153, 337-343.

Deuser, W.G., Ross, E.H., 1989. Seasonally abundant planktonic foraminifera of the Sargasso Sea: succession, deep-water fluxes, isotopic compositions, and paleoceanographic implications. Journal of Foraminiferal Research, 19, 268-293.

Duplessy, J.C., Labeyrie, L., Juilet-Leclerc, A., Maître, F., Duprat, J., Sarnthein, M., 1991. Surface salinity reconstruction of the North Atlantic Ocean during the last glacial maximum. Oceanologica Acta 14, 311-324.

Emeis, K.-C., H.-M. Schulz, U. Struck, T. Sakamoto, H. Doose, H. Erlenkeuser, M. Howell, D. Kroon, M. Paterne, 1998. Stable isotope and temperature records of sapropels from ODP Sites 964 and 967: Constraining the physical environment of sapropel formation in the Eastern Mediterranean Sea. In: Robertson, A.H.F., Emeis, K.-C., Richter C., and Camerlenghi A. (Editors), Proc. ODP, Sci. Res., 160. Ocean Drilling Program, College Station, TX, pp. 309-331.

Emeis, K.-C., Struck, U., Schulz, H.-M., Bernasconi, S., Sakamoto, T. and Martinez-Ruiz, F., 2000. Temperature and salinity of Mediterranean Sea surface waters over the last 16,000 years: Constraints on the physical environment of S1 sapropel formation based on stable oxygen isotopes and alkenone unsaturation ratios. Palaeogeography, Palaeoclimatology, Palaeoecology, 158, 259-280.

Emeis, K.-C., Schulz, H., Struck, U., Rossignol-Strick, M., Erlenkeuser, H., Howell, M.W., Kroon, D., Mackensen, H., Ishizuka, S., Oba, T., Sakamoto, T., Koizumi, I., 2003 . Eastern Mediterranean surface water temperatures and $\delta^{18}O$ composition during deposition of sapropels in the late Quaternary. Paleoceanography, 18, DOI 10.1029/ 2000PA000617.

Fairbanks, R.G., Sverdlove, M., Free, R., Wiebe, P.H., Bé, A.W.H., 1982. Vertical distribution of living planktonic foraminifera from the Panama Basin. Nature 298, 841-844.

Fontugne, M.R., Calvert, S.E., 1992. Late Pleistocene variability of the organic carbon isotopic composition of organic matter in the eastern Mediterranean: monitor of changes in organic carbon sources and atmospheric CO_2 concentrations. *Paleoceanography 7*, 1-20.

Fontugne, M., Arnold, M., Labeyrie, L., Paterne, M., Calvert, S., Duplessy, J.C., 1994. Paleoenvironment, sapropel chronology, and Nile river discharge during the last 20,000 years as indicated by deep-sea sediment records in the eastern Mediterranean, Radiocarbon 34, 75-88.

Ganssen, G., Troelstra, S.R., 1987. Palaeoenvironmental changes from stable isotopes in planktonic foraminifera from Eastern Mediterranean Sapropels. Marine Geology 75, 221-230.

Garrett, C., Outerbridge, R., Thompson, K., 1993. Inter-annual variability in Mediterranean heat budget and buoyancy fluxes. Journal of Climatology 6, 900-910.

Gasse, F., 2000. Hydrological changes in the African tropics since the last glacial maximum, Quat. Sci. Rev. 19, 189-211.

Grossman, E.L., 1987. Stable isotopes in modern benthic foraminifera: a study of vital effect, J. Foram. Res., 17, 48-61.

Hassan, F.A., 1997. The dynamics of a riverine civilization: a geoarchaeological perspective on the Nile Valley, Egypt. World Archaeology 29, 51-74.

Hayes, A., Rohling, E.J., De Rijk, S., Kroon, D., Zachariasse, W.J., 1999. Mediterranean planktonic foraminifera faunas during the last glacial cycle. Marine Geology 153, 239-252.

Hayes, A., Kucera, M., Rohling, E., and Kallel, N., 2003. Foraminifer assemblage-based SST reconstruction using Artificial Neural Networks records distinct cooling events associated with the Mediterranean Holocene sapropel, Geophysical Research Abstracts, 5 (CD-ROM), EGS-EUG-AGU 28th assembly, Nice, Abstract P1393.

Hemleben, C., Meischner, D., Zahn, R., Almogi-Labin, A., Erlenkeuser, H., Hiller, B., 1996. Three hundred eighty thousand year long stable isotope and faunal records from the Red Sea: influence of global sea level change on hydrography. Paleoceanography 11, 147-156.

Hemleben, C., Spindler, M., Anderson, O.R., 1989. Modern Planktonic Foraminifera. Springer, New York, 363pp.

Hemleben, Ch., Spindler, M., 1983. Recent advances in research on living planktonic foraminifera. In: Reconstruction of marine paleoenvironments, Utrecht Micropaleontological Bulletin 30, 141-170.

Hoelzmann, P., Kruse, H.J., Rottinger, F., 2000. Precipitation estimates for the eastern Saharan palaeomonsoon based on a water balance model of the West Nubian palaeolake basin. Global and Planetary Change 26, 105–120

Jenkins, J.A., Williams D.F., 1984. Nile water as a cause of eastern Mediterranean sapropel formation; evidence for and against. Marine Micropaleontology 9, 521-534.

Jorissen, F.J., Asioli, A., Borsetti, A.M., Capotondi, L., De Visscher, J.P., Hilgen, F.J., Rohling, E.J., Van der Borg, K., Vergnaud-Grazzini, C., Zachariasse, W.J., 1993. Late Quaternary central Mediterranean biochronology. Marine Micropaleontology 21, 169-189.

Kallel, N., Paterne, M., Duplessy, J.C., Vergnaud-Grazzini, C., Pujol, C., Labeyrie, L., Arnold, M., Fontugne, M., Pierre, C., 1997a. Enhanced rainfall in the Mediterranean region during the last sapropel event. Oceanologica Acta 20, 697-712.

Kallel, N., Paterne, M., Labeyrie, L., Duplessy, J.C., Arnold, M., 1997b. Temperature and salinity records of the Tyrrhenian Sea during the last 18,000 years. Palaeogeography, Palaeoclimatology, Palaeoecology 135, 97-108.

Kim, S.T., O'Neil, J.R., 1997. Equilibrium and nonequilibrium oxygen isotope effects in synthetic calcites. Geochimica et Cosmochimica Acta 61, 3461-3475.

Kucera, M., and Darling, K.F., 2002. Cryptic species of planktonic foraminifera: their effect on palaeoceanographic reconstructions, Phil. Trans. Roy. Soc. London Ser. A – Math. Phys. Eng. Sci. 360, 695-718.

Labeyrie, L., Labracherie, M., Gorfti, N., Pichon, J.J., Vautravers, M., Arnold, M., Duplessy, J.C., Paterne, M., Michel, E., Duprat, J., Caralp, M., Turon, J.L., 1996. Hydrographic changes of the Southern ocean (southeast Indian sector) over the last 230 kyr. Paleoceanography 11, 57-76.

Maslin, M.A., Shackleton, N.J., Pflaumann, U., 1995. Surface water temperature, salinity, and density changes in the northeast Atlantic during the last 45,000 years: Heinrich events, deep water formation, and climatic rebounds. Paleoceanography 10, 527-544.

Maynard, K., Royer, J.F., Chauvin, F. Impact of greenhouse warming on the west African summer monsoon. Climate Dynamics (on-line number DOI 10.1007/s00382-002-0242-z).

McKenzie, J.A., 1993. Pluvial conditions in the eastern Sahara following the penultimate deglaciation: implications for changes in atmospheric circulation patterns with global warming. Palaeogeography, Palaeoclimatology, Palaeoecology 103, 95-105.

Mercone, D., Thomson, J., Croudace, I.W., Siani, G., Paterne, M., Troelstra, S., 2000. Duration of S1, the most recent sapropel in the eastern Mediterranean Sea, as indicated by accelerator mass spectrometry radiocarbon and geochemical evidence. Paleoceanography 15, 336-347.

Mercone, D., Thomson, J., Abu-Zied, R.H., Croudace, I.W., Rohling, E.J., 2001. High-resolution geochemical and micropalaeontological profiling of the most recent eastern Mediterranean sapropel. Marine Geology 177, 25-44.

Mielke, K.M., 2001. Reconstructing surface carbonate chemistry and temperature in palaeoceans: Geochemical results from Laboratory experiments and the fossil record, M.Sc. thesis, University California Davis, Davis CA, 166pp.

Müller, P.J., Kirst, G., Ruhland, G., von Storch, I., Rosell-Mélé, A., 1998. Calibration of the alkenone paleotemperature index UK'37 based on core tops from the eastern South Atlantic and the global ocean (60°N-60°S). Geochim. Cosmochim. Acta, 62, 1757-1772.

Murat, A., 1984. Sequences et paleoenvironnements marins Quaternaires. Une marge active: l'arc Hellenique oriental, *Ph.D.(3^{ieme} cycle) dissertation, Univ. of Perpignan, France*: 280 pp.

Myers, P.G., Hayes, K., Rohling, E.J., 1998. Modelling the paleao-circulation of the Mediterranean: The Last Glacial Maximum and the Holocene with emphasis on the formation of sapropel S1. Paleoceanography 13, 586-606.

Myers, P.G., Rohling, E.J., 2000. Modelling a 200 year interruption of the Holocene sapropel S1. Quaternary Research 53, 98-104.

NASA, 1995. Wadi Kufra radar image P-45719 http://southport.jpl.nasa.gov/imagemaps/html/srl-wadik.html.

National Institute of Standards & Technology, 1992. Report of Investigation, Reference Materials 8543-8546.

Nof, D., 1981. On the dynamics of equatorial outflows with application to the Amazon's basin. Journal of Marine Research 39, 1-29.

O'Neil, J.R., Clayton, R.N., Mayeda, T.K., 1969. Oxygen isotope fractionation on divalent metal carbonates. Journal of Chemical Physics 51, 5547-5558.

Ortiz, J.D., Mix, A.C., Rugh, W., Watkins, J.M., Collier, R.W., 1996. Deep-dwelling planktonic foraminifera of the northeastern Pacific Ocean reveal environmental control of oxygen and carbon isotope disequilibria. Geochimica et Cosmochimica Acta 60, 4509-4523.

Pachur, H.J., 2001. Holozäne Klimawechsel in den nördlichen Subtropen. Nova Acta Leopoldina NF88 331, 109-131.

Pachur, H.J., Kröpelin, S., 1987. Wadi Howar: Paleoclimatic evidence from an extinct river system in the southeastern Sahara. Science 237, 298-301.

Palmer, M.R., Pearson, P.N., Cobb, S.J., 1998. Reconstructing past ocean pH-depth profiles. Science 282, 1468-1471.

Parisi, E., 1987. Carbon and Oxygen isotope composition of Globerinoides ruber in two deep sea cores from the Levantine Basin (eastern Mediterranean). Marine Geology 75, 201-219.

Pawlowski J., and Holzmann, M., 2002. Molecular phylogeny of Foraminifera - a review. European J. Protistology, 38, 1-10.

Pearson P.N., Palmer, M.R., 1999. Middle Eocene seawater pH and atmospheric carbon dioxide concentrations. Science 284, 1824-1826.

Pearson P.N., Palmer, M.R., 2000. Estimating Paleogene atmospheric pCO2 using boron isotope analysis of foraminifera. GFF 122, 127-128.

Peeters, F., 2000. The distribution and stable isotope composition of living planktic foraminifera in relation to seasonal changes in the Arabian Sea. PhD thesis Free University Amsterdam, NSG 20000104, 184 pp.

Pierre, C., 1999. The oxygen and carbon isotope distribution in the Meditteranean water masses. Marine Geology 153, 41-55.

POEM group, 1992. General circulation of the eastern Mediterranean. Earth-Science Reviews 32, 285-309.

Pujol, C., Vergnaud-Grazzini, C., 1989. Palaeoceanography of the last deglaciation in the Alboran Sea (western Mediterranean): Stable isotopes and planktonic foraminiferal records. Marine Micropaleontology 15, 153-179.

Pujol, C., Vergnaud-Grazzini, C., 1995. Distribution patterns of live planktic foraminifers as related to regional hydrography and productive systems of the Mediterranean Sea. Marine Micropaleontology 25, 187-217.

Ravelo, A.C. and Fairbanks, R.G., 1995. Carbon isotopic fractionation in multiple species of planktonic foraminifera from core-tops in the tropical Pacific, J. Foram. Res., 25, 53-74.

Reiss, Z., Halicz, E., Luz, B., 1999. Late-Holocene foraminifera from the SE Levantine Basin. Isr. J. Earth Sci. 48, 1-17.

Reynolds, L.A., Thunell, R.C., 1989. Seasonal succession of planktonic foraminifera: results from a four-year time-series sediment trap experiment in the northeast Pacific. Journal of Foraminiferal Research 19, 253-267.

Roether, W., Well., R., Oxygen consumption in the eastern Mediterranean, Deep-Sea Res. I, 48, 1535-1551.

Rohling, E.J., 1994. Review and new aspects concerning the formation of Mediterranean sapropels. Marine Geology 122, 1-28.

Rohling, E.J., 1999. Environmental controls on salinity and δ18O in the Mediterranean. Paleoceanography 14, 706-715.

Rohling, E.J., 2000. Paleosalinity: confidence limits and future applications. Marine Geology 163, 1-11.

Rohling, E.J., Bigg, G.R., 1998. Paleosalinity and delta18O: a critical assessment. Journal of Geophysical Research 103, 1307-1318.

Rohling, E.J., Cooke, S., 1999. Stable oxygen and carbon isotope ratios in foraminiferal carbonate, in: Sen Gupta, B.K. (ed.), Modern Foraminifera. Kluwer Academic, Dordrecht, The Netherlands, pp.239-258.

Rohling, E.J., De Rijk, S., 1999. The Holocene Climate Optimum and Last Glacial Maximum in the Mediterranean: the marine oxygen isotope record. Marine Geology 153, 57-75.

Rohling, E.J., Gieskes, W.W.C., 1989. Late Quaternary changes in Mediterranean Intermediate Water density and formation rate. Paleoceanography 4, 531-545.

Rohling, E.J., Hilgen, F.J., 1991. The eastern Mediterranean climate at times of sapropel formation: a review. Geologie en Mijnbouw 70, 253-264.

Rohling, E.J., Cane, T.R., Cooke, S., Sprovieri, M., Bouloubassi, I., Emeis, K.C., Schiebel, R., Kroon, D., Jorissen, F.J., Lorre, A., Kemp, A.E.S., 2002. African monsoon variability during the previous interglacial maximum, Earth Planet. Sci. Lett., 202, 61-75.

Rohling, E.J., De Rijk, S., Myers, P., and Haines, K., 2000 Traditional palaeoceanography and numerical modelling : the Mediterranean Sea at times of sapropel formation, in Hart, M.B. (ed.) "Climates: Past and Present", Geol. Soc. Spec. Publ., 181, 135-149.

Rohling, E.J., Den Dulk, M., Pujol, C., Vergnaud-Grazzini, C., 1995. Abrupt hydrographic change in the Alboran Sea (western Mediterranean) around 8000 yrs BP, Deep-Sea Research 42, 1609-1619.

Rohling, E.J., Jorissen F.J., De Stigter, H.C., 1997. 200 year interruption of Holocene sapropel formation in the Adriatic Sea. Journal of Micropaleontology 16, 97-108.

Rohling, E.J., Jorissen, F.J., Vergnaud-Grazzini, C., Zachariasse, W.J., 1993. Northern Levantine and Adriatic Quaternary planktic foraminifera: reconstruction of paleoenvironmental gradients. Marine Micropaleontology 21, 191-218.

Rosell-Melé, A., Bard, E., Emeis, K.-C., Grimalt, J.O., Müller, P., Schneider, R., Bouloubassi, I., Epstein, B., Fahl, K., Fluegge, A., Freeman, K., Goni, M., Gütner, U., Hartz, D., Hellebust, S., Herbert, T., Ikehara, M., Ishiwatari, R., Kawamura, K., Kenig, F., de Leeuw, J., Lehman, S., Mejanelle, L., Ohkouchi, N., Pancost, R., D. Pelejero, C., Prahl, F., Quinn, J., Rontani, J.-F., Rostek, F., Rullkötter, J., Sachs, J., Blanz, T., Sawada, K., Schulz-Bull, D., Sikes, E., Sonzoni, C., Ternois, Y., Versteegh, G., Volkman, J., Wakeham S., 2001. Precision of the current methods to measure the proxy Uk'37 and absolute abundance in sediments: Results of an inter-laboratory comparison study. Geochem. Geophys. Geosyst., (G3), 2, paper number 2000GC000141.

Rossignol-Strick, M., 1983. African monsoons, an immediate climatic response to orbital insolation. Nature 304, 46-49.

Rossignol-Strick, M., 1985. Mediterranean Quaternary sapropels, an immediate response to the African monsoon to variation of insolation. Palaeogeography, Palaeoclimatology, Palaeoecology 49, 237-263.

Rossignol-Strick, M., 1987. Rainy periods and bottom water stagnation initiating brine concentrations, 1: The late Quaternary. Paleoceanography 2, 330-360.

Rossignol-Strick, M., Nesteroff, W., Olive, P., Vergnaud-Grazzini, C., 1982. After the deluge: Mediterranean stagnation and sapropel formation. Nature 295, 105-110.

Rostek, F., Ruhland, G., Bassinot, F.C., Müller, P.J., Labeyrie, L., Lancelot, Y., Bard, E., 1993. Reconstructing sea surface temperature and salinity using $\delta^{18}O$ and alkenone records. Nature 364, 319-321.

Rozanski, K., 1985. Deuterium and oxygen-18 in European groundwaters – links to atmospheric circulation in the past, Chem. Geol. (Isot. Geosc. Sect.) 52, 349-363.

Ryther, J.H., Menzel, D.W., Corwin, N., 1967. Influence of the Amazon River Outflow on the ecology of the western tropical Atlantic I. Hydrography and Nutrient Chemistry. Journal of Marine Research 25, 69-83.

Schiebel, R., Hemleben, Ch., 2000. Interannual variability of planktic foraminiferal populations and test flux in the eastern North Atlantic Ocean (JGOFS). Deep-Sea Research II, 47, 1809-1852.

Schiebel, R., Waniek, J., Bork, M. and Hemleben, Ch., 2001. Planktic foraminiferal production stimulated by chlorophyll redistribution and entrainment of nutrients. Deep-Sea Research I, 48, 721-740.

Schiebel, R., Waniek, J., Zeltner, A., Alves, M., 2002. Impact of the Azores Front on the distribution of planktic foraminifers, shelled gastropods, and coccolithophorids. Deep-Sea Research II 49, 4035-4050.

Schmidt, G.A., 1999a. Error analysis of paleosalinity calculations. Paleoceanography 14, 422-429.

Schmidt, G.A., 1999b. Forward modelling of carbonate proxy data from planktonic foraminifera using oxygen isotope tracers in a global ocean model. Paleoceanography 14, 482-497.

Schmuker, B., 2000. Recent Planktonic foraminifera in the Caribbean Sea: distribution, ecology and taphonomy, Diss. ETH 13559, Zürich, Switzerland, 167 pp.

Schmuker, B. Schiebel, R., 2002 . Planktic foraminifers and hydrography of the eastern and northern Caribbean Sea. Marine Micropaleontology 46, 387-403.

Simstich, J., Sarnthein, M., and Erlenkeuser, H., 2003. Paired $\delta^{18}O$ signals of *Neogloboquadrina pachyderma* (s) and *Turborotalita quinqueloba* show thermal stratification structure in Nordic Seas. Marine Micropaleontology 48, 107-125.

Sonntag, C., Klitzsch, E., Löhnert, E.P., El Shazly, E.M., Münnich, K.O., Junghans, Ch., Thorweihe, U., Weistroffer, K., Swailem, F.M., 1979. Paleoclimatic information from deuterium and oxygen-18 in carbon-14-dated north Saharan groundwaters. In: Isotope Hydrology 1978, Vol. II, Int. At. Energy Agency, Vienna, pp. 569-580.

Spero, H.J., 1992. Do planktic foraminifera accurately record shifts in the carbon isotopic composition of sea water ΣCO_2 ? Mar. Micropaleontol., 19, 275-285.

Spero, H.J, and Lea, D.W., 1993. Intraspecific stable isotope variability in the planktic foraminifera *Globigerinoides sacculifer*: results from laboratory experiments, Mar. Micropaleontol., 22, 221-234.

Spero, H.J., and Williams, D.F., 1988. Extracting environmental information from planktonic foraminiferal $\delta^{13}C$ data. Nature 335. 717-719.

Spero, H.J., Lerche, I., and Williams, D.F., 1991. Opening the carbon isotope "vital effect" black box, 2, quantitative model for interpreting foraminiferal carbon isotope data, Paleoceanography, 6, 639-655.

Spero, H.J. Mielke, K.M., Kalve, E.M., Lea, D.W., Pak, D.K., 2003. Multi-species approach to reconstructing Eastern Equatorial Pacific thermocline hydrography during the past 360ky. Paleoceanography, 18, DOI 10.1029/ 2002PA000814.

Stanev, E.V., Friedrich, H.J., Botev, S.V., 1989. On the seasonal response of intermediate and deep water to surface forcing in the Mediterranean Sea. Oceanologica Acta 12, 141-149.

Stanley, D.J., Maldonado, A., 1979. Levantine Sea-Nile Cone lithostratigraphic evolution: quantitative analysis and correlation with paleoclimatic and eustatic oscillations in the Late Quaternary. Sedimentary Geology 23, 37-65.

Stewart, I.A., Darling, K.F., Kroon, D., Wade, C.M., and Troelstra S.R., 2001. Genotypic variability in subarctic Atlantic planktic foraminifera, Mar. Micropaleontol., 43, 143-153.

Struck, U., Emeis, K.C., Voss, M., Krom, M.D., Rau, G.H., 2001. Biological productivity during sapropel S5 formation in the Eastern Mediterranean Sea: Evidence from stable isotopes of nitrogen and carbon. Geochimica et Cosmochimica Acta 65, 3249–3266.

Tang, C.M., Stott, L.D., 1993. Seasonal salinity changes during Meditteranean sapropel deposition 9000 years B.P.: evidence from isotopic analyses of individual planktonic foraminifera. Paleoceanography 8, 473-493.

Thomson, J., Higgs, N.C., Wilson, T.R.S., Croudace, I.W., De Lange, G.J., Van Santvoort, P.J.M., 1995. Redistribution and geochemical behaviour of redox-sensitive elements around S1, the most recent eastern Mediterranean sapropel. Geochimica et Cosmochimica Acta 59, 3487-3501.

Thunell, R.C., Reynolds, L.A., 1984. Sedimentation of planktonic foraminifera: seasonal changes in species flux in the Panama Basin. Micropaleontology 30 243-262.

Thunell, R.C., 1978. Distribution of recent planktonic foraminifera in surface sediments of the Mediterranean Sea. Marine Micropaleontology 3, 147-173.

Thunell, R.C., Williams, D.F., 1989. Glacial-Holocene salinity changes in the Mediterranean Sea: hydrographic and depositional effects. Nature 338, 493-496.

Troelstra, S.R., Ganssen, G.M., Van der Borg, K., De Jong, A.F.M., 1991. A Late Quaternary stratigraphic framework for eastern Mediterranean sapropel S1 based on AMS 14C dates and stable isotopes. Radiocarbon 33, 15-21.

Ufkes, E., Jansen, J.H.F., Brummer, G.J.A., 1998.

Tables 1-4

Table 1. Schematic presentation of $\delta^{18}O$ and $\delta^{13}C$ trends expected in equilibrium calcite precipitated within the various Mediterranean surface to intermediate water masses, as discussed in the text, along with their expected variability (more dots = higher variability).

	$\delta^{18}O$	$\delta^{18}O$ variability	$\delta^{13}C$	$\delta^{13}C$ variability
Fresh top-layer/lenses	– –	●●●●	– to o	●●●
Summer mixed layer	–	●●●	o to ++	●
Summer subthermocline	+	●●	– to – –	●●
Winter mixed layer	+	●●	– to +	●
Intermediate water	++	●	– – –	●●●

Table 2a. Reported deviations from $\delta^{18}O$ of *G. ruber* or $\delta^{18}O_{equilibrium\ calcite}$. For *G. ruber*, the deviation given is relative to equilibrium, which is dependent on temperature according to $T(°C) = 1.49 - 4.8(\delta^{18}O_{ruber} - \delta^{18}O_{equilibrium\ calcite})$ (Requires local calibration (Spero et al, 2003)).

Species	Temperature (°C)			Source	Location
	15.0	20.0	25.0		
G. ruber	-0.02	-1.06	-2.10	Spero et al, 2003	Culture
Deviations from $\delta^{18}O_{G.\ ruber}$ (values shown are $\delta^{18}O_{species} - \delta^{18}O_{ruber}$ vpdb)					
G. sacculifer† (>650μm)	-0.51	-0.35	-0.19	Spero et al, 2003	Culture
G. menardii	0.00	0.07	0.13	Mielke, 2001	Culture
N. dutertrei	-0.61	-0.38	-0.05	Bouvier-Soumagnac and Duplessy, 1985	Plankton tow in Indian Ocean
G. bulloides (11 chambered)	-0.45	-0.40	-0.34	Bemis et al, 1998	Culture
G. bulloides (12 chambered)	-0.35	-0.33	-0.31		
G. bulloides (13 chambered)	-0.27	-0.28	-0.29		
O. universa (low light)	0.33	0.33	0.33		
O. universa (high light)	0.00	0.00	0.00		
N. pachyderma	0.40	0.62	0.84	von Langen et al, 2000	Culture
Deviations from $\delta^{18}O_{equilibrium\ calcite}$ for deep dwelling species at ~6°C					
G. scitula	-0.4			Ortiz et al, 1996	Plankton tow in northeastern Pacific
G. hexagona	-0.4			Ortiz et al, 1996	Plankton tow in northeastern Pacific
N. pachyderma (s)**	-1			Bauch et al, 1997	Plankton tow in Arctic Ocean
N. pachyderma (s)**	-0.9 to –1.0			Simstich et al., 2003	Plankton tow in Nordic Seas
N. pachyderma (s)**	-0.7			Ortiz et al, 1996	Plankton tow in northeastern Pacific
*G. calida***	-0.6			Ortiz et al, 1996	Plankton tow in northeastern Pacific
Deviations from $\delta^{18}O_{equilibrium\ calcite}$ from a plankton tow near Bermuda††					
	Mean	St. Dev.			
G. ruber (white)	-2.03	0.70		(Williams et al, 1981)	Plankton tow near Bermuda
G ruber (pink)	-2.28	0.19			
G. conglobatus	-2.03	0.16			
G. siphonifera	-0.55	0.76			
G. truncatulinoides	-1.04	0.17			
*G. hirsuta****	-1.05	0.01			

† Deviation dependent on test size and on light influence. Individuals taken from 250-350μm fraction are offset by ~0.3‰ (Spero et al, 2003).

** Relative to dwelling depth (may calcify at shallower depths (Ortiz et al, 1996)).

†† Size (140–510μm) and temperature (27.6–19.4°C) are variable (Williams et al, 1981).

*** Only two data points are available for *G. hirsuta*

Table 2b. Deviation from $\delta^{13}C_{DIC}$ varies as a function of the equation: $\delta^{13}C_{DIC} = \delta^{13}C_s + \Delta\delta^{13}C_o Q_{10}^{(T-To)/10}$ where Q_{10} is the change in metabolic rate over a change of 10°C (not constant over broad temperature changes and requires local calibration) (Ortiz et al, 1996).

Species	Deviation from DIC	Source	Location
G. ruber	+0.94	Bemis et al, 1998	Culture
G. sacculifer (>650μm)	-0.73	Spero et al, 2003	Culture
G. sacculifer (250-350mm)	+0.19		
G. menardii	0.00	Mielke, 2001	Culture
N. dutertrei	-0.50	Bouvier-Soumagnac and Duplessy, 1985	Plankton tow in Indian Ocean
G. bulloides†	-3.65	Bemis et al, 2000	Culture
O. universa (low light)	-1.20	Bemis et al, 1998	Culture
O. universa (high light)	-0.30	Bemis et al, 1998	Culture
G. scitula	-1.1	Ortiz et al 1996	Plankton tow in northeastern Pacific
G. hexagona	-0.8	Ortiz et al 1996	Plankton tow in northeastern Pacific
N. pachyderma (sinistral)*	-0.75	Ortiz et al 1996	Plankton tow in northeastern Pacific
*G. calida**	-0.25	Ortiz et al 1996	Plankton tow in northeastern Pacific

† Dependent on size.

* Relative to dwelling depth (may calcify at shallower depths (Ortiz et al, 1996)).

Table 3. Model parameters used in the main run discussed in the present paper.

Plot depth (cm)	Interval	Monsoon intensification factor (M)	Mon-soon box	Interface shoaling[1]	T_s[2] °C	T_w[2] °C
39.71-29.37	Post S5	0	N	N	21.4	15.4
50.65-41.06	Upper 'lobe'	2	Y	Y	22.9	16.9
55.72-52.10	Interval	0	N	Y	23.4	17.4
60.64-57.00	Top lower lobe	3	Y	Y	22.7	16.7
62.92-61.03	Base lower lobe	3	Y	Y	21.0	15.0
74.24-63.29	Pre S5	0	N	N	19.1	13.1

(1) Concerns the intermediate to surface water interface. If shoaling is applied (periods of sapropel formation, see text), the total depth of the surface system in the model is set to 100m, versus 150m where no shoaling is applied.

(2) Temperatures derived from the mean values for the identified intervals in the alkenone SST record, as explained in the text

Table 4. Summary of the stable isotope ranges and variability within S5 for the various species analysed, and their inferred palaeohabitat based on the qualitative arguments in section 4.1. These inferred habltats are further assessed with a box-model (section 4.2.), and the endresults are compared with modern observations in Table 5.

	N	Mean $\delta^{18}O$	Variability[1]	Mean $\delta^{13}C$	Variability[1]	Inferred Habitat [2]
G. ruber (w)	45	-0.87	0.35 (0.57)	+0.07	0.18 (0.27)	Fresh-S.ml
G. ruber (p)	43	-1.32	0.33 (0.38)	+0.63	0.33 (0.37)	? Spring ?
G. sacculifer	27	-0.83	0.48 (0.49)	+1.10	0.24 (0.31)	S.ml
G. sacculifer (tril.)	26	-1.07	0.33 (0.50)	+1.24	0.24 (0.35)	S.ml
O. universa	47	+0.03	0.34 (0.41)	+1.23	0.21 (0.30)	S.ml
G. glutinata	30	-0.25	0.42 (0.50)	-0.71	0.43 (0.61)	Spring
G. bulloides	41	-0.23	0.62 (0.60)	-1.06	0.47 (0.51)	Spring
H. pelagica	15	-0.35	0.48 (0.62)	-0.79	0.24 (0.31)	
G. siphonifera	47	+0.67	0.32 (0.33)	-0.23	0.21 (0.21)	Winter ml
N. pachyderma (d)	17	+0.43	0.22 (0.39)	-1.41	0.31 (0.59)	Ssth / Int
G. scitula	18	+0.69	0.28 (0.38)	-1.50	0.19 (0.27)	(Ssth) / Int

[1] Non-bracketed values: mean of the 1σ values for the four key intervals within S5 (in effect a detrended variance estimate). Bracketed values: straight 1σ values through entire S5. A large offset between the two indicates underlying trends through S5.

[2] S.ml.= summer mixed layer; Spring = spring bloom conditions; Winter ml. = winter mixed layer; Ssth = summer subthermocline waters; Int. = intermediate water; Fresh-Sml = freshwater affected layer/lenses in the summer mixed layer.

Table 5. Comparison of modern observations with palaeohabitats inferred in the present study.

	Summary of modern habitat preferences within Mediterranean [a]	Additional observations outside Mediterranean	Inferred Mediterranean habitat during S5 [b]	Agreement Yes/No
G. ruber (white)	Upper 50 m (summer), less abundant also in upper 100 m (winter) [1].	Associated with freshwater dilution in Atlantic/Caribbean [2]	S.ml + lenses	Y
G. ruber (pink)	Very shallow (~20 m), with possible second peak just above summer thermocline [1]		? Spring or bimodal?	?N?
G. sacculifer	Not many found, but together with *trilobus* types [1]		S.ml	Y
G. sacculifer (*trilobus* type)	Summer mixed layer (20-50 m) [1]		S.ml	Y
O. universa	Summer mixed layer (to thermocline) [1]	Summer mixed layer down to thermocline [2]	S.ml	Y
G. glutinata	Rare, in winter conditions and to depths of 200 m (Mediterranean campaigns did not sample spring) [1].	N Atlantic: spring and fall dominance to considerable depth (~200 m) [3].	Spring	Y
G. bulloides	Mainly winter and early spring. Great depth range, from very shallow to mesopelagic [1]		Spring	~Y
G. siphonifera	Winter mixed layer, peaks at considerable depth [1]		Winter ml	Y
N. pachyderma (dextral)	Year-round, mesopelagic (50-200 m) [1]. Linked to density stratification and Deep Chlorophyll Maximum [4,5]		Ssth / Int	Y
G. scitula	Not known from the Mediterranean.	Lives deep in N Atlantic and Caribbean (>100 m) [2,3]	(Ssth) / Int	Y
G. inflata	Mainly winter, but year-round at frontal settings [1,4]		Winter ml [6]	Y

(a) Summary of of modern Mediterranean habitat observations based on late summer and winter plankton tows by Pujol and Vergnaud-Grazzini (1995) for entire Mediterranean. For species reported from the eastern Mediterranean specifically, most weight is given to their habitat descriptions in that basin. Where additional observations from other studies are included, the relevant reference is indicated with superscript numbering.

(b) S.ml.= summer mixed layer; Spring = spring bloom conditions; Winter ml. = winter mixed layer; Ssth = summer subthermocline waters; Int. = intermediate water; Sml + lenses = summer mixed layer with affinity for freshwater diluted conditions.

(1) Pujol and Vergnaud-Grazzini (1995)
(2) Schmuker, 2000; Schiebel et al. (2002)
(3) Schiebel and Hemleben, 2000
(4) Rohling et al. (1995)
(5) Rohling and Gieskes (1989)
(6) Derived in this study from the Late Glacial to Holocene record in core LC21 (Fig. 12).

Figure Captions

Figure 1. Summary plot of stable O isotope and alkenone SST records for the three S5 sapropels investigated. The scale of the SST records has been adjusted so that 1°C corresponds with 0.23‰ on the $\delta^{18}O$ scales (see text) (simplified after Rohling et al., 2002a). Development of stratigraphic relationship between the investigated sections and the presence of a small hiatus in S5 of ODP Hole 967C as summarised in the text and extensively discussed in Cane et al. (2002) and Rohling et al. (2002a).

Figure 2. Side-by-side plots of the $\delta^{18}O$ and $\delta^{13}C$ records (in ‰ VPDB) for the various planktic foraminiferal species analysed from S5 in core KS205. Means and standard deviations are shown for the various intervals through S5 identified in Table 2.

Figure 3. Schematic representation of the model used to calculate property changes in the various surface and intermediate water masses. *V* stands for volume, *T* for temperature, δ for $\delta^{18}O$, *S* for salinity, *E* for evaporation, *P* for precipitation (onto sea), *R* for runoff, *B* for Black Sea influence (treated in analogy the present, as part of *R*; cf. Rohling, 1999), and *Q* for the exchange fluxes through the Strait of Gibraltar. The model resolves for the residence time of water in the boxes, and iteratively solves the property changes for the appropriate (integer) number of years.

Figure 4. Comparison between the alkenone-based mean SST and seasonal range (red bars) used in the oxygen isotope model, and the annual mean (blue) and summer+winter SST (black) values obtained from the preliminary application of the Artificial Neural Network method for deriving Mediterranean SST (Hayes et al., 2003). ANN values reported with 1σ uncertainty limits.

Figure 5. Changes in the mean $\delta^{18}O$ and $\delta^{13}C$ values of the various species analysed for the intervals identified in Table 2 through sapropel S5 in core KS205, all plotted on the same scale. Grey band is the visible extent (dark colouration) of S5.

Figure 6. Comparison between the modelled traces of $\delta^{18}O$ for equilibrium calcite (see text) and the mean values of $\delta^{18}O$ of the various species in the key intervals through S5 in core KS205 (Table 2, Figure 2). All values in ‰ VPDB. The analytical series are simply shifted to obtain the best agreement in trends and absolute values (see text), and the inferred offsets are evaluated in comparison with observed offsets of the various species from isotopic equilibrium (section 4.3). Abbreviations: *mon* = monsoon box; *sml* = summer mixed layer; *ssth* = summer sub-thermocline layer; *wml* = winter mixed layer; ***int*** = intermediate water.

Figure 7. As Figure 5, but for the actual data rather than means+stdevs. The inferred offsets between analytical scales and equilibrium scales are kept exactly identical in Figures 5 and 6.

Figure 8. As Figure 5 and 6, but now for the data in S5 of ODP Holes 971A and 967C. The inferred offsets between analytical scales and equilibrium scales are again kept exactly identical to those in Figures 5 and 6.

Figure 9. Assessment of the S:$\delta^{18}O_{water}$ relationships in the main model run using z_{mon} = 5m and M = 3.0 (lower lobe) and 2.0 (upper lobe). The impacts of two scenarios are evaluated: (1) monsoon runoff $\delta^{18}O$ = –8‰ (top panels); and (2) monsoon runoff $\delta^{18}O$ = –10‰ (see text section 4.4).

Figure 10. As Figure 8, but here to investigate sensitivity to a change in model set-up, to z_{mon} = 1.5m, for M = 1.6 (lower lobe) and 1.2 (upper lobe) (see text section 4.5 for explanations).

Figure 11. Comparison between the modelled $\delta^{18}O$ traces through S5 for equilibrium calcite in the various surface and intermediate water boxes for main model run (left-hand panel; related to Figure 8) and the sensitivity test (right-hand panel; related to Figure 9). Abbreviations as in Figure 5.

Figure 12. Comparison between analytical $\delta^{18}O$ and $\delta^{13}C$ series for various foraminiferal species (in ‰ VPDB) through Holocene sapropel S1 in core LC21 from the SE Aegean Sea, and Eemian sapropel S5 from core KS205.

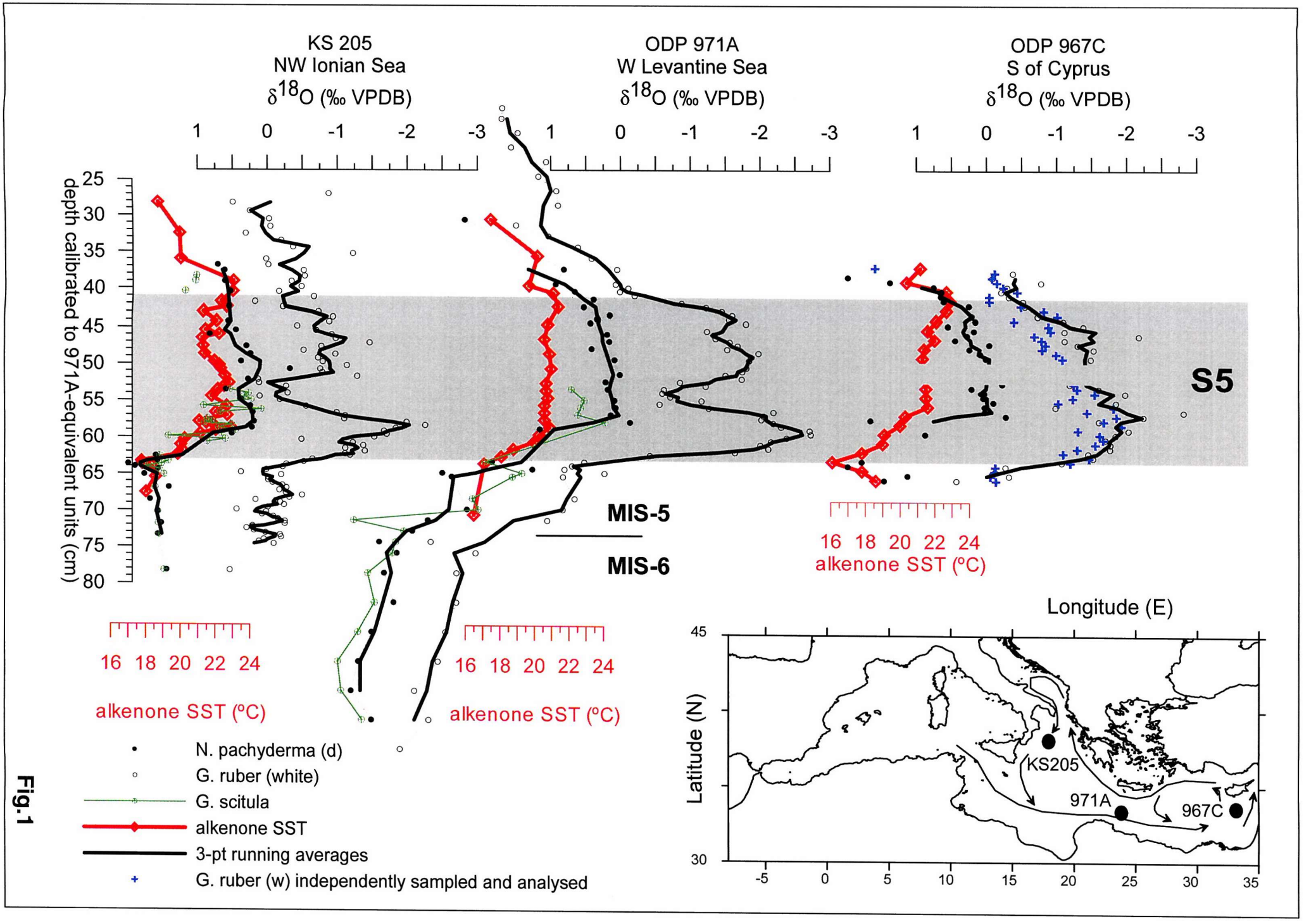
KS 205
NW Ionian Sea
δ18O (‰ VPDB)
ODP 971A
W Levantine Sea
δ18O (‰ VPDB)
ODP 967C
S of Cyprus
δ18O (‰ VPDB)
1 0 -1 -2 -3
depth calibrated to 971A-equivalent units (cm)
25 30 35 40 45 50 55 60 65 70 75 80
S5
MIS-5
MIS-6
16 18 20 22 24
alkenone SST (ºC)
Longitude (E)
Latitude (N)
45
30
-5 0 5 10 15 20 25 30 35
KS205
971A
967C
N. pachyderma (d)
G. ruber (white)
G. scitula
alkenone SST
3-pt running averages
G. ruber (w) independently sampled and analysed

Fig.1

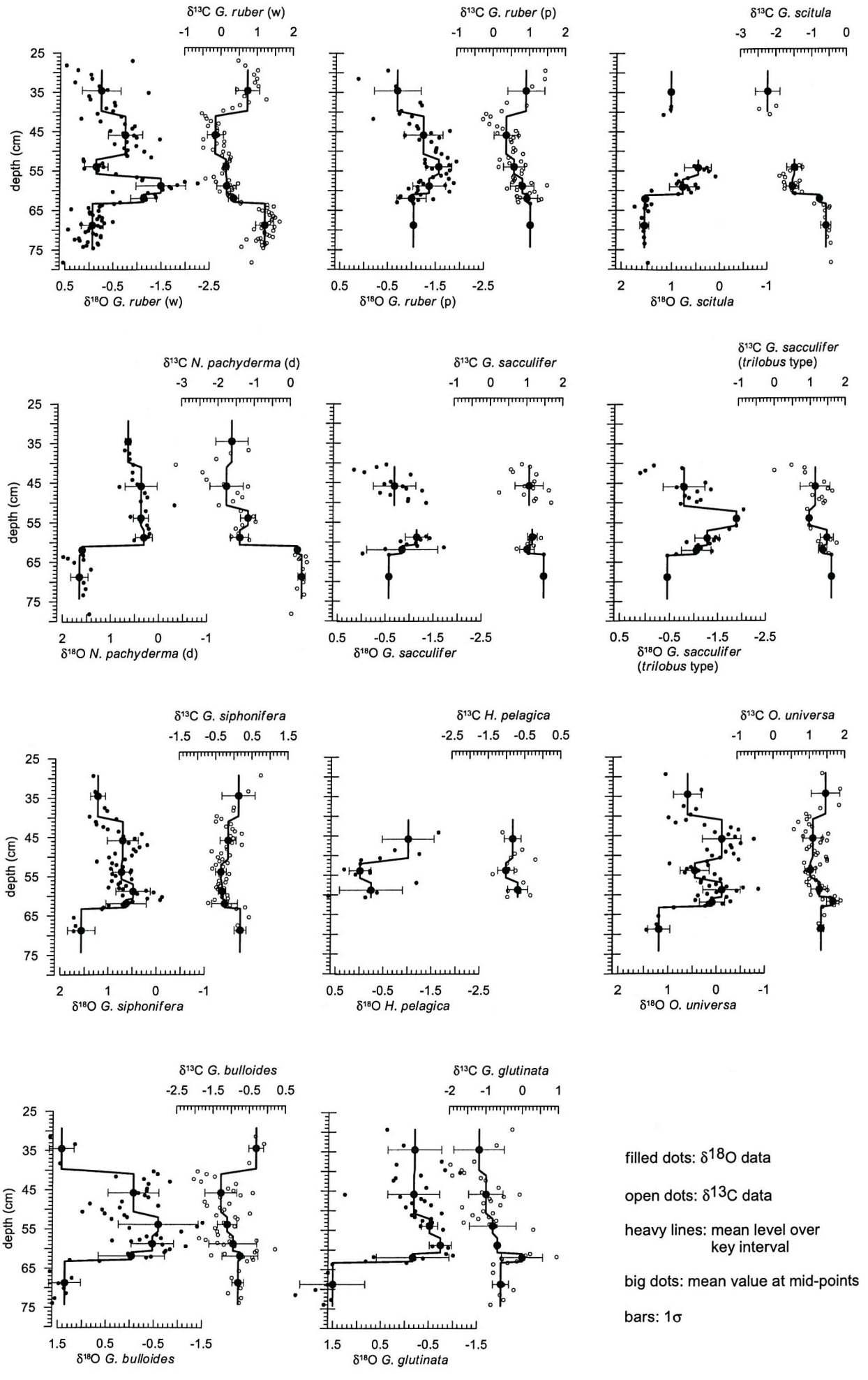
δ13C G. ruber (w)
δ18O G. ruber (w)
δ13C G. ruber (p)
δ18O G. ruber (p)
δ13C G. scitula
δ18O G. scitula
δ13C N. pachyderma (d)
δ18O N. pachyderma (d)
δ13C G. sacculifer
δ18O G. sacculifer
δ13C G. sacculifer (trilobus type)
δ18O G. sacculifer (trilobus type)
δ13C G. siphonifera
δ18O G. siphonifera
δ13C H. pelagica
δ18O H. pelagica
δ13C O. universa
δ18O O. universa
δ13C G. bulloides
δ18O G. bulloides
δ13C G. glutinata
δ18O G. glutinata
depth (cm)
filled dots: δ18O data
open dots: δ13C data
heavy lines: mean level over key interval
big dots: mean value at mid-points
bars: 1σ

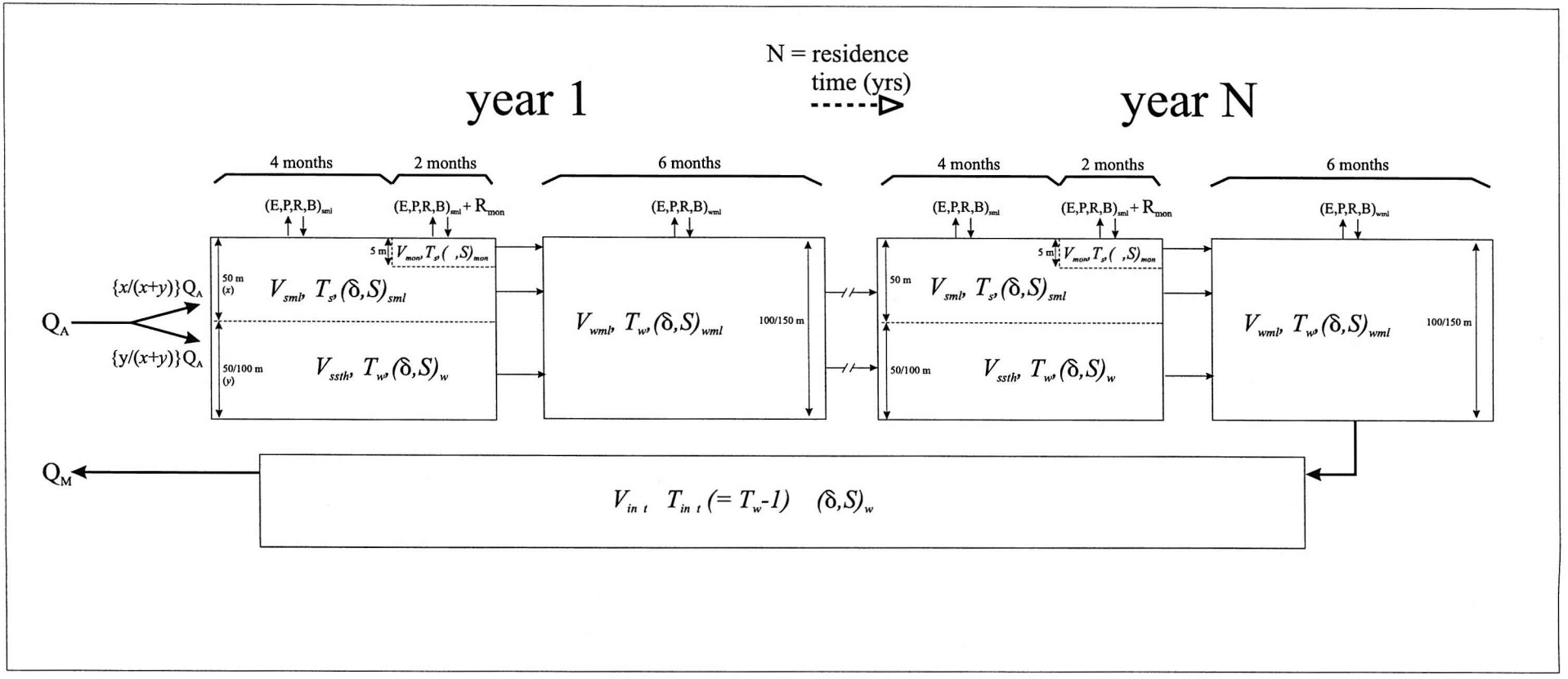
N = residence time (yrs)
year 1
year N
4 months
2 months
6 months
4 months
2 months
6 months
(E,P,R,B)sml
(E,P,R,B)sml + Rmon
(E,P,R,B)wml
(E,P,R,B)sml
(E,P,R,B)sml + Rmon
(E,P,R,B)wml
5 m
Vmon, Ts, (,S)mon
50 m (x)
Vsml, Ts, (δ,S)sml
50/100 m (y)
Vssth, Tw, (δ,S)w
Vwml, Tw, (δ,S)wml
100/150 m
{x/(x+y)}QA
{y/(x+y)}QA
QA
QM
Vin t, Tin t (= Tw-1) (δ,S)w

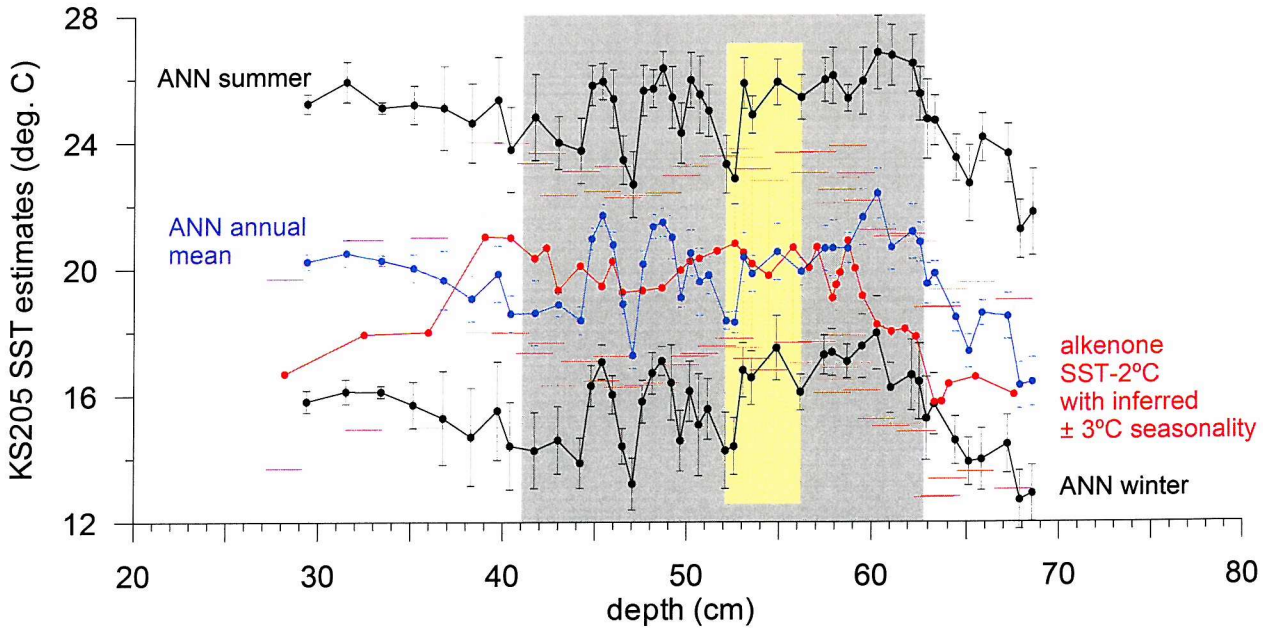
28
24
20
16
12
KS205 SST estimates (deg. C)
ANN summer
ANN annual
mean
alkenone
SST-2°C
with inferred
± 3°C seasonality
ANN winter
20
30
40
50
60
70
80
depth (cm)

Figure 4

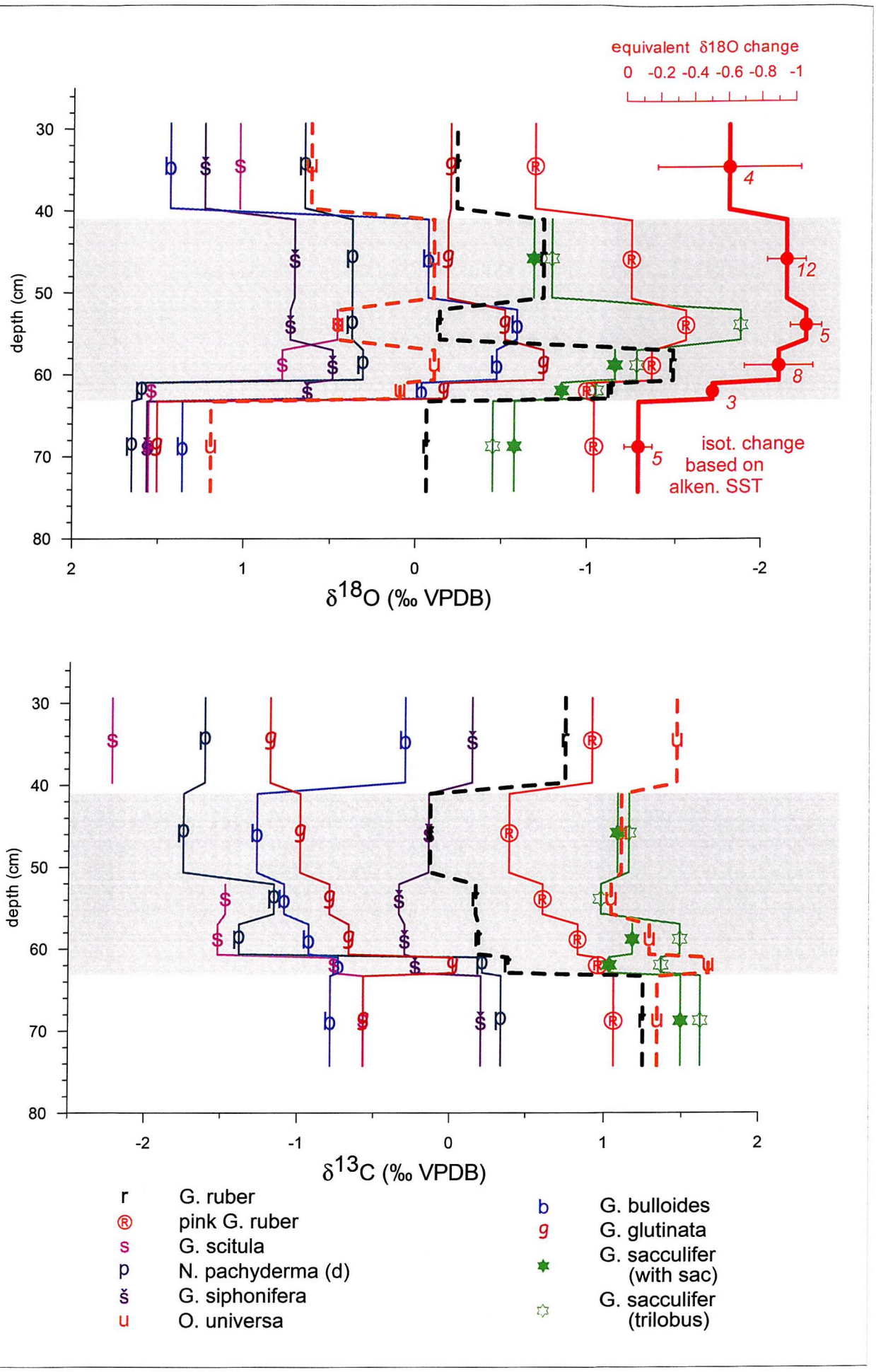
equivalent δ18O change
0 -0.2 -0.4 -0.6 -0.8 -1
depth (cm)
30
40
50
60
70
80
2
1
0
-1
-2
δ18O (‰ VPDB)
4
12
5
8
3
5
isot. change
based on
alken. SST
δ13C (‰ VPDB)
r G. ruber
® pink G. ruber
s G. scitula
p N. pachyderma (d)
š G. siphonifera
u O. universa
b G. bulloides
g G. glutinata
G. sacculifer (with sac)
G. sacculifer (trilobus)

Fig.5

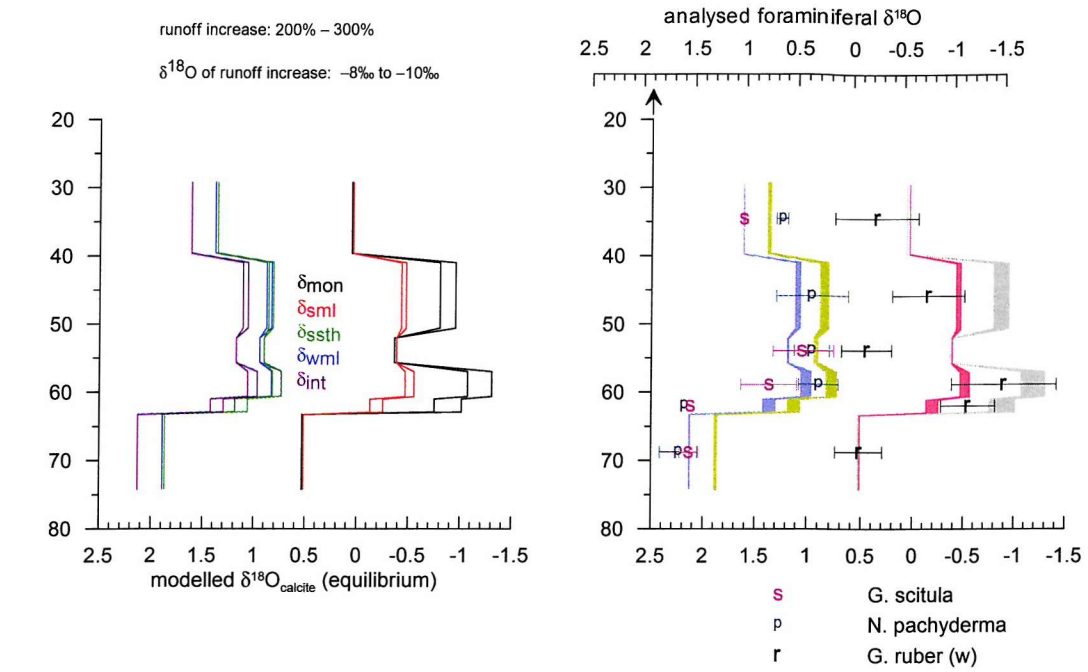
runoff increase: 200% – 300%
δ18O of runoff increase: –8‰ to –10‰
δmon
δsml
δssth
δwml
δint
modelled δ18Ocalcite (equilibrium)
analysed foraminiferal δ18O
s G. scitula
p N. pachyderma
r G. ruber (w)

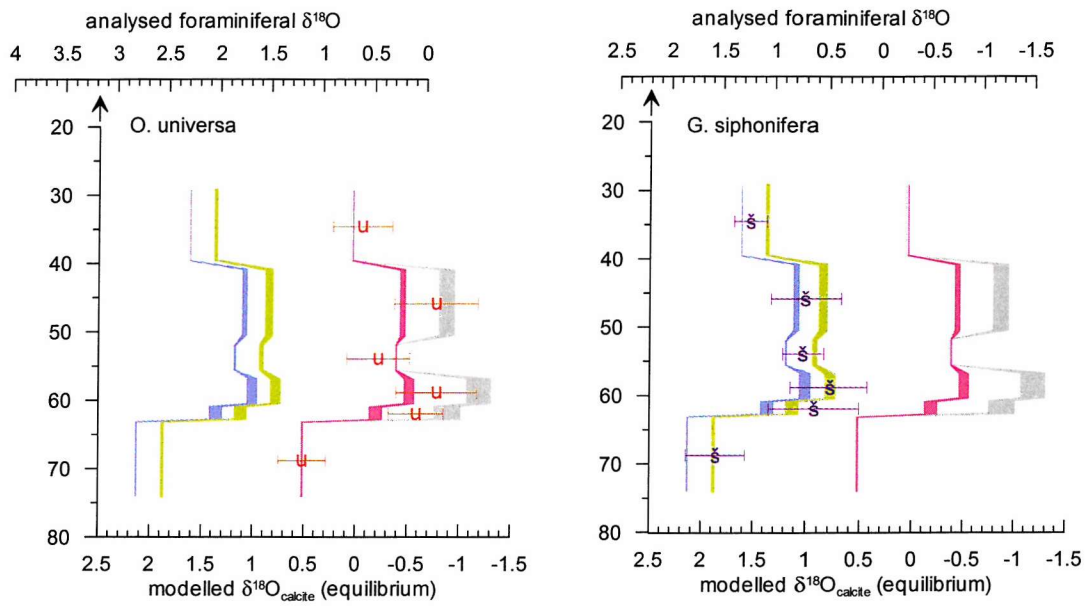
analysed foraminiferal δ18O
O. universa
G. siphonifera
modelled δ18Ocalcite (equilibrium)

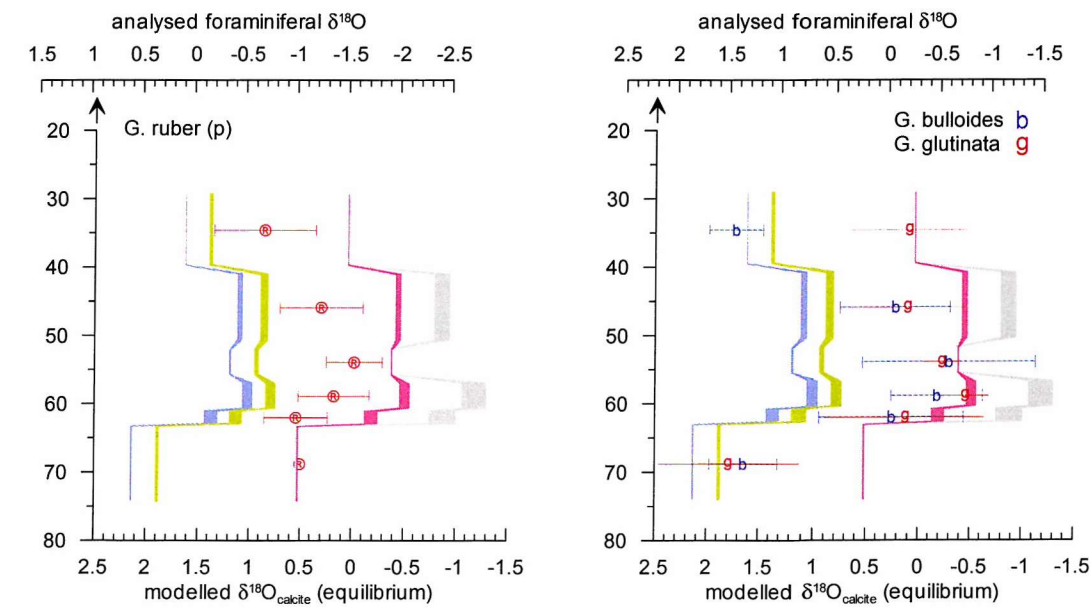
analysed foraminiferal δ18O
G. ruber (p)
G. bulloides b
G. glutinata g
modelled δ18Ocalcite (equilibrium)

Fig.6

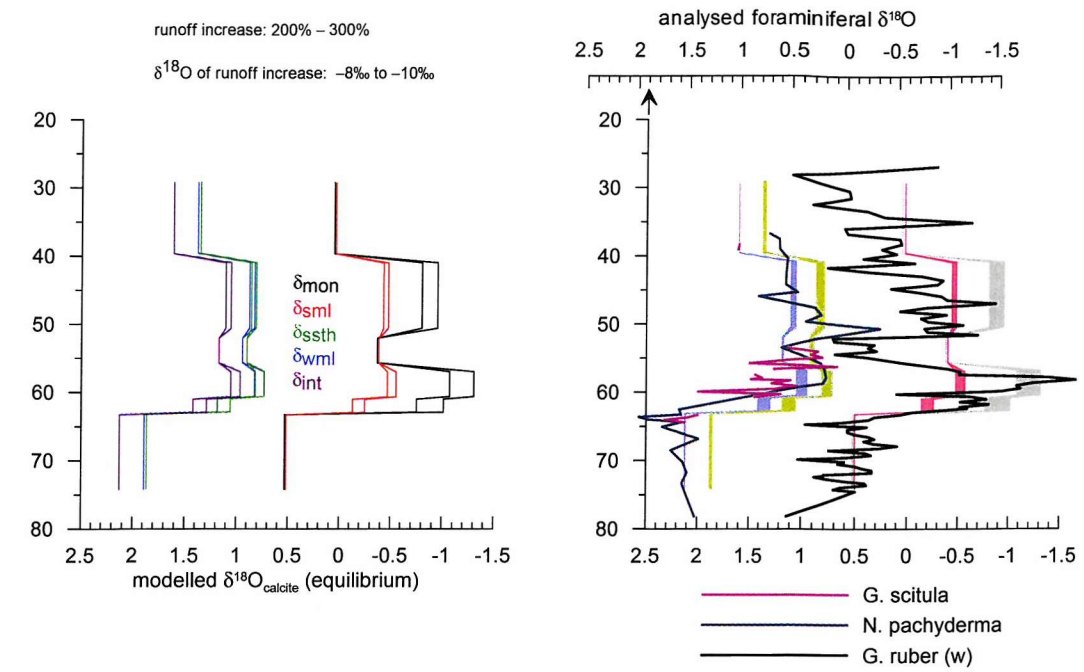
runoff increase: 200% – 300%
δ18O of runoff increase: –8‰ to –10‰
δmon
δsml
δssth
δwml
δint
modelled δ18Ocalcite (equilibrium)

analysed foraminiferal δ18O
G. scitula
N. pachyderma
G. ruber (w)

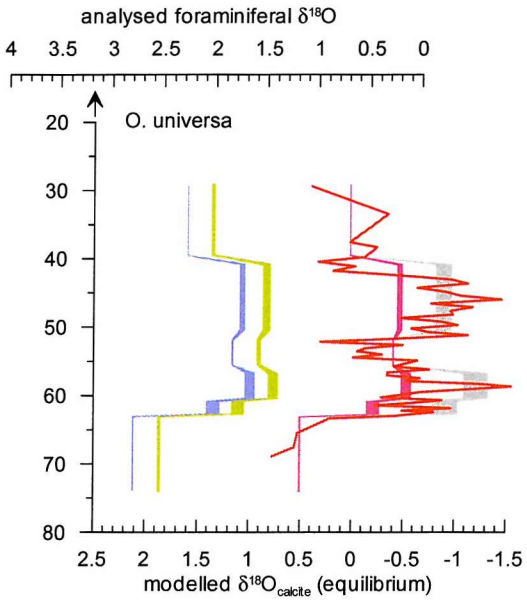
analysed foraminiferal δ18O
O. universa
modelled δ18Ocalcite (equilibrium)

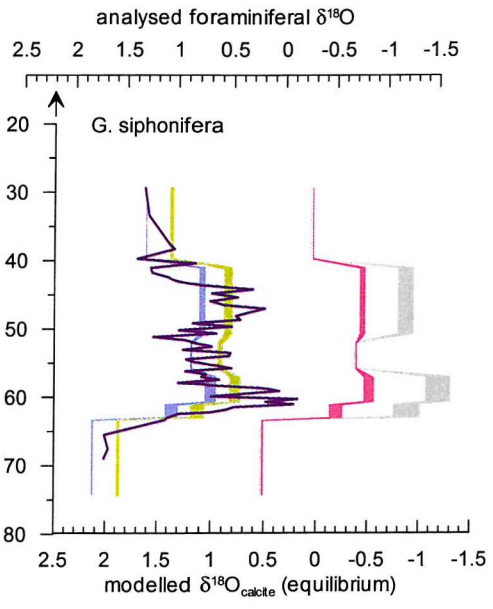
analysed foraminiferal δ18O
G. siphonifera
modelled δ18Ocalcite (equilibrium)

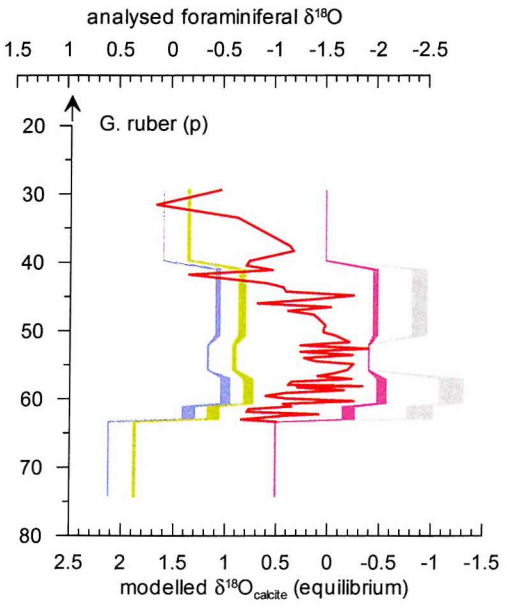
analysed foraminiferal δ18O
G. ruber (p)
modelled δ18Ocalcite (equilibrium)

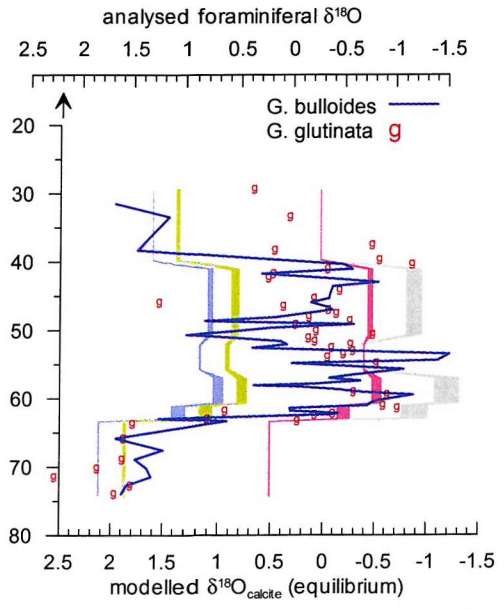
analysed foraminiferal δ18O
G. bulloides
G. glutinata
modelled δ18Ocalcite (equilibrium)

Fig.7

western Levantine core ODP 971A

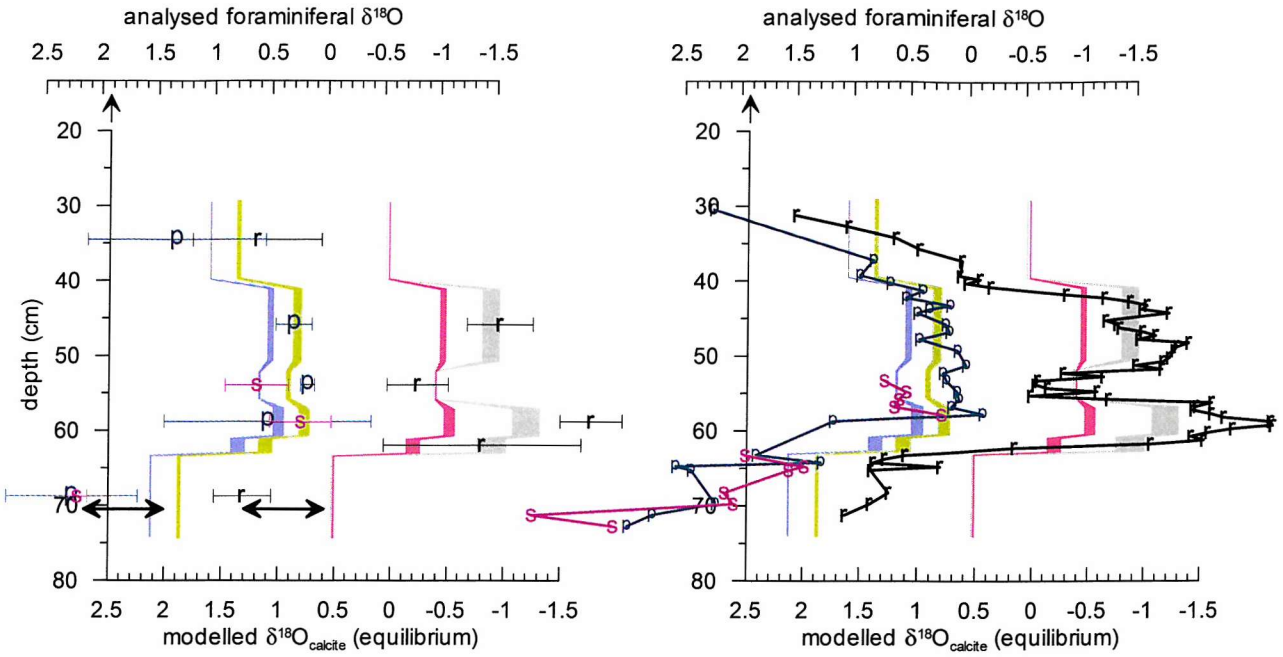

systematic offset before S5, relative to those intervals in KS205

s G. scitula
p N. pachyderma
r G. ruber (w)

eastern Levantine core ODP 967C

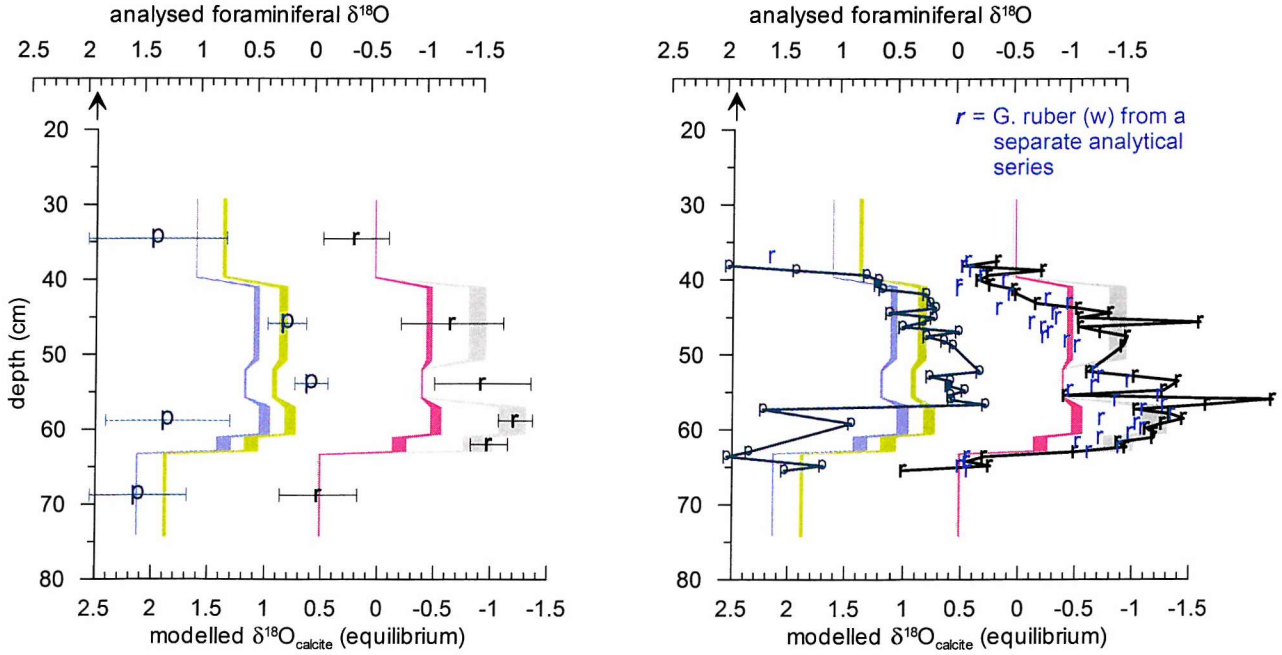

Fig.8

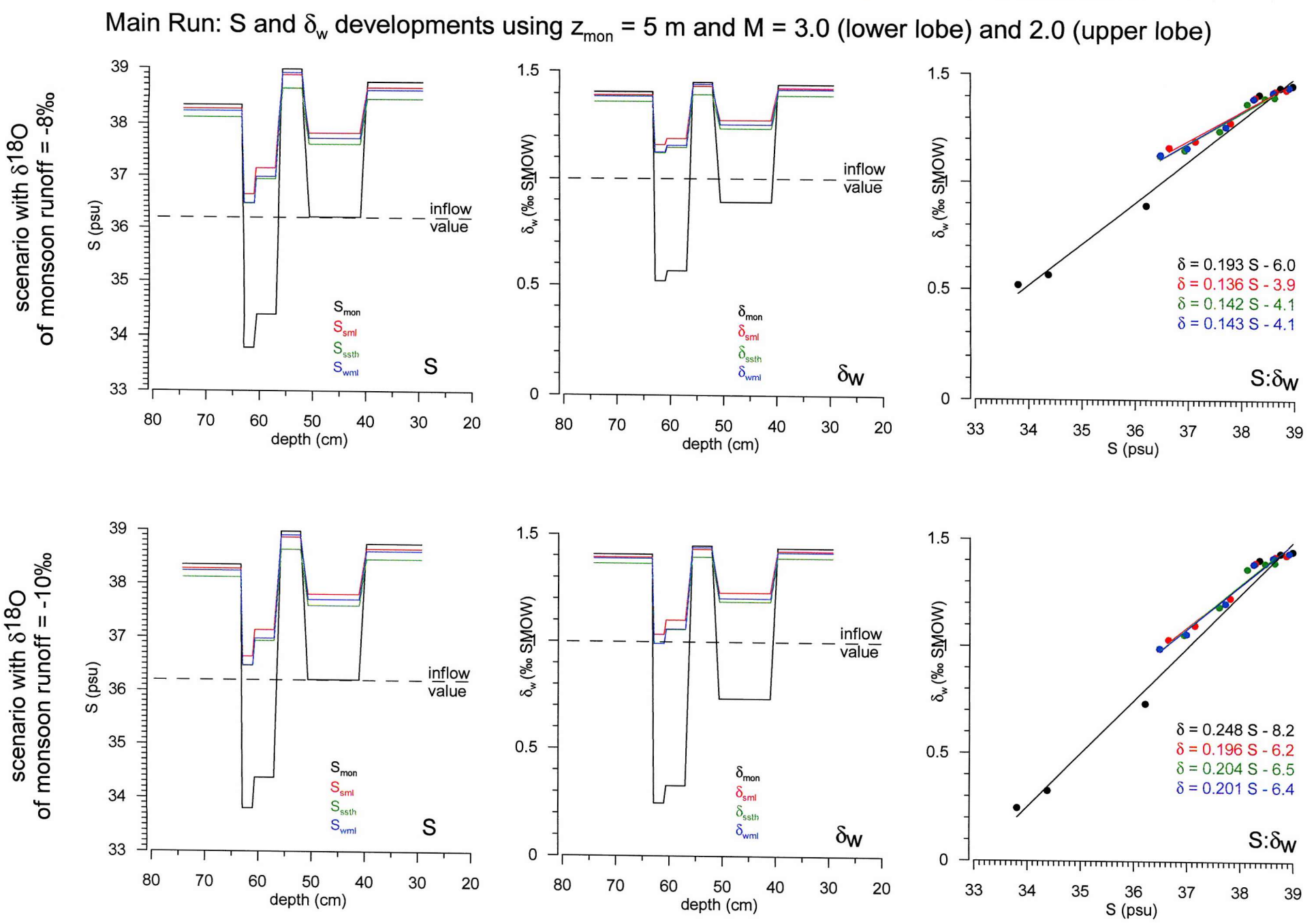
Main Run: S and δ_w developments using z_{mon} = 5 m and M = 3.0 (lower lobe) and 2.0 (upper lobe)
scenario with $\delta^{18}O$ of monsoon runoff = -8‰
scenario with $\delta^{18}O$ of monsoon runoff = -10‰
S (psu)
depth (cm)
inflow value
S_{mon}
S_{sml}
S_{ssth}
S_{wml}
S
δ_w (‰ SMOW)
δ_{mon}
δ_{sml}
δ_{ssth}
δ_{wml}
δ_w
S (psu)
δ = 0.193 S - 6.0
δ = 0.136 S - 3.9
δ = 0.142 S - 4.1
δ = 0.143 S - 4.1
S:δ_w
δ = 0.248 S - 8.2
δ = 0.196 S - 6.2
δ = 0.204 S - 6.5
δ = 0.201 S - 6.4
S:δ_w

Fig.9

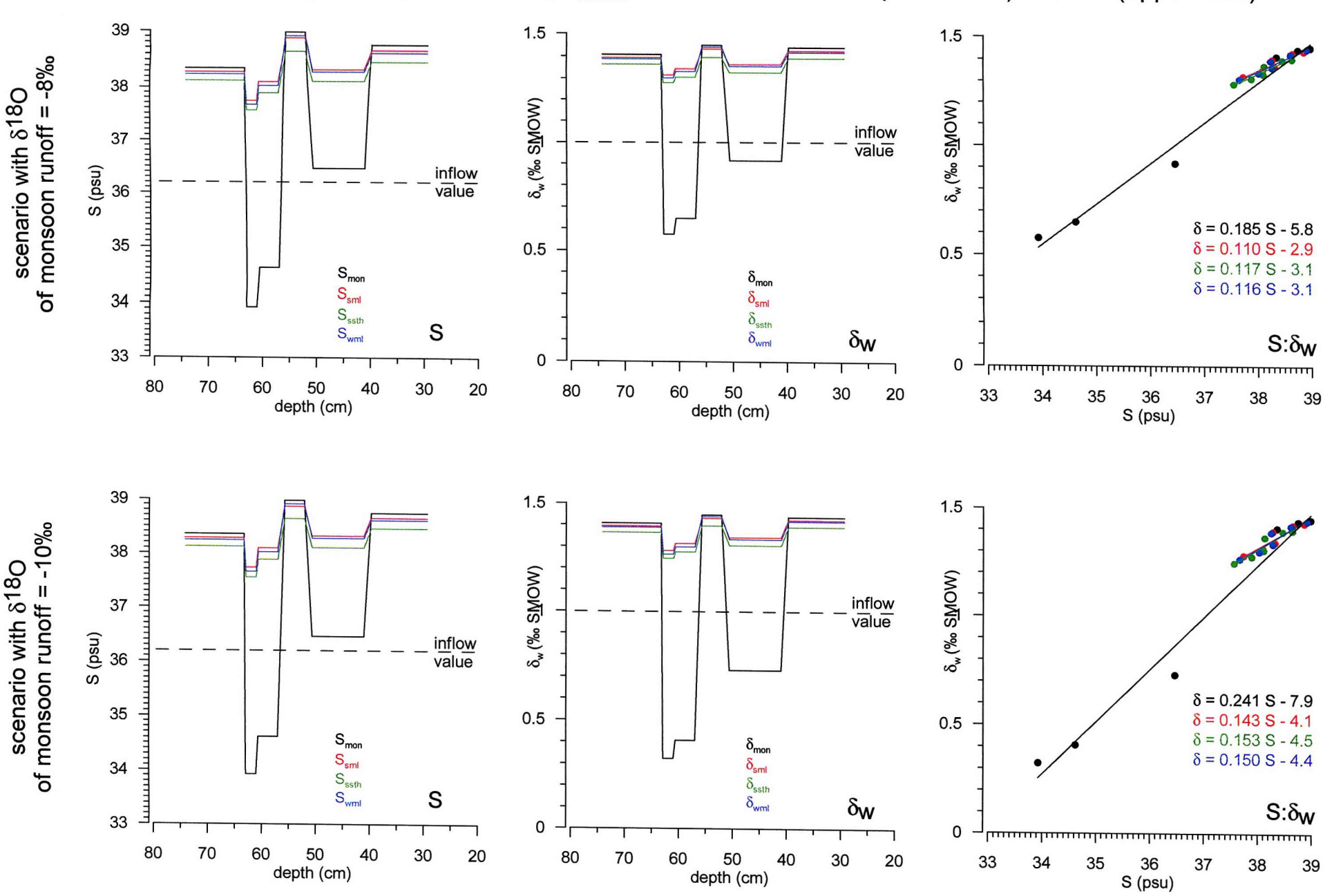
S and δ_w developments using z_{mon} = 1.5 m and M = 1.6 (lower lobe) and 1.2 (upper lobe)
scenario with $\delta^{18}O$ of monsoon runoff = -8‰
scenario with $\delta^{18}O$ of monsoon runoff = -10‰
S (psu)
depth (cm)
inflow value
S_{mon}
S_{sml}
S_{ssth}
S_{wml}
S
δ_w (‰ SMOW)
δ_{mon}
δ_{sml}
δ_{ssth}
δ_{wml}
δ_w
S (psu)
δ = 0.185 S - 5.8
δ = 0.110 S - 2.9
δ = 0.117 S - 3.1
δ = 0.116 S - 3.1
S:δ_w
δ = 0.241 S - 7.9
δ = 0.143 S - 4.1
δ = 0.153 S - 4.5
δ = 0.150 S - 4.4
S:δ_w

Fig.10

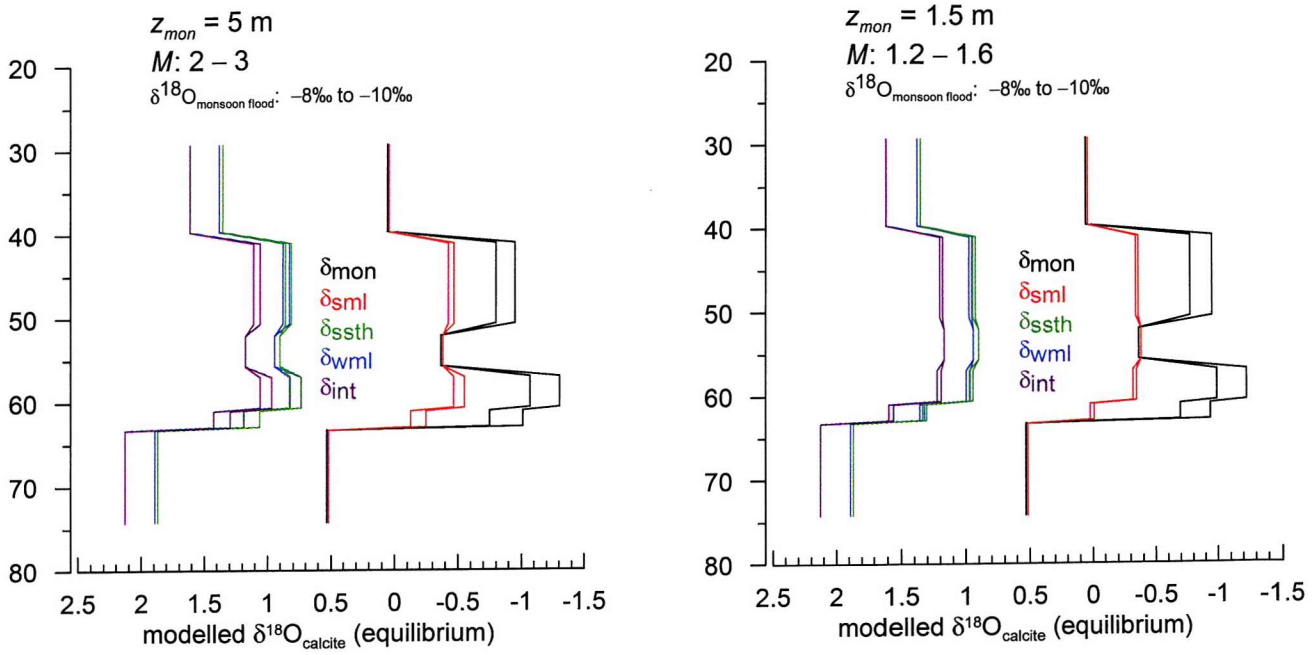
z_{mon} = 5 m
M: 2 – 3
$\delta^{18}O_{monsoon\ flood}$: –8‰ to –10‰
δmon
δsml
δssth
δwml
δint
20
30
40
50
60
70
80
2.5
2
1.5
1
0.5
0
-0.5
-1
-1.5
modelled $\delta^{18}O_{calcite}$ (equilibrium)
z_{mon} = 1.5 m
M: 1.2 – 1.6
$\delta^{18}O_{monsoon\ flood}$: –8‰ to –10‰
δmon
δsml
δssth
δwml
δint
20
30
40
50
60
70
80
2.5
2
1.5
1
0.5
0
-0.5
-1
-1.5
modelled $\delta^{18}O_{calcite}$ (equilibrium)

Fig.11

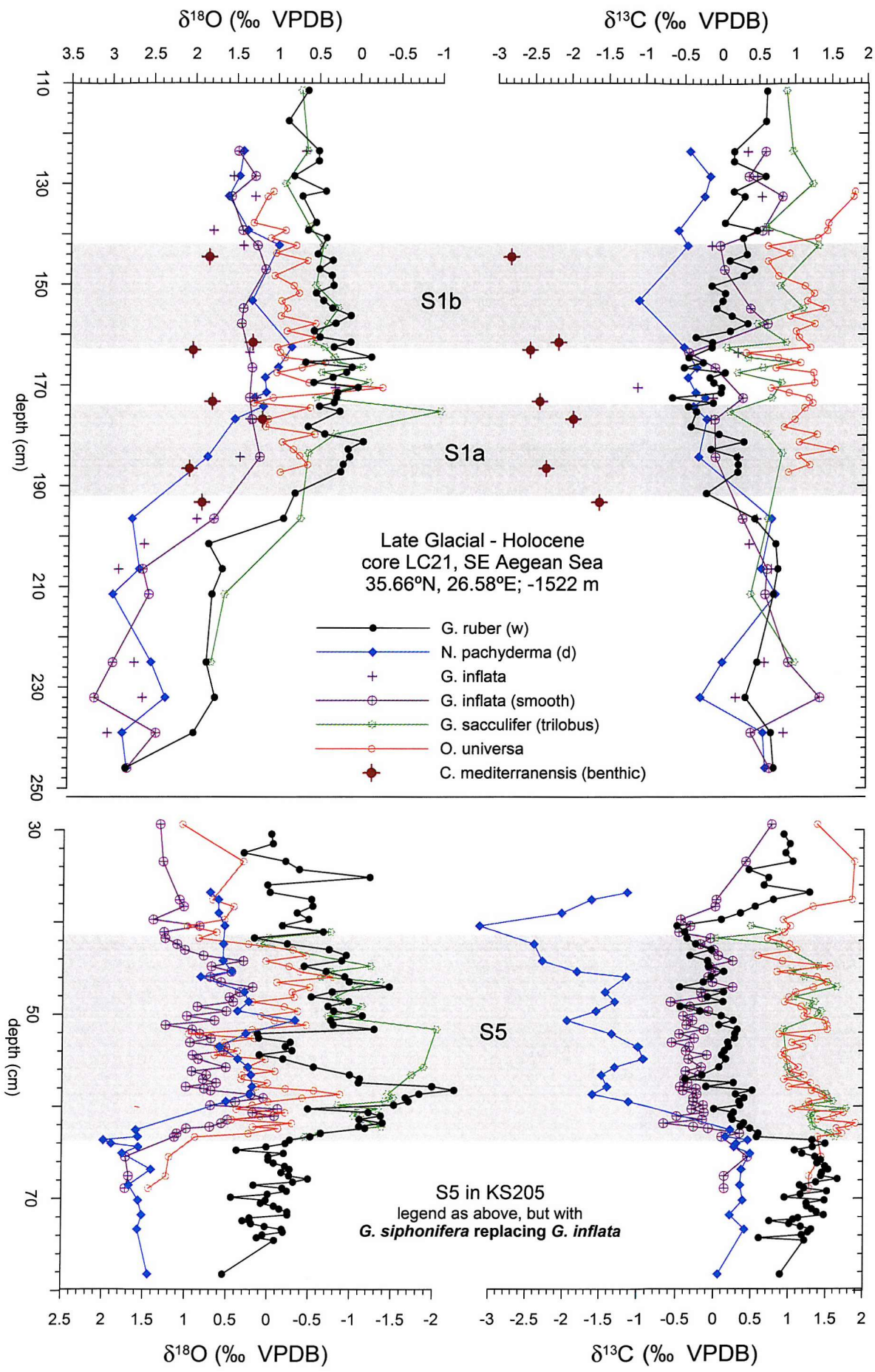
δ18O (‰ VPDB)
δ13C (‰ VPDB)
depth (cm)
S1b
S1a
Late Glacial - Holocene
core LC21, SE Aegean Sea
35.66°N, 26.58°E; -1522 m
G. ruber (w)
N. pachyderma (d)
G. inflata
G. inflata (smooth)
G. sacculifer (trilobus)
O. universa
C. mediterranensis (benthic)
S5
S5 in KS205
legend as above, but with
G. siphonifera replacing G. inflata

Fig.12